VOLUME 35 APRIL 1957

NUMBER 4

Canadian Journal of Physics

Editor: H. E. DUCKWORTH

Associate Editors:

L. G. ELLIOTT, *Atomic Energy of Canada, Ltd., Chalk River*
J. S. FOSTER, *McGill University*
G. HERZBERG, *National Research Council of Canada*
L. LEPRINCE-RINGUET, *Ecole Polytechnique, Paris*
B. W. SARGENT, *Queen's University*
G. M. VOLKOFF, *University of British Columbia*
W. H. WATSON, *University of Toronto*
G. A. WOONTON, *McGill University*

Published by THE NATIONAL RESEARCH COUNCIL

OTTAWA CANADA

CANADIAN JOURNAL OF PHYSICS

(Formerly Section A, Canadian Journal of Research)

Under the authority of the Chairman of the Committee of the Privy Council on Scientific and Industrial Research, the National Research Council issues THE CANADIAN JOURNAL OF PHYSICS and six other journals devoted to the publication, in English or French, of the results of original scientific research. Matters of general policy concerning these journals are the responsibility of a joint Editorial Board consisting of: members representing the National Research Council of Canada; the Editors of the Journals; and members representing the Royal Society of Canada and four other scientific societies.

EDITORIAL BOARD

Representatives of the National Research Council

A. N. Campbell, *University of Manitoba*
G. E. Hall, *University of Western Ontario*
H. G. Thode, *McMaster University*
D. L. Thomson, *McGill University*
W. H. Watson (Chairman), *University of Toronto*

Editors of the Journals

D. L. Bailey, *University of Toronto*
T. W. M. Cameron, *Macdonald College*
H. E. Duckworth, *McMaster University*
K. A. C. Elliott, *Montreal Neurological Institute*
G. A. Ledingham, *National Research Council*
Léo Marion, *National Research Council*
R. G. E. Murray, *University of Western Ontario*

Representatives of Societies

D. L. Bailey, *University of Toronto*
Royal Society of Canada
T. W. M. Cameron, *Macdonald College*
Royal Society of Canada
H. E. Duckworth, *McMaster University*
Royal Society of Canada
Canadian Association of Physicists
K. A. C. Elliott, *Montreal Neurological Institute*
Canadian Physiological Society
R. G. E. Murray, *University of Western Ontario*
Canadian Society of Microbiologists
H. G. Thode, *McMaster University*
Chemical Institute of Canada
T. Thorvaldson, *University of Saskatchewan*
Royal Society of Canada

Ex officio

Léo Marion (Editor-in-Chief), *National Research Council*
F. T. Rosser, Director, Division of Administration, *National Research Council*

Manuscripts for publication should be submitted to Dr. Léo Marion, Editor-in-Chief, Canadian Journal of Physics, National Research Council, Ottawa 2, Canada.

(For instructions on preparation of copy, see **Notes to Contributors** (inside back cover).)

Proof, correspondence concerning proof, and orders for reprints should be sent to the Manager, Editorial Office (Research Journals), Division of Administration, National Research Council, Ottawa 2, Canada.

Subscriptions, renewals, requests for single or back numbers, and all remittances should be sent to Division of Administration, National Research Council, Ottawa 2, Canada. Remittances should be made payable to the Receiver General of Canada, credit National Research Council.

The journals published, frequency of publication, and prices are:

Canadian Journal of Biochemistry and Physiology	Monthly	$3.00 a year
Canadian Journal of Botany	Bimonthly	$4.00 a year
Canadian Journal of Chemistry	Monthly	$5.00 a year
Canadian Journal of Microbiology	Bimonthly	$3.00 a year
Canadian Journal of Physics	Monthly	$4.00 a year
Canadian Journal of Technology	Bimonthly	$3.00 a year
Canadian Journal of Zoology	Bimonthly	$3.00 a year

The price of single numbers of all journals is 75 cents.

Canadian Journal of Physics

Issued by THE NATIONAL RESEARCH COUNCIL OF CANADA

VOLUME 35 APRIL 1957 NUMBER 4

THE LATTICE SPACINGS OF NICKEL SOLID SOLUTIONS[1]

W. B. PEARSON AND L. T. THOMPSON[2]

ABSTRACT

New lattice spacing measurements in terminal nickel solid solutions with Cr, Mn, Co, Zn, Ga, Ge, In, and Sn solutes are reported and discussed, and the relationship of lattice distortion and the depression of the solidus temperature is examined in solid solutions of the First Long Period elements in nickel.

INTRODUCTION

Measurements, most of which have been carried out in recent years, of the lattice spacings of nickel solid solutions containing as solutes the transition metal elements of the First Long Period* provide one of the most systematic sources of information on lattice spacing variation in transition metal alloys. These measurements are particularly interesting because of the definite kinks found in the lattice spacing – composition curves of vanadium, chromium, manganese, and iron dissolved in nickel. Taylor and Floyd (1952) associated the change of slope in the curve of lattice spacing vs. composition in the Ni–Cr solid solution with the occurrence of ordering in the Ni_3Cr region. The curve (Fig. 1) obtained by a combination of their measurements with those of Pearson, carried out in 1950, but reported for the first time here, shows that the bend occurs at about 20 at. % Cr. It does not, therefore, appear to be due to the superlattice ordering at Ni_3Cr which takes place at temperatures below 570° C. Similarly in the lattice spacings of the Ni–V solid solution (Fig. 1), although the bend occurs in the region of the compound Ni_3V, the slopes of the lattice spacing curves at higher and lower compositions are considerably different and nearly linear suggesting that the effect is independent of the ordering process which takes place on formation of Ni_3V. The large change of slope found in the iron solid solution at about 60 at. % Fe (Fig. 3) is associated with the formation of the alloy "Invar." Bradley *et al.* (1937) also found indications of a slight bend in the lattice spacing curve at about 22 at.

[1]Manuscript received November 5, 1956.

Contribution from the Division of Pure Physics, National Research Council, Ottawa, Canada.

Issued as N.R.C. No. 4245.

[2]Now with Defence Research Board, Ottawa, Canada.

*Notably, for instance, NiTi: Taylor and Floyd (1952); Ni–V: Pearson and Hume-Rothery (1952); Ni–Cr: Taylor and Floyd (1952) and Pearson (unpublished, reported here for the first time); Ni-Mn: Tyler and Hume-Rothery and Pearson (unpublished, reported here for the first time); Ni-Fe: Owen and Sully (1941), Bradley *et al.* (1937), Jette and Foote (1936); Ni–Co: Taylor (1950); Ni–Cu: Owen and Pickup (1934), Coles (1956).

% iron in the 'permalloy' region; however, this bend was not apparent in the work of Jette and Foote (1936) or of Owen and Sully (1941).

In contrast to the work on transition metal solutes in Ni, very little has been done recently on the behavior of the B group elements dissolved in Ni. On the other hand such an examination may well be important, for investigation of these solutes dissolved in Cu, Ag, and Au has been largely responsible for an understanding of the distortion caused by solutes of different valencies in solid solutions (cf. Raynor 1949; also Owen 1947). Previously measurements of lattice spacings of the Ni–Zn solid solution have been made by Tamara and Ôsawa (1935), but the lattice spacing of $a = 3.503$ kX given for pure nickel (accepted value $a \simeq 3.5167$ kX) indicates that the results are not too reliable. Measurements of several alloys in the Ni–Ga solid solution were made by Hellner (1950), but he failed to notice the formation of a Ni_3Ga superlattice in the solid solution region (Pearson 1954). Weibke and Pleger (1937) measured the lattice spacings of alloys in the Ni–In solid solution, but they found a rather low lattice spacing for pure nickel ($a = 3.514$ kX). Measurements of the lattice spacings of the Ni–Sn solid solution made by Mikulas *et al.* (1937) and by Jette and Foote (1935) are in rather good agreement with each other. Finally lattice spacings of the Ni–Sb solid solution have been measured by Ôsawa and Shibata (1940).

We have thus undertaken anew systematic measurements on the lattice spacings of the B group solutes in nickel with three main interests in view: (i) to gain further understanding of the electronic behavior of Ni as solvent in relation to that of the succeeding monovalent metals Cu, Ag, and Au; (ii) to see if any further systematic information can be gained about the bends which occur in the lattice spacing–composition curves of certain Ni solid solutions (somewhat similar bends have also been found in some Cr and some Fe solid solutions); and finally (iii) to examine the relationship of macroscopic lattice distortion (as determined by lattice spacing variation) and the depression of the solidus temperature caused by a solute, for we expect that the solidus depression should show a certain dependence on the distortion of the crystal lattice. Nickel, as we shall show, is a rather interesting solvent from this point of view, as all of the transition metal and B group metal solutes are (nominally at least) of larger size than the solvent atom.

EXPERIMENTAL METHODS

The alloys have been prepared from Mond nickel shot (typical analysis: 99.95% nickel, 0.02% carbon, 0.02% iron) kindly supplied by the International Nickel Co. and electrolytic hydrogen-treated Cr (99.9%), Mn (99.9%), and Co (99.9%) from Johnson, Matthey & Co. Ltd., 99.999% Zn from the New Jersey Refining Co. Ltd., 99.9% Ga, from Johnson, Matthey & Co. Ltd. or Mackay Inc., 99.999% Ge from various sources, 'spec pure' Cd and Sn from Johnson, Matthey & Co. Ltd., and 99.9% In from the same firm or from the Indium Corporation of America. With the exception of the Ni–Zn and Ni–Cd alloys they were all melted *in vacuo* in an induction furnace in pure alumina crucibles and then homogenized for several days at 1100° C. in

alumina collars sealed in evacuated silica tubes. Filings were prepared and strain-relieved, generally at 800° C. The composition of the actual X-ray powders was determined by chemical analyses of both components and also of iron. The first series of powders prepared was found to contain generally as much as 0.5% Fe which was picked up during the filing process. The measurements of these samples were therefore discarded, and subsequently the iron was carefully removed from the powders with a magnet by heating them *in vacuo* to a temperature above their Curie point so that the iron remained ferromagnetic but not the alloys. The iron content of most powders examined then generally lay in the range 0.02 to 0.25 wt. %.

The Ni–Zn and Ni–Cd alloys were prepared by interdiffusion by heating together mixtures of filings of the pure metals in sealed silica tubes for a sufficient time to attain equilibrium.

Lattice spacings were determined from powder photographs taken in a 19 cm. diam. Unicam camera in a thermostatically controlled room. CuK_α radiation was generally used throughout the work. Scattered radiation from Ni–Co alloys was absorbed with aluminum foil placed between the specimen and the X-ray film. Lattice spacings were calculated using the extrapolation method of Nelson and Riley. The X-ray measurements on any specimen were reproducible to 0.0001 kX, but factors involving the alloys (impurities, chemical analyses, etc.) made the general reproducibility of the measurements from different alloys somewhat less, particularly it seems in the Ni–Ge system.

EXPERIMENTAL RESULTS

The lattice spacing of Mond nickel shot (a = 3.5169 kX at 18° C.) was found to be higher than that of Johnson and Matthey spectroscopically pure Ni (a = 3.5165 kX at 18° C.), which was absolutely cobalt-free and contained only trivial amounts of other metallic impurities. This agrees with the observations of Coles (1956).

The lattice spacing variations in the systems Ni–Cr, Ni–Mn, Ni–Co, Ni–Zn, Ni–Ga, Ni–Ge, Ni–In, and Ni–Sn, together with measurements by others on Ni–Ti, Ni–V, Ni–Fe, and Ni–Cu solid solutions, are shown in a series of diagrams (Figs. 1–5). We should notice the sudden change in slope of the lattice spacing curves in the Ni–V, Ni–Cr, Ni–Mn, and Ni–Fe solid solutions at about 24, 20, 60, and 60 at. % solute respectively. Smaller changes of slope may also exist in the Ni–Zn, Ni–Ga, Ni–Ge, and Ni–In systems. Measurements on the Ni–Sb solid solution by Ôsawa and Shibata (1940, 1942) apparently indicate a steplike increase in the lattice spacing – composition curve at 6 wt. % Sb which they attributed to the occurrence of a superlattice.

It is possible to compare the present work with that of other investigators in several of the systems. The agreement with Taylor and Floyd (1952) on the lattice spacings of the Ni–Cr solid solution is excellent, and good agreement is also found with Taylor (1950) in the Ni–Co system and with Weibke and Pleger (1937) in the Ni–In system. Because of the Ni_3Ga superlattice only one of Hellner's measurements on the Ni–Ga solid solution can

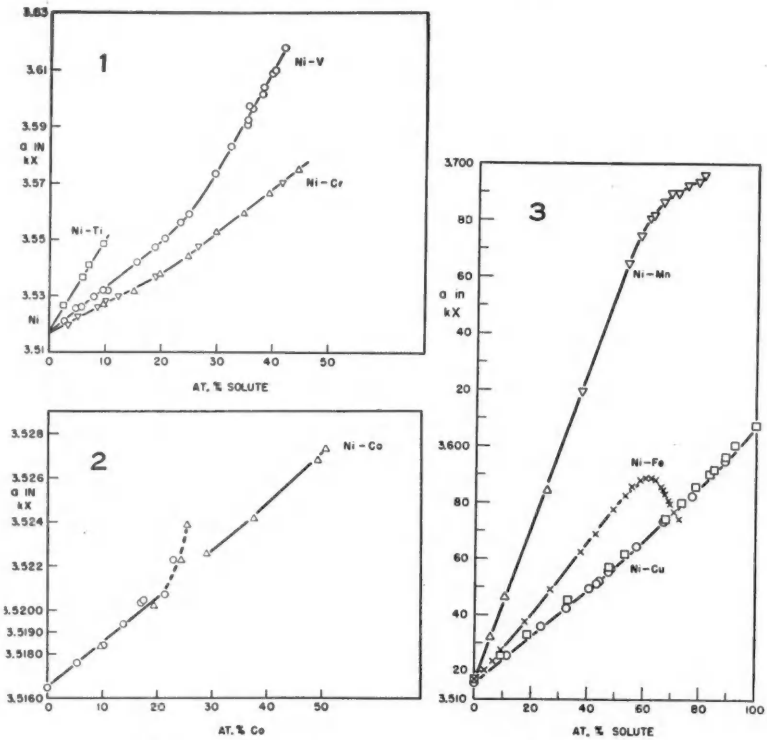

FIG. 1. Lattice spacings of terminal nickel solid solutions.

□ Ni–Ti Taylor and Floyd (1952)
○ Ni–V Pearson and Hume-Rothery (1952)
△ Ni–Cr Taylor and Floyd (1952)
▽ Ni–Cr Pearson

FIG. 2. Lattice spacings of the Ni–Co solid solution.

△ Taylor (1950)
○ Present work

FIG. 3. Lattice spacings of terminal nickel solid solutions.

△ Ni–Mn Pearson
▽ Ni–Mn Tyler
× Ni–Fe Owen and Sully (1941)
○ Ni–Cu Coles (1956)
□ Ni–Cu Owen and Pickup (1934)

be compared with our results and the agreement is reasonable. In the Ni–Sn system our results lie slightly higher than the measurements of Mikulas *et al.* (1937) and of Jette and Foote (1935), which agree with each other. However, it appears that only in the present investigation were the actual X-ray powders chemically analyzed, and as the analytical totals deviate from 100% by no more than 0.09%, we have confidence in these new measurements.

The solubility of Cd in Ni appears to be rather small at 800° C. We prepared a number of alloys by the method which was successful for the Ni–Zn solid solutions; however, as the alloys regularly showed a loss of weight during sintering and the X-ray films frequently showed extra reflections

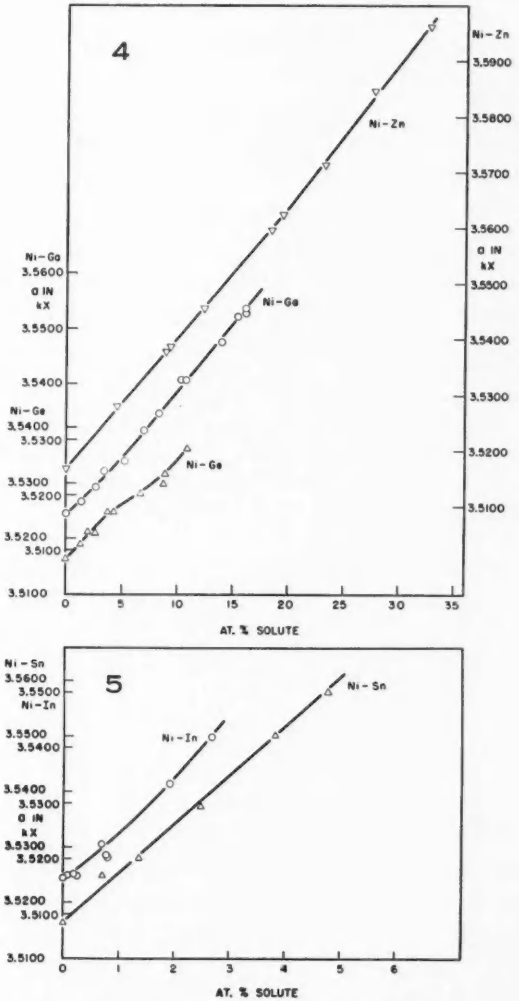

FIG. 4. Lattice spacings of terminal nickel solid solutions.

▽ Ni–Zn
○ Ni–Ga
△ Ni–Ge
} Present work

FIG. 5. Lattice spacings of terminal nickel solid solutions.

○ Ni–In
△ Ni–Sn
} Present work

due to some impurity phase we have rejected the results. The lattice spacing of heterogeneous alloys quenched from 800° C. was found consistently to be $a = 3.5180$ kX.

DISCUSSION OF RESULTS

(*a*) *Lattice Distortion*

Fig. 6 shows the total initial lattice distortion Δa, per atomic per cent solute for the elements of the First Long Period dissolved in nickel, together with the sizes of the solute atoms relative to nickel.* It is perhaps remarkable

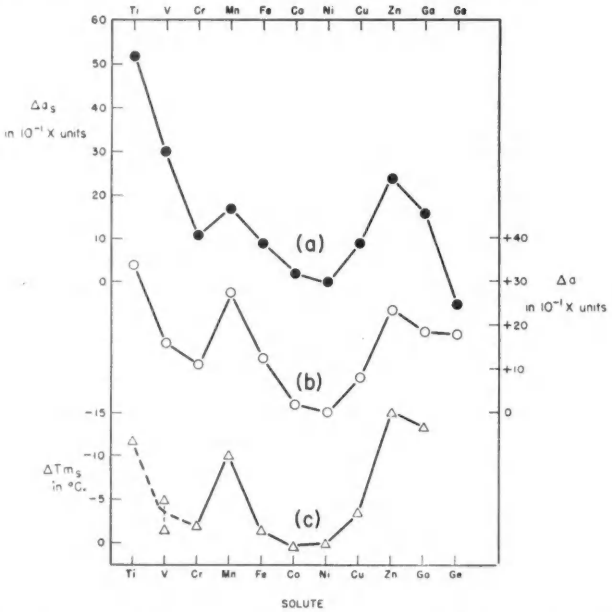

FIG. 6. (*a*) Difference in sizes of solute atoms relative to Ni (see text), plotted as the increase in lattice spacing expected per atomic per cent solute dissolved in nickel.
(*b*) Total observed initial lattice distortion per atomic per cent solute in terminal nickel solid solutions.
(*c*) Initial solidus depression in ° C. per atomic per cent solute in terminal nickel solid solutions.

how well the relative variation in lattice distortion (except with Ge as solute) follows the relative variation of solute atom size. In the Ni–Ge solid solution it is apparent that specific electronic or valence effects contribute to the observed lattice distortion.

*The relative atom sizes for a hypothetical face-centered cubic lattice have been calculated for the body-centered cubic metals from the interatomic distances, which were increased by 3% to allow for increase in coordination Following the lead of Raynor (1949) the interatomic distances of Zn and Ge were taken as the closest distances of approach of the atoms in the pure metals and the same procedure was followed for hexagonal Ti. The atomic diameter of Ga was calculated from the observed lattice distortion in Cu, Ag, and Au as solvents using Raynor's relationships for the data of the Group II and IVB solutes in the same solvents. The size of the Mn atom was obtained by taking a face-centered cubic unit cell which had the same volume as the face-centered tetragonal γ-Mn unit cell at room temperature. This is the most satisfactory method of estimating its size as Christian and Basinski have shown that cubic γ-Mn transforms to tetragonal γ-Mn without change of volume.

At present the only apparently successful quantitative analysis of lattice spacing variation in terminal solid solutions is that given by Raynor (1949) for the B group solutes dissolved in Cu, Ag, and Au. In this analysis the total observed distortion was divided into parts due to a size effect and to a valence effect and, for solvent and solutes which lay in the same period, the valence distortion was found to be proportional to the square of the valence difference of solvent and solute. It can be seen from Fig. 6 (*a*) and (*b*) that a similar analysis of solid solutions in nickel (taking the same sizes as were used by Raynor for Zn, Ga, and Ge atoms) would not lead to this same dependence of the electronic component of lattice distortion on the square of the valence difference of solvent and solute.

With our present picture of the nature of a solute ion in solid solution (derived largely from an understanding of electrical measurements) it is perhaps hard to understand the nature of a size effect which can be separated entirely from an electronic effect in the general way found by Raynor. It is therefore of particular interest to note that the factors which control the sizes of the transition metal atoms in the pure state also appear to play a large part in determining their apparent sizes when they are dissolved in nickel. The number of *s*-electrons does not vary greatly throughout the series of transition metals, but the *d*-electron content varies more or less regularly from one element to the next and, although it is known that these electrons contribute to the cohesion of the lattice, the cohesion is certainly *not* a linear function of the *d*-electron content of the metal (cf. Hume-Rothery, Irving, and Williams 1951). The correspondence between the observed distortion in nickel and the relative solute sizes obtained from the pure metals is therefore perhaps rather closer than might have been expected, since the electronic state of the solutes in nickel is presumably different to that in the pure metals. However, judging by known data, the same observation appears to be generally true for solid solutions of most of the transition metals in each other, although there are some obvious exceptions to this rule. In an attempt to gain more knowledge of the relative electronic states of these solutes in nickel, measurements of the resistivity of these alloys are being undertaken.

(*b*) *Bends in Lattice Spacing Curves*

In the terminal iron solid solutions of the Fe–Co and Fe–Cr systems sharp bends are found in the lattice spacing – composition curves at the same compositions as bends also occur in the curves of Curie temperature and saturation magnetic moment as functions of composition. This correspondence does not appear to hold in nickel solid solutions and this is perhaps not surprising if the magnetic interactions are weaker. In the Ni–Mn solid solution, for instance, the saturation magnetic moment first increases for additions of up to 8 or 10 at. % Mn after which it decreases very rapidly (Sadron 1932); however, the few lattice spacing measurements which we have obtained in this region certainly indicate that the lattice spacing changes linearly as a function of composition up to about 50 at. % Mn.

Both Owen and Yates (1936) and Esser *et al.* (1938) have shown that the lattice spacing of pure nickel as a function of temperature passes through a small anomaly in the region of the Curie point, and it would therefore be

expected that the lattice spacing – composition curve of alloys should show an anomaly at the composition at which the Curie point passes through room temperature. The lattice spacing – composition curves shown in Figs. 1 and 3 indicate that this anomaly must be rather small and not bigger than the general scatter of the experimental measurements, for it has not been possible to observe it, except perhaps in the Ni–Cu system where Coles' (1956) measurements showed a change in the rate of deviation from Vegard's law in this region.

It does not seem possible to find any explanation of the large bends in the lattice spacing – composition curve of the Ni–V, Ni–Cr, and Ni–Mn systems in terms of Brillouin zone overlaps, and even if the bend in the Ni–Fe solid solution were in part due to magnetic interactions which changed rapidly with composition in that region, there seems to be no clear evidence that this should also be the case in the other solid solutions. It is, however, probably significant that in the Ni–V and Ni–Cr solid solutions the rate of lattice distortion beyond the bend increases, whereas, when Mn or Fe is solute there is a decrease in the rate of distortion of the lattice as a function of composition beyond the bend in the curve of lattice spacing vs. composition. This change thus follows changes in the sequence of other physical properties which occur between Cr and Mn and which probably result from a change in the distribution of electrons in the *d*-band as the second half of the *d*-band starts to be filled.

(*c*) *Correlation of Lattice Distortion and Solidus Depression*

The solidus depression, ΔTm_a,* in a terminal solid solution may be expected to show some correlation with the total lattice distortion, Δa, as determined from lattice spacing measurements, for the energy stored in the lattice as the result of a positive distortion (i.e. an increase in lattice spacing) should lessen the total thermal energy required to disrupt the lattice in the melting process. In other words we would expect the solidus temperature to depend very largely on the properties of the crystalline lattice of the solid phase. Indeed, when we compare (Fig. 6 (*b*) and (*c*)) the total lattice distortion and solidus depression for nickel solid solutions we find an excellent qualitative correlation. Such a correlation is lost if we compare estimated size or electronic components of the distortion with the solidus depression, showing as expected that it is only for the *total* distortion that the relationship exists. The relationship is perhaps more remarkable when it is remembered that the lattice spacing measurements were made at room temperature and there is no *a priori* reason to expect that the same relative distortions should be found in the various solid solutions in the vicinity of the melting point of the alloys.

When we compare similar data for solid solutions in Cu and in Au we find that, although many of the features are similar, a general correlation of solidus depression and lattice distortion does not exist. This may be due to the relative lattice distortions near the melting point being different in these solvents from those observed at room temperature, or it may in part be due

*°C. per atomic per cent solute.

to the fact that some solutes cause positive distortions and others negative distortions of the Cu and Au lattices, while nickel is unique as a solvent in having a smaller diameter than all of the solute atoms and each solute causes a positive distortion of the lattice. If a negative distortion of the solvent lattice (i.e. a contraction) occurs, it seems unlikely that this should necessarily lead to an increase in the solidus temperature for, although the cohesion of the solvent atoms may increase, any strain energy in the lattice would still be expected to contribute towards a lowering of the melting point.

A thorough discussion of "Melting and Crystal Structure" was given by Ubbelohde (1950).

ACKNOWLEDGMENTS

The lattice spacings of nickel–chromium and nickel–manganese solid solutions were measured in Dr. W. Hume-Rothery's Laboratory at the University of Oxford and we are indebted to him for permission to publish these results here. Measurements on the more concentrated solutions of Mn in Ni, as yet unpublished, were made by Mr. D. N. Tyler in the same Laboratory. We also wish to thank Mrs. D. M. Rimek who heat treated many of the alloys, Mr. W. Stockdale who carried out the chemical analyses, and Miss B. J. Anderson and Miss J. M. LePage who assisted in some of the work.

REFERENCES

Bradley, A. J., Jay, A. H., and Taylor, A. 1937. Phil. Mag. **23**, 545.
Coles, B. R. 1956. J. Inst. Metals, **84**, 346.
Esser, H., Eilender, W., and Bungardt, K. 1938. Arch. Eisenhüttenw. **12**, 157.
Hellner, E. 1950. Z. Metallkunde, **41**, 480.
Hume-Rothery, W., Irving, H. M., and Williams, R. J. P. 1951. Proc. Roy. Soc. A, **208**, 431.
Jette, E. R. and Foote, F. 1935. Metallwirtschaft, **14**, 165.
——— 1936. Trans. Am. Inst. Mining Met. Engrs. **120**, 259.
Mikulas, W., Thomassen, L., and Upthegrove, C. 1937. Trans. Am. Inst. Mining Met. Engrs. **124**, 111.
Ôsawa, A. and Shibata, N. 1940. Nippon Kinzoku Gakkai-Shi, **4**, 362.
——— 1942. Sci. Repts. Tôhoku Imp. Univ. (i), **30**, 245.
Owen, E. A. 1947. J. Inst. Metals, **73**, 471.
Owen, E. A. and Pickup, L. 1934. Z. Krist. A, **88**, 116.
Owen, E. A. and Sully, A. H. 1941. Phil. Mag. **31**, 314.
Owen, E. A. and Yates, E. L. 1936. Phil. Mag. **21**, 809.
Pearson, W. B. 1954. Nature, **173**, 364.
Pearson, W. B. and Hume-Rothery, W. 1952. J. Inst. Metals, **80**, 641.
Raynor, G. V. 1949. Trans. Faraday Soc. **45**, 698.
Sadron, C. 1932. Ann. phys. **17**, 371.
Tamara, K. and Ôsawa, A. 1935. Kinzoku-no-Kenkyu, **12**, 131.
Taylor, A. 1950. J. Inst. Metals, **77**, 585.
Taylor, A. and Floyd, R. W. 1952. J. Inst. Metals, **80**, 577.
Ubbelohde, A. R. 1950. Quart. Revs. **4**, 356.
Weibke, F. and Pleger, I. 1937. Z. anorg. Chem. **231**, 197.

LATTICE DISTORTION IN TERMINAL SOLID SOLUTIONS OF THE FIRST LONG PERIOD TRANSITION METALS AND COPPER[1]

W. B. Pearson

ABSTRACT

Collected data of the gross lattice distortion in solid solutions of the First Long Period elements in each other and in copper are given together with similar data for B group solutes in Cu, Ag, and Au. It is shown that there is no correlation between the size of the lattice distortion and the solid solubility of the First Long Period transition metals in copper.

The whole of the X-ray work on metals and alloys has recently been reviewed and a compilation of the most reliable structural and lattice spacing data is in the course of publication (Pearson 1957*a*). Using these collected data we have now calculated the initial lattice distortion (expressed as change of lattice spacing per atomic per cent solute) in terminal solid solutions of the transition metals of the First Long Period in each other and with the B group elements as solutes. This information is of particular interest in relation to the other physical properties of transition metal alloys such as electrical resistivity and thermoelectricity and to recent considerations of their electronic nature (e.g. Friedel 1956).

Information about the local, microscopic distortion caused by a substitutional solute in a solvent lattice can be gained from examination of the diffuse X-ray scattering accompanying the spectral reflections (cf. Averbach *et al.* 1953, 1954; Warren and Averbach 1953); on the other hand lattice spacing variation gives a direct measurement of the gross or macroscopic distortion of the solvent lattice due to the solute. In Fig. 1 we show all the available data for the initial* macroscopic lattice distortion per atomic per cent of solute in the terminal solid solutions of the transition metals of the First Long Period plotted as a function of the atomic number of the solute, and in Fig. 2 we show the same information as a function of the atomic number of the solvent. In each case we have shown the actual distortion (Δa) rather than the proportional distortion ($\Delta a/a$) as this can more conveniently be compared with the relative sizes of the solvent or solute atoms, which are also plotted in Figs. 1 and 2. The method used to obtain the sizes of the atoms and to compare them in terms of a (hypothetical) face-centered cubic lattice has been described by Pearson (1957*b*).

The factors causing lattice distortion are still not too well understood and in the only successful quantitative interpretation, which is due to Raynor (1949), the total distortion caused by the B group solutes in solid solution

[1]Manuscript received November 5, 1956.
Contribution from the Division of Pure Physics, National Research Council, Ottawa, Canada.
Issued as N.R.C. No. 4241.

*Details of references from which the data were collected can be found in Pearson (1957*a*). We have taken the best average of the initial slope of the lattice spacing – composition curves.

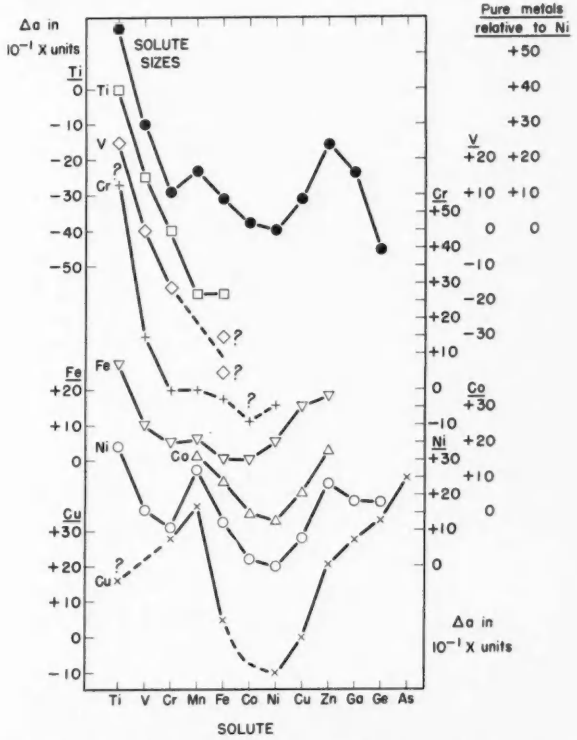

FIG. 1. Initial lattice distortion per atomic per cent solute in terminal solid solutions of the transition metals and copper plotted for the various solvents as a function of the atomic number of the solute, together with the difference of the solute sizes relative to nickel, plotted as the increase in lattice spacing expected per atomic per cent dissolved in nickel.

? V–Fe: the two points mark the probable limits of the somewhat uncertain size of the lattice distortion.

? Cr–Ti: the value of the *initial* lattice distortion is not too certain.

? Cr–Co: obtained from very old measurements made in the region of 25 wt. % Co.

? Cu–Ti: the results of two recent investigations differ rather widely. The value plotted is a mean value weighted slightly in favor of the work which appears to be the most reliable.

in Cu, Ag, or Au was separated into components due to the relative sizes and relative valencies of the solutes and solvent. The occurrence of other factors causing lattice distortion has also been recognized (Raynor 1949; Axon and Hume-Rothery 1948) but it is not possible to calculate them a priori. With our present physical picture of a screened solute ion in these solid solutions—a concept largely derived from an understanding of electrical measurements—it is perhaps hard to see how a size effect can exist independent of the electronic or valence effect as found by Raynor. It is therefore interesting to note in Figs. 1 and 2 that the lattice distortion in transition metal alloys generally follows the relative variation in the solute or solvent

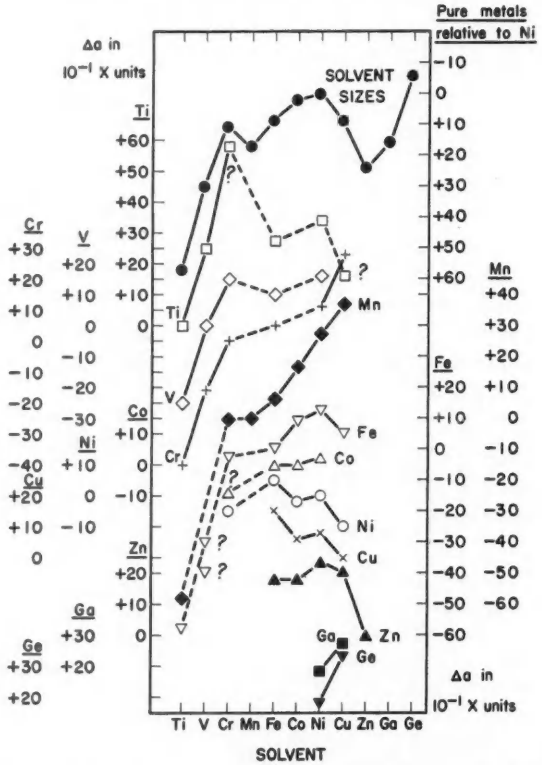

FIG. 2. Initial lattice distortion per atomic per cent solute in terminal solid solutions of the transition metals and copper plotted for the various solutes as a function of the atomic number of the solvent, together with the difference of the solvent sizes relative to nickel, plotted as the increase in lattice spacing expected per atomic per cent dissolved in nickel. For comments on ? V–Fe, ? Cr–Ti, ? Cr–Co, and ? Cu–Ti see caption to Fig. 1.

atom sizes.* This is certainly not the case in the solid solutions of the B group solutes in Cu, Ag, and Au (Fig. 3), for the sizes of the solutes of the First and Second Long Periods decrease in the elements following Zn and Cd respectively, while the distortion which they cause in Cu, Ag, and Au continues to increase. However, it can also be seen from Fig. 3 that although the solute size is not the major factor in causing the lattice distortion in these solid solutions, it does exert some influence.

Although we do not intend in the present note to discuss these lattice distortion data in any detail, we do, however, examine them in relation to one of the most interesting unsolved problems of metallurgical chemistry;

*There are of course notable exceptions to this, such as some solid solutions in which Mn is the solute.

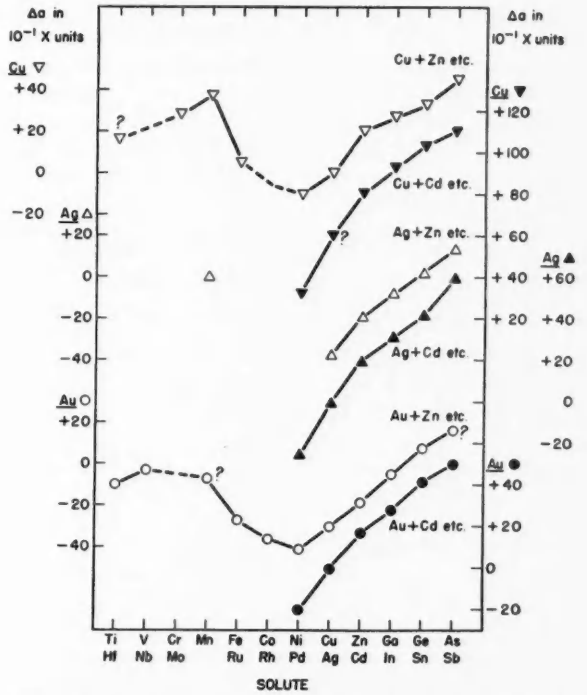

FIG. 3. Initial lattice distortion per atomic per cent solute in solid solutions in Cu, Ag, or Au plotted as a function of the atomic numbers of the B group solutes of the First and Second Long Periods. ? indicates some uncertainty in the observed lattice distortion values.

that is to the relative variation of solid solubility of the transition metals in copper. In Table I we compare the total measured lattice distortion and

TABLE I

Solute	Solid solubility	Δa, total measured distortion per at. % solute in 10^{-1} X units	Δa_s, pure metal sizes relative to Cu. expected distortion per at. % solute in 10^{-1} X units	Δa_v, apparent 'electronic' distortion of Cu lattice per at. % solute in 10^{-1} X units
Ni	100%	−10	− 9	− 1
Co	Very small at low temperature	?	− 7	—
Fe	Very small at low temperature, ~5% at 1090° C.	+ 5	0	+ 5
Mn	100%	+37	+ 8	+29
Cr	Very small	+28	+ 2	+26
V	Probably very small	?	+21	—
Ti	About 6 at. %	~+16	+48	~−32?

also the apparent 'electronic' distortion* of the copper lattice with the solid solubility limits of the various transition elements of the First Long Period. This shows, surprisingly perhaps, that there is no correlation between a small solid solubility and a large lattice distortion, and the factors which restrict the solid solubility of Co, Fe, Cr, and V in Cu do not at the same time lead to a large distortion of the copper lattice, so that the behavior of the transition metal solutes is again seen to be different to that of the B group solutes.

REFERENCES

AVERBACH, B. L., FLINN, P. A., and COHEN, M. 1953. Acta Met. **1**, 665.
——— 1954. Acta Met. **2**, 92.
AXON, H. J. and HUME-ROTHERY, W. 1948. Proc. Roy. Soc. A, **193**, 1.
FRIEDEL, J. 1956. Can. J. Phys. **34**, 1190.
PEARSON, W. B. 1957*a*. The lattice spacings and structures of metals and alloys (The Pergamon Press, Ltd., London).
PEARSON, W. B. and THOMPSON, L. T. 1957*b*. Can. J. Phys. **35**, 349.
RAYNOR, G. V. 1949. Trans. Faraday Soc. **45**, 698.
WARREN, B. G. and AVERBACH, B. L. 1953. Modern research techniques in physical metallurgy (American Society for Metals, Cleveland, Ohio).

*Calculated by the method of Raynor (1949) using the solute atom sizes of Pearson (1957*b*).

THE VELOCITY DEPENDENCE OF ČERENKOV RADIATION FROM μ-MESONS[1]

C. H. Millar and E. P. Hincks

ABSTRACT

The intensity–velocity relationship of the Čerenkov light emitted by μ-mesons passing through Plexiglas has been studied for the velocity range $0.83c$ to $0.99970c$ (84 Mev. to 4.2 Bev.). No departure of the observed from the theoretical intensity was found in the high velocity region, in disagreement with the results of Bassi, Bianchi, and Manduchi (1952). In the low velocity region slightly less radiation was observed than expected, but this is attributed to an optical effect in the apparatus rather than to a departure from theory of the Čerenkov light emission.

INTRODUCTION

The classical theory (Frank and Tamm 1937) of Čerenkov radiation by a moving, charged particle gives for the energy radiated in a distance x in a medium of refractive index n

$$W = (e^2x/c^2)\int_{\beta n>1}(1-1/\beta^2n^2)\,\nu\,d\nu, \tag{1}$$

where β $(=v/c)$ and e are the velocity and charge respectively of the moving particle, ν is the frequency of the emitted light, and c is the velocity of light *in vacuo*. Ginsburg (1940) has obtained by a quantum calculation a formula closely coincident with the above. From (1) it will be seen that after the particle velocity exceeds a threshold value ($\beta_{\text{threshold}} = 1/n$) W at first increases rapidly with particle velocity, but as β approaches unity, W asymptotically approaches a constant maximum or 'plateau' value.

Experimental evidence has been reported that the velocity dependence of the intensity of Čerenkov light from mesons passing through Plexiglas deviates significantly from that given in equation (1). Bassi, Bianchi, and Manduchi (1952) reported a plateau intensity of Čerenkov light from fast cosmic-ray μ-mesons whose relative value was about 25% too high when compared with the intensity of light from mesons in a velocity range corresponding to a steeply rising portion of the theoretical curve. Winckler, Mitchell, Anderson, and Peterson (1955), on the other hand, using artificially produced π-mesons observed good agreement with the steeply rising part of the expected intensity curve, but obtained a slight indication that the plateau commenced at a lower velocity than theoretically predicted. Since some Čerenkov counters in use at Chalk River depend on this intensity–velocity relationship to measure particle energies, we have carried out an experiment using cosmic-ray μ-mesons to investigate these reported anomalies.

[1]Manuscript received December 10, 1956.
Contribution from Physics Division, Atomic Energy of Canada Limited, Chalk River, Ontario.
Issued as A.E.C.L. No. 410.

EXPERIMENTAL PROCEDURE AND OBSERVATIONS

The general method of this experiment was to select a vertically-directed μ-meson beam by means of a coincidence telescope and to study the light output from a Čerenkov counter placed in this beam. The energies of the mesons were determined by their ranges after leaving the Čerenkov counter.

Since the experiment was carried out at Chalk River (altitude 475 ft.), and since a considerable thickness of absorber was always present either within or above the telescope, about 99% of the particles selected by the telescope were μ-mesons. The contamination of the beam by the remainder of the particles was estimated to have a negligible effect on the experimental results. In addition, an auxiliary experiment was performed in which showers were detected by recording coincident pulses in trays of Geiger counters placed nearby but out of the telescope beam. The results indicated that in the region of the most probable Čerenkov light output by mesons the effect of showers was also negligible.

The Čerenkov counter consisted of a 13 in.$\times$13 in.$\times$5 in. block of Type II Plexiglas viewed by two RCA No. 5819 photomultiplier tubes centrally positioned on opposite edges of the block. The Plexiglas was surrounded by MgO reflecting powder and a thin aluminum light shield.

It should be noted that the photomultiplier tubes used had an 'S-4' spectral sensitivity so that they responded only to visible and ultraviolet light in a

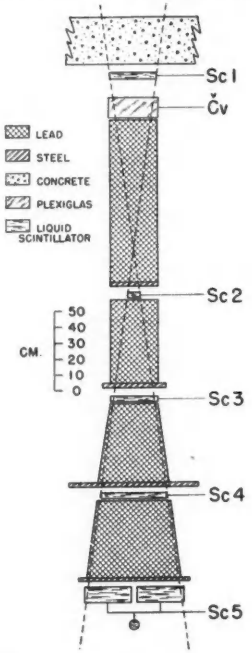

FIG. 1. Arrangement of counters and absorber for Part I of experiment.

restricted wavelength band. Thus the term "Čerenkov light" as used in this work refers to light in the region from 3200 to 6000 Å.

The experiment was carried out in two phases. The first phase was designed to look for any anomalous intensity variation of Čerenkov radiation that might occur in the high velocity or plateau region. The arrangement of apparatus for this part of the experiment is shown in Fig. 1, and is described below.

Vertically directed charged particles were selected by a triple coincidence between the two top liquid scintillation counters (Sc1, Sc2) and the Čerenkov counter (Čv). For a selected event the pulse height from the Čerenkov counter was measured by a 30-channel kicksorter and automatically recorded on an IBM punch card. On the same card was recorded which, if any, of the three lower scintillation counters (Sc3, Sc4, Sc5) had detected a particle in coincidence with the selected event. By sorting the cards according to this latter coincidence information it was possible to obtain pulse height distributions from the Čerenkov counter measured simultaneously for particles of four adjacent range bands.

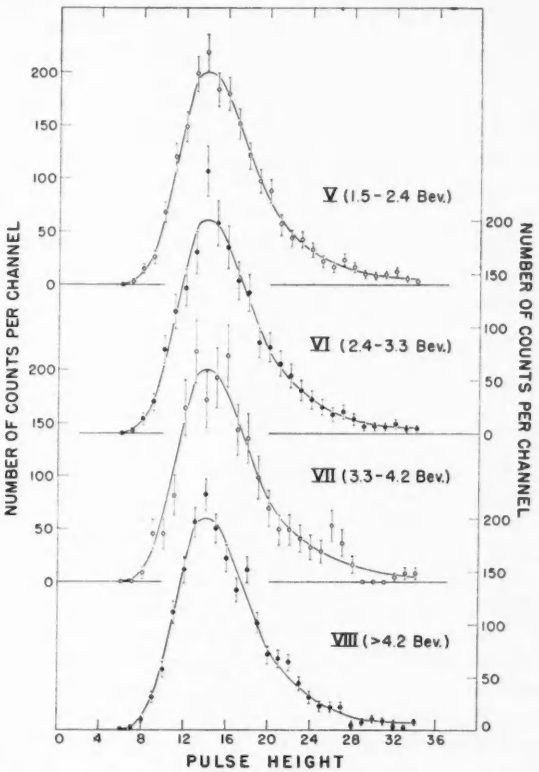

FIG. 2. Pulse height distributions from Čerenkov counter measured in Part I of experiment.

A μ-meson required a minimum kinetic energy of 1.5 Bev. when passing the central plane of the Čerenkov detector in order to penetrate the absorber and produce a signal in Sc2. The corresponding energies to reach counters Sc3, Sc4, and Sc5 were 2.4, 3.3, and 4.2 Bev. respectively. Thus Čerenkov light distributions were obtained for μ-mesons in three 0.9 Bev. energy bands between the above limits, and also in a fourth band comprising all energies above 4.2 Bev. These four distributions (V–VIII) are shown in Fig. 2. (The bands are numbered in order of increasing energy over both parts of the experiment.) The experimental points have been normalized so that each distribution contains the same total number of counts and one may be compared with the the other through the solid curves, which are identical in each plot. All four experimental distributions are of the same shape, and in particular have the same *most probable* light intensity as far as can be determined by visual inspection.

Assuming that the shapes of the four distributions are, in fact, identical, a quantitative estimate of the degree of equality of the peak positions may be made by comparing average values of light intensity calculated for the region covered by the kicksorter. These average values—denoted by A—are thus for a restricted range from zero to about $2\frac{1}{2}$ times the most probable pulse height. The comparison of individual values of A for each curve with the A for all data combined is shown in Table I and it may be seen that within the indicated standard errors all the values are identical. We conclude that the *most probable* values are constant to the same accuracy (within $\pm\sim 1\%$) as are these A values, and this conclusion is strengthened by a comparison of the r.m.s. deviations from A for each of the four distributions. These values, also listed in Table I, themselves agree to within $\pm\sim 1\%$ and prove that the calculated values of A are not influenced significantly by any changes in shape of the wings of the curves.

TABLE I

SUMMARY OF NUMERICAL RESULTS (PART I)

Band number	Energy range (Bev.)	Velocity range	'Average' pulse height (A)	Normalized 'average' pulse height	Normalized r.m.s. deviation from 'average'	% pulses greater than 34.5
V	1.5–2.4	0.9978–$0.9991c$	16.77 ± 0.12	0.998 ± 0.006	0.281	1.4 ± 0.3
VI	2.4–3.3	0.9991–$0.99952c$	16.72 ± 0.16	0.995 ± 0.009	0.276	2.3 ± 0.5
VII	3.3–4.2	0.99952–$0.99970c$	16.98 ± 0.22	1.010 ± 0.012	0.275	2.9 ± 0.8
VIII	>4.2	$>0.99970c$	16.83 ± 0.11	1.001 ± 0.005	0.275	3.3 ± 0.4
V–VIII	>1.5	$>0.9978c$	16.81 ± 0.07	1.000	(0.276)	(2.5 ± 0.3)

It appears then that the *most probable* Čerenkov light output remains constant to within 1% for μ-meson energies from 1.5 Bev. up to above 4.2 Bev. This conclusion does not, however, apply to the true *mean* Čerenkov intensity since a few large pulses formed a tail to each distribution which was not measured. These pulses, whose size fell above the range of the kicksorter, were of course not included in the calculations of the A values used above to

compare the peak positions. Their number did, in fact, show a significant increase with meson energy as shown in the last column of Table I. This suggests that the *mean* Čerenkov intensity may be increasing, perhaps as a result of secondary Čerenkov radiation from knock-on electrons. However, lack of knowledge of the size distribution of these large pulses as well as the lack of adequate protection against showers in our apparatus prevents any quantitative determination of the variation of *mean* Čerenkov light output with meson energy.

In the second phase of the experiment the energy bands studied were lowered by reducing the amount of lead absorber, the arrangement of apparatus being as shown in Fig. 3. Here the initial particle selection was by a triple coincidence

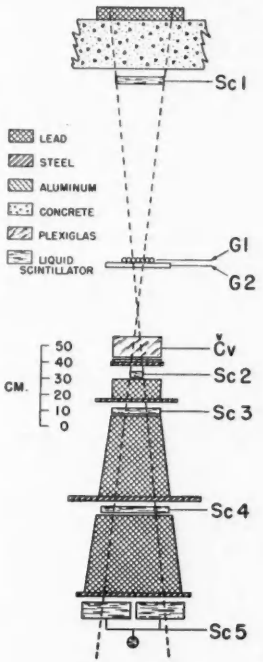

FIG. 3. Arrangement of counters and absorber for Part II of experiment.

between liquid scintillation counters Sc1 and Sc2, and the coincidence output of the crossed Geiger counter trays G1 and G2. The absorber thicknesses which the mesons had to penetrate to reach scintillation counters Sc2, Sc3, and Sc4 were adjusted to correspond roughly to those used by Bassi *et al.* (1952). Additional absorber and the scintillation counter Sc5 were included in order to overlap the energy bands studied in the first part of this experiment and thus to enable normalization of the one set of results to the other. Because

of the small thickness of absorber required for the lowest energy group, an additional 86.5 g./cm.^{2} of lead was placed above the concrete roof to help filter out the soft component of the cosmic radiation. The boundary values of the meson energy bands in this second experiment were 0.084, 0.27, 1.02, and 1.85 Bev., and four simultaneous pulse height distributions were obtained as previously. The results are shown in Fig. 4, where again the four curves have been normalized to equal areas.

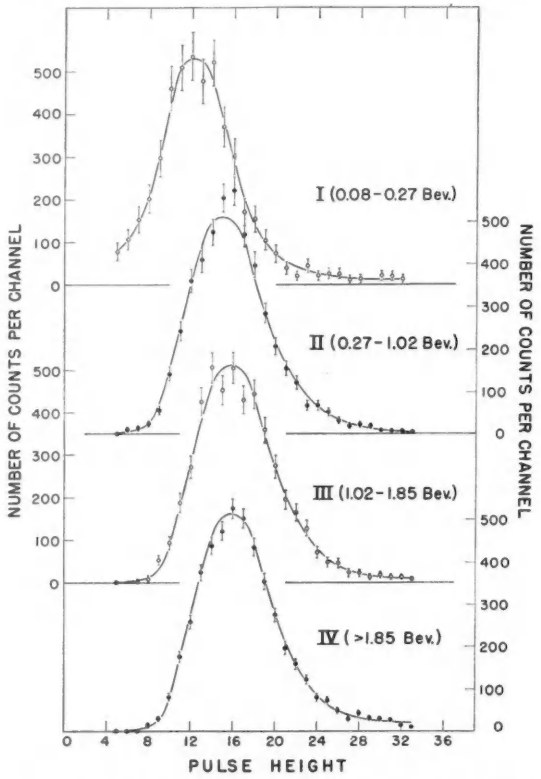

FIG. 4. Pulse height distributions from Čerenkov counter measured in Part II of experiment. Note that the arbitrary pulse height scale differs from that in Fig. 2.

In this instance there are obvious peak shifts as well as shape changes among the various curves so that we are not justified in using average values to compare peak positions as was done previously. Instead the peak positions and their uncertainties have been estimated from individual curves fitted to the sets of experimental points.

The results of the second part of the experiment are summarized in Table II. The most probable pulse height values for each energy group are normalized

to make that for the >1.85 Bev. group equal to unity in accordance with the results of the earlier runs. To compare our results directly with those of Bassi *et al.*, the 1.02–1.85 Bev. and >1.85 Bev. energy groups were added to give a >1.02 Bev. group which corresponds exactly to the energy band reported by Bassi to give an anomalously large Čerenkov intensity. This comparison is shown in the last column of the table.

TABLE II

SUMMARY OF NUMERICAL RESULTS (PART II)

Band number	Energy range (Bev.)	Velocity range	Peak pulse height	Peak pulse height (normalized)	Results of Bassi *et al.**
I	0.084–0.27	0.83–0.960*c*	12.30±0.30	0.769±0.020	0.88±0.03
II	0.27–1.02	0.960–0.9956*c*	15.15±0.17	0.947±0.013	0.97±0.03
III	1.02–1.85	0.9956–0.9985*c*	15.90±0.17	0.994±0.014	—
IV	>1.85	>0.9985*c*	16.00±0.13	1.000†	—
III+IV	>1.02	>0.9956*c*	15.96±0.10	0.998±0.005	1.26±0.03

*Results of Bassi *et al.* (1952) normalized to theoretical curve at energy band II.
†Energy band IV has been taken as the plateau value consistent with the normalization made in Part I.

It will be seen that our observed value of the *most probable* Čerenkov light output remains constant to within the estimated uncertainty of 1% down to a meson energy of 1.02 Bev. Below this energy the *most probable* intensity decreases to somewhat lower values than reported by Bassi *et al.*

DISCUSSION OF RESULTS

If equation (1) is normalized to the plateau intensity (W_{max}), assuming n to be constant,[2] the expression for the relative intensity I of Čerenkov radiation becomes

$$I = W/W_{max} = \frac{(1-1/\beta^2 n^2)}{(1-1/n^2)}. \tag{2}$$

For convenience in comparing the radiation from particles of different masses, the quantity I may be plotted as a function of $(\gamma-1)$, the kinetic energy of the particle in units of its rest mass, where

$$\gamma = (1-\beta^2)^{-\frac{1}{2}}. \tag{3}$$

The solid curve in Fig. 5 shows such a plot for Plexiglas, whose index of refraction is 1.49 in the visible region.

The normalized peak position for each of the four high energy groups studied in the first part of this experiment is shown as a black bar whose width is twice the standard error for the group. The cross-hatched bars show the normalized peak positions obtained in the second part of the experiment with energy groups III and IV added together. The vertical lines in groups I and II show the positions at which the bars should correspond to the theoretical curve when one takes into account the finite thickness of the counter

[2]It is only necessary for a comparison with experiment that n be independent of ν over that part of the spectrum where the detector has a significant response. It may be shown that within the sensitivity region of the photomultiplier the effect of the variation of n is negligible.

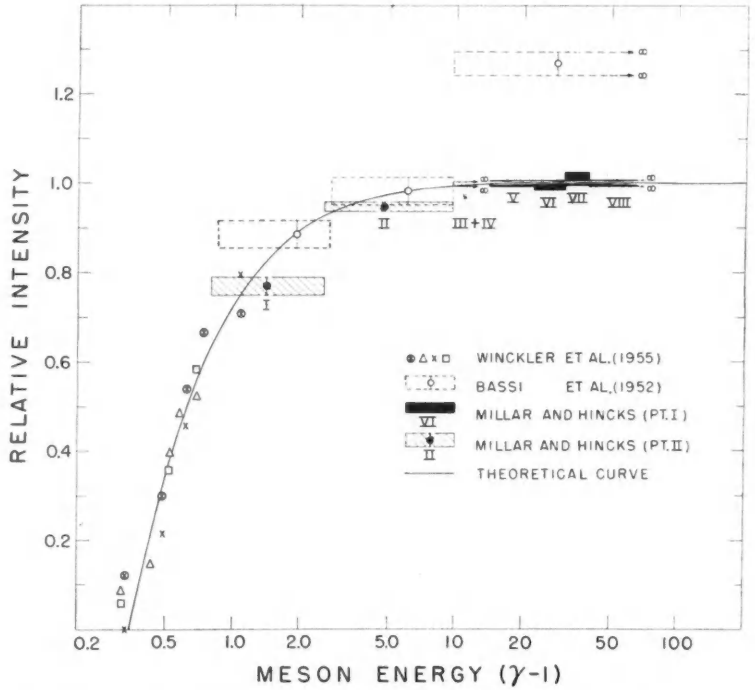

FIG. 5. Comparison with theory of various experimental observations of relative Čerenkov light intensity as a function of meson energy. Note that the results from different experiments have been independently normalized.

and the sea level meson spectrum corrected for the effect of the absorber above the telescope.

The dotted blocks show the results of Bassi *et al.* normalized by fitting the effective mean value of their middle energy group to the theoretical curve. Mean positions for the various groups are taken from Bassi's paper. These authors call their values "average" values, but since they describe no method for measuring very large amplitude pulses, it is probable that these "average" values are calculated for a limited region about the *most probable* pulse height as was the case with the A values used for comparison purposes in the first part of our experiment. Thus the variation of their "average" values should be consistent with the theoretical intensity–velocity relationship and therefore directly comparable with our relative data on *most probable* intensities.

The various experimental points in the figure are from the work of Winckler *et al.* (1955) and are for π-mesons of specific energies as shown. We have renormalized intensities and have made an approximate energy adjustment in order to fit these points to the 'thin counter' curve of Fig. 5. This procedure is not entirely valid since the variation in Čerenkov emission as the particles

slow down in passing through the counter becomes very large at the lower energies, an effect that is properly taken into account in the calculated curve of Winckler's paper. On the other hand the *shapes* of Winckler's curve and of the thin counter curve are very similar except near the threshold, and so Fig. 5 demonstrates fairly well the agreement between his experimental points and theory.

From Fig. 5 it will be seen that we do not observe any anomalously large Čerenkov light output from high energy μ-mesons corresponding to that found by Bassi *et al.* The apparent constancy to within 1% of the peak positions above 1.5 Bev. (bands V, VI, VII, VIII) which has already been noted is in agreement with the expected increase of 0.3% in the same energy range. The least squares fit of a linear relationship between I and $1/\beta^2$ to these four experimental points gives an increase of $(+0.5\pm1.1)\%$, which indicates the accuracy to which the theoretical curve is verified.

On the other hand, our low energy groups give slightly less light than predicted, group I being 7% low and group II about $2\frac{1}{2}\%$ low. Though this may, in fact, indicate a true departure from the theoretical curve in the energy region where Winckler *et al.* find some hint of a discrepancy, we believe that this apparent disagreement is due to an optical effect in our particular Čerenkov counter which is discussed below.

Čerenkov radiation is emitted at an angle to the particle direction of $\cos^{-1}(1/\beta n)$. For high energies β approaches unity and the maximum angle becomes $\cos^{-1}(1/n)$. For Plexiglas this maximum angle is 47.8°, which is about 6° greater than the critical angle ($\sin^{-1}(1/n) = 42.1°$) for a Plexiglas–air interface. Thus in our experiment all the Čerenkov light from the selected high energy μ-mesons (which enter the counter within 6° of the vertical) is totally reflected at the bottom surface of the Plexiglas, and continues outwards to the edges of the counter by a series of total internal reflections at the top and bottom surfaces. However, as the meson energy decreases, the angle of the Čerenkov cone decreases so that, for the oblique mesons first and ultimately for all mesons, more and more of the light strikes the Plexiglas–air boundary at less than the critical angle and depends on the diffuse reflectivity of the MgO to reflect it out to the photomultipliers. This transition region commences at the upper end of energy band II and continues throughout groups II and I until at the lower end of group I all the initial reflection is diffuse.

Inaccurate knowledge of the parameters involved prevents an exact calculation of the effect of this transition on the observed signal. However, since there will be a few per cent loss at each diffuse reflection as compared with practically no loss for total internal reflection, and since, on the average, the light will be reflected several times before reaching the photomultipliers, it would appear that this effect could easily be large enough to account for the difference between our observed results and the theoretical curve. The observation that in our experiment the fractional discrepancy increases with decreasing energy, while in Bassi's experiment—where no such transition effect should occur—this discrepancy is not found gives qualitative support to this hypothesis.

CONCLUSION

On the basis of our observations we conclude that there is no high energy anomaly in the intensity of Čerenkov light produced by μ-mesons passing through Plexiglas up to energies somewhat above 4.2 Bev. ($v = 0.99970c$). An apparently low output in the 100 to 1000 Mev. region is attributed to optical effects in our counter rather than to a disagreement between theory and experiment.

We believe that our results taken together with those of Winckler *et al.* (1955) establish the validity of the theoretical Čerenkov intensity relation to within a few per cent from threshold up to a velocity $\beta = 0.99970$, well into the saturation region.

ACKNOWLEDGMENT

The authors wish to express their thanks to M. Bercovitch for lending them the Čerenkov counter used in this experiment, to G. C. Hanna for his assistance in the original setting up of the electronic equipment, and to A. S. C. Hyde and Mrs. P. I. K. Lennox for technical and computational assistance.

REFERENCES

Bassi, P., Bianchi, A. M., and Manduchi, C. 1952. Nuovo cimento, **9**, 861.
Frank, I. and Tamm, I. 1937. Compt. rend. acad. sci. U.R.S.S. **14**, 109.
Ginsburg, V. L. 1940. J. Phys. (U.S.S.R.), **2**, 441.
Winckler, J. R., Mitchell, E. N., Anderson, K. A., and Peterson, L. 1955. Phys. Rev. **98**, 1411.

HIGH RESOLUTION RAMAN SPECTROSCOPY OF GASES

VIII. ROTATIONAL SPECTRA OF ACETYLENE, DIACETYLENE, DIACETYLENE-d_2, AND DIMETHYLACETYLENE[1]

J. H. CALLOMON[2] AND B. P. STOICHEFF

ABSTRACT

The pure rotational Raman spectra of acetylene (C_2H_2), diacetylene (C_4H_2 and C_4D_2), and dimethylacetylene (C_4H_6) have been photographed with a 21-ft. grating spectrograph. The rotational constants were found to be $B_0(C_2H_2) = 1.1769$ cm^{-1}, $B_0(C_4H_2) = 0.14689$ cm^{-1}, $B_0(C_4D_2) = 0.12767$ cm^{-1}, and $B_0(C_4H_6) = 0.1122$ cm^{-1}. An analysis shows that r_0(C—H) in diacetylene is shorter than in acetylene and cyanoacetylene; in dimethylacetylene at least one of the carbon–carbon bonds is longer than in the closely related molecule methylacetylene.

A. INTRODUCTION

The present paper is part of a program of bond length determinations in which the dependence of various bonds on their environment is studied (Herzberg and Stoicheff 1955), especially of bonds in non-polar molecules. A detailed discussion of the results obtained from the rotational Raman spectra of diacetylene (C_4H_2 and C_4D_2) and dimethylacetylene (C_4H_6) is given here together with a brief report on the rotational Raman spectrum of acetylene (C_2H_2).

There have been two determinations of the moment of inertia of diacetylene: one from bands in the photographic infrared (Jones 1952) and another from the near infrared spectrum (Craine and Thompson 1953), both in good agreement. From this value and assumed values of the C—H and C≡C bond lengths, it was shown that the central C—C bond was unusually short. However, in order to establish the validity of the assumed bond lengths, the moments of inertia of two additional isotopic molecules must be determined. Since a sample of diacetylene-d_2 was available, the pure rotational Raman spectrum was photographed. At the same time, photographs of the pure rotational Raman spectrum of the ordinary diacetylene were also obtained.

Although the infrared spectrum of dimethylacetylene has been studied several times, the rotational structure of a parallel band has not yet been resolved. In the present investigation photographs of the pure rotational Raman spectrum were obtained showing a closely-spaced rotational structure which is just resolved. From an analysis of this spectrum, a value for the large moment of inertia was obtained. This result is discussed in terms of probable dimensions of the dimethylacetylene molecule.

B. EXPERIMENTAL PROCEDURE

"Pure" grade acetylene was obtained from a cylinder supplied by the Matheson Company, and sublimed *in vacuo* before using. The diacetylene

[1]Manuscript received December 21, 1956.
Contribution from the Division of Pure Physics, National Research Council, Ottawa, Canada.
Issued as N.R.C. No. 4244.
[2]National Research Laboratories Postdoctorate Fellow; present address: University College, London, England.

was prepared from 1,4-dichloro-2-butyne, and the diacetylene-d_2 was prepared by exchange from heavy water and diacetylene (Callomon 1956). The sample of dimethylacetylene was supplied by the Farchan's Research Laboratories.

The apparatus used to photograph the spectra was that described in I of this series (Stoicheff 1954) with some modifications. Four lamps of increased length replaced the previous two, resulting in an intensity gain of approximately two. A two-lens condensing system (Callomon 1956) was used to match the apertures and aperture stops of the 21-ft. grating with the mirror system in the Raman tube.

The spectra of acetylene and dimethylacetylene were photographed at a pressure of 30 cm. Hg in exposure times of 10 hours. The gas pressures of diacetylene and diacetylene-d_2 were 15 cm. Hg and the exposure times were 6 hours.

Several more intense plates of the diacetylene spectra were obtained in 30 minutes with the well-known method of placing a cylindrical lens in front of the photographic plate of the 21-ft. grating spectrograph (Humphreys 1903; Bowen 1938). The plano-convex cylindrical lens used in this work is made of fused quartz and has a focal length of about 20 cm. Its length is 15 cm., its height 3 cm., and its maximum thickness about 2 mm. The lens is mounted with independent translation and rotation relative to three mutually perpendicular axes, the most critical adjustment being the alignment of the cylinder axis at right angles to the rulings of the grating.

With this lens, the final image height at the photographic plate is reduced from 3 cm. to about 2 mm., resulting in an intensity gain of almost 15. The length of the lens covers a wavelength region of about 200 Å in the second order of the 21-ft. grating, and in this region a resolving power of approximately 100,000 has been obtained with the lens, which is adequate for the present investigations. As a check, and in order to detect any errors which may have been introduced by the use of the cylindrical lens, the spectra of a number of substances, including C_4H_2 and C_4D_2, were photographed with and without the cylindrical lens. These gave identical results.

C. ROTATIONAL ANALYSIS

Photographs of the pure rotational Raman spectra of acetylene, the two diacetylenes, and dimethylacetylene are shown in Fig. 1.

(*a*) *Acetylene*

The mean values of the Raman displacements $|\Delta\nu|$ of the rotational lines obtained from the Stokes and anti-Stokes branches are listed in Table I. For a linear molecule, the displacements are given by

$$|\Delta\nu| = (4B_0-6D_0)(J+3/2)-8D_0(J+3/2)^3.$$

Values of the constants were obtained by plotting the values of $|\Delta\nu|/(J+3/2)$ against $(J+3/2)^2$ in the usual way. The graph is shown in Fig. 2. The intercept is $4B_0$ (neglecting $6D_0$) and the slope $8D_0$, giving

$$B_0 = 1.1769\pm0.0003,\ D_0 = 1.9\pm0.4\times10^{-6}\ \text{cm}^{-1}.$$

PLATE I

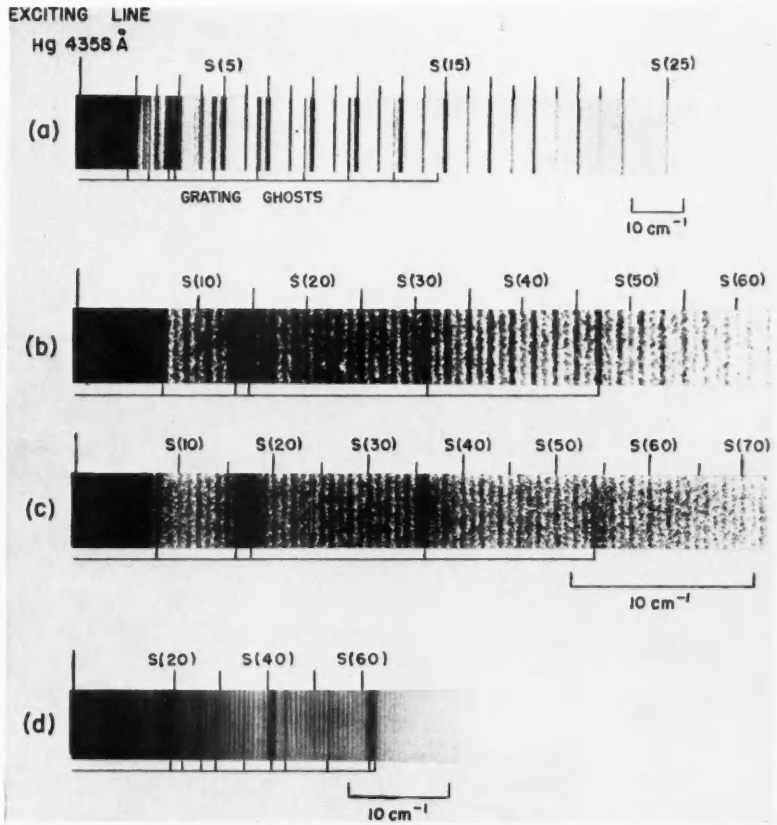

FIG. 1. Pure rotational Raman spectra (Stokes branches) of: (*a*) acetylene, C_2H_2; (*b*) diacetylene, C_4H_2; (*c*) diacetylene-d_2, C_4D_2; (*d*) dimethylacetylene, C_4H_6 (this photograph was made by moving the photographic paper parallel to the spectral lines during enlargement).

TABLE I

OBSERVED WAVE NUMBER SHIFTS OF THE ROTATIONAL RAMAN LINES OF ACETYLENE (C_2H_2)

J	$\lvert\Delta\nu\rvert$, cm^{-1}	J	$\lvert\Delta\nu\rvert$, cm^{-1}
0	———	13	68.20_6
1	11.84_7	14	72.92_8
2	16.44_2	15	77.60_5
3	21.16_9	16	82.32_1
4	25.91_3	17	87.01_1
5	30.58_8	18	91.74_9
6	35.30_0	19	96.38_5
7	40.00_4		
8	44.73_3	20	101.06_8
9	49.40_8	21	105.74_1
		22	———
10	54.13_7	23	115.15_3
11	58.81_5	24	———
12	63.53_5	25	124.46_0

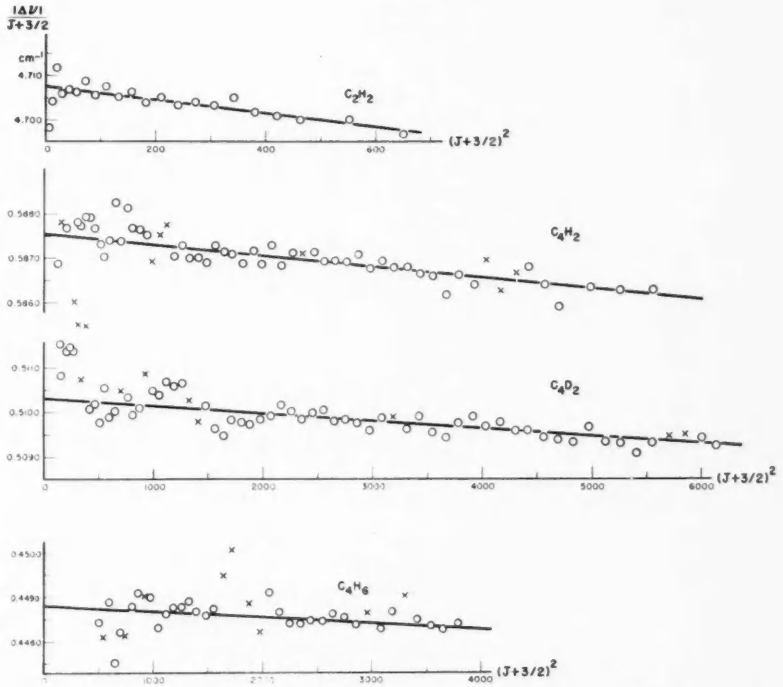

FIG. 2. $|\Delta\nu|/(J+3/2)$ graphs for the ground state of acetylene, diacetylene, diacetylene-d_2, and dimethylacetylene.

This value of B_0 is in good agreement with values reported from the infrared spectrum of C_2H_2, but favors slightly the value 1.1769 cm^{-1} obtained by Herzberg and Spinks (1934) and Bell and Nielsen (1950) rather than the

lower values of about 1.1766 cm^{-1} obtained by Wiggins, Shearer, Shull, and Rank (1954), Allen, Tidwell, and Plyler (1956), and Christensen, Eaton, Green, and Thompson (1956). For comparison, a value of D_0 was obtained from the simple expression $D_0 \approx 4B^3/\omega^2$ (ω = 1974 cm^{-1}) and also from a valence force field calculation. These yielded 1.67×10^{-6} cm^{-1} and 1.60×10^{-6} cm^{-1} respectively, which are slightly lower than the observed value.

(*b*) *Diacetylene and Diacetylene-d_2*

The displacements of the rotational Raman lines on plates taken with the cylindrical lens are listed in Table II and the plots of $|\Delta\nu|/(J+3/2)$ against $(J+3/2)^2$ are shown in Fig. 2. The constants obtained were:

for C_4H_2: $B_0 = 0.14689\pm0.00004$, $D_0 = (3.2\pm0.6)\times10^{-8}$ cm^{-1},

for C_4D_2: $B_0 = 0.12767\pm0.00005$, $D_0 = (2.3\pm0.8)\times10^{-8}$ cm^{-1}.

TABLE II

OBSERVED WAVE NUMBER SHIFTS OF THE ROTATIONAL RAMAN LINES OF DIACETYLENE (C_4H_2) AND DIACETYLENE-d_2 (C_4D_2)

J	$\|\Delta\nu\|$, cm^{-1}		J	$\|\Delta\nu\|$, cm^{-1}		J	$\|\Delta\nu\|$, cm^{-1}	
	C_4H_2	C_4D_2		C_4H_2	C_4D_2		C_4H_2	C_4D_2
7	4.95$_2$*	——	31	19.09$_9$*	16.58$_7$	55	33.15$_2$	28.80$_5$*
8	5.55$_1$*	4.87$_6$*	32	19.68$_9$*	17.10$_8$	56	33.74$_1$	29.30$_2$
9	6.16$_6$	5.38$_1$*	33	20.25$_2$	17.61$_6$	57	34.31$_8$	29.82$_9$
10	6.74$_9$	5.88$_2$*	34	20.84$_9$	18.12$_8$	58	34.90$_2$	30.31$_7$
			35	21.42$_5$	18.62$_4$*	59	35.46$_2$	30.82$_1$
11	7.34$_8$	6.38$_5$	36	22.01$_2$	19.11$_7$*	60	36.07$_6$	31.35$_0$
12	7.97$_3$*	6.90$_6$	37	22.59$_5$	19.64$_0$			
13	8.52$_1$	7.41$_5$	38	23.19$_7$	20.13$_0$	61	36.64$_8$	31.86$_9$
14	9.07$_6$*	7.92$_3$	39	23.77$_3$	20.63$_3$	62	37.27$_1$*	32.36$_4$
15	9.67$_0$*	8.43$_7$	40	24.36$_5$	21.15$_4$	63	37.81$_3$*	32.88$_1$
16	10.28$_6$	8.96$_0$*				64	38.42$_5$*	33.37$_3$
17	10.87$_3$	9.44$_5$*	41	24.94$_3$	21.66$_6$	65	39.02$_3$	33.88$_5$
18	11.46$_4$	9.98$_4$*	42	25.54$_1$	22.17$_3$	66	39.58$_2$	34.38$_7$
19	12.05$_2$	10.45$_6$	43	26.11$_5$	22.68$_7$	67	40.14$_7$	34.89$_2$
20	12.63$_4$	10.96$_9$	44	26.72$_1$	23.20$_1$	68	——	35.39$_7$
			45	27.28$_7$	23.72$_2$	69	41.33$_5$	35.93$_1$
21	13.21$_5$	11.47$_0$	46	27.88$_8$	24.22$_5$	70	——	36.41$_8$
22	13.79$_5$	11.99$_8$	47	28.47$_5$*	24.72$_7$			
23	14.39$_1$	12.49$_2$	48	29.06$_3$	25.24$_3$	71	42.50$_2$	36.92$_6$
24	15.00$_0$	13.00$_6$	49	29.63$_9$	25.75$_6$	72	——	37.41$_9$
25	15.56$_8$	13.52$_8$*	50	30.22$_8$	26.25$_4$	73	43.67$_8$	37.94$_3$*
26	16.17$_3$	14.03$_4$				74	——	38.46$_9$*
27	16.74$_9$	14.53$_7$	51	30.81$_3$	26.76$_5$	75	——	38.97$_9$
28	17.33$_6$	15.04$_8$	52	31.40$_6$	27.27$_1$	76	——	39.48$_3$
29	17.91$_9$	15.58$_1$	53	31.97$_8$	27.77$_2$	77	——	39.98$_2$
30	18.48$_9$*	16.08$_1$	54	32.57$_5$	28.29$_7$	78	——	40.48$_6$

*Lines blended with grating ghosts.

The standard deviation of observed line positions (of lines not blended with grating ghosts) from the values calculated with the above constants was 0.02 cm^{-1}. The uncertainties quoted for B_0 and D_0 refer to random errors only. As a check, the spectra of both molecules photographed without the cylindrical lens were measured and evaluated. These spectra were somewhat weaker and less extensive than those photographed with the cylindrical lens. A graphical analysis yielded the following values of the rotational constants:

for C_4H_2: $B_0 = 0.1469_2\pm0.0001$, $D_0 = (4.0\pm1)\times10^{-8}$ cm^{-1},

for C_4D_2: $B_0 = 0.1275_2\pm0.0001$, $D_0 = (3.8\pm1)\times10^{-8}$ cm^{-1},

confirming the values of B_0 obtained above, but with slightly larger values of

D_0. As already mentioned, the spectra photographed with the cylindrical lens were more extensive and, for this reason, are considered to give somewhat better values of the constants.

The value of B_0 for C_4H_2 determined here is slightly larger than the values obtained by Jones ($B_0 = 0.14641 \pm 0.00015$ cm^{-1}) and by Craine and Thompson ($B_0 = 0.1463_8 \pm 0.001$ cm^{-1}). The difference is most likely due to the effects of superimposed "hot" bands in the earlier investigations which did not permit the evaluation of the centrifugal distortion constant D_0.

The observed values of D_0 were compared with the values obtained from the simple formula $4B^3/\omega^2$, and also from a simple valence force field calculation:

	C_4H_2	C_4D_2
D_0 (observed)	3.2×10^{-8} cm^{-1}	2.3×10^{-8} cm^{-1}
D_0 (calculated) $= 4B^3/\omega^2$	1.66 ($\omega = 874$ cm^{-1})	1.13 ($\omega = 858$ cm^{-1})
Using a valence force field	1.64	1.14

The observed values are approximately twice the calculated ones. Such a large discrepancy has also been noticed in the D_0 value of cyanogen (Møller and Stoicheff 1954), where the ratio of observed to calculated values was 1.7. The cause is not yet understood but a systematic experimental error cannot be ruled out altogether.

In diacetylene, as in cyanogen, there is a low-lying vibrational level (ν_9) at about 220 cm^{-1}, and at ordinary temperatures, about 40% of the molecules are thermally excited to this level. The B value for this level (B') is probably slightly different from B_0 and the centrifugal distortion constant is most likely nearly equal to D_0. The rotational Raman spectra of molecules in the different vibrational levels are therefore superimposed with a slight relative displacement (but in this case not resolved) according to the value of α_9. An approximate value of α_9 was calculated according to the method of Shaffer and Nielsen (1941) giving -0.00010 cm^{-1}. The true value of B_0 should therefore not differ through this cause from the value derived here by more than -0.00004 cm^{-1}. Also, the values of B_0 for C_4H_2 and C_4D_2 would be affected almost equally, so that their difference, which is important in bond length determinations, is not affected.

(*c*) *Dimethylacetylene*

The observed spectrum consists of a series of finely spaced lines which are just barely resolved, extending to about 30 cm^{-1} on either side of the exciting line. Unfortunately, this region is also overlapped by many grating ghosts. Nevertheless, it was possible to measure approximately 80 Stokes and anti-Stokes lines, and their wave number shifts are listed in Table III. These rotational lines arise from transitions with $\Delta J = 2$ and hence are part of the S branches. Since the dimethylacetylene molecule is a symmetric top, the displacements from the exciting line are given by the equation (in simplified form)

$$|\Delta\nu| = 4B_0(J+3/2) - 8D_J(J+3/2)^3.$$

TABLE III

OBSERVED WAVE NUMBER SHIFTS OF THE ROTATIONAL RAMAN LINES OF DIMETHYLACETYLENE (C_4H_6)

J	$\lvert\Delta\nu\rvert$, cm^{-1}	J	$\lvert\Delta\nu\rvert$, cm^{-1}
21	10.09	41	———*
22	10.53*	42	19.53*
23	10.98	43	19.95*
24	11.41	44	20.43
25	11.88	45	20.86*
26	12.32*	46	21.30*
27	12.79	47	21.75
28	13.25	48	22.20
29	13.70*	49	22.65
30	14.14	50	23.10
31	14.57	51	23.55
32	15.03	52	23.99
33	15.48	53	24.45*
34	15.93	54	24.88
35	16.38*	55	25.35
36	16.83	56	25.82*
37	17.27	57	26.24
38	17.72	58	26.68
39	18.20*	59	27.12
40	18.68*	60	27.58

*Lines blended with grating ghosts.

A plot of $|\Delta\nu|/(J+3/2)$ against $(J+3/2)^2$, shown in Fig. 2, gave the rotational constants:

$$B_0 = 0.1122_0 \pm 0.0002 \text{ cm}^{-1} \text{ and } D_J = 1.3 \times 10^{-8} \text{ cm}^{-1}.$$

D. BOND LENGTHS

In using the moments of inertia of isotopic molecules to determine bond lengths, the assumption is made that the bond lengths are the same in the various isotopic species of a molecule. As is well known, this assumption is strictly correct only for the equilibrium bond lengths, r_e, but is often applied to effective bond lengths, r_0. The latter approximation breaks down because of zero-point vibration effects and, as might be expected, these are largest for bonds involving hydrogen atoms. Thus, in several investigations in which deuterated isotopes were used to determine values of r_0(C—H), it was found that consistent results could only be obtained by assuming differences between r_0(C—H) and r_0(C—D). Differences of 0.002 Å were found in HCN (Nethercot, Klein, and Townes 1952) and of 0.005 to 0.009 Å in methyl groups of several molecules (Miller, Aamodt, Dousmanis, Townes, and Kraitchman 1952; Costain 1955; Heath, Thomas, Sherrard, and Sheridan 1955).

Since pure rotational Raman spectra yield only values of B_0 and not B_e (hence r_0 and not r_e), the limitations of the assumption that r_0 values are equal in isotopic molecules must be kept in mind.

(*a*) *Acetylene*

The effective internuclear distances r_0(C≡C) and r_0(C—H) for the acetylene molecule were calculated from existing values of the rotational constants,

namely $B_0(C_2H_2) = 1.1766$ and $1.1769\ cm^{-1}$, $B_0(C_2HD) = 0.9911$ and $0.9914\ cm^{-1}$ (Overend and Thompson 1955; Herzberg, Patat, and Spinks 1934), and $B_0(C_2D_2) = 0.8479\ cm^{-1}$ (Saksena 1952; Overend and Thompson 1956). With the assumption that $r_0(C—H) = r_0(C—D)$, the average values were found to be $r_0(C\equiv C) = 1.208_5$ Å and $r_0(C—H) = 1.057_2$ Å. When these are compared with the most recent values for the equilibrium internuclear distances $r_e(C\equiv C) = 1.204_7$ Å and $r_e(C—H) = 1.058_5$ Å (Christensen, Eaton, Green, and Thompson 1956), it is found that $r_e(C—H)$ is slightly larger than $r_0(C—H)$. This is an indication that the above $r_0(C—H)$ cannot be a true mean internuclear distance in the ground vibrational level and hence that $r_0(C—H)$ does not equal $r_0(C—D)$. An analysis of the existing data on the three isotopic molecules shows that $r_0(C—H) - r_0(C—D)$ probably has a value in the range 0.0005 to 0.0035 Å. If the mean value $r_0(C—H) - r_0(C—D) = 0.002$ Å is assumed, then $r_0(C\equiv C) = 1.206_7$ Å and $r_0(C—H) = 1.061$ Å.

(*b*) *Diacetylene*

The present rotational constants of the two diacetylene molecules give the following values for the moments of inertia:

$$I_0(C_4H_2) = (190.54 \pm 0.06) \times 10^{-40}\ \text{g. cm.}^2,$$

$$I_0(C_4D_2) = (219.40 \pm 0.09) \times 10^{-40}\ \text{g. cm.}^2$$

These two values together with several assumed values of $r_0(C\equiv C)$ ranging from 1.203 to 1.207 Å were used to calculate $r_0(C—C)$ and $r_0(C—H)$ and the results are shown in the graph of Fig. 3. The solid lines of Fig. 3 show the

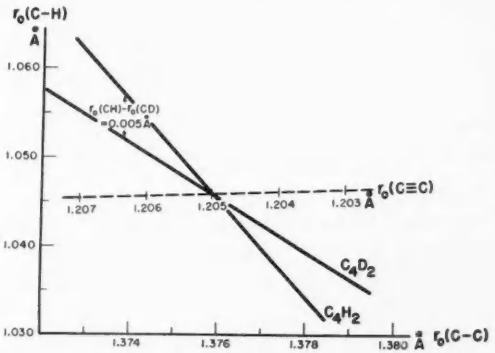

FIG. 3. Graphical determinations of $r_0(C—H)$ and $r_0(C—C)$ in the diacetylene molecule assuming various values of $r_0(C\equiv C)$. The solid lines give the relationships of these parameters in diacetylene and diacetylene-d_2 assuming $r_0(C\equiv C) = 1.205$ Å. The broken line is the locus of the points of intersection of corresponding solid lines with other assumed values of $r_0(C\equiv C)$.

relationship between these parameters for each molecule, assuming the value $r_0(C\equiv C) = 1.205$ Å, the length of this bond in the closely related molecule

cyanoacetylene.[3] The intersection of the two curves corresponds to the values

$$r_0(\text{C—H}) = r_0(\text{C—D}) = 1.046 \pm 0.009 \text{ Å},$$

$$r_0(\text{C—C}) = 1.376 \pm 0.002 \text{ Å},$$

$$r_0(\text{C}\equiv\text{C}) = 1.205 \text{ Å (assumed)}.$$

The estimated errors in the bond lengths refer to random errors in B_0. As usual, the value of the CH bond length has a rather large uncertainty since its value is very sensitive to small changes in the rotational constants. The locus of the point of intersection of corresponding solid lines with other assumed values of $r_0(\text{C}\equiv\text{C})$ is also shown in Fig. 3, as a broken line. From this line it is observed that a change in the assumed value of $r_0(\text{C}\equiv\text{C})$ changes only $r_0(\text{C—C})$ and not the CH bond length, which remains at the low value of 1.046 Å. If it is now assumed that $r_0(\text{CH}) \neq r_0(\text{CD})$ (shown in Fig. 3 as the vertical difference between the solid lines) a larger value can be obtained for the CH bond length. For example, if $r_0(\text{CH}) - r_0(\text{CD}) = 0.005$ Å, as in cyanoacetylene,[3] then $r_0(\text{C—C}) = 1.374$ Å and $r_0(\text{CH}) = 1.057$ Å. Again this is a rather short CH bond length. Thus it would seem that the CH bond length in diacetylene is shorter than that in acetylene and cyanoacetylene.

The bond lengths of the diacetylene molecule given above are in general agreement with the values found for similar bonds in other molecules (see, for example, Herzberg and Stoicheff 1955). In particular, the carbon–carbon single bond, which in diacetylene is adjacent to two triple bonds, is considerably shorter than other carbon–carbon single bonds. For example, with two adjacent triple bonds, the C—C bond has a length of 1.380 Å, while with only one adjacent triple bond the C—C bond has a length of 1.460 Å. This result was first shown by Pauling, Springall, and Palmer (1939) from electron diffraction data and has also been confirmed from the spectra of diacetylene, dicyanogen, and cyanoacetylene. From the present analysis, however, it appears that in addition the C—H bonds in diacetylene are slightly shorter than in other similar molecules.

(c) Dimethylacetylene

The structure of the dimethylacetylene molecule is shown in Fig. 4, along with the designation of the structural parameters. Dimethylacetylene is a symmetric top molecule with the four carbon atoms in a linear chain. The

[3]Westenberg and Wilson (1950) measured the microwave spectra of 10 isotopic species of cyanoacetylene involving the atoms H, D, C^{12}, C^{13}, N^{14}, and N^{15}, and used the data to evaluate four bond-lengths assuming $r_0(\text{C—H}) = r_0(\text{C—D})$. The bond lengths have been briefly recalculated, assuming $r_0(\text{C—H})$ not equal to $r_0(\text{C—D})$ and, as the values are overdetermined from the data, they were adjusted to give the minimum standard deviation (0.10 Mc./s.) between the observed and calculated values. The values found were:

	Westenberg and Wilson
$r_0(\text{C—H}) = 1.069 \pm 0.006$ Å $r_0(\text{C—D}) = 1.064$	1.057 Å
$r_0(\text{C}\equiv\text{C}) = 1.204_7 \pm 0.001$	1.203
$r_0(\text{C—C}) = 1.378_1 \pm 0.002$	1.382
$r_0(\text{C}\equiv\text{N}) = 1.157_9 \pm 0.001$	1.157

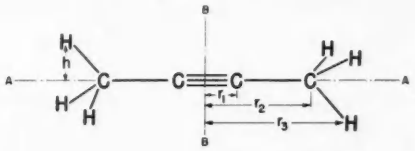

FIG. 4. The structure and structural parameters of the dimethylacetylene molecule.

moment of inertia about any axis perpendicular to this line and passing through the center of the molecule is given by

$$I_B = 2[m_C(r_1^2 + r_2^2) + 3m_H(r_3^2 + h^2/2)].$$

This expression is valid whether free or hindered rotation is assumed for dimethylacetylene. Numerically the value of this moment of inertia calculated from B_0 is

$$I_B^0 = (249.46 \pm 0.45) \times 10^{-40} \text{ g.cm.}^2$$

The evaluation of one moment of inertia is, of course, inadequate for the determination of the dimensions of dimethylacetylene; however, since the structure of dimethylacetylene is closely related to that of methylacetylene, it seemed of interest to calculate the moment of inertia I_B using the methylacetylene parameters. The values

$$r_0(\text{C—C}) = 1.460 \pm 0.002 \text{ Å}, \; r_0(\text{C}\equiv\text{C}) = 1.207 \pm 0.002 \text{ Å},$$

$$r_0(\text{C—H}) = 1.097 \pm 0.010 \text{ Å}, \text{ and } \angle\text{HCH} = 108°14 \pm 1°,$$

found by Trambarulo and Gordy (1950) from the microwave spectrum of methylacetylene were used in the calculation and yielded a value $I_B^0 = 247.60 \times 10^{-40}$ g. cm.^{2} This value of the moment of inertia of dimethylacetylene is significantly smaller than that determined here from the rotational spectrum and suggests that at least one of the bond lengths in dimethylacetylene is larger than the value found in methylacetylene. If the change is assumed to be wholly in the C—C or C≡C bonds, the lengths are found to be 1.469 Å and 1.221 Å, respectively, the remaining parameters being those of methylacetylene. These two values are to be compared with the bond lengths 1.460 ± 0.003 Å and 1.207 ± 0.002 Å as found for similar bonds in several molecules (Herzberg and Stoicheff 1955). Unfortunately the present data on dimethylacetylene are not sufficient to determine these two bond lengths independently.

Other related molecules such as dimethyldiacetylene and dimethyltriacetylene have been investigated by electron and X-ray diffraction methods (Bastiansen 1956; Jeffrey and Rollet 1952). While the results appear to be in general agreement with values of 1.21 Å for the C≡C bond length and of 1.46 Å for the C—C bond length, the limits of accuracy range from 0.01 to 0.02 Å and would completely overshadow any small differences in bond lengths such as are indicated by the Raman spectrum of dimethylacetylene.

The present results on acetylene, diacetylene, and dimethylacetylene show that fairly accurate values of the rotational constants of molecules having even relatively large moments of inertia can be obtained from their pure

rotational Raman spectra. There are, however, certain limitations. Firstly, it appears that, while the present techniques are adequate for resolving rotational lines having a spacing as narrow as 0.4 cm^{-1}, the practical limit of resolution is about 0.3 cm^{-1}, because of line broadening by pressure and finally because of the width of the exciting line itself (about 0.25 cm^{-1}). A spacing of 0.3 cm^{-1} corresponds to a moment of inertia of about 350×10^{-40} g. $cm.^2$ for molecules having nuclei with spin $\neq 0$ (and twice this value for those with nuclei of zero spin). Secondly, the rotational Raman spectra of all but asymmetric top molecules give the value of only one moment of inertia. Therefore, some assumptions about the molecular structure usually have to be made in order to determine the internuclear distances of molecules with several parameters. The number of assumptions can, of course, be reduced by investigating the rotational Raman spectra of isotopic molecules, but since rather large amounts of a pure sample must be used in this work, one is limited to deuterated molecules at present.

REFERENCES

ALLEN, H. C., TIDWELL, E. D., and PLYLER, E. K. 1956. J. Research NBS, **57**, 213.
BASTIANSEN, O. 1956. Acta Chem. Scand. **10**, 261.
BELL, E. E. and NIELSEN, H. H. 1950. J. Chem. Phys. **18**, 1382.
BOWEN, I. S. 1938. Astrophys. J. **88**, 113.
CALLOMON, J. H. 1956. Can. J. Phys. **34**, 1046.
COSTAIN, C. C. 1955. J. Chem. Phys. **23**, 2037.
CRAINE, G. D. and THOMPSON, H. W. 1953. Trans. Faraday Soc. **49**, 1273.
CHRISTENSEN, M. T., EATON, D. R., GREEN, B. A., and THOMPSON, H. W. 1956. Proc. Roy. Soc. (London), A, **238**, 15.
HEATH, G. A., THOMAS, L. F., SHERRARD, E. I., and SHERIDAN, J. 1955. Discussions Faraday Soc. **19**, 38.
HERZBERG, G., PATAT, F., and SPINKS, J. W. T. 1934. Z. Physik, **92**, 87.
HERZBERG, G. and SPINKS, J. W. T. 1934. Z. Physik, **91**, 386.
HERZBERG, G. and STOICHEFF, B. P. 1955. Nature, **175**, 79.
HUMPHREYS, W. J. 1903. Astrophys. J. **18**, 324.
JEFFREY, G. A. and ROLLET, J. S. 1952. Proc. Roy. Soc. (London), A, **213**, 86.
JONES, A. V. 1952. J. Chem. Phys. **20**, 860.
MILLER, S. L., AAMODT, L. C., DOUSMANIS, G., TOWNES, C. H., and KRAITCHMAN, J. 1952. J. Chem. Phys. **20**, 1112.
MØLLER, C. K. and STOICHEFF, B. P. 1954. Can. J. Phys. **32**, 635.
NETHERCOT, A. H., KLEIN, J. A., and TOWNES, C. H. 1952. Phys. Rev. **86**, 798.
OVEREND, J. and THOMPSON, H. W. 1955. Proc. Roy. Soc. (London), A, **232**, 291.
——— 1956. Proc. Roy. Soc. (London), A, **234**, 306.
PAULING, L., SPRINGALL, H. D., and PALMER, K. J. 1939. J. Am. Chem. Soc. **61**, 927.
SAKSENA, B. D. 1952. J. Chem. Phys. **20**, 95.
SHAFFER, W. H. and NIELSEN, A. H. 1941. J. Chem. Phys. **9**, 847.
STOICHEFF, B. P. 1954. Can. J. Phys. **32**, 330.
TRAMBARULO, R. and GORDY, W. 1950. J. Chem. Phys. **18**, 1613.
WESTENBERG, A. A. and WILSON, E. B., Jr. 1950. J. Am. Chem. Soc. **72**, 199.
WIGGINS, T. A., SHEARER, J. N., SHULL, E. R., and RANK, D. H. 1954. J. Chem. Phys. **22**, 547.

RHEOLOGY OF THE EARTH: THE BASIC PROBLEM OF GEODYNAMICS[1]

A. E. SCHEIDEGGER

ABSTRACT

A discussion is given of the data which are available to provide information on the rheological behavior of the Earth's mantle and crust. It is shown that a fundamental distinction has to be made between stress durations that are "short" (up to 4 hours), "intermediate" (4 hours to 15,000 years), and "long" (longer than 15,000 years). For short durations, the behavior of the Earth is well known from the results of seismological investigations. However, these results should not be applied directly to the longer time durations. For intermediate time durations, the Earth shows an elastic aftereffect. One obtains a value for the (Kelvin) viscosity if it is assumed that the damping of the variation of latitude is caused by a Kelvin effect. The same (Kelvin) viscosity is arrived at if the strain rebound characteristics of earthquake aftershock sequences are also interpreted in terms of an elastic aftereffect. For stresses of long duration, some information may be obtained from the uplift of Fennoscandia. It appears that viscous creep is the prevailing phenomenon. If this information is combined with some further considerations, indications are that the Earth behaves like a Bingham body. Then, the fact that orogenetic phenomena are concentrated in narrow bands may be due to the existence of solutions of the Bingham equation exhibiting rheological instability.

1. INTRODUCTION

The chief problem of the science of geodynamics is to determine deformations within the Earth and upon its surface. On the surface, the present-day deformations are known and the task is to explain the latter in terms of stresses that could be considered as reasonable. In any definite deformation theory, it is a matter of mathematical analysis to determine the stresses from the boundary conditions. If it were possible to formulate an exact deformation theory applying to the Earth as a whole, it would be, in principle, a straightforward (though not necessarily easy) matter to calculate the stresses from the (known) strains and then to look for causes of the latter. Unfortunately, it is a fact that the deformation theory applying to the Earth is not known, thus leaving the matter of finding the causes of its present-day appearance wide open to speculation. It is thus evident that the basic problem of geodynamics is to determine the rheological conditions in the Earth. The explanation of the present-day physiography would then follow provided our mathematical resources were equal to the task.

As stated above, it is quite clear that the principal difficulty is the problem of determining the proper rheological condition for the various layers of the Earth, including the criteria applicable for possible fracture. The difficulties inherent in finding the rheological conditions applicable to the Earth arise from two causes. First, the state of the material in all but the uppermost few kilometers of the Earth's crust is not easy to envisage. Pressures and temperatures are such that it is unlikely that they can be duplicated in the laboratory

[1]Manuscript received November 26, 1956.
Contribution from the Dominion Observatory, Ottawa, Vol. 3, No. 4.
Published by permission of the Deputy Minister, Department of Mines and Technical Surveys, Ottawa, Ontario.

in the near future, leaving only theoretical guessing to determine the behavior of the material under consideration. Second, the time elements involved are for the greater part such that, even if experiments involving the correct temperatures and pressures could be performed, the human life span would be millions of times too short to obtain the desired answers. This, again, forces one to speculate.

The time element in the rheological equations is a concept which, in general, has not been sufficiently noted. Terms like "rigid" and "fluid" have a meaning only if it is stated what the time intervals are over which the stresses in question are applied. In order to survey what *can* be said about the rheology of the material within the Earth, it is therefore necessary to make a distinction between various typical duration-intervals for the stresses. It is convenient to classify stresses according to whether their duration is "short", "intermediate", or "long". We shall consider stresses as short if they have a typical duration of the order of 3 seconds, as intermediate if their typical duration is of the order of 3 years, and as long if their typical duration is of the order of 100 million years. It will be noted that the ratio of subsequent typical stress durations is 3×10^7. As limits for the interval for which stresses may be considered as short, intermediate, or long, one may take the geometric mean between the "typical" durations, i.e. about 4 hours and 15,000 years.

The ratio of subsequent typical durations, being 3×10^7, is very large. It can therefore not be expected that the rheological behavior deduced for one typical duration can be extrapolated for another. The various typical durations have to be studied separately.

It now appears that it is possible to make some progress in determining the rheology of the Earth. It is true enough that the exact rheological equation cannot be given, but there are a number of data known which permit one to set a limit to the boundless a priori possibilities. We shall first discuss some of the possible classifications of rheological bodies and then proceed to investigate the various time ranges.

2. RHEOLOGY

Let us discuss first briefly some of the implications of the science of "rheology".

In order to determine the motion of a continuous material, there are various steps that must be observed. In the first place, one must decide upon a description of the deformation. Once this has been achieved, one must express various physical laws: the condition of continuity, the law of motion, and boundary conditions.

Finally, one needs a connection between the dynamical quantities (e.g. the stresses) and the kinematical quantities (i.e. the strains). The latter is called "rheological condition".

The schemes applicable to the treatment of deformations of continuous matter have been discussed, e.g. by the writer (Scheidegger 1956), in general terms. It is, however, very difficult to operate with the general equations in particular problems and one is therefore forced to introduce simplifications.

Originally, one had only the "classical" materials: viscous fluids and ideally elastic substances. The mathematical treatment of these substances has been carried to a high degree of refinement; convenient monographs on it have been given by Lamb (1945) for viscous fluids and by Love (1934) for elastic bodies.

An extension of the classical bodies to approximate some of the more commonly found natural bodies is usually done by, first of all, restricting oneself to infinitesimal strains. This, of course, is a severe limitation of generality and, in fact, usually quite an inconsistent procedure as, if any type of true rheological effects occur at all, the displacements become large, at least after the elapse of sufficient time. Nevertheless, a very approximate idea of the physical possibilities may be obtained by assuming the strains as infinitesimal. At any rate, it is customary to do this in most engineering literature, whether it is justified or not. A convenient summary of this type of treatment has been given by Reiner (1949). We shall present here the more important cases as well as discuss some special integrals which will be of signifieance later on.

In terms of infinitesimal strain terminology, the part of the rheological equation referring to the deviatoric components can be written for the Hooke solid as follows (where τ_{ik} are the stresses and ϵ_{ik} the strains):

$$\tau_{ik} = 2\mu\epsilon_{ik} \quad (i \neq k) \tag{2.1}$$

and for the viscous (Newtonian) liquid as follows:

$$\tau_{ik} = 2\eta\dot{\epsilon}_{ik} \quad (i \neq k). \tag{2.2}$$

Combination of both gives (after Reiner)

$$\dot{\epsilon}_{ik} = \dot{\tau}_{ik}/(2\mu_M) + \tau_{ik}/(2\eta_M) \quad (i \neq k). \tag{2.3}$$

A similar combination with appropriate constants can be set up for the isotropic components. The quantities μ_M and η_M are constants of the body; they are often referred to as (Maxwell) rigidity and viscosity. However, it should be noted that the names "rigidity" and "viscosity" are not very good ones. The ordinary viscous fluid is obtained if, in (2.3), $\mu_M \to \infty$ in which case η_M becomes the fluid viscosity. Similarly, for $\eta_M \to \infty$ one obtains an elastic solid with rigidity μ_M. It is for this reason that the two constants μ_M and η_M have been called "rigidity" and "viscosity". However, "Maxwell constants" would be a better name.

The rheological equation (2.3) describes a liquid which shows stress relaxation. That the latter occurs can be seen immediately if it is assumed that the deformation is kept constant (i.e. $\dot{\epsilon} = 0$). Then the stress diminishes exponentially with a time constant τ,

$$\tau = \eta_M/\mu_M. \tag{2.4}$$

Furthermore, if a constant stress is applied, it is seen that deformation occurs at a constant *rate*. This phenomenon is called *creep*.

Stress relaxation phenomena have been studied extensively by Maxwell. Hence the name "Maxwell liquid" for the material at present under consideration.

The equations of the Hooke solid and of the viscous liquid in their infinitesimal-strain form as displayed in (2.1) and (2.2) can also be combined in a different manner, viz.

$$\tau_{ik} = 2\mu_K\epsilon_{ik}+2\eta_K\dot{\epsilon}_{ik} \quad (i \neq k), \tag{2.5}$$

where again a similar combination with appropriate constants could be written down for the isotropic components ($i = k$). Again, the quantities μ_K and η_K are constants of the body which, again, are often referred to as "rigidity" and "viscosity", respectively. Again, these names are not very good. One notes that a "Kelvin solid" becomes an elastic solid if $\eta_K = 0$ and a viscous fluid if $\mu_K = 0$. These are the opposite limits to those required to yield the same classical bodies in the case of Maxwell liquids. The use of Maxwell liquids and Kelvin bodies has given rise to much confusion. Consequently, we should prefer to call μ_K and η_K "Kelvin constants".

The Kelvin solid is characterized by an elastic aftereffect; if a stress change is performed, the body will eventually reach that state which would correspond to Hooke's law, but only exponentially. The time constant is again η/μ. A loading–unloading diagram has therefore the characteristics shown in Fig. 1.

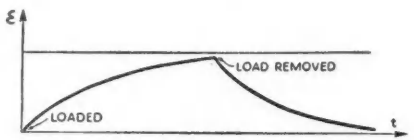

FIG. 1. Loading–unloading curve of a Kelvin body.

The elastic aftereffect characteristic of a Kelvin body also causes free oscillations to be damped; as this will be of importance later on, let us try to calculate the damping constant. The equation of motion of a Kelvin body is

$$\mu x+\eta\dot{x} = -c\ddot{x}, \tag{2.6}$$

where c is some constant of the system. Trying for a solution

$$x = \exp[(\alpha+i\omega)t], \tag{2.7}$$

one obtains

$$\mu+\eta(\alpha+i\omega) = -c(\alpha^2-\omega^2+2\alpha i\omega). \tag{2.8}$$

Equating real and imaginary parts yields

$$\mu+\eta\alpha = -c(\alpha^2-\omega^2), \tag{2.9}$$

$$\omega\eta = -c2\alpha\omega, \tag{2.10}$$

and hence one obtains

$$\alpha = -\eta/(2c), \tag{2.11}$$

$$\omega = \sqrt{\frac{\mu}{c}-\frac{\eta^2}{4c^2}}. \tag{2.12}$$

Finally, eliminating the constant c yields

$$\alpha^2+\frac{2\mu\alpha}{\eta}+\omega^2 = 0. \tag{2.13}$$

The last equation can be used to determine μ/η if α and ω are measured in a given system.

Since the rheological equations for Maxwell and Kelvin bodies each contain two arbitrary constants, it may appear that either can be used to describe any particular phenomenon provided these constants are adjusted properly. It can be shown, however, that this is not the case as long as the phenomenon considered is transient. The character of the transience is completely defined by the type of equation that is used. In order to explain an observed motion by one *or* the other of the two equations, one has to change completely the physical cause of the motion.

Finally, it may be remarked that more generalized bodies are obtained if one introduces a yield stress ν_{ik} into Eq. (2.5). Setting $\mu = 0$ to avoid further complication, one then has

$$\tau_{ik} = \nu_{ik}+2\eta\dot{\epsilon}_{ik}, \tag{2.14}$$

which is the constitutive equation of a "Bingham solid". Here, η is called the "plastic viscosity". Further complications can be achieved by including in the constitutive equations more and more terms. However, the basic shortcomings of this type of theory outlined in the beginning of this section are thereby not overcome. Nevertheless, the various rheological equations discussed here, and commonly employed by engineers, give a useful indication of the types of inelastic behavior that might be encountered.

3. STRESSES OF SHORT DURATION

According to the above, we consider stresses as of short duration if the typical times involved are of the order of 3 seconds—or if the upper limit of their duration is about 4 hours. As might well be expected, the rheological behavior of the various layers of the Earth is best known for this time range. It is found that (infinitesimal) elasticity theory gives a good description of the phenomena for small displacements and it is therefore natural to classify the findings as to whether they apply to the material being stressed *below* or *beyond* the elastic limit.

(*a*) *Stresses below the Elastic Limit*

Stresses of short duration (in the above sense) below the elastic limit occur in the Earth during the passing of earthquake waves. Seismology, therefore, yields important information bearing upon the question under consideration. It is found that the upper layers of the Earth, to a depth of 2900 km., behave as an elastic solid, below as an elastic fluid.

Seismology, directly, yields only the variation of seismic velocity with depth. In order to determine the elastic parameters therefrom, one has to make certain assumptions regarding the density variation within the Earth; Bullen (1953) studied various possibilities. Characteristic values are about

2×10^{12} c.g.s. for the rigidity, and 5×10^{12} for the modulus of elasticity in the mantle of the Earth.

Bullen's estimates start at the layer just below the Mohorovičić discontinuity. Above this discontinuity the crust is very heterogeneous. The elastic constants of the various types of rocks for short-duration stresses can be measured in the laboratory. A typical value is Young's modulus $E = 4\times10^{11}$ c.g.s., Poisson's number $\sigma = 0.25$.

(*b*) *Stresses above the Elastic Limit*

(*i*) *Crust*

A significant number of experiments have been made to determine the modes of disintegration of various types of rock samples. The first experiments along these lines were done early in the century to determine the modes of failure of such rocks as can be used as building materials. After Bridgman (1949) initiated the development of high pressure techniques, Griggs (1936) and others investigated the deformation of many rock samples under extreme conditions. All these experiments must be taken as investigations belonging in the present category of short-duration stresses.

From these investigations it appears that most crustal rocks fracture in a manner as postulated by Mohr's theory; i.e. one observes two preferred failure planes inclined at an angle of $\phi < 45°$ toward the direction of maximum pressure and parallel to the intermediate principal stress. The value of the stress under which the samples break would be expected to be given by an envelope in Mohr's diagram. As this is rather difficult to tabulate, an idea of the magnitude of the stresses involved can be obtained by listing the maximum stress differences that the material can support in a state of pure shear. A typical value is 10^{10} c.g.s. (Benioff and Gutenberg 1951).

A different mode of fracture is observed under pure tension. The tensile strength is much below the compressive strength of rocks, presumably owing to the presence of Griffith cracks. It is unlikely, however, that such a state exists in the Earth anywhere but on the very surface.

(*ii*) *Mantle*

Stress changes of short duration above the elastic limit occur in the mantle at the focus of an earthquake during the actual shock. The fact that the phenomenon of an earthquake is at all possible indicates that the material of the mantle has some resemblance to an "ordinary" solid. The earthquakes seem to correspond to sudden shear fractures wherein it is very characteristic that most of the displacements along the fracture surfaces are essentially parallel to the surface of the Earth (cf. Hodgson 1955; Scheidegger 1955).

There are indications that modes of sudden displacement different from shear fracture may occur in the mantle. The seismic waves emanating from the focus of an earthquake do not always permit an interpretation in terms of an "orange being sliced". Thus, there are indications that, in certain cases, the distribution of waves is such that it would correspond to a multipole of higher order. The physical significance of this in terms of an envisageable fracture pattern is not yet quite clear.

Finally, because it has often been thought that the dissipation of energy in seismic waves might be an indication of an anelastic behavior of the Earth in the short time range, a remark might be added here regarding this possibility. The case, in fact, has been satisfactorily dealt with by Jeffreys (1952, p. 107): The damping of seismic waves increases with frequency. Hence it must be due to scattering. If it were due to anelasticity, it would have to increase with period, and this is not the case.

4. STRESSES OF INTERMEDIATE DURATION

The next task is to investigate the rheological behavior of the Earth under stresses of intermediate duration. As outlined above, we assume intermediate duration to mean from 4 hours to 15,000 years, the typical duration being about 3 years. As might be expected, it is much more difficult to obtain an idea of the rheological behavior of the Earth in this time range than for short stresses. The information which we do have, thus, comes only from two sources: (*a*) from the damping of the variation of latitude, and (*b*) from the release of stresses in earthquake sequences.

(*a*) *The Damping of the Variation of Latitude*

An analysis of the observations on latitude variation yields the result that, after an annual term (probably due to the movement of air masses) has been taken out, a period of approximately 420 days exists. On the assumption that this motion is due to random impulses of unknown origin, it is possible to say that the damping causes the motion to decrease to a value of $1/e$ of the original between 3 (Jeffreys 1952) and 13 (cf. Bondi and Gold 1955) periods. It had originally been thought that this damping would be caused by motions in the core of the Earth (Jeffreys 1952). However, in a renewed discussion of the problem, Bondi and Gold (1955) claim that the motion of the core can *not* account for the observed damping. The damping would therefore have to be due to a Kelvin effect in the mantle of the Earth. Under this assumption, it is possible to obtain an estimate for the value of η/μ occurring in the constitutive equation of a Kelvin body. Indeed, assuming

$$T = 2\pi/\omega = 420 \text{ days} \tag{4.1}$$

and the damping as of the order of 10 periods

$$1/\alpha = -4200 \text{ days} \tag{4.2}$$

yields for the ratio of the Kelvin constants according to (2.13)

$$\eta_K/\mu_K \cong 2 \text{ days} = 1.72\times10^5 \text{ sec.} \tag{4.3}$$

From the above considerations, the two Kelvin constants cannot be obtained separately. One may be tempted to use for μ_K the "rigidity" for the mantle as deduced from seismology and confirmed by a discussion of the Earth's bodily tides (Jeffreys 1952), viz.

$$\mu_K \cong 2\times10^{12} \text{ c.g.s.,} \tag{4.4}$$

which would yield

$$\eta_K \cong 3\times10^{17} \text{ c.g.s.,} \tag{4.5}$$

and then to say that the "rigidity" and the "viscosity" of the Earth's mantle have the "values" shown in (4.4) and (4.5). However, this leads to a fallacy. The names "viscosity" and "rigidity" have no properly defined meaning *per se*, unless it is specified to which rheological equation they refer. There might be some justification for using the elastic μ for the time range presently under consideration, particularly as the discussion of the Earth's tides gave the same result, but then the viscosity η_K obtained above in (4.4) and (4.5) is a "Kelvin constant" and has no direct relation with the *creep* viscosity occurring in the rheological equation of a Maxwell body.

The above result that the Earth behaves as a Kelvin body with the constants (4.4) and (4.5) in the time range under consideration depends, as indicated, on the assumption that the motion in the core cannot account for the damping. This, however, is by no means established (Gutenberg 1956). Alternatively, it has also been tried to explain the Chandler wobble as caused by a Maxwell effect, in which case it leads to a higher (Maxwell) viscosity.

(*b*) *Earthquake Sequences*

After an earthquake occurs in some part of the world, it often happens that the first, "principal" shock is followed by a series of aftershocks of diminishing magnitude. Benioff (1951) has studied a series of such aftershock sequences regarding the time dependence of their magnitudes. The "magnitude" of an earthquake, as defined by Gutenberg and Richter (1942), permits an interpretation in terms of "strain release". The total energy of an (elastically) strained body is proportional to the square of the strain; hence the strain release in a sudden shock should be proportional to the square root of the energy release J. The energy release J (in ergs) is connected with the earthquake magnitude M by the equation

$$\log J = 12.0+1.8\ M. \tag{4.6}$$

Benioff (1951) used the "old" equation of Gutenberg and Richter as given above for his studies; if the "new" (corrected) equation (Gutenberg and Richter 1956) is used, the essence of the results is not changed, as the interest lies solely in the relaxation times involved. If the magnitude of each shock of an aftershock sequence is known, it is therefore possible to plot a quantity

$$S = \sum J_i^{\frac{1}{2}}, \tag{4.7}$$

which is proportional to the cumulative strain release. If this be done, one obtains graphs of the type shown in Fig. 2.

Such graphs suggest the following interpretation. The principal shock occurs when the strain accumulation has reached a critical value. This starts a break along an existing or new fault. As soon as this has happened, the fault will be "greased" so that any strain accumulating can be released, apart for "bumps" that cause the motion to be somewhat discontinuous. One can thus picture an earthquake aftershock sequence to be the expression of the strain release of a body in which, after loading, the stress has been suddenly removed.

The resemblance of curves of the type shown in Fig. 2 to the strain-release curves of a Kelvin body (Fig. 1) is rather striking and would be even more so if the aftershock sequence had not been plotted on semilogarithmic paper. The maximum S reached in Fig. 2 corresponds to the unstrained position of the Kelvin body, the zero value of S to the loaded position. Naturally, the curve of Fig. 2 cannot be expected to come to a complete levelling-off as, in

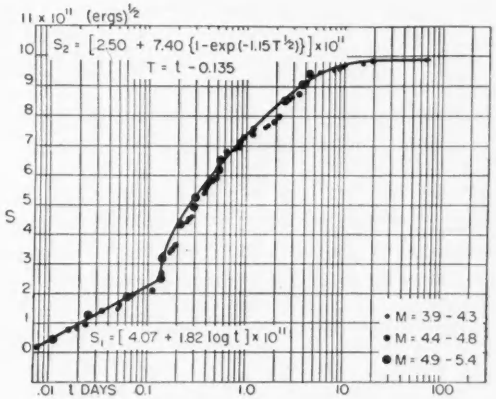

FIG. 2. Accumulated strain release diagram of an earthquake aftershock sequence (after Benioff 1951). The curve shows the same pattern as the unloading diagram of a Kelvin body. In order to make this comparison, note that the state of zero strain corresponds to 10×10^{11} ergs$^{\frac{1}{2}}$; the fully loaded position corresponds to $S = 0$ ergs$^{\frac{1}{2}}$.

addition to the strain release, it must be expected that a constant build-up of stress occurs at a slow rate which, presumably, never comes to a stop. Thus, after a few years, one would expect the same pattern to repeat itself.

The study of strain release in earthquake aftershock sequences thus yields the result that the latter occur in a fashion that can be explained in terms of elastic afterworking of a Kelvin body. Moreover, the relaxation time (i.e. the time in which the strain drops to $1/e$ times the initial value) turns out to be of the order of 2 days. This, however, is equal to the ratio η/μ of the Kelvin constants. It thus turns out that the interpretation of earthquake sequences in the above fashion leads to the same value for η/μ as that obtained from the damping of the variation of latitude. It would be strange indeed if this coincidence should be accidental. We can thus summarize the findings of this paragraph as follows: Under stress of intermediate duration, indications are that the mantle behaves like a Kelvin body with the Kelvin constants of the order of magnitude indicated above.

A final remark should be made regarding the possibility of fractures. The occurrence of earthquakes makes it evident that the Kelvin-type behavior subsists only up to a certain limit of stress. If this limit is exceeded, a fracture-type process (an earthquake) occurs. What the limiting stress is

and what the mode of fracture is (i.e. whether it is, for example, governed by Mohr's criterion), no-one can say. Caution, however, should be used in applying to the Earth strength values from short-duration experiments with rocks or such like. In other words, we can *not* make direct use of the results from laboratory experiments to draw conclusions regarding the mode of fracture to be expected in the Earth under intermediate-duration stresses. One direct piece of evidence is that most earthquakes show displacements essentially parallel to the surface, as was already mentioned above. However, since the stress state producing the earthquakes is not yet known, the field is wide open for speculation. Mohr's criterion is just one of many that *could* be valid.

Finally, a remark should be added explaining why we did not take into account any evidence resulting from tidal friction, which, at first glance, would fall into the time interval at present under consideration. Jeffreys (1952, p. 227) has shown that the damping of the Chandler wobble and the tidal friction cannot be due to the same cause. If the time constant obtained from tidal friction is applied to the Chandler wobble, assuming the two effects as being due to the same cause, the wobble should be damped out in a few days instead of in some 12 years. Since Jeffreys has also shown that friction in shallow seas can very well account for tidal friction, it is not necessary to try to resolve the discrepancy in time constants by assuming some rheological peculiarities.

5. STRESSES OF LONG DURATION

We finally come to the crucial problem of trying to elucidate the rheological behavior of the material in the Earth's crust and mantle under stresses of long duration. By long duration we mean, as stated earlier, from 15,000 years upwards, with characteristic duration of 100 million years. Needless to say, the behavior in such time intervals is only very vaguely known.

At the lower limit of this time interval is the rise of some ancient shields since the melting of the overlying ice caps which were present during the last ice age. It is generally assumed that the ice melted approximately 20,000 years ago and that, for example, Fennoscandia has been (and still is) rising since that time owing to the principle of isostasy, buoyancy providing the driving force.

A discussion of the postglacial uplift of Fennoscandia with respect to its possible significance regarding the viscosity in the Earth's mantle and crust has been given by Gutenberg (1941) and by Vening Meinesz (1937). The results are summarized in an article by Benioff and Gutenberg (1951). Accordingly, the uplift of Fennoscandia proceeds at a rate of the order of centimeters per century; "viscosities" (assuming Maxwell behavior) calculated therefrom are of the order of (Haskell 1935)

$$\eta_M = 10^{22} \text{ c.g.s.} \tag{5.1}$$

(Note that the Maxwell viscosity has no relation to the Kelvin viscosity mentioned in the last section.) No value can be given for the other Maxwell constant (the rigidity), since all the processes that can be investigated are steady-state processes; i.e. $\dot{\tau} = 0$ in Eq. (2.3). The term containing it may therefore possibly be neglected, i.e. μ_M is set equal to infinity.

It is also possible to interpret the uplift of Fennoscandia in terms of a Kelvin effect, but the physical picture is then somewhat different from that above: the driving force causing the uplift is the expression of elastic afterworking (and not of buoyancy) after the ice melted. The relaxation constant in a Kelvin body is equal to η_K/μ_K; if this is set equal to, say, 10,000 years, one has in c.g.s. units:

$$\eta_K/\mu_K = 3\times 10^{11} \text{ sec.}$$

No value for the rigidity can be given. The time constant obtained in this manner is obviously not the same as the corresponding one obtained in (4.3) for the intermediate time range. One is therefore faced with having to accept that, in the two time ranges, either the Earth has the *same type* of rheological behavior (Kelvin type), but with *different* constants, or else different types of behavior (Kelvin and Maxwell) with correspondingly unrelated constants. The latter possibility would appear as the more reasonable, especially since it is known that many bodies show increasing tendency towards Maxwell behavior in long time-intervals.

The above interpretation of the uplift of Fennoscandia has been criticized by Lyustikh (1950), who claims that the figure of viscosity calculated in this manner has no meaning. This is because, according to Lyustikh, the uplift of Fennoscandia took place also before the last glaciation and therefore cannot be caused by isostatic forces.

However, if we accept that the uplift of Fennoscandia is an expression of creep during the past 20,000 years, then it is more likely that there will be even more creep in longer time intervals. It is a general experience that creep becomes the more pronounced the longer the stresses apply. Thus, we may assume that the Earth's mantle and crust show creep effects if the stress relaxation time is long compared with 20,000 years. However, this cannot possibly be the whole story. It is well known that mountain ranges can persist over several millions of years; in fact the eventual disappearance of mountains is not at all due to a creep effect, but to the gradual wearing down by the action of wind and water. This implies that the material, to a certain depth at least, also must have a non-vanishing yield stress. Introduction of a yield stress into the equation of a Maxwell liquid produces that of a Bingham body. Noting that, in all processes that are at present accessible to discussion, no indication as to the prevailing Maxwell rigidity μ_M can be obtained, it may thus be permissible to neglect the term containing the latter and therefore to use the Bingham equation as shown in (2.14).

It remains to attempt to give an estimate for the yield strength ν_{ik} $(i \neq k)$ occurring in the Bingham equation. Since the *presence* of a yield stress may be deduced from the existence of mountains, it appears valid to attempt to extract some information regarding its *value* from the same source.

The stability of mounds of various materials has been discussed extensively by Terzaghi (1943), who postulated the following formula

$$H = \frac{\nu}{\rho g} N. \tag{5.2}$$

Here, ν is the yield stress (to shear), H the critical height of the mound which

can just support its own weight, g as usual the gravity acceleration, and N a function of the angle β of the slope of the mound. This function is shown graphically in Fig. 3.

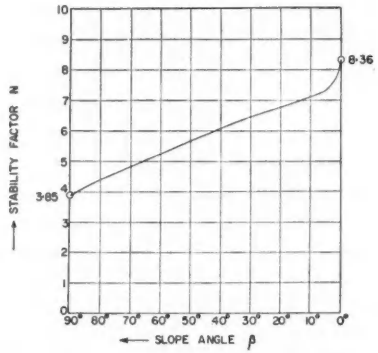

FIG. 3. Graph of stability factor versus slope angle of a mound (after Terzaghi 1943).

If we assume, as a crude approximation, that mountains also satisfy Eq. (5.2), then we obtain an estimate for the yield stress by putting $H = 8$ km., $\rho = 3$, $g = 980$ cm./sec., and $N \backsim 6$ (corresponding to a slope angle of 45°). This yields

$$\nu = 4 \times 10^9 \text{ c.g.s.} \tag{5.3}$$

This value is estimated for the surface of the Earth. It is an upper limit if it is assumed that mountains would be higher if they could support themselves. At a depth, it must be assumed that the yield strength is lower, in conformity with the trend of most materials to become weaker if the pressure and temperature increase. It is interesting to observe that this is of the same order of magnitude as the laboratory strength of rocks.

Thus, combining the phenomenology of the uplift with that of the persistence of mountains suggests that, under stresses of long duration, a rheological equation similar to that of a Bingham body should apply. However, there is a further puzzling factor. This is that the orogenetic phenomena occur in bands of rather narrow width. In these bands, stresses of intermediate time duration are created so that the well-known tectonic effects of folding, faulting, and earthquakes occur. The motion of the displacements in these bands seems to be in no simple relation to the boundaries of the bands (Hodgson 1955; Scheidegger 1955) but generally parallel to the surface of the Earth. For the explanation of this, one can think of the following possibilities:

(i) The bands occur because the crust of the Earth is built up of "stable masses", viz. the continents and ocean blocks, which are in "collision" owing to contraction of the Earth's interior, continental drift, or some other cause. It would naturally be the boundaries of the blocks that would be subject to the greatest deformations. A difficulty with this explanation is that the oro-

genetic bands are known to extend to great depths as evidenced by deep focus earthquakes, whereas it is generally assumed that the "stable blocks" do not extend much below the Mohorovičić discontinuity. It thus appears that the "collisions" could have no more than a triggering effect for the stress concentration, but could not be its actual cause.

(ii) The bands occur because the material is thixotropic: At the edges of the stable blocks a stress concentration is created in the upper regions, which causes motions in the intermediate time intervals. These, in turn, change the rheological equation so as to make the material more yielding. However, this "explanation" is actually nothing but an ad hoc hypothesis and therefore just a restatement of the observations. It explains nothing and is merely a tautology.

(iii) The bands occur because the rheological equation for long-term stresses allows this type of instability to occur. It must be expected that an equation of the Bingham type has integrals in which the deformation becomes unstable in narrow bands. The actual position of the bands could be triggered by the "stable masses" as indicated under (i). This is suggested by an analogy with the bands of plastic instability observed by Bijlaard (1936). However, not sufficient information is available to make this conclusion more definite.

6. CONCLUSION

In conclusion, we may emphasize once more that the behavior of the material in the Earth's crust and mantle is substantially different in the three time ranges which we have been considering.

(*a*) In the short range (up to 4 hours) the material behaves as an elastic solid with a rigidity of about 2×10^{12} c.g.s. and a modulus of elasticity E of about 5×10^{12} c.g.s. If the elastic limit is exceeded, the material undergoes brittle fractures.

(*b*) In the intermediate time range (4 hours to 15,000 years) the material still behaves as an elastic solid with similar elastic constants, but with a significant aftereffect. The relaxation time is about 2 days, the "viscosity" (Kelvin constant) η_K about 3×10^{17} c.g.s. It appears that there is a critical stress which, if exceeded, causes a fracture-type process. The limits of strength referring to this fracture-type process are not known. The process itself is probably very similar to that discussed under (*a*) as, once a fracture starts to move, this occurs in a time interval characteristic of (*a*).

(*c*) In long-duration stresses, creep is the significant phenomenon, i.e. the material yields indefinitely at a constant rate if the stresses stay constant. The relaxation time appears to be of the order of 20,000 years upward. The "viscosity" (Maxwell constant) η_M is probably about 10^{22} to 10^{23} c.g.s. From the relative persistence of mountain chains it may also be assumed that a low yield stress is present so that the rheological equation is essentially that of a Bingham body. The concentration of orogenetic phenomena in narrow bands may be due to rheological instability. For easy reference, the results arrived at in this paper are put together in Table I.

TABLE I

Time interval	Applicable to:	Behavior	Constants
Up to 4 hours ("short")	Seismic wave transmission	Elastic solid with strength limit	μ (rigidity) 2×10^{12} c.g.s. E (Young's modulus) 5×10^{12} c.g.s. Strength limit 10^{10} c.g.s.
4 hours to 15,000 years ("intermediate")	Chandler wobble Earthquake aftershocks Faulting Earth's tides	Kelvin body with strength limit	μ_K ("rigidity") 2×10^{12} c.g.s. η_K ("viscosity") 3×10^{17} c.g.s. Strength limit: present, value unknown
Longer than 15,000 years ("long")	Large scale orogenesis Uplift of Fennoscandia Polar wandering	Bingham body	μ_M ("rigidity") term containing it may possibly be neglected η_M ("viscosity") 10^{22} c.g.s. ν (yield stress) 4×10^{9} c.g.s. at surface

Any investigation of geodynamic problems should take the above facts into consideration. In general, the creation of an orogenetic system will take place during millions of years; it is therefore *not* permissible to apply rigidities, "viscosities", etc. calculated from short- and intermediate-duration data to global considerations concerned with the distribution of orogenetic elements. Much unsatisfactory work has had its origin in this fundamental mistake.

On the other hand, the *local* tectonics is governed by the laws of the intermediate time-range: During the over-all orogenetic process, the local stresses may be assumed to reach large values in periods substantially less than 15,000 years. If a certain critical stress-difference is exceeded, a fracture-like process occurs which is felt as an earthquake and can possibly be recognized physiographically as a fault.

The laws of the short time-range seem to have no application to geodynamics. They appear to be of importance solely in the propagation of elastic waves through the Earth.

ACKNOWLEDGMENTS

The writer is indebted to Dr. P. L. Willmore of the Dominion Observatory in Ottawa for carefully reading the manuscript of this paper and making many valuable suggestions. The remark that it is sometimes possible to describe any one phenomenon either as a Maxwell process or as a Kelvin process, if the underlying physical picture is changed, is due to Dr. Willmore, whom the writer wishes to thank.

REFERENCES

BENIOFF, H. 1951. Bull. Seismol. Soc. Amer. **41**, 31.
BENIOFF, H. and GUTENBERG, B. 1951. *In* Internal constitution of the earth, *edited by* B. Gutenberg (Dover Publications, New York), p. 382.
BIJLAARD, P. P. 1936. Rapport ass. gén., assoc. géod. U.G.G.I., Edimbourg.
BONDI, H. and GOLD, T. 1955. Monthly Notices Roy. Astron. Soc. **115**, 41.
BRIDGMAN, P. W. 1949. The physics of high pressure, New impression with supplement (G. Bell, London).

BULLEN, K. E. 1953. An introduction to the theory of seismology (Cambridge University Press, London).
GRIGGS, D. 1936. J. Geol. **44**, 541.
GUTENBERG, B. 1941. Bull. Geol. Soc. Amer. **52**, 721.
——— 1956. Nature, **177**, 887.
GUTENBERG, B. and RICHTER, C. F. 1942. Bull. Seismol. Soc. Amer. **32**, 163.
——— 1956. Bull. Seismol. Soc. Amer. **46**, 105.
HASKELL, N. W. 1935. Physics, **6**, 265.
HODGSON, J. H. 1955. Geofis. pura e appl. **32**, 31.
JEFFREYS, H. 1952. The earth, 3rd ed. (Cambridge University Press, London).
LAMB, SIR H. 1945. Hydrodynamics (Dover Publications, New York).
LOVE, A. E. H. 1934. A treatise on the mathematical theory of elasticity (Cambridge University Press, London).
LYUSTIKH, E. N. 1956. Izvest. Akad. Nauk S.S.S.R., Ser. Geofiz. 360.
REINER, M. 1949. Twelve lectures on theoretical rheology (North-Holland Pub. Co., Amsterdam).
SCHEIDEGGER, A. E. 1955. Trans. Roy. Soc. Can. IV (3) **44**, 65.
——— 1956. Can. J. Phys. **34**, 498.
TERZAGHI, K. 1943. Theoretical soil mechanics (Chapman & Hall, Ltd., London).
VENING MEINESZ, A. 1937. Proc. Koninkl. Akad. Wetenschap. **40**, 654.

VARIATIONS IN THE AMOUNTS OF POSITRONIUM FORMED IN LIQUIDS AND AMORPHOUS SOLIDS[1]

R. E. GREEN[2] AND R. E. BELL[3]

ABSTRACT

Measurements are reported of the intensity, I_2, of the long-lived (τ_2) component of positron annihilations in a number of liquids and amorphous solids. Large variations in I_2 have been found with different samples of similar substances. It is shown, for example, that I_2 for fused quartz of good quality is about 51% of all the positron decays, and that an earlier published value of 29% probably referred to a 96% silica glass rather than to pure fused quartz. The new value, taken with the results of angular correlation measurements, gives convincing evidence that the annihilation of triplet positronium in condensed materials proceeds mainly by the "pickoff" mechanism. It is shown that the addition of NO_3^- and NO_2^- ions to water in increasing concentration depresses I_2 from its normal value of $(21\pm5)\%$ to a value at least as low as 2% without any marked change in τ_2. This behavior is explained in terms of the formation of the positron compound $e^+NO_3^-$ in the water. This hypothesis explains the shape of the curve of I_2 as a function of NO_3^- ion concentration and also gives a cross section for the capture of positrons by NO_3^- in rough agreement with expectation.

INTRODUCTION

The measurements described here show that the amount of positronium formed when positrons are stopped in certain liquids and amorphous solids is much less constant than has hitherto been supposed. Previously Bell and Graham (1953) had detected a long-lived (τ_2) component in the decay of positrons in a number of amorphous substances, and attributed it to the formation of triplet positronium; this conclusion is now widely accepted. They measured the intensity, I_2, of this component with fair accuracy in only four substances, fused quartz ($I_2 = 29\%$), polystyrene (36%), polyethylene (29%), and fused borax (32%). The error attached to each of these figures was $\pm5\%$. For a large number of other samples, Bell and Graham refrained from quoting definite figures for I_2, remarking only that the value of I_2 for these substances seemed "consistent with the figure of $\sim30\%$" found for the four samples referred to above. They also mentioned that I_2 for teflon was about 33%. On these grounds they assumed that all substances showing the τ_2 component would also show an intensity I_2 of around 30%. The impression that this is true has been strengthened by subsequent measurements by other observers as follows: polystyrene $(27\pm3)\%$ (Ferguson and Lewis 1953), benzene $(31\pm3)\%$ (Berko and Zuchelli 1956), teflon $(31\pm5)\%$ (Gerholm 1956). It will be noticed, however, that these measurements have added only one new substance, benzene, to the list. Graham, Paul, and Henshaw (1956) have found a component in liquid helium with a mean life

[1]Manuscript received November 12, 1956.
Contribution from the Radiation Laboratory, Department of Physics, McGill University, Montreal, and Nuclear Physics Branch, Atomic Energy of Canada Ltd., Chalk River, Ontario. Issued as A.E.C.L. No. 412.
[2]Now at Atomic Energy of Canada, Ltd., Chalk River, Ontario, Canada.
[3]Formerly on staff of Atomic Energy of Canada, Ltd.

of 2.7×10^{-9} sec. and an intensity greater than 30%, but their more recent work (Graham, unpublished) seems to show that this is not the usual τ_2 component.

This accepted constancy of I_2 led to apparent difficulties in the interpretation of the experiments, but the additional measurements to be reported here show that this constancy was largely due to the chance selection of samples.

In a very recent publication, Landes, Berko, and Zuchelli (1956) have shown that I_2 is quite different in molten naphthalene (29%) from what it is in crystalline naphthalene (9%). This work appears to be the first recognition of large changes in I_2. The present results, however, are concerned only with amorphous substances, including liquids. Berko and Zuchelli's value of 29% for molten naphthalene adds one more substance to the list of amorphous samples having I_2 near 30%.

EXPERIMENTAL PROCEDURE

For the measurements, sources of Na^{22} were dissolved or embedded in the sample materials and viewed by two diphenylacetylene 6342 scintillation counters. One counter was biased to accept only pulses from the 1.28 Mev. gamma rays emitted practically simultaneously with the positrons from the source; the other was differentially biased to accept only the upper part of the Compton electron pulse distribution from the 511 kev. annihilation quanta. The distribution in time of the annihilation quanta relative to the 1.28 Mev. gamma rays was measured with a time-to-amplitude converter (Green and Bell 1956) and a 28-channel kicksorter (Skarsgard and Bell 1954). The time calibration of the apparatus was performed by inserting known delays by means of cables, and observing the shifts of the centroid of a prompt coincidence distribution. The use of this converter, which we shall describe in another publication, enabled the whole delay distribution to be measured during a single counting interval. With a source of 10 μc. of Na^{22}, a time spectrum containing a total of over 200,000 counts could be recorded in about 2 hours. We call such a measurement a long run, and one having about one-tenth as many counts a short run.

The Na^{22} source material was prepared by a 45 Mev. proton bombardment of "Superpure" aluminum in the McGill synchrocyclotron, with subsequent chemical separation of Na^{22} by ion exchange. The specific activity after separation was about 0.1 μc./μgm. About 10 μc. of the dissolved material was deposited over an area of 1 cm.^{2} on a mica sheet of thickness 1.8 to 2.0 mg./cm.^{2} and diameter 4 cm. and evaporated to dryness. A similar sheet was placed over the source and the two sheets were waxed together at the edges with black sealing wax. This source will be referred to as the sandwich source. Mica was chosen for the sandwiching material because of its chemical inertness and because it shows no long-lived component of positron decay. A certain fraction of the positrons from the source will annihilate in the mica, reducing the measured intensity I_2 proportionately. This fraction can be estimated from a curve published by Rosenfeld, Swanson, and Warshaw

(1956) as something below 10% for the 1 Mev. positron spectrum of C^{11}. Owing to the effects of backscattering, it will vary somewhat with the effective atomic number of the surrounding sample. Taking account of the lower energy (0.57 Mev.) of the Na^{22} positron spectrum, we correct I_2 for this effect by multiplying by 1.10 for water and organic substances, and by 1.15 for quartz and similar substances. The effect of these corrections on the conclusions of the experiments is small.

In one measurement on water, the Na^{22} source was dissolved directly in distilled water contained in a lead cell. The only correction to I_2 in this case is for the fraction of positrons escaping from the water and annihilating in the lead walls. The correction factor to I_2 was estimated from the dimensions of the cell as 1.04. In another case the active water was in a Pyrex cell; since Pyrex glass is fairly similar to water in behavior (see below), no correction was applied for annihilation in the glass walls.

One sample of fused quartz, made from "Vitreosil" (stated to be >99.8% SiO_2), was directly activated by a 70 Mev. proton irradiation in the cyclotron, the reaction being

$$Si^{28}(p, 4p3n)Na^{22}.$$

After 2 weeks' decay, the sample was found to contain no activity other than Na^{22} in a detectable amount. The Na^{22} in this case was distributed throughout the body of the fused quartz sample. The sample was surrounded by further fused quartz so that no positron could reach any other substance; this source therefore does not require any correction to the measured value of I_2. The radiation damage to this piece of quartz was undoubtedly appreciable, since about 10^{18} protons per cm.^{2} passed through it at 70 Mev. The discoloration of the quartz was not very marked, however, and it is likely that the heating effect of the proton beam on the sample caused at least a partial annealing of the radiation damage while the bombardment was in progress. This view is supported by the fact that the part of the quartz sample nearer to the water-cooled target clamp, and just outside the direct proton beam, showed more discoloration than the part that was more heavily bombarded and less well cooled. We refer to this specimen as the activated quartz sample.

RESULTS

Fig. 1 gives the results for three different high-silica glasses. Curve (*a*) shows the time delay spectrum for the activated sample of fused quartz, measured in a long run. The τ_2 component in this curve is extraordinarily prominent, and its decay is observed over a factor of 1000 with no sign of departure from the exponential shape. The mean life, τ_2, is $(1.53\pm0.05)\times 10^{-9}$ sec. Fig. 1 also shows the method of evaluating the intensity I_2 of the τ_2 component. The straight line representing the τ_2 component is extrapolated back to the point where the center of a prompt resolution curve would lie (point P in Fig. 1); for the samples examined in this paper, this point is 3.5×10^{-10} sec. to the left of the center of the τ_1 peak of the quartz curve, since the τ_1 mean life involved is 3.5×10^{-10} sec. with an uncertainty of perhaps

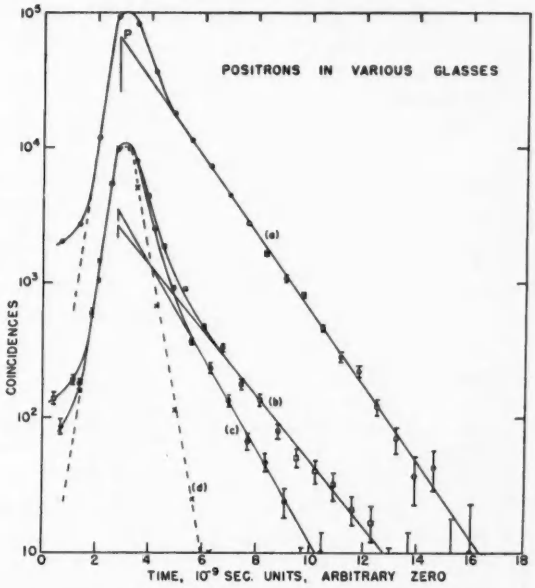

FIG. 1. Time spectra of the decay of positrons in three different high-silica glasses: (*a*) Vitreosil, >99.8% pure fused quartz; (*b*) Vycor, 96% fused quartz; (*c*) Pyrex, ~80% fused quartz. Curve (*d*) shows the shape of the curve observed when the Na^{22} source is replaced by Co^{60}, whose gamma–gamma coincidences are essentially prompt. The curves were taken at different times and their centers do not coincide exactly. The point *P* of curve (*a*) is used in evaluating I_2; see the text.

$\pm 1\times10^{-10}$ sec. (Bell and Graham 1953). For a value of τ_2 of 1.5×10^{-9} sec., this uncertainty will cause an error of only $\pm 7\%$ of the value of I_2. The point *P* having been located, the value of I_2 is given almost exactly by the area under the τ_2 line to the right of *P*, divided by the area of the entire curve (i.e. the sum of all the counts in the individual channels). A small further correction is required because of the finite width of the prompt response curve compared with the value of τ_2. This correction is analogous to the correction for finite duration of the counting interval when a rapidly decaying source is being counted. It is easily shown that the correction factor is given by $(\tau_0/\tau_2)\times[\sinh(\tau_0/\tau_2)]^{-1}$, where τ_0 is the half width at half height of the prompt resolution curve. For the times involved here, this factor is usually about 0.95, and varies little from sample to sample. The value of τ_0 can be judged well enough from the width of the τ_1 peak in the curve. The same procedure for evaluating I_2 was followed in all the curves. The statistical errors in evaluating I_2 are seldom large, but the systematic errors are appreciable, and we have purposely assigned rather generous errors to I_2. The conclusions of the experiment are not affected by the errors assigned.

The value of I_2 for the activated quartz sample, evaluated from Fig. 1, is $(53\pm8)\%$. It is noticed at once that both τ_2 and I_2 for this sample are

quite different from those reported by Bell and Graham for fused quartz ($\tau_2 = 1.8\times10^{-9}$ sec., $I_2 = (29\pm5)\%$). It becomes clear on enquiry that the samples of "fused quartz" that one finds in the laboratory are not very well defined in composition. Taken with the variability in structure owing to the method of preparation of the quartz, it is perhaps not surprising that both τ_2 and I_2 should be found to vary with different samples.

Fig. 1 also shows the results of short runs made with the sandwich source on a pair of "Vycor" quartz windows (96% SiO_2) in curve (*b*), and on a sample of Pyrex glass (~80% SiO_2) in curve (*c*). The Vycor has $\tau_2 = 1.75\times10^{-9}$ sec., $I_2 = (32\pm6)\%$, and the Pyrex $\tau_2 = 1.22\times10^{-9}$ sec., $I_2 = (35\pm7)\%$. Thus the three samples of Fig. 1, all quite similar substances, show among themselves both a variable τ_2 and a variable I_2. It will be noticed that the Vycor result is close to that given by Bell and Graham for their "piece of fused quartz laboratory ware", which in fact is often made of Vycor. Curve (*d*) of Fig. 1 shows the shape of the curve for prompt coincidences from a Co^{60} source, using the same biases on the scintillation counters as in the positron experiments.

Samples of "Homosil" and "Ultrasil" optical-grade fused quartz, the latter stated to be the best available for ultraviolet transmission, showed $I_2 = (49\pm8)\%$, essentially the same result as the activated quartz sample. We conclude that fused quartz of good quality has $I_2 = (51\pm6)\%$, and that even a 4% addition of other oxides to silica in a glass, as in Vycor, seriously depresses the value of I_2.

Fig. 2 shows the results of three short runs for distilled water. Curve (*a*) is for water with Na^{22} dissolved in it, held in a Pyrex cell, curve (*b*) is for the same kind of source in a lead cell, and curve (*c*) is for the sandwich source immersed in water. The three curves are all very similar, and after correction for wall loss for (*b*), and mica loss for (*c*), they yield the following values of I_2:

$$(a)\ 22.3\%, \qquad (b)\ 21.9\%, \qquad (c)\ 20.6\%.$$

The value of I_2 for water may therefore be given as $(21\pm5)\%$. Earlier runs on the sandwich source in water using the conventional single-channel delayed coincidence apparatus with $2\tau_0 = 2\times10^{-9}$ sec. also gave values of I_2 around 21%, in agreement with the above figures. In all cases the indicated value of τ_2 was about 1.80×10^{-9} sec., in reasonable agreement with Bell and Graham's value of 1.7×10^{-9} sec. Analysis of Bell and Graham's published diagram for water also yields I_2 about 20%. The agreement of I_2 from curves (*a*) and (*b*) with that from curve (*c*) is evidence that the small correction factor for mica loss adopted here is sufficiently accurate.

A measurement with the sandwich source in *p*-dioxane gave $\tau_2 = 2.67\times10^{-9}$ sec., $I_2 = (36\pm7)\%$, in almost exact agreement with Berko and Zuchelli's results (1956) on benzene. The identity of these results is interesting because the *p*-dioxane molecule has a benzene ring structure.

A very interesting effect is observed with water solutions of sodium nitrate in various concentrations. Fig. 3 shows a set of results for pure water, and

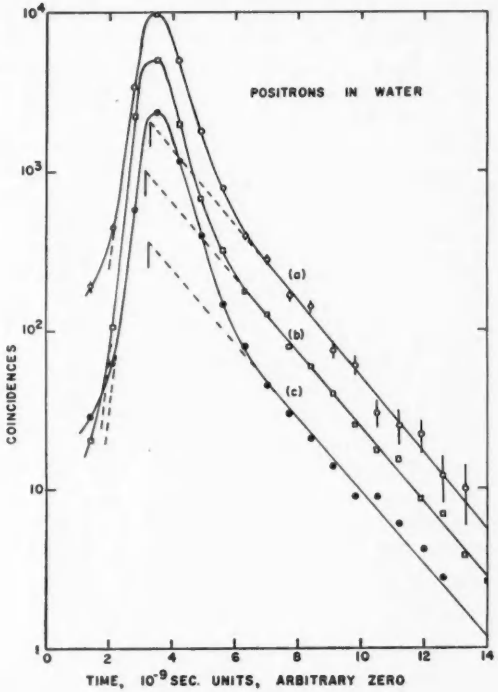

FIG. 2. Time spectra of the decay of positrons in water: (*a*) water in a Pyrex cell, (*b*) water in a lead cell, (*c*) water surrounding the mica sandwich source. The statistical errors are shown only for curve (*a*). Those for curve (*c*) are similar, and those for curve (*b*) are somewhat smaller. The curves were taken at different times and their centers do not coincide exactly.

for $NaNO_3$ concentrations of 0.25 *M*, 0.5 *M*, 2.5 *M*, and 5 *M*.* It will be seen that the effect of adding $NaNO_3$ to water is to depress the value of I_2 without substantially changing τ_2. At the highest concentrations, 2.5 *M* and 5 *M*, the results become uncertain statistically, and the values for I_2 are only rough estimates. Any defects in the experimental techniques at these low levels will give values of I_2 that are too high. Fig. 4 summarizes the results of Fig. 3 in a curve of the experimental value of I_2 as a function of concentration of $NaNO_3$. Two points in Fig. 4 have been taken from runs that were omitted from Fig. 3 in the interests of clarity. Fig. 4 shows that I_2 falls very rapidly as $NaNO_3$ is first added to the water, but seems to decrease more slowly as the concentration is made large. The curve shown in Fig. 4 is drawn according to equation (5) of the discussion section.

The behavior of $NaNO_3$ is presumably to be attributed to the NO_3^- ion, because sodium hydroxide, for example, shows no effect on I_2 and only a

*M = moles per liter of solution.

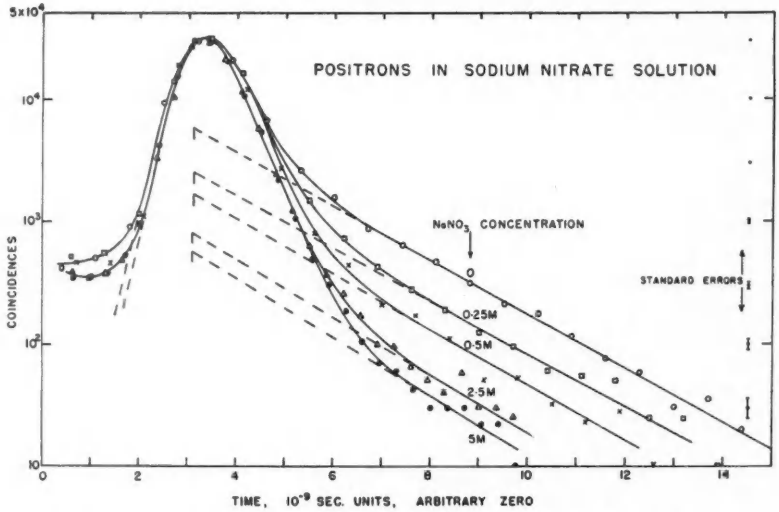

FIG. 3. Time spectra of the decay of positrons in water solutions of sodium nitrate of concentration 0 M, 0.25 M, 0.5 M, 2.5 M, and 5.0 M, showing the decrease of I_2 as the concentration is increased. A change of range of the time-to-amplitude converter occurs between the 0.5 M curve and 2.5 M curve.

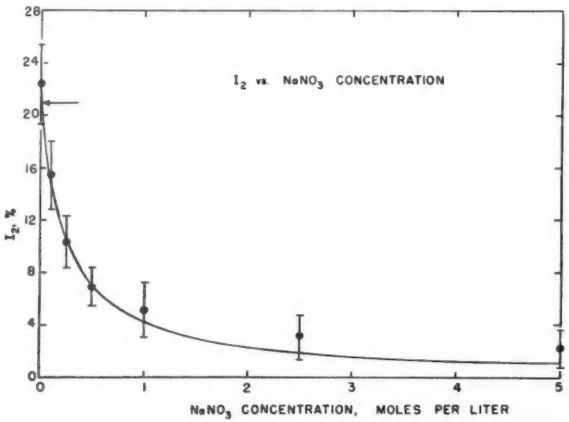

FIG. 4. Points: experimental values of I_2, observed from runs like those of Fig. 3, as a function of sodium nitrate concentration. Curve: theoretical shape computed from equation (5), fitted to $I_2 = 21\%$ for pure water (arrow) and to $I_2 = 10.5\%$ for 0.25 M $NaNO_3$.

small effect on τ_2 at concentrations as high as 10 M. On the other hand, nitric acid (HNO_3) shows the same effect as an equal concentration of sodium nitrate. It has also been observed that sodium nitrite ($NaNO_2$) shows almost the same effect as sodium nitrate, differing only in requiring a slightly higher concentration for the same degree of suppression of I_2.

Several other salts were found to depress the value of I_2 slightly in concentrated water solution, but in every case the concentration was high enough (2–10 M) to affect the bulk properties of the water (mass density, electron density, etc.). Some salts leave I_2 relatively unaffected and modify τ_2 to a small extent. Table I is a list of the salts tried, their concentrations, and their measured values of τ_2 and I_2. None of them possesses the apparently highly specific effect of suppressing positronium formation in dilute solution shown by $NaNO_3$, HNO_3, and $NaNO_2$, although a wider search would presumably reveal other substances with a similar behavior.

TABLE I

EXPERIMENTAL VALUES OF τ_2 AND I_2 FOR VARIOUS SALTS DISSOLVED IN WATER. ALL MEASUREMENTS WERE MADE WITH THE MICA SANDWICH SOURCE. THE ASSIGNED STANDARD ERROR IN τ_2 IS ± 0.10, AND IN I_2 IS ± 5 IN ABSOLUTE VALUE, OR ± 3 FOR COMPARISON OF DIFFERENT ENTRIES IN THIS TABLE AMONG THEMSELVES

Entry No.	Sample	Concentration	τ_2 (10^{-9} sec.)	I_2 (%)
1	H_2O	Pure	1.80	21
2	HCl	5 M	1.83	16
3	NaCl	5.2 M	1.76	15
4	KCl	3.9 M	1.68	17
5	NH_4Cl	5.2 M	1.72	14
6	$ZnCl_2$	6.3 M	1.82	16
7	$BaCl_2$	1.7 M	1.72	17
8	$AlCl_3$	3.9 M	1.71	20
9	$LaCl_3$	Sat.	1.80	18
10	NaOH	10 M	1.49	21
11	$NaC_2H_3O_2$	7.6 M	1.91	19
12	K_2CO_3	5.8 M	1.57	17
13	Na_2CO_3	1.3 M	1.77	20
14	Na_2SO_4	3.3 M	1.75	16

DISCUSSION

The preceding results have shown that it is possible to find substances all having roughly the same value of τ_2 but with I_2 varying from $\sim 2\%$ to 53%. In terms of positronium formation by the incident positrons, these figures represent only the triplet positronium formation, i.e. three-quarters of the total; the total formation therefore ranges from $\sim 3\%$ to 71% of all the incident positrons. The high value for fused quartz has an immediate application in the interpretation of angular correlation experiments on the annihilation radiation. Page *et al.* (1955, 1956) have found a narrow component in the two-photon angular correlation curve for fused quartz; a similar effect has been noted by Stewart (1955) for teflon. Page *et al.* evaluated the fraction of all their coincidences appearing in the narrow component, and found $(17.6 \pm 1.5)\%$, later given simply as 18%. A narrow component can arise only when a positron in a slowly moving positronium atom annihilates with the electron to which it is bound. If the τ_2 component in fused quartz decayed mainly by conversion to singlet positronium, as suggested by Bell and Graham (1953), then essentially all the positronium formed would decay from the singlet state, and the fraction appearing in Page's narrow component would be equal to the total positronium formation. On Bell and Graham's original result for what they called fused quartz, this would be $\frac{4}{3}(29\%) = 39\%$. If,

on the other hand, the τ_2 component represents annihilations of triplet positronium mainly by "pickoff" annihilation with electrons bound to neighboring atoms or molecules (Garwin 1953), only the singlet positronium would yield a narrow component, and again on Bell and Graham's original result, the fraction in the narrow component would be $\frac{1}{3}(29\%) = 10\%$. Page *et al.* were puzzled by the failure of their narrow-component fraction, 18%, to agree with either value predicted by Bell and Graham's result. Assuming pickoff, the discovery in this work that good fused quartz has $I_2 \sim 51\%$ allows us to predict a narrow-component fraction of $\frac{1}{3}(51\%) = 17\%$, in agreement with that found by Page *et al.* This agreement is strong evidence that the pickoff mechanism is in fact the main process determining the lifetime τ_2.

The effect of $NaNO_3$ in suppressing the formation of positronium is difficult to discuss conclusively. A concentration of 0.1 M, corresponding to less than two molecules of $NaNO_3$ per thousand water molecules, produces a distinct reduction in I_2 (see Fig. 4) without appreciably affecting τ_2. It must be emphasized that this strong effect is a quite different effect from the ortho-para-positronium conversion found by Deutsch (1951) for NO and NO_2 in gases. The present effect is not one of conversion, which would be reflected mainly as a variation of τ_2 rather than I_2, but one of inhibition of the formation of positronium. Dulit, Gittelman, and Deutsch (1956) have observed that the amount of positronium formed in argon can be influenced by adding small amounts of a polyatomic gas; their results, however, show an increase in positronium formation as the concentration of the polyatomic gas is increased, followed by a decrease to the value characteristic of the polyatomic gas itself. They do not give quantitative figures. This behavior can be understood qualitatively (Deutsch 1955) on Ore's picture (1949) of the energetics of positronium formation. In a similar way, Deutsch and Brown (1952) and Deutsch and Dulit (quoted by Deutsch 1955) have shown that the enhancement of positronium formation in argon caused by an applied electric field can be nullified by the presence of a small amount of a polyatomic gas.

No similar simple explanation of the present results for NO_3^- and NO_2^- in water seems to be available. In the first place, it would require great boldness to apply Ore's picture to the complicated liquid medium and it could only be expected to be a very general guide. In the second place, water itself is polyatomic, as well as the additives NO_3^- and NO_2^-, and it is difficult to see how the additives could reduce the amount of positronium formed so drastically—according to Fig. 4, by a factor of 10 or more. It would also be difficult to explain why the other polyatomic ions from the salts appearing in Table I do not have a comparable effect; these other ions are the acetate, sulphate, carbonate, hydroxyl, and ammonium ions. Of course none of the above arguments can rule out the energetics of positronium formation as an influencing factor on I_2, but they do show that an additional mechanism is necessary to explain the results.

An alternative hypothesis is the following. Since HNO_3 is a stable compound, we may suppose that a positron may replace the proton and still form a stable compound. This compound would be written $e^+NO_3^-$; the paral-

lel notation for nitric acid would be $H^+NO_3^-$. The work of Ore (1948, 1952) is not conclusive on the subject of the stability of such positron compounds, but he has demonstrated that e^+H^- is stable in free space, and Simons (1953) has shown the same for e^+Cl^-. We therefore assume provisionally that $e^+NO_3^-$ is likely to be stable, or at least that $e^+NO_3^-$ is not dissociated by water within a few times 10^{-10} sec. after its formation. Given these conditions, NO_3^- ions in water would capture positrons to form $e^+NO_3^-$. The lifetime of this compound against annihilation would be of the same order as that of singlet positronium, for the positron would be situated in a comparable density of electrons of favorable spin orientation. Thus the positrons captured by the NO_3^- ions would be lost from the τ_2 component in the decay curves and would appear instead with a short lifetime of the order of τ_1. We now show that this hypothesis explains the shape of the curves of Fig. 4.

The fate of a positron in pure water—whether it will form positronium or not—is presumably decided within some average time of decision short compared with the τ_1 lifetime of about 3×10^{-10} sec. We call this short time T_D. During this time interval there is repeated capture and loss of electrons by the positron, and speaking in terms of averages, there is a probability Γ_p per unit time of its forming positronium and a probability Γ_f of its remaining free or annihilating in a free collision. The total probability of forming positronium is $\Gamma_p T_D$ and the total probability, $(\Gamma_p+\Gamma_f)T_D$, is unity. The fractional formation of positronium is $\Gamma_p T_D$, and the τ_2 component represents three-quarters of this, so that we have, from the water experiments,

$$I_2 = \tfrac{3}{4}(\Gamma_p T_D) = 0.21. \tag{1}$$

Upon adding NO_3^- ions to the water, we introduce a positron capture process with a rate $N\bar{\sigma}\bar{v}$ where N is the density of NO_3^- ions, $\bar{\sigma}$ is the mean capture cross section, and $\bar{v}$ is the mean relative velocity of the positron and the NO_3^- ions. We then have, instead of (1),

$$I_2 = \tfrac{3}{4}\,\Gamma_p T_D/(\Gamma_p+\Gamma_f+N\bar{\sigma}\bar{v})T_D. \tag{2}$$

With the use of (1) and the fact that $(\Gamma_p+\Gamma_f)T_D = 1$, we get

$$I_2 = 0.21/(1+N\bar{\sigma}\bar{v}\,T_D). \tag{3}$$

If the concentration of NO_3^- is varied, we vary only N in equation (3), so that we have

$$I_2 = 0.21/(1+kM), \tag{4}$$

where M is the molarity of the $NaNO_3$ solution, and k is a constant. The experiments show that I_2 is about half normal, i.e. $1+kM$ is about 2, when $M = 0.25$ (Fig. 4), and we get finally

$$I_2 = 0.21/(1+4M). \tag{5}$$

The solid curve in Fig. 4 is a graph of expression (5); the agreement with the measured points is good except at the two highest concentrations where, as already remarked, the measurements of I_2 are unreliable and the experimental values may be too high.

A further confirmation of the NO_3^- capture mechanism consists of showing that the positron capture cross section $\bar{\sigma}$ of NO_3^- is of a reasonable magnitude, viz. of the order of the geometrical cross section of the NO_3^- ion. In order to estimate $\bar{\sigma}$ we must estimate T_D. If positronium formation occurs during the time when the positrons are slowing down from, say, 1000 ev. to 10 ev. as suggested by the electron capture calculations of Jackson (1955), and if the inelastic processes by which this slowing down takes place have cross sections of the order of πa_0^2, then the time T_D is of the order of 10^{-13} sec. The positron velocities over this interval are around 4×10^8 cm. sec.$^{-1}$ We have seen that $1+kM$ is equal to 2, i.e. $N\bar{\sigma}\bar{v}\ T_D = 1$, when $M = 0.25$, i.e. when $N = 1.5\times10^{20}$ cm.$^{-3}$ We get from these values of N, $\bar{v}$, and T_D,

$$\bar{\sigma} = [N\bar{v}T_D]^{-1} = 1.7\times10^{-16}\ \text{cm.}^2 \tag{6}$$

This value of $\bar{\sigma}$ is about equal to $2\pi a_0^2$, in the expected range of magnitude. The above estimates are probably rough enough to allow a factor of 10 change in either direction, but the order of magnitude would still support the hypothesis of $e^+NO_3^-$ formation.

It is now necessary to consider the substances in Table I, which do not show the positron compound effect. We can divide the entries in Table I into four classes: entries 2 to 9, chlorides; entry 10, hydroxide; entry 11, acetate; and entries 12 to 14, salts having divalent negative ions. We dispose of the last group at once by noting that it would be necessary to have two positrons present simultaneously in order to produce a positron analogue of, say, Na_2SO_4. The remaining three negative ions, Cl^-, OH^-, and $C_2H_3O_2^-$, must now be supposed not to form stable compounds such as e^+Cl^- in the presence of water; these compounds may of course be stable in free space, as indeed Simons has shown for e^+Cl^- (1953). The behavior of the NO_3^- and NO_2^- ions now seems much less remarkable than it did at first sight, because they represent two out of five monovalent negative ions tried in the experiments.

We may note in passing that in an experiment like that of Pond (1954), where the defect in the two-quantum annihilation rate (i.e. the three-quantum rate) was measured in benzene as a function of the concentration of a dissolved free radical, the quantity measured is proportional to the product $\tau_2 I_2$. In Pond's experiment, the three-quantum rate decreased with increasing concentration of the free radical because τ_2 was being reduced by the action of the free radical in causing ortho–para–positronium conversion (Berko and Zuchelli 1956). An experiment like Pond's performed on water solutions of $NaNO_3$ should show a similar effect because of the decrease in I_2, and the shape of the curve of three-quantum rate as a function of concentration should not be very different. The experiment could also be done by direct detection of the three-quantum annihilations in the manner of the early experiment by Rich (1951).

Returning to the subject of fused quartz, we find that nearly pure fused quartz has I_2 about 51%, while both 96% quartz (Vycor) and 80% quartz (Pyrex) have I_2 about two-thirds this amount. In both the latter cases the

added substance is mainly boric oxide. Here we have a case where I_2 varies much less violently than in the case of $NaNO_3$ in water, and which resembles, so far as it goes, the gas results of Dulit, Gittelman, and Deutsch (1956) mentioned earlier. It is therefore likely that the energetics of positron capture are responsible for these results. Similar remarks probably apply to the salts in Table I that show slight effects on I_2.

We wish to thank Mrs. N. Hollbach and Dr. L. Yaffe for the chemical separation of the Na^{22} source material. Valuable suggestions have been received during the course of this work from Dr. J. S. Foster and Dr. J. D. Jackson. One of us (R.E.G.) was supported by National Research Council scholarships.

REFERENCES

BELL, R. E. and GRAHAM, R. L. 1953. Phys. Rev. **90**, 644.
BERKO, S. and ZUCHELLI, A. J. 1956. Phys. Rev. **102**, 724.
DEUTSCH, M. 1951. Phys. Rev. **82**, 455.
——— 1955. *In* Beta- and gamma-ray spectroscopy, *edited by* K. Siegbahn (North-Holland Pub. Co., Amsterdam).
DEUTSCH, M. and BROWN, S. C. 1952. Phys. Rev. **85**, 1047.
DULIT, E. P., GITTELMAN, B., and DEUTSCH, M. 1956. Bull. Am. Phys. Soc. II, **1**, No. 1, 69.
FERGUSON, A. T. G. and LEWIS, G. M. 1953. Phil. Mag. **44**, 1339.
GARWIN, R. L. 1953. Phys. Rev. **91**, 157.
GERHOLM, T. R. 1956. Arkiv Fysik, **10**, 523.
GRAHAM, R. L., PAUL, D. A. L., and HENSHAW, D. G. 1956. Bull. Am. Phys. Soc. II, **1**, No. 1, 68.
GREEN, R. E. and BELL, R. E. 1956. Unpublished.
JACKSON, J. D. 1955. Phys. Rev. **99**, 1653.
LANDES, H. S., BERKO, S., and ZUCHELLI, A. J. 1956. Phys. Rev. **103**, 828.
ORE, A. 1948. Phys. Rev. **73**, 1313.
——— 1949. University of Bergen Yearbook, No. 9, p. 1.
——— 1952. University of Bergen Yearbook, No. 5, p. 1.
PAGE, L. A., HEINBERG, M., WALLACE, J., and TROUT, T. 1955. Phys. Rev. **98**, 206.
PAGE, L. A. and HEINBERG, M. 1956. Phys. Rev. **102**, 1545.
POND, T. A. 1954. Phys. Rev. **93**, 478.
RICH, J. A. 1951. Phys. Rev. **81**, 140.
ROSENFELD, A. H., SWANSON, R. A., and WARSHAW, S. D. 1956. Phys. Rev. **103**, 43.
SIMONS, L. 1953. Phys. Rev. **90**, 165.
SKARSGARD, H. M. and BELL, R. E. 1954. Unpublished.
STEWART, A. T. 1955. Phys. Rev. **99**, 594.

STEADY STATE HEAT TRANSFER TO FULLY DEVELOPED TURBULENT FLOW IN A CURVED CHANNEL[1]

A. W. MARRIS

ABSTRACT

A vorticity transfer analogy theory of turbulent heat transfer is developed first for the case of fully developed turbulent flow under zero transverse pressure and temperature gradients such as that in the annulus between concentric cylinders rotating with different angular velocities or in a "free vortex". The mean flow is assumed to be two-dimensional. The theory, which requires that the turbulence be statistically isotropic, yields a temperature distribution in agreement with experiment except in narrow regions immediately adjacent to the boundaries. An argument is given to show that the boundary layer thickness should be of the order of the reciprocal of the square root of the mean velocity, these boundaries are introduced, and Nusselt moduli are defined and their dependence on Reynolds and Prandtl numbers is investigated.

The temperature distributions for the case of non-zero transverse temperature and pressure gradients, i.e. for the case of flow in a curved channel in which the fluid does not flow back into itself, are then obtained and the applicability of the simpler equations for zero transverse gradients to this case is investigated.

SUMMARY OF NOMENCLATURE

r, θ, z	= cylindrical polar co-ordinates of reference point of channel, referred to center of curvature of channel as origin (see Fig. 2).
R_1, R_2	= boundaries of channel (see Fig. 2).
R	= parameter such that $R_1 < R < R_2$.
U, V, W	= components of mean flow velocity in θ, r, z directions respectively ($V = W = 0$).
u', v', w'	= components of fluctuating turbulent velocities in θ, r, z directions respectively.
ξ', η', ζ'	= components of fluctuating turbulent vorticities in θ, r, z directions respectively.
P	= mean pressure at reference point.
ρ	= density of fluid, assumed constant.
$F_V(r)$	= eddy diffusivity for vorticity.
$\zeta = \frac{1}{r}\frac{\partial}{\partial r}(rU)$	= z component of mean vorticity.
C_1, C_2	= parameters in vorticity distribution.
ν	= kinematic viscosity of fluid.
t	= temperature at reference point.
t_{R_1}, t_{R_2}, t_R	= temperature at $r = R_1$, $r = R_2$, $r = R$.
$a_H = k/s\rho$	= molecular thermal diffusivity of fluid.
k	= molecular thermal conductivity of fluid, assumed constant.

[1]Manuscript received November 5, 1956.
Contribution from the Department of Civil Engineering, The University of British Columbia, Vancouver, B.C.

s = specific heat of fluid, assumed constant.

$F_H(r)$ = eddy diffusivity for heat transfer.

P_1, P_2 $= -\dfrac{1}{C_1\rho}\dfrac{\partial P}{\partial\theta}, \dfrac{1}{C_2\rho}\dfrac{\partial P}{\partial\theta}.$

P_1, P_2 $= -\lim\limits_{\partial P/\partial\theta\to 0}\dfrac{1}{C_1\rho}\dfrac{\partial P}{\partial\theta}, \lim\limits_{\partial P/\partial\theta\to 0}\dfrac{1}{C_2\rho}\dfrac{\partial P}{\partial\theta}.$

$\lambda = F_H(r)/F_V(r)$ = analogy parameter.

Q_1 $= \lambda P_1.$

Q_2 $= \lambda P_2.$

T $= -rq_r/s\rho.$

q_r = radial heat flow per unit area per second at r (see Fig. 2).

ϵ_1, ϵ_2 = width of boundary layers at $r = R_1$, $r = R_2$.

$N_{Re} = (R_2-R_1)U_m/\nu$ = Reynolds number for channel.

U_m = mean velocity in channel.

N_{Pr} $= \nu/a_H = s\mu/k =$ Prandtl number.

Q_1' $= Q_1/U_m.$

Q_2' $= Q_2/U_m.$

$\alpha_1, \beta_1, \gamma_1, \delta_1, \alpha_2, \beta_2, \gamma_2, \delta_2, \phi_2$ = parameters in the radial temperature distribution.

g $= \dfrac{T}{U_m}\dfrac{1}{\partial t/\partial\theta} = -\dfrac{q_r}{s\rho U_m\partial t/r\partial\theta}.$

t_m = mean mixed fluid temperature.

INTRODUCTION

In this work heat transfer phenomena for turbulent flow in annuli and curved channels are investigated by postulating eddy diffusivities for heat analogous to eddy diffusivities for vorticity which latter have earlier been shown to be capable of yielding formulae for the mean velocity distribution which agree with experiment as long as the ratio of the radius of curvature of the channel to the channel width is relatively small, i.e. so that the flow does not approximate to straight channel flow.

Whereas it has become apparent that fruitful insight into the ultimate micromechanism of turbulence, and particularly the effect of solid boundaries on this mechanism, is not likely to be obtained from such a phenomenological investigation, it is felt that such an approach must retain a value for the design physicist and engineer in that it represents the most tangible means of predicting with adequate accuracy the effect of the geometry and general flow conditions on these mean phenomena (Goldstein 1950; Klebanoff 1954; Laufer 1951).

This then is the main justification for this work, the need for applicable formulae to yield temperature distribution and heat transfer data in the numerous problems of rotary motion that arise in the fields of engineering and in meteorology and oceanography. Moreover, while such semiempirical results

probably cannot be used as a starting point for any fundamental theory of turbulence (this because of the generally slow response of the macroscopic results of the turbulence to changes in the microscopic activity), it would seem that they must be at least an approximate end-point to such a theory, and as such possibly serve as a guide in its construction.

BACKGROUND

In cylindrical co-ordinates the Reynolds equations expressing the components of mean velocity in terms of the time average of the turbulent velocity and vorticity components take the form, for steady motion,

$$(1)\qquad U\frac{\partial U}{r\partial\theta}+V\frac{\partial U}{\partial r}+W\frac{\partial U}{\partial z}+\frac{UV}{r}=-\frac{\partial}{r\partial\theta}\left(\frac{P}{\rho}+\frac{\overline{q'^2}}{2}\right)+\overline{v'\zeta'-w'\eta'}+\nu\left[\nabla^2U-\frac{U}{r^2}+\frac{2}{r^2}\frac{\partial V}{\partial\theta}\right],$$

$$(2)\qquad U\frac{\partial V}{r\partial\theta}+V\frac{\partial V}{\partial r}+W\frac{\partial W}{\partial z}-\frac{U^2}{r}=-\frac{\partial}{\partial r}\left(\frac{P}{\rho}+\frac{\overline{q'^2}}{2}\right)+\overline{w'\xi'-u'\zeta'}+\nu\left[\nabla^2V-\frac{V}{r^2}-\frac{2}{r^2}\frac{\partial U}{\partial\theta}\right],$$

$$(3)\qquad U\frac{\partial W}{r\partial\theta}+V\frac{\partial W}{\partial r}+W\frac{\partial W}{\partial z}=-\frac{\partial}{\partial z}\left(\frac{P}{\rho}+\frac{\overline{q'^2}}{2}\right)+\overline{u'\eta'-v'\xi'}+\nu\nabla^2W,$$

where

$$(4)\qquad \nabla^2=\frac{1}{r^2}\frac{\partial^2}{\partial\theta^2}+\frac{\partial^2}{\partial r^2}+\frac{1}{r}\frac{\partial}{\partial r}+\frac{\partial^2}{\partial z^2},$$

$$(5)\qquad \overline{q'^2}=\overline{u'^2+v'^2+w'^2},$$

$$(6)\qquad \xi'=\frac{\partial w'}{\partial r}-\frac{\partial v'}{\partial z},$$

$$(7)\qquad \eta'=\frac{\partial u'}{\partial z}-\frac{\partial w'}{r\partial\theta},$$

$$(8)\qquad \zeta'=\frac{\partial v'}{r\partial\theta}-\frac{\partial u'}{\partial r}-\frac{u'}{r}.$$

The equations of continuity for the mean and turbulent velocity components are respectively

$$(9)\qquad \frac{\partial U}{r\partial\theta}+\frac{\partial V}{\partial r}+\frac{\partial W}{\partial z}+\frac{V}{r}=0,$$

$$(10)\qquad \frac{\partial u'}{r\partial\theta}+\frac{\partial v'}{\partial r}+\frac{\partial w'}{\partial z}+\frac{v'}{r}=0.$$

For two-dimensional mean flow in circles,

$$(11)\qquad V=W=0$$

and apart from the pressure gradient $\partial P/r\partial\theta$ all derivatives with respect to θ,

and the mean derivatives with respect to z, vanish, so that equations (1) and (2) become

$$(12)\quad \frac{1}{\rho}\frac{\partial P}{r\partial\theta} = \overline{v'\zeta'-w'\eta'}+\nu\left[\frac{\partial^2 U}{\partial r^2}+\frac{1}{r}\frac{\partial U}{\partial r}-\frac{U}{r^2}\right] = \overline{v'\zeta'-w'\eta'}+\nu\left[\frac{\partial}{\partial r}\frac{1}{r}\frac{\partial}{\partial r}(rU)\right]$$

$$= \overline{v'\zeta'-w'\eta'}+\nu\frac{\partial\zeta}{\partial r},$$

$$(13)\quad \frac{1}{\rho}\frac{\partial P}{\partial r}+\frac{\partial}{\partial r}\frac{\overline{q'^2}}{2} = \frac{U^2}{r}+\overline{w'\xi'-u'\zeta'},$$

where, by equation (10),

$$(14)\quad \overline{v'\zeta'-w'\eta'} = -\frac{1}{r^2}\frac{\partial}{\partial r}(r^2\overline{u'v'})$$

and

$$(15)\quad \overline{w'\xi'-u'\zeta'} = \frac{\partial}{\partial r}\frac{q'^2}{2}-\frac{\partial}{\partial r}\overline{v'^2}-\frac{\overline{v'^2}}{r}+\frac{\overline{u'^2}}{r}.$$

It is an experimental result (Taylor 1937) that for flow in circles under zero transverse pressure gradient, for example for flow in the annulus between concentric rotating cylinders, the mean velocity distribution is given by

$$(16)\quad rU = \text{const.}$$

over all the channel except for the narrow region immediately adjacent to the walls. Putting $\partial P/r\partial\theta = 0$ in equation (12) above, one sees that this is only possible if

$$(17)\quad v'\zeta'-w'\eta' = F_V(r)\left[\frac{\partial}{\partial r}\frac{1}{r}\frac{\partial}{\partial r}(rU)\right],$$

$F_V(r)$ being any non-zero function of r. The argument for the vorticity transfer theory is that for statistically isotropic turbulence it predicts just this result (Goldstein 1938). Near the solid boundary the turbulence is known to be non-isotropic and the mean velocity distribution is no longer given by $rU = \text{const.}$

While equation (17) may not represent the whole story of the effect of the turbulent micromechanism on the mean motion, its form, once $F_V(r)$ is determined, lends itself as a basis for producing a mean velocity distribution formula of use in design problems. Further one may develop from it, on an analogy basis, expressions for mean temperature distributions in such a curved channel. The general sluggishness of the response of such mean phenomena to the microscopic impulses, which tends to prohibit an investigation of the latter from an $F_V(r)$ determined from mean distribution, has perhaps the compensating advantage of giving stability and reproducibility of these mean distributions.

THE EDDY DIFFUSIVITY FOR CURVED CHANNEL FLOW

Assuming that the relation

$$(17)\quad \overline{v'\zeta'-w'\eta'} = F_V(r)\left[\frac{\partial}{\partial r}\frac{1}{r}\frac{\partial}{\partial r}(rU)\right]$$

holds, at least in the region not immediately adjacent to the solid boundaries for the case when $\partial P/r\partial\theta$ is small but not zero, i.e. for flow in a curved channel with a depth to breadth ratio sufficiently large for the flow to be two-dimensional, one would have for the region of statistically isotropic turbulence

$$\frac{1}{\rho}\frac{\partial P}{\partial\theta} = (\nu+F_V(r))\left[\frac{\partial}{\partial r}\frac{1}{r}\frac{\partial}{\partial r}(rU)\right] = (\nu+F_V(r))\frac{\partial\zeta}{\partial r}, \tag{18}$$

U being the mean transverse velocity at radius r (see Fig. 2) and $\partial P/\partial\theta$ the mean pressure gradient in the flow direction.

Differentiating equation (13) with respect to θ one has

$$\partial^2 P/\partial r\partial\theta = 0, \tag{19}$$

so that $\partial P/\partial\theta$ is independent of r. It follows from equation (18) that, assuming $\partial P/\partial\theta$ to be also independent of θ,

$$(\nu+F_V(r))\frac{\partial\zeta}{\partial r} = \frac{A}{r}, \quad \text{where } A = \frac{1}{\rho}\frac{\partial P}{\partial\theta} = \text{constant}. \tag{20}$$

Wattendorf (1935) obtained for such a flow a radial vorticity distribution for which the vorticity is not constant as in the case of Taylor's Couette type flow (equation (16)) but which is representable by the equations (Marris 1956)

$$\zeta = \zeta_1 = C_1/(r-R_1) \quad \text{for } R_1 < r < R \tag{21}$$

and

$$\zeta-\zeta_0 = \zeta_2-\zeta_0 = C_2/(R_2-r) \quad \text{for } R < r < R_2, \tag{22}$$

$r = R_1$ and R_2 being the boundaries of the region of turbulence under consideration, and R a parameter such that $R_1 < R < R_2$. The parameter C_1 is positive and C_2 is negative.

One obtains immediately from equation (20)

$$F_V(r)+\nu = F_{V_1}(r)+\nu = P_1(r-R_1)^2/r \quad \text{for } R_1 < r < R \tag{23}$$

and

$$F_V(r)+\nu = F_{V_2}(r)+\nu = P_2(R_2-r)^2/r \quad \text{for } R < r < R_2, \tag{24}$$

where

$$P_1 = -\frac{1}{C_1\rho}\frac{\partial P}{\partial\theta}, \tag{25}$$

$$P_2 = \frac{1}{C_2\rho}\frac{\partial P}{\partial\theta}, \tag{26}$$

and since $\partial P/\partial\theta$ is negative, P_1 and P_2 are both positive.

By equations (14) and (17)

$$\overline{v'\zeta'-w'\eta'} = -\frac{1}{r^2}\frac{\partial}{\partial r}(r^2\overline{u'v'}) = F_V\frac{\partial\zeta}{\partial r} = \frac{1}{\rho r}\frac{\partial P}{\partial\theta}-\nu\frac{\partial\zeta}{\partial r}. \tag{27}$$

Equation (27) integrates to give for the total shear stress (Eskinazi and Yeh 1956)

$$\frac{\tau}{\rho} = -\overline{u'v'} + \nu r \frac{\partial}{\partial r}\left(\frac{U}{r}\right) = -\frac{1}{2}\frac{\partial P}{\partial \theta}\frac{1}{\rho}\left(\frac{r_n^2}{r^2} - 1\right), \tag{28}$$

where r_n is the radius at which $\tau = 0$.

Eskinazi and Yeh (1956) measured the distribution of both $\overline{u'v'}/U_{\max}^2$ and $\tau/U_{\max}^2$ for flow in a curved channel of the type here considered, for which $R_1 = 27$ in., $R_2 = 30$ in., and $U_{\max} = 98.36$ ft./sec. They find that $r_n = 27.96$ in. Their results are shown in Fig. 1. The discrepancy between the value of the

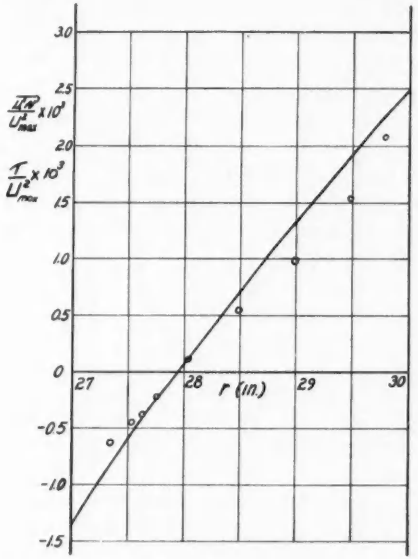

FIG. 1. Radial shear stress distribution for Eskinazi's channel. Full line is total shear stress $\tau/U_{\max}^2$. Points are values of $\overline{u'v'}/U_{\max}^2$.

total stress τ and the value of $\overline{u'v'}$ agrees with that found by Laufer (1951) for the case of straight channel flow.

From equations (21), (22), and (27), one has

$$\frac{\overline{u'v'}}{U_{\max}^2} = \frac{1}{2}\frac{\partial P}{\partial \theta}\frac{1}{\rho U_{\max}^2}\left(\frac{r_n^2}{r^2} - 1\right) + \Delta, \tag{29}$$

where

$$\Delta = -\frac{\nu C_1}{U_{\max}^2 r^2}\int_{r_n}^{r}\frac{r^2 dr}{(r-R_1)^2} \quad \text{for } R_1 < r < R \tag{30}$$

and

$$\Delta = \frac{\nu C_2}{U_{\max}^2 r^2}\int_{r_n}^{r}\frac{r^2 dr}{(R_2-r)^2} \quad \text{for } R < r < R_2. \tag{31}$$

From Eskinazi's mean velocity distribution (see below, and also Fig. 5) one obtains $C_1/U_{\max} = 0.0357$, $C_2/U_{\max} = -0.044$, and $R = 28.75$ in.

(approx.). The distribution of the correction, positive for $r < r_n$, and negative for $r > r_n$, was found to be such as to decrease the error; however with the values of C_1/U_{max} and C_2/U_{max} chosen, the magnitude of Δ is insufficient to account for more than a small fraction of the discrepancy.

HEAT TRANSFER IN CURVED CHANNELS UNDER ZERO TRANSVERSE PRESSURE AND TEMPERATURE GRADIENTS

When $\partial P/\partial\theta = 0$ equation (18) gives

$$(\nu+F_V(r))\left[\frac{\partial}{\partial r}\frac{1}{r}\frac{\partial}{\partial r}(rU)\right] = (\nu+F_V(r))\frac{\partial\zeta}{\partial r} = 0 \tag{32}$$

so that ζ = const. irrespective of $F_V(r)$.

It is verified experimentally (Taylor 1937) that for such flow in the channel between concentric rotating cylinders, $\zeta = 0$, and that in a so-called free vortex, $\zeta = 0$, except in regions near the center of the vortex. One obtains (see equations (21) and (22)) $C_1 = C_2 = 0$ and $\zeta_0 = 0$ so that the constants P_1 and P_2 of equations (25) and (26) are indeterminate, taking the form 0/0.

To overcome this difficulty one will regard this case as the limiting case of channel flow and set

$$P_1 = -\lim_{\partial P/\partial\theta\to 0}\frac{1}{C_1\rho}\frac{\partial P}{\partial\theta} \tag{33}$$

and

$$P_2 = \lim_{\partial P/\partial\theta\to 0}\frac{1}{C_2\rho}\frac{\partial P}{\partial\theta}, \tag{34}$$

where P_1 and P_2 are positive and finite. The eddy diffusivities for vorticity will then be taken as given as before by equations (23) and (24).

Referring to the polar element in Fig. 2 the equation analogous to equation (18) representing the steady state heat condition in a curved channel is

$$\begin{aligned} U\frac{\partial t}{\partial\theta} &= \frac{\partial}{\partial r}\left[(a_H+F_H(r))\,r\frac{\partial t}{\partial r}\right]+\frac{1}{r}\frac{\partial}{\partial\theta}\left[(a_H+F_H(r))\frac{\partial t}{\partial\theta}\right] \\ &= \frac{\partial}{\partial r}\left[(a_H+F_H(r))\,r\frac{\partial t}{\partial r}\right]+\frac{(a_H+F_H(r))}{r}\frac{\partial^2 t}{\partial\theta^2}, \end{aligned} \tag{35}$$

where $F_H(r)$ is the radius-dependent eddy diffusivity for heat analogous to $F_V(r)$ of equation (18).

With $\partial^2 t/\partial\theta^2$ small, equation (35) becomes

$$U\frac{\partial t}{\partial\theta} = \frac{\partial}{\partial r}\left[(a_H+F_H(r))\,r\frac{\partial t}{\partial r}\right]. \tag{36}$$

For rotary annular flow (i.e. such that the liquid flows back into itself), no heat is transferred in the flow direction but only radially through the fluid, and one has

$$\partial t/\partial\theta = 0 \tag{37}$$

and from equation (36)

$$\frac{\partial}{\partial r}\left[(a_H+F_H(r))\,r\frac{\partial t}{\partial r}\right] = 0. \tag{38}$$

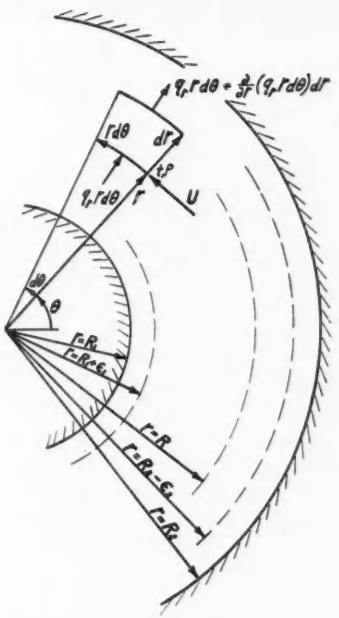

FIG. 2. Channel parameters and polar element.

It is seen that equation (38) does not involve the mean radial velocity distribution.

Integrating equation (38) one has

$$(a_H + F_H(r))\ \partial t/\partial r = T/r, \tag{39}$$

where T is independent of r. Neglecting a_H in comparison with $F_H(r)$ one has

$$\partial t/\partial r = T/F_H(r)r, \tag{40}$$

$$t - t_R = T \int_R^r \frac{dr}{F_H(r)r}. \tag{41}$$

Asserting analogy between the eddy diffusivities for heat and vorticity one has from equations (23) and (24), neglecting ν in comparison with $F_V(r)$,

$$F_H(r) = \lambda F_V(r) = \lambda P_1(r-R_1)^2/r = Q_1(r-R_1)^2/r \quad \text{for } R_1 < r < R \tag{42}$$

and

$$F_H(r) = Q_2(R_2-r)^2/r \quad \text{for } R < r < R_2. \tag{43}$$

λ being taken as a positive constant, Q_1 and Q_2 are positive constants.

Continuity of $F_H(r)$ at $r = R$ yields

$$\frac{Q_1}{Q_2} = \left[\frac{R_2-R}{R-R_1}\right]^2. \tag{44}$$

By equations (40), (42), and (43) one has

$$(45)\quad t-t_R = \frac{T}{Q_1}\int_R^r \frac{dr}{(r-R_1)^2} = \frac{T}{Q_1(R-R_1)}\left[\frac{r-R}{r-R_1}\right] \quad \text{for } R_1 < r < R$$

and

$$(46)\quad t-t_R = \frac{T}{Q_2}\int_R^r \frac{dr}{(R_2-r)^2} = \frac{T}{Q_2(R_2-r)}\left[\frac{r-R}{R_2-r}\right] \quad \text{for } R < r < R_2.$$

For the particular case of constant eddy diffusivity for heat one has

$$(47)\qquad t-t_R = \frac{T'}{F_H}\log\frac{r}{R}, \quad R_1 < r < R_2,$$

where T' and F_H are constant.

Using equation (44) to eliminate Q_2 from equation (46) one has

$$(45a)\qquad (t-t_R)\left(\frac{Q_1}{T}\right) = \frac{1}{R-R_1}\left[\frac{r-R}{r-R_1}\right] \quad \text{for } R_1 < r < R$$

and

$$(46a)\qquad (t-t_R)\left(\frac{Q_1}{T}\right) = \frac{1/(R-R_1)^2}{R_2-R}\left[\frac{r-R}{R_2-r}\right] \quad \text{for } R < r < R_2.$$

T may be identified with the radial heat flux across the annulus, see equation (58) below, and there is evidence that Q_1 and Q_2 depend linearly on U_m (Marris 1956), see below, section "Nusselt modulus". It follows that there is only the one radius-dependent quantity, Q_1/U_m, to be determined by experiment.

Taylor's (1937) experimental results for flow under zero transverse temperature and pressure gradients in the annulus between concentric rotating cylinders of radii $R_1 = 1.865$ cm. and $R_2 = 3.745$ cm. are shown as curve 1 of Fig. 3. The mean velocity distribution is given by Ur = const. over the region

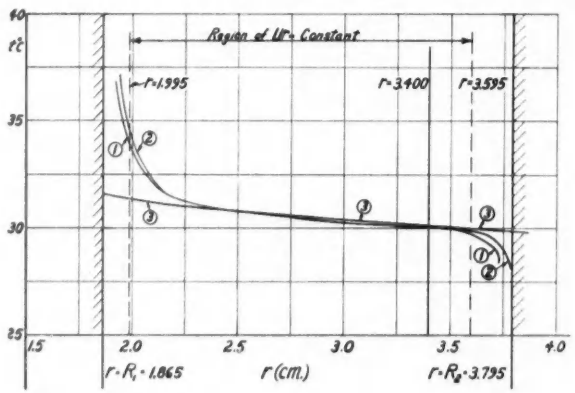

FIG. 3. Radial temperature distribution for flow under zero transverse temperature and pressure gradients.
Curve 1. Taylor's experimental distribution.
Curve 2. Distribution calculated from equations (50) and (51).
Curve 3. Distribution calculated from equation (52), case constant F_H.

(48) $$1.995 < r < 3.595.$$

Taking

(49) $$R = 3.4 \text{ cm.}, \qquad t_R = 30.05° \text{ C.}, \qquad T/Q_1 = -0.617,$$

one has by equation (45*a*)

(50) $$t-30.05 = -\frac{0.617}{3.400-1.865}\left[\frac{r-3.400}{r-1.865}\right] = 0.402\left[\frac{3.400-r}{r-1.865}\right] \quad \text{for } 1.865 < r < 3.400$$

and by equation (46*a*)

(51) $$t-30.05 = -0.103\left[\frac{r-3.400}{3.795-r}\right] \quad \text{for } 3.40 < r < 3.795.$$

Curve 2 of Fig. 3 is calculated from equations (50) and (51). The calculated curve is seen to fit the experimental curve well except in a region immediately adjacent to the outside wall of the annulus.

The constancy of Ur would seem to require that the turbulence be statistically isotropic (a necessary condition for equation (18) to hold). One would also think statistical isotropy necessary for the analogy relative F_H/F_V = constant. It would therefore seem reasonable to expect equations (50) and (51) to fail outside the region Ur = const.

Also on Fig. 3 is shown for reference the temperature distribution obtained from

(52) $$t-t_R = 2.44 \log(r/3.4), \quad 1.865 < r < 3.795 \text{ cm.},$$

i.e. from equation (47) with $T'/F_H = 2.44$, for constant diffusivity. The distribution is seen to be generally too flat and to fall well below the experimental distribution for almost a third of the channel width.

NUSSELT MODULUS FOR FLOW IN CIRCULAR CHANNEL UNDER ZERO PRESSURE GRADIENT

The Nusselt moduli for heat transfer for the case of the Couette flow between concentric cylinders (or for "free" vortex) will be defined by

(53) $$\text{Nu}_1 = \frac{q_{R_1}(R_2-R_1)}{k(t_{R_1}-t_{R_2})},$$

(54) $$\text{Nu}_2 = \frac{q_{R_2}(R_2-R_1)}{k(t_{R_1}-t_{R_2})},$$

where q_{R_1} and q_{R_2} are the quantities of heat per second per unit area being transferred radially across the solid boundaries $r = R_1$, $r = R_2$, respectively, t_{R_1} and t_{R_2} are the temperatures of these boundaries, and k is the molecular thermal conductivity of the fluid.

It must be noted that equations (53) and (54) are not the conventional definitions (Kreith 1955) of Nusselt moduli in that total temperature difference between the channel walls is employed rather than the difference between a wall temperature and the mean flow temperature. The above definitions are employed in order to maintain symmetry and simplicity in the analysis and at the same time produce expressions for experimentally measurable quantities.

One has

$$q_r/s\rho = -(a_H + F_H(r))\partial t/\partial r, \qquad a_H = k/s\rho, \tag{55}$$

and equation (55) will hold for all r such that $R_1 < r < R_2$, when a suitable form is given to $F_H(r)$.

Also (by considering no heat accumulation in the polar element of Fig. 2)

$$U\frac{\partial t}{\partial \theta} = -\frac{1}{s\rho}\frac{\partial (rq_r)}{\partial r}. \tag{56}$$

(Equation (56) of course follows from equations (36) and (55).)

For the case being considered, $\partial t/\partial\theta = 0$, so that from equation (56)

$$rq_r = \text{const.} = R_1 q_{R_1} = R_2 q_{R_2} = -s\rho T \text{ (see equation (39))} \tag{57}$$

and also

$$R_1 \mathrm{Nu}_1 = R_2 \mathrm{Nu}_2. \tag{58}$$

It will be assumed that the inner cylinder (of radius R_1) rotates with peripheral velocity U_1 (i.e. angular velocity U_1/R_1) and the outer cylinder (radius R_2) is at rest.

Except in the case of liquid metals the value of the Nusselt modulus is governed largely by the thickness of the layers of laminar flow adjacent to the boundaries. Buffer layers will not be considered in the present analysis. The flow channel is considered to be divided into four regions as follows (see Fig. 2) with the velocity and temperature distributions as given.

(*1*) *Inner Boundary* $R_1 < r < R_1 + \epsilon_1$

$$U = U_1 R_1/r \tag{59}$$

$$t = t_{R_1} - q_{R_1}(r - R_1)/k \tag{60}$$

(*2*) *Turbulent Region, Inner Section* $R_1 + \epsilon_1 < r < R$

$$U = D/r \tag{61}$$

$$t = t_R + \frac{T}{Q_1(R - R_1)}\left[\frac{r - R}{r - R_1}\right] \tag{62}$$

(*3*) *Turbulent Region, Outer Section* $R < r < R_2 - \epsilon_2$

$$U = D/r \tag{63}$$

$$t = t_R + \frac{T}{Q_2(R_2 - r)}\left[\frac{r - R}{R_2 - r}\right] \tag{64}$$

(*4*) *Outer Boundary* $R_2 - \epsilon_2 < r < R_2$

$$U = 0 \text{ (approx.)} \tag{65}$$

$$t = t_{R_2} + q_{R_2}(R_2 - r)/k \tag{66}$$

One then has by equations (60), (62), (64), and (66)

$$\begin{aligned} t_{R_1} - t_{R_2} &= (t_{R_1} - t_{R_1 + \epsilon_1}) + (t_{R_1 + \epsilon_1} - t_R) + (t_R - t_{R_2 - \epsilon_2}) + (t_{R_2 - \epsilon_2} - t_{R_2}) \\ &= \frac{q_{R_1}}{k}\epsilon_1 + \frac{T}{Q_1(R - R_1)}\left[\frac{R_1 - R}{\epsilon_1}\right] - \frac{T}{Q_2(R_2 - R)}\left[\frac{R_2 - R}{\epsilon_2}\right] + \frac{q_{R_2}}{k}\epsilon_2, \end{aligned} \tag{67}$$

where $(R_1+\epsilon_1)-R$ and $(R_2-\epsilon_2)-R$ are written as R_1-R and R_2-R respectively. Using equation (57) one has

$$(68)\qquad t_{R_1}-t_{R_2} = \left[\epsilon_1+\frac{R_1\epsilon_2}{R_2}\right]\frac{q_{R_1}}{k}+\left[\frac{1}{Q_1\epsilon_1}+\frac{1}{Q_2\epsilon_2}\right]\frac{R_1 q_{R_1}}{s}$$
$$= \left[\epsilon_2+\frac{R_2\epsilon_1}{R_1}\right]\frac{q_{R_2}}{k}+\left[\frac{1}{Q_1\epsilon_1}+\frac{1}{Q_2\epsilon_2}\right]\frac{R_2 q_{R_2}}{s}.$$

By equations (59), (55), and (68) one obtains for the Nusselt moduli

$$(69)\qquad \mathrm{Nu}_1 = \frac{R_2-R_1}{\left[\epsilon_1+\frac{R_1}{R_2}\epsilon_2\right]+\left[\frac{1}{Q_1\epsilon_1}+\frac{1}{Q_2\epsilon_2}\right]a_H R_1},$$

$$(70)\qquad \mathrm{Nu}_2 = \frac{R_2-R_1}{\left[\epsilon_2+\frac{R_2}{R_1}\epsilon_1\right]+\left[\frac{1}{Q_1\epsilon_1}+\frac{1}{Q_2\epsilon_2}\right]a_H R_2},$$

and

$$(58)\qquad R_1\mathrm{Nu}_1 = R_2\mathrm{Nu}_2.$$

Equations (69) and (70) show the very great dependence of Nu_1 and Nu_2 on the boundary layer thicknesses ϵ_1 and ϵ_2. These must now be investigated.

For case of flow through a channel with $\partial P/\partial\theta \neq 0$, one would have

$$(23)\qquad F_{V_1} = -\nu+P_1(r-R_1)^2/r, \quad R_1+\epsilon_1 < r < R,$$

$$(24)\qquad F_{V_2} = -\nu+P_2(R_2-r)^2/r, \quad R < r < R_2-\epsilon_2,$$

and

$$(25)\qquad P_1 = -\frac{1}{C_1\rho}\frac{\partial P}{\partial\theta},$$

$$(26)\qquad P_2 = \frac{1}{C_2\rho}\frac{\partial P}{\partial\theta},$$

where P_1 and P_2 are both positive. One has

$$(71)\qquad \frac{F_{V_1}}{\nu} = \frac{P_1(r-R_1)^2}{\nu r}-1 \quad \text{for } R_1+\epsilon_1 < r < R,$$

$$(72)\qquad \frac{F_{V_2}}{\nu} = \frac{P_2(R_2-r)^2}{\nu r}-1 \quad \text{for } R < r < R_2-\epsilon_2,$$

or, near the boundaries,

$$(73)\qquad \frac{F_{V_1}}{\nu} = \frac{P_1R_1}{\nu}\left(1-\frac{R_1}{r}\right)^2-1,$$

$$(74)\qquad \frac{F_{V_2}}{\nu} = \frac{P_2R_2}{\nu}\left(1-\frac{r}{R_2}\right)^2-1,$$

and it is seen that for regions of negative F_{V_1} and F_{V_2} to be excluded then

$$(75)\qquad \frac{r}{R_1} > 1+\sqrt{\nu/P_1R_1}, \quad \text{i.e. } r > R_1+\sqrt{R_1\nu/P_1},$$

and

$$\frac{r}{R_2} < 1-\sqrt{\nu/P_2R_2}\,, \quad \text{i.e. } r < R_2-\sqrt{R_2\nu/P_2}\,. \tag{76}$$

These boundary regions of negative F_V would seem to be incompatible with any physical conception of the turbulent mixing process, so that equations (73) and (74) are to be considered valid only outside this range.

One therefore postulates boundary layers at least as thick as these regions of negative F_V and takes

$$\epsilon_1 = \sqrt{R_1\nu/P_1}\,, \tag{77}$$

$$\epsilon_2 = \sqrt{R_2\nu/P_2}\,. \tag{78}$$

In further justification of equations (77) and (78) it may be remarked that in the case of rectilinear turbulent flow through a circular pipe, the relegation of the region for which the eddy diffusivity for momentum is negative into the boundary layer yields a boundary layer whose thickness seems to depend on Reynolds number in the experimentally required way (Marris 1954).

Taking $P_1 = \lambda Q_1$, $P_2 = \lambda Q_2$, and assuming that the foregoing argument holds in the limiting case of zero pressure gradient, one writes

$$\epsilon_1 = \sqrt{R_1\nu/\lambda Q_1}, \tag{77a}$$

$$\epsilon_2 = \sqrt{R_2\nu/\lambda Q_2}, \tag{77b}$$

and so

$$\mathrm{Nu}_1 = \frac{(R_2-R_1)\,\nu^{-\frac{1}{2}}}{\left[\left(\frac{R_1}{\lambda}\right)^{\frac{1}{2}}+\frac{1}{N_{\mathrm{Pr}}}(\lambda R_1)^{\frac{1}{2}}\right]\left[\frac{1}{Q_1^{\frac{1}{2}}}+\left(\frac{R_1}{R_2}\right)^{\frac{1}{2}}\frac{1}{Q_2^{\frac{1}{2}}}\right]}, \tag{79}$$

or if λ is taken as unity

$$\mathrm{Nu}_1 = \frac{(R_2-R_1)\,\nu^{-\frac{1}{2}}}{R_1^{\frac{1}{2}}\left[1+\frac{1}{N_{\mathrm{Pr}}}\right]\left[\frac{1}{Q_1^{\frac{1}{2}}}+\left(\frac{R_1}{R_2}\right)^{\frac{1}{2}}\frac{1}{Q_2^{\frac{1}{2}}}\right]}, \tag{80}$$

where $N_{\mathrm{Pr}} = \nu/a_H = s\mu/k$ is the Prandtl modulus. Also

$$\mathrm{Nu}_2 = (R_1/R_2)\mathrm{Nu}_1. \tag{58}$$

Equations (79) and (80) may be tentatively developed a little further. For flow past a rectilinear boundary it can be shown that the adjacent-to-boundary region in which the eddy diffusivity for vorticity becomes negative is $O\sqrt{N/(h/\nu)\sqrt{(\tau_0/\rho)}}$, where N is constant in von Kármán's velocity distribution law, h is the channel depth, τ_0 is the shear at the boundary, and for fully developed turbulence the shear velocity $\sqrt{\tau_0/\rho}$ is proportional to U_m. For this case then

$$\epsilon = O\sqrt{\frac{N'}{h}\,\frac{\nu}{U_m}}\,.$$

A similar result holds for the necessary boundary layer thickness when the vorticity transfer theory is applied to flow in a pipe of circular section (Marris

1954). These results can be identified with equations (77*a*) and (77*b*) if Q_1 and Q_2 contain the mean flow velocity U_m as a factor.

For the case of pressure flow in a channel $\partial P/\partial\theta$ is proportional to U_m^2 provided the Reynolds number is high enough. The fact that the velocity distribution obtained by integrating the vorticity distribution (from which C_1 and C_2 were derived) is capable of being fitted to experimental distributions for varying U_m when the velocity is expressed by the quotient U/U_m would indicate that C_1 and C_2 contain U_m as a factor (Marris 1956). Thus it again follows that Q_1 and Q_2 are each proportional to U_m.

The final justification for believing Q_1 and Q_2 contain U_m as a linear factor is that the kinematic viscosity ν would be expected to occur in equations (77) and (79) in the Reynolds number grouping.

Writing

$$Q_1 = Q_1' U_m, \tag{81}$$

$$Q_2 = Q_2' U_m, \tag{82}$$

where Q_1' and Q_2' are functions of R_1 and R_2 alone, equation (80) now becomes

$$\mathrm{Nu}_1 = \frac{\left(\frac{R_2}{R_1}-1\right)^{\frac{1}{4}} N_{\mathrm{Re}}^{\frac{1}{4}}}{\left(1+\frac{1}{N_{\mathrm{Pr}}}\right)\left[\frac{1}{Q_1'^{\frac{1}{4}}}+\left(\frac{R_1}{R_2}\right)^{\frac{1}{4}}\frac{1}{Q_2'^{\frac{1}{4}}}\right]}, \tag{83}$$

where Q_1' and Q_2' are independent of U_m and functions only of the radii.

It follows that for a given channel

$$\mathrm{Nu}_1 = \frac{Z N_{\mathrm{Re}}^{\frac{1}{4}} N_{\mathrm{Pr}}}{(1+N_{\mathrm{Pr}})}, \qquad \mathrm{Nu}_2 = \frac{R_2}{R_1}\mathrm{Nu}_1, \tag{84}$$

where Z is a function of the radii, and that for low Prandtl number (liquid metals) Nu_1, Nu_2 vary as $N_{\mathrm{Re}}^{\frac{1}{4}} N_{\mathrm{Pr}}$.

TEMPERATURE DISTRIBUTION FOR TURBULENT HEAT TRANSFER FOR TWO-DIMENSIONAL PRESSURE FLOW IN A CHANNEL OF CONSTANT RADIUS OF CURVATURE

From equations (21) and (22) for the radial vorticity distribution for two-dimensional curved channel flow, one has

$$\frac{1}{r}\frac{\partial}{\partial r}(rU) = \frac{C_1}{r-R_1} \quad \text{for } R_1 < r < R \tag{85}$$

and

$$\frac{1}{r}\frac{\partial}{\partial r}(rU) - \zeta_0 = \frac{C_2}{R_2-r} \quad \text{for } R < r < R_2. \tag{86}$$

Integrating equations (85) and (86) one obtains for the mean radial velocity distribution across the channel

$$U = C_1\left[1+\frac{R_1 \log(r-R_1)}{r}\right]+\frac{D_1}{r} \quad \text{for } R_1 < r < R \tag{87}$$

and

$$(88) \qquad U = -C_2\left[1+\frac{R_2\log(R_2-r)}{r}\right]+\frac{\zeta_0 r}{2}+\frac{D_2}{r} \quad \text{for } R < r < R_2.$$

Like the eddy diffusivities (equations (23) and (24)) these velocity distributions have their origin in the experimentally observed vorticity distribution and must be regarded as empirical on this account. They were derived previously (Marris 1956) on a mixing length basis analogous to that used by von Kármán and Goldstein for flow in straight pipes and rectilinear channels, a way which showed that a reasonable assumption concerning the dependence of mixing length on channel curvature would give rise on Prandtl's hypothesis to the eddy diffusivities and consequent vorticity distribution. One can say perhaps that the status of the mean velocity distributions is thus raised from empirical to semiempirical, and hope that sometime the mixing lengths referred to may be approximately deducible from fundamental considerations.

The velocity distributions of equations (87) and (88), while they must fail in the immediate vicinity of the channel walls, giving velocities of minus infinity instead of zero, seem however capable of being fitted to experimentally observed velocity distributions for channels of relatively small radius of curvature, the fit breaking down at the inner wall of a 2 inch wide channel when the radius of curvature exceeds about 2 feet (Marris 1956).

That the functional form of F_V allows such a fit for small radius of curvature, and the same functional form F_H gives a radial temperature distribution in agreement with experiment for the Couette channel of small radius, would seem to be justification for taking the analogy parameter $\lambda = F_H/F_V$ as independent of r.

Considering now the temperature distribution in the curved channel, one has by equation (36), neglecting the molecular diffusivity a_H,

$$(89) \qquad U\frac{\partial t}{\partial \theta} = \frac{\partial}{\partial r}\left[F_H(r)\, r\, \frac{\partial t}{\partial r}\right]$$

and from equations (87) and (88) for the heat transfer case

$$(90) \qquad \left[C_1\left[1+\frac{R_1\log(r-R_1)}{r}\right]+\frac{D_1}{r}\right]\frac{\partial t}{\partial \theta} = \frac{\partial}{\partial r}\left[F_H(r)\, r\, \frac{\partial t}{\partial r}\right] \quad \text{for } R_1 < r < R,$$

$$(91) \qquad \left[-C_2\left[1+\frac{R_2\log(R_2-r)}{r}\right]+\frac{\zeta_0 r}{2}+\frac{D_2}{r}\right]\frac{\partial t}{\partial \theta} = \frac{\partial}{\partial r}\left[F_H(r)\, r\, \frac{\partial t}{\partial r}\right] \text{ for } R<r<R_2.$$

There seems to be experimental evidence that F_V, C_1, D_1, C_2, D_2, ζ_0 depend linearly on the mean flow velocity U_m provided U_m is great enough to ensure fully developed turbulence (Marris 1956; Wattendorf 1935). Thus it is possible to fit equations (87) and (88) with experiment when they are divided through by U_m to give similar expressions for U/U_m (Wattendorf 1935). The fact that F_V and ζ depend linearly on U_m is further indicated by equations (27) and (28) and from the experimental fact that a continuous experimental plot of $\overline{u'v'}/U_m^2$ for varying U_m is obtainable (see equation (28)). Equations (90) and (91) can thus be written

$$(92)\quad \left[A_1\left[1+\frac{R_1\log(r-R_1)}{r}\right]+\frac{Br}{r}\right]U_m\frac{\partial t}{\partial\theta}=\frac{\partial}{\partial r}\left[F_H(r)\,r\,\frac{\partial t}{\partial r}\right]\quad \text{for } R_1<r<R$$

and

$$(93)\quad \left[A_2\left[1+\frac{R_2\log(R_2-r)}{r}\right]+\frac{B_2}{r}+E_2r\right]U_m\frac{\partial t}{\partial\theta}=\frac{\partial}{\partial r}\left[F_H(r)\,r\,\frac{\partial t}{\partial r}\right]$$

$$\text{for } R<r<R_2,$$

where

$$(94)\quad A_1=\frac{C_1}{U_m},\qquad B_1=\frac{D_1}{U_m},\qquad A_2=-\frac{C_2}{U_m},\qquad B_2=\frac{D_2}{U_m},\qquad E_2=\frac{\zeta_0}{2U_m},$$

and A_1, B_1, A_2, B_2, E_2 are all positive functions of the channel radii.

From equations (92) and (93) one obtains

$$(95)\quad F_H(r)\,r\,\frac{\partial t}{\partial r}=U_m\frac{\partial t}{\partial\theta}\int_R^r\left[A_1\left[1+\frac{R_1\log(r-R_1)}{r}\right]+\frac{B_1}{r}\right]dr\quad \text{for } R_1<r<R,$$

$$(96)\quad F_H(r)\,r\,\frac{\partial t}{\partial r}=U_m\frac{\partial t}{\partial\theta}\int_R^r\left[A_2\left[1+\frac{R_2\log(R_2-r)}{r}\right]+\frac{B_2}{r}+E_2r\right]dr$$

$$\text{for } R<r<R_2,$$

taking $\partial t/\partial r$ as zero at $r=R$.

Equations (95) and (96), like equations (87) and (88), fail near the boundaries $r=R_1$, $r=R_2$, because the logarithmic terms become very large negative causing $\dfrac{r\partial t/\partial r}{\partial t/\partial\theta}$ to become negative.

The constants A_1 and A_2 in the velocity distribution are small compared with B_1 and B_2 (E_2 is also small), and the velocity in the center region of the stream is very nearly given by $V=k/r$ as in the case of flow in an annulus under zero pressure gradient. The effect of the terms $A_1R_1\log(r-R_1)/r$ and $A_2R_2\log(R_2-r)/r$ is negligible in the center region of the stream but they become large negative in the vicinity of the boundaries of the region, cancelling out the positive terms in the expression and thereby causing the rapid decrease in U at the boundaries.

Whereas these terms could be integrated in series, it is considered that the boundary velocity distribution is too uncertain to warrant this arithmetic complication. Instead, the expressions on the right-hand sides of the inequalities

$$(97)\quad \log\left(1-\frac{R_1}{r}\right)>-\frac{R_1}{r-R_1},$$

$$(98)\quad \log\left(1-\frac{r}{R_2}\right)>-\frac{r}{R_2-r}$$

will be used instead of the logarithm terms to represent the velocity decay at the boundaries.

For $R_1<r<R$, by equation (95),

$$F_H(r)\, r \frac{\partial t}{\partial r} = U_m \frac{\partial t}{\partial \theta} \int_R^r \left[A_1 + \frac{B_1}{r} + \frac{A_1 R_1}{r} \left(\log\left(1 - \frac{R_1}{r}\right) + \log r \right) \right] dr$$

$$(99) \qquad = U_m \frac{\partial t}{\partial \theta} \left[A_1(r-R) + \frac{A_1 R_1}{2} \left(\log \frac{r}{R} \right)^2 + (B_1 + A_1 R_1 + A_1 R_1 \log R) \log \frac{r}{R} - A_1 R_1 \log \frac{r - R_1}{R - R_1} \right]$$

and for $R < r < R_2$, by equation (96),

$$F_H(r)\, r \frac{\partial t}{\partial r} = U_m \frac{\partial t}{\partial \theta} \int_R^r \left[A_2 + \frac{B_2}{r} + E_2 r + \frac{A_2 R_2}{r} \left(\log\left(1 - \frac{r}{R_2}\right) + \log R_2 \right) \right] dr$$

$$(100) \qquad = U_m \frac{\partial t}{\partial \theta} \left[A_2(r-R) + \frac{E_2}{2}(r^2 - R^2) + (B_2 + A_2 R_2 \log R_2) \log \frac{r}{R} + A_2 R_2 \log \frac{R_2 - r}{R_2 - R} \right].$$

Setting

$$(42) \quad F_H(r) = \lambda F_V(r) = Q_1(r - R_1)^2/r = Q_1' U_m (r - R_1)^2/r \quad \text{for } R_1 < r < R$$

and

$$(43) \quad F_H(r) = Q_2(r - R_2)^2/r = Q_2' U_m (r - R_2)^2/r \quad \text{for } R < r < R_2$$

and neglecting the small and slowly varying term $\frac{1}{2} A_1 R_1 (\log r/R)^2$ in equation (99), one obtains from equations (99) and (100) the expressions for radial mean temperature gradient

$$(101) \quad t - t_R \Big/ \frac{1}{Q_1'} \frac{\partial t}{\partial \theta} = I_1 =$$

$$\int_R^r \frac{A_1(r-R) + (B_1 + A_1 R_1 + A_1 R_1 \log R) \log (r/R) - A_1 R_1 \log [(r - R_1)/(R - R_1)]}{(r - R_1)^2}\, dr$$

for $R_1 < r < R$

and

$$(102) \quad t - t_R \Big/ \frac{1}{Q_2'} \frac{\partial t}{\partial \theta} = I_2 = \int_R^r \left(\frac{A_2(r-R) + \frac{1}{2} E_2 (r^2 - R^2)}{(R_2 - r)^2} + \frac{(B_2 + A_2 R_2 \log R_2) \log (r/R) + A_2 R_2 \log [(R_2 - r)/(R_2 - R)]}{(R_2 - r)^2} \right) dr$$

for $R < r < R_2$.

Evaluating the integrals I_1 and I_2, one obtains

$$(103) \quad t - t_R \Big/ \frac{1}{Q_1'} \frac{\partial t}{\partial \theta} = \left(\alpha_1 + \frac{\beta_1}{r - R_1} \right) \log \frac{r - R_1}{R - R_1} + \gamma_1 \frac{R - r}{r - R_1} + \delta_1 \frac{r}{R_1 - r} \log \frac{r}{R} \quad \text{for } R_1 < r < R,$$

where

$$(104)\qquad \begin{cases} \alpha_1 = A_1(2+\log R)+\dfrac{B_1}{R_1}, \\ \beta_1 = A_1R_1, \\ \gamma_1 = A_1\left[\dfrac{R-2R_1}{R-R_1}\right], \\ \delta_1 = A_1(1+\log R)+\dfrac{B_1}{R_1} = \alpha_1-A_1, \end{cases}$$

and

$$(105)\qquad t-t_R \Big/ \frac{1}{Q_2'}\frac{\partial t}{\partial \theta} = \left(\alpha_2+\frac{\beta_2}{R_2-r}\right)\log\frac{R_2-r}{R_2-R}+\gamma_2\frac{r-R}{R_2-r}+\delta_2\frac{r}{R_2-r}\log\frac{r}{R}+\phi_2\frac{(r-R)^2}{(R_2-r)} \qquad \text{for } R<r<R_2,$$

where

$$(106)\qquad \begin{cases} \alpha_2 = E_2R_2+A_2(1+\log R_2)+\dfrac{B_2}{R_2}, \\ \beta_2 = A_2R_2, \\ \gamma_2 = \dfrac{A_2(2R_2-R)}{R_2-R}+E_2R_2, \\ \delta_2 = A_2\log R_2+\dfrac{B_2}{R_2} = \alpha_2-A_2-E_2R_2, \\ \phi_2 = -\tfrac{1}{2}E_2. \end{cases}$$

CORRELATION WITH EXPERIMENTAL DATA

The mean radial velocity distributions given by equations (87) and (88) are fitted to the experimental distribution of Wattendorf (1935) for water flow in a channel for which $R_1 = 20$ cm., $R_2 = 25$ cm., and $R = 23$ cm. (approximately), and to the recently obtained distribution of Eskinazi and Yeh (1956) for air flow in a channel with $R_1 = 27$ in., $R_2 = 30$ in., and $R = 28.75$ in. (approximately).

For Wattendorf's channel one has for the ratio of the mean velocity at r to the mean flow velocity (Marris 1956)

$$(107)\qquad \begin{cases} \dfrac{U}{U_m} = 0.0766+\dfrac{3.527}{r}\log_{10}(r-20)+\dfrac{20.7}{r} & \text{for } 20<r<23, \\ \dfrac{U}{U_m} = 0.0596+\dfrac{3.431}{r}\log_{10}(25-r)+0.02373r+\dfrac{9.20}{r} & \text{for } 23<r<25, \end{cases}$$

so that $A_1 = C_1/U_m = 0.0766$, $B_1 = D_1/U_m = 20.7$, $A_2 = -C_2/U_m = 0.0596$, $B_2 = \zeta_0/2U_m = 0.02373$, and $E_2 = D_2/U_m = 9.2$.

The plot of equation (107) together with Wattendorf's experimental results is shown in Fig. 4.

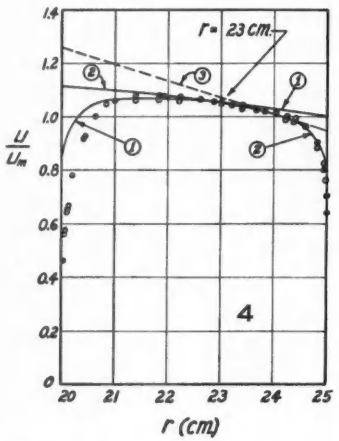

FIG. 4. Radial velocity distribution for Wattendorf's channel.
Curves 1 and 2. Plot of equation (107).
Curve 3. $U/U_m = 25/r$.
Points are Wattendorf's experimental readings.

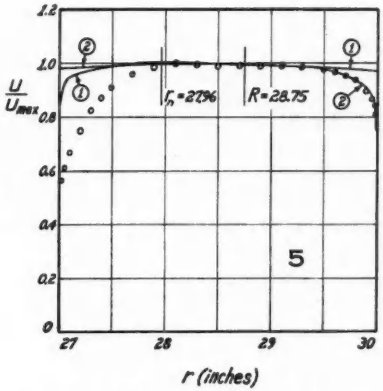

FIG. 5. Radial velocity distribution for Eskinazi's channel.
Curves 1 and 2. Plot of equation (108).
Points are Eskinazi's experimental readings.

For Eskinazi's channel one has for the ratio of the mean velocity at r to the maximum velocity

$$(108)\quad \begin{cases} \dfrac{U}{U_{\max}} = 0.0357+\dfrac{2.220}{r}\log_{10}(r-27)+\dfrac{27}{r} & \text{for } 27 < r < 28.75, \\ \dfrac{U}{U_{\max}} = 0.0440+\dfrac{3.040}{r}\log_{10}(30-r)+0.03202r+\dfrac{0.479}{r} & \text{for } 28.75<r<30, \end{cases}$$

so that $C_1/U_{\max} = 0.0357$, $D_1/U_{\max} = 27$, $C_2/U_{\max} = -0.044$, $\zeta_0/2U_{\max} = 0.03202$, and $E_2/U_{\max} = 0.479$.

The plot of equation (108) together with Eskinazi's experimental results is shown in Fig. 5.

Comparing Figs. 4 and 5 it is seen that the present theory fails near the linear boundary when the radius of curvature becomes large. This was remarked on previously (Marris 1956), the same having been found to be true when the theory was correlated to Wattendorf's experimental data for a channel of larger radius of curvature.

Eskinazi's distribution can be fitted in the region adjacent to the inner wall by taking a larger value of $C_1/U_{\max}$, say $C_1/U_{\max} = 0.1416$, but only at the expense of the fit in the center region of the channel.

Owing to unavailability of data it is not possible to compare the temperature distribution given by equations (103) to (106) directly with experimental data. What will be done instead will be to employ the Wattendorf channel quoted above, for which the most satisfactory over-all fit is obtained for the mean velocity distribution, and determine the temperature distribution that would occur in it.

Using the above values of A_1, B_1, A_2, B_2, and E_2 the radial temperature distribution given by equations (103) and (105) becomes, for this channel,

$$(109)\quad t-t_R \Big/ \frac{1}{Q_1'}\frac{\partial t}{\partial \theta}$$

$$= \left(3.290+\frac{3.528}{r-20}\right)\log_{10}\frac{r-20}{3}-0.4341\left(\frac{23-r}{r-20}\right)+\frac{3.120}{r-20}\,r\log_{10}\frac{23}{r} \quad \text{for } 20<r<23$$

and

$$(110)\quad t-t_R \Big/ \frac{1}{Q_2'}\frac{\partial t}{\partial \theta}$$

$$= \left(2.802+\frac{3.431}{25-r}\right)\log_{10}\frac{25-r}{2}+1.398\,\frac{r-23}{25-r}+1.2920\,\frac{r}{25-r}\log_{10}\frac{r}{23}$$

$$-0.0119\,\frac{(r-23)^2}{25-r} \quad \text{for } 23 < r < 25.$$

The radial temperature distribution as calculated from equations (109) and (110) is shown in Fig. 6. The distribution fails near the outside boundary $r = R_2$ owing to the velocity distribution (88) giving $U = -\infty$ at $r = R_2$. The error would seem to include all r such that $24 < r < 25$. The extrapolated temperature distribution is shown by the dotted curve.

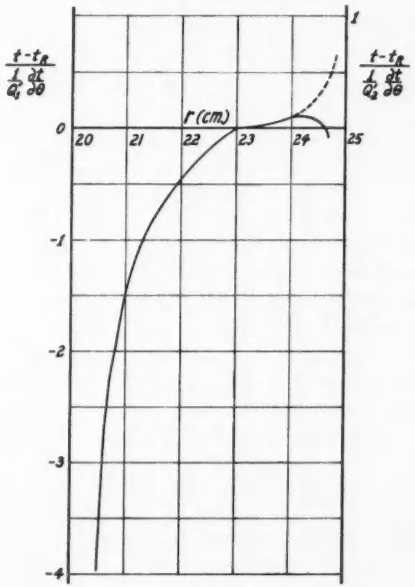

FIG. 6. Radial temperature distribution as calculated from equations (109) and (110), for non-zero transverse temperature and pressure gradients. Extrapolated curve near outer boundary is shown dotted.

Using equations (44), (45), and (46) for the case of flow under zero transverse temperature and pressure gradients, for this case also, one would write

$$t-t_R \Big/ \frac{1}{Q_1'}\frac{\partial t}{\partial \theta} = \frac{g}{(R-R_1)}\left[\frac{r-R}{r-R_1}\right] \quad \text{for } R_1 < r < R \tag{111}$$

and

$$t-t_R \Big/ \frac{1}{Q_2'}\frac{\partial t}{\partial \theta} = \frac{g}{R_2-R}\left[\frac{r-R}{R_2-R}\right] \quad \text{for } R < r < R_2, \tag{112}$$

where

$$g = \frac{T}{U_m}\frac{1}{\partial t/\partial\theta} = \frac{-q_r}{s\rho U_m\, \partial t/r\partial\theta} \text{ approx. (see equation (57))} \tag{113}$$

and

$$Q_1 = U_m Q_1', \tag{81}$$

$$Q_2 = U_m Q_2'. \tag{82}$$

For the channel being considered one would then have

$$t-t_R \Big/ \frac{1}{Q_1'}\frac{\partial t}{\partial \theta} = \frac{g}{3}\left[\frac{r-23}{r-20}\right] \quad \text{for } 20 < r < 23, \tag{114}$$

$$t-t_R \Big/ \frac{1}{Q_2'}\frac{\partial t}{\partial \theta} = \frac{g}{2}\left[\frac{r-23}{25-r}\right] \quad \text{for } 23 < r < 25. \tag{115}$$

The temperature distributions given by equations (114) and (115) for $g = 0.15$, 1.5, and 3.0 are shown by curves 2, 3, and 4 of Fig. 7. Curve 1 of Fig. 7 is the distribution as calculated from equations (109) and (110) and is given for reference.

It is seen that in the $R_1 < r < R$ region $t-t_R$ as given by equation (114) is increasingly less than $t-t_R$ as given by equation (109) as g decreases from about 2.25 and that in the outer region of the channel the values of $t-t_R$ as calculated from equation (115) are strikingly greater than the values as calculated from equation (110) for all $g > 0.15$. For $g = 0.15$, the values of $t-t_R$ as calculated from equation (115) and equation (110) are substantially the same until the point of failure of equation (110) is reached.

The conclusion seems to be that the employment of equations (114) and (115) and the foregoing Nusselt modulus analysis to the case of non-zero transverse temperature and pressure gradients would only be possible if g was given two different values, a relatively high value in the inner region of the channel and a low value in the outer region.

SUMMARY AND CONCLUSION

A radial temperature distribution for Couette flow in the annulus between concentric rotating cylinders which agrees satisfactorily with experiment (Taylor 1937) except in the immediate neighborhood of the outer wall of the channel is obtained by using an eddy diffusivity for heat which is a constant times the eddy diffusivity for vorticity which latter yields the velocity distribution for flow in channels of relatively small radius of curvature.

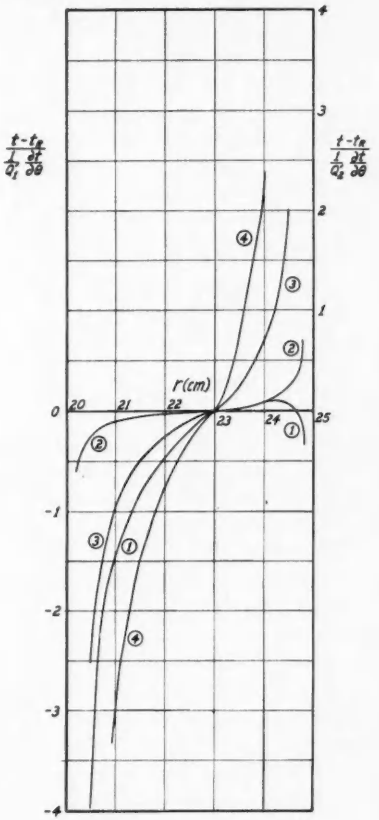

FIG. 7. Radial temperature distribution for non-zero transverse temperature and pressure gradients using equations (114) and (115).
Curve 1. Reference curve as calculated from equations (109) and (110).
Curve 2. $g = 0.15$.
Curve 3. $g = 1.5$.
Curve 4. $g = 3.0$.

The temperature distribution is given by the relatively simple formulae

$$t - t_R = \frac{T}{Q_1(R - R_1)} \left[\frac{r - R}{r - R_1} \right] \quad \text{for } R_1 < r < R, \tag{45}$$

$$t - t_R = \frac{T}{Q_2(R_2 - R)} \left[\frac{r - R}{R_2 - r} \right] \quad \text{for } R < r < R_2, \tag{46}$$

where $r = R$ is a circle dividing the annulus into two regions such that for $R_1 < r < R$ the effect of the inner wall predominates and for $R < r < R_2$ the effect of the outer wall predominates. For the case of flow in a curved channel (see below) for which $\partial t/\partial\theta$ and $\partial P/\partial\theta$ are not zero the point $r = R$ is that at which $\partial t/\partial r = 0$.

The temperature distribution given by equations (45) and (46) is independent of the velocity distribution provided $\partial P/\partial\theta = 0$ but the eddy diffusivities for heat are taken as analogous to eddy diffusivities for vorticity under a condition of isotropic turbulence and therefore it is expected that the temperature distribution could only be valid over the region of isotropic turbulence.

The distributions (45) and (46) agree with experiment over a region somewhat in excess of the region of Ur = constant.

The annulus is then divided into three regions, laminar layer at inside wall, turbulent region, and laminar layer at outside wall, and Nusselt moduli for the channel of the forces,

$$\text{Nu}_1 = \frac{q_{R_1}(R_2-R_1)}{k(t_{R_1}-t_{R_2})}, \tag{53}$$

$$\text{Nu}_2 = \frac{q_{R_2}(R_2-R_1)}{k(t_{R_1}-t_{R_2})}, \tag{54}$$

are defined and constructed on this basis that the laminar boundary layers are of width $O(1/U_m)^{\frac{1}{2}}$. As in the case when the vorticity transfer theory is applied to flow in a pipe (Marris 1954) the laminar layers are shown to be of necessity at least this width in order that the eddy diffusivities do not become negative.

For a given channel the Nusselt modulus of the form given above seems to vary simply as $N_{\text{Re}}{}^{\frac{1}{2}}/(1+1/N_{\text{Pr}})$ where N_{Re} and N_{Pr} are respectively the Reynolds and Prandtl numbers.

The case of turbulent flow through a channel for which $\partial P/\partial\theta$ and $\partial t/\partial\theta$ are not zero is then considered. It is necessary however to assume that $\partial t/\partial\theta$ is independent of r as well as of θ; however there is evidence that this approximation causes but little error (1–2%) away from the boundaries (Marris 1955; Seban and Shimazaki 1951).

The temperature distribution is calculated on the basis of the velocity distribution for the $\partial P/\partial\theta = 0$, $\partial t/\partial\theta = 0$ case. It appears that such an adaptation would require different values for the parameter

$$g = \frac{-q_r}{s\rho U_m\, \partial t/r\partial\theta} \tag{116}$$

for the inner and outer regions of the channel, and on this account would seem to be unsatisfactory.

One closes with a remark concerning the differences in heat transfer coefficients at boundaries convex and concave to the flow.

It is known that for Nusselt moduli defined by

$$\text{Nu}_1' = \frac{q_{R_1}(R_2-R_1)}{k(t_{R_1}-t_m)} \tag{117}$$

for heat flow outwards from the inner (convex) surface and by

$$\text{Nu}_2' = \frac{q_{R_2}(R_2-R_1)}{k(t_{R_2}-t_m)} \tag{118}$$

for heat flow inwards from the outer (concave) surface, then (Kreith 1955):

(119) $$\mathrm{Nu}_2' > \mathrm{Nu}_1'.$$

Consider two points A and B in the turbulent region at distance x from the inner and outer walls respectively, where

(120) $$\epsilon_1, \epsilon_2 < x < R-R_1, R_2-R,$$

i.e. so that

(121) $$r_A = R_1+x,$$

(122) $$r_B = R_2-x.$$

By equations (42) and (43)

(123) $$F_{H_A} = F_H(R_1+x) = \frac{Q_1 x^2}{R_1+x},$$

(124) $$F_{H_B} = F_H(R_2-x) = \frac{Q_2 x^2}{R_2-x},$$

so that

(125) $$\frac{F_{H_B}}{F_{H_A}} = \frac{Q_2(R_1+x)}{Q_1(R_2-x)} = \left[\frac{R-R_1}{R_2-R}\right]^2 \frac{R_1+x}{R_2-x}$$

by equation (44).

It follows that

(126) $$\frac{F_{H_B}}{F_{H_A}} > \frac{R_1}{R_2}\left[\frac{R-R_1}{R_1-R}\right]^2$$

for all x satisfying the inequality (120).

If

(127) $$\frac{R-R_1}{R_2-R} > \sqrt{R_2/R_1},$$

as seems to be the case for a channel of relatively small radius of curvature,

(128) $$F_{H_B}/F_{H_A} > 1$$

and Nu_2' would be expected to be greater than Nu_1'.

ACKNOWLEDGMENTS

This work is part of a program carried out under National Research Council Grant G 514 and under a National Research Council Summer Research Associateship, 1956.

The author expresses his thanks to Professor Eskinazi of Syracuse University for remitting to him his experimental data, and for his interest.

REFERENCES

ESKINAZI, S. and YEH, H. 1956. J. Aeronaut. Sci. **23**, No. 1, 23.
GOLDSTEIN, S. 1938. Modern developments in fluid dynamics (Oxford at the Clarendon Press), p. 214.
——— 1950. Statistical theory of turbulence, Lecture No. 6, Institute for Fluid Dynamics and Applied Mathematics, University of Maryland.
KLEBANOFF, P. S. 1954. Natl. Advisory Comm. Aeronaut. Tech. Note 3178.
KREITH, F. 1955. Trans. ASME, **77**, 1247.
LAUFER, J. 1951. Natl. Advisory Comm. Aeronaut. Rept. 1053.
MARRIS, A. W. 1954. Can. J. Phys. **32**, 419.
——— 1955. Can. J. Technol. **33**, 470.
——— 1956. Can. J. Phys. **34**, 1134.
TAYLOR, G. I. 1937. Proc. Roy. Soc. (London), A, **151**, 496.
SEBAN, R. A. and SHIMAZAKI, T. T. 1951. Trans. ASME, **73**, 803.
WATTENDORF, F. L. 1935. Proc. Roy. Soc. (London), A, **148**, 565.

DIFFUSION IN MULTICOMPONENT METALLIC SYSTEMS[1]

J. S. KIRKALDY

ABSTRACT

Onsager's phenomenological scheme for diffusion in multicomponent liquid systems is examined for suitability as a description of metallic interdiffusion. Subject to certain restrictions and approximations a set of non-linear differential equations is obtained which can be simply applied to important boundary conditions. A solution of the set for the system iron, carbon, silicon is shown to provide a good fit to Darken's experimental results.

1. INTRODUCTION

The present purpose is to find a convenient and concise mathematical framework for the description of interdiffusion in multicomponent metallic solid solutions, for the correlation of available experimental results, and for the calculation of concentration distributions corresponding to simple boundary conditions. The subject of diffusion mechanisms will be introduced only insofar as it might assist in the simplification of the phenomenological equations.

2. ONSAGER'S PHENOMENOLOGICAL SCHEME

Onsager (1945–46) in his consideration of interdiffusion of liquid electrolytes assumed as a generalization of Fick's first law (Fick 1855) that the diffusion current of each component is a linear function of all the concentration gradients. Accordingly, in one dimension,

$$J_i = -\sum_k D'_{ik} \frac{\partial C_k}{\partial x}, \quad (i = 1, 2, \ldots), \tag{1}$$

where the diffusion coefficients D'_{ik} are assumed to be functions of the C_k.

Some authors (Darken 1951; Bardeen and Herring 1951) have expressed the view that the expression

$$J_i = -\sum_k M_{ik} \frac{\partial \mu_k}{\partial x}, \quad (i = 1, 2, \ldots), \tag{2}$$

where the μ_k are the partial molal free energies, is more fundamental since the virtual forces for diffusion are represented as the free energy gradients. Equation (2) has been used successfully by Bardeen and Herring (1951) in the description of radioactive and chemical diffusion in pure metals and binary alloys. However, this form is not very useful for the solution of practical alloy problems since few of the thermodynamic data are available, nor are they easy to obtain. On the other hand, concentration gradients are relatively easy to measure, and it is usually the variation of concentration in diffusion-dependent alloy transformations which we desire. Accordingly, we will focus our attention on equations (1) and investigate methods for their simplification and manipulation.

[1]Manuscript received December 20, 1956.
Contribution from Aluminum Laboratories Limited, Kingston, Ontario, and the Department of Metallurgical Engineering, McGill University, Montreal, Quebec.

In all the discussions it is specified that distance is measured in numbers of lattice planes, that concentration is measured in atoms per unit cell (Birchenall *et al.* 1948), and that the total number of lattice sites is very closely conserved. This specification of concentration units is fundamentally different from the usual ones (mole fraction, g./cm.^{3}, or weight per cent) since it implies that in a binary interstitial solution the solvent atoms have no concentration gradient even though the interstitial solute atoms are distributed non-uniformly. For practical purposes, at small solute concentrations, the four specifications are approximately equivalent.

For simplicity it will be assumed that interstitial components diffuse interstitially and that substitutional components diffuse by a simple exchange mechanism, ignoring thereby the complications involved in a vacancy mechanism and the associated Kirkendall effect.

Consider now an n-component system with r components diffusing interstitially (numbered 1 to r) and $n-r$ components diffusing by an exchange mechanism. In this case equation (1) applies subject to the conditions that

$$\sum_{i=r+1}^{n} J_i = 0 \quad \text{and} \quad \sum_{i=r+1}^{n} C_i = \text{constant}. \tag{3}$$

With these equations, (1) reduces to

$$J_i = -\sum_{k=1}^{n-1} D_{ik} \frac{\partial C_k}{\partial x}, \tag{4}$$

where $D_{ik} = D'_{ik}$, $1 \leqslant k \leqslant r$, and $D_{ik} = D'_{ik} - D'_{in}$, $r+1 \leqslant k \leqslant n-1$. One of the J_i is of course dependent. In agreement with Darken (1951) we see that with a suitable choice of coordinate system we can always reduce the n phenomenological equations for an n-component system involving n^2 diffusion coefficients to $n-1$ equations involving $(n-1)^2$ coefficients.

Onsager (1945–46) demonstrated by invoking his hypothesis of "microscopic reversibility" that for a liquid diffusing system subject to no bulk flow and no pressure gradients, the D'_{ik} can be related to thermodynamic quantities by

$$\sum_j \frac{\partial \mu_i}{\partial C_j} D'_{jk} = \sum_j \frac{\partial \mu_k}{\partial C_j} D'_{ji}. \tag{5}$$

These subsidiary relations allow the further reduction of the number of independent coefficients from $(n-1)^2$ to $n(n-1)/2$. Darken (1951) has recommended the application of the same relationship to metallic systems. This is probably a valid procedure since the usual assumption of conservation of lattice sites is approximately equivalent to Onsager's conditions on liquid diffusion. However, in systems which show porosity and lateral distortion associated with the Kirkendall effect, large pressure gradients have necessarily been present. Consequently, in such cases, some doubt is cast on the applicability of equation (5).

In any case, for the present these equations are of little practical use since none of the required thermodynamic data are available and they are generally quite difficult to measure. We have therefore to treat a system of n components with $n-1$ differential equations involving $(n-1)^2$ diffusion coefficients.

While this might appear quite unmanageable for three components and out of reason for four, we shall see that in special cases the values of the D's are such that major simplifications are possible and accordingly the equations can be manipulated and integrated with reasonable facility.

3. MANIPULATION OF THE DIFFERENTIAL EQUATIONS

If we subject equations (4) for an n-component system to the corresponding continuity equations

$$\frac{\partial J_i}{\partial x}+\frac{\partial C_i}{\partial t}=0, \tag{6}$$

we obtain the $n-1$ simultaneous diffusion equations in one dimension:

$$\frac{\partial C_i}{\partial t}=\sum_{k=1}^{n-1}\frac{\partial}{\partial x}\left[D_{ik}\frac{\partial C_k}{\partial x}\right]. \tag{7}$$

Following a procedure often used in binary diffusion (the Boltzmann–Matano analysis (Boltzmann 1894; Matano 1933)) we seek parametric solutions of the form

$$C_i = C_i(\lambda), \quad \lambda = x/\sqrt{t}, \tag{8}$$

which must satisfy the non-linear ordinary differential equations

$$-\frac{\lambda}{2}\frac{dC_i}{d\lambda}=\sum_{k=1}^{n-1}\frac{d}{d\lambda}\left[D_{ik}\frac{dC_k}{d\lambda}\right]. \tag{9}$$

Solutions of these latter exist such that all $dC_i/d\lambda$ vanish as $\lambda \to \pm\infty$. This implies, in view of $\lambda = x/\sqrt{t}$, that appropriate initial conditions $C_i(x, 0)$ are single step functions at the origin. Solutions of (9) therefore apply to the semi-infinite diffusion couple for which the initial conditions are

$$\begin{aligned} C_i &= C_i^0 \quad \text{for } x > 0 \text{ and } t = 0 \quad (\text{i.e. } \lambda = \infty), \\ C_i &= C_i^1 \quad \text{for } x < 0 \text{ and } t = 0 \quad (\text{i.e. } \lambda = -\infty). \end{aligned} \tag{10}$$

Equations (9) can be integrated once to obtain

$$\int_{C_i^0}^{C_i}\lambda dC_i = -2\sum_{k=1}^{n-1}D_{ik}\frac{dC_k}{d\lambda}. \tag{11}$$

Since these equations relate the diffusion coefficients to the properties of the measured experimental curves, we can use them for the experimental determination of the coefficients. In binary alloys the procedure is a standard one and is relatively simple to carry out since there is only one coefficient to be determined from a single curve. For higher order alloys it is apparent that the extent of the experimentation and computation would be prohibitive if no approximations were made. In most cases suitable approximations should be made apparent by the experimental results.

4. ANALYSIS OF EXPERIMENTS ON THE IRON, SILICON, CARBON SYSTEM

Darken (1949) has performed an interesting series of experiments on carbon diffusion in γ-iron in the presence of other soluble alloying elements. In one example he prepared a diffusion couple in which the carbon (component

1) was in approximately equal concentrations on both sides of the weld while the silicon (component 2) was present essentially on one side of the couple only. Fig. 1 indicates the initial concentration distributions as well as the observed carbon distribution (points) after a 13-day anneal at 1050° C.

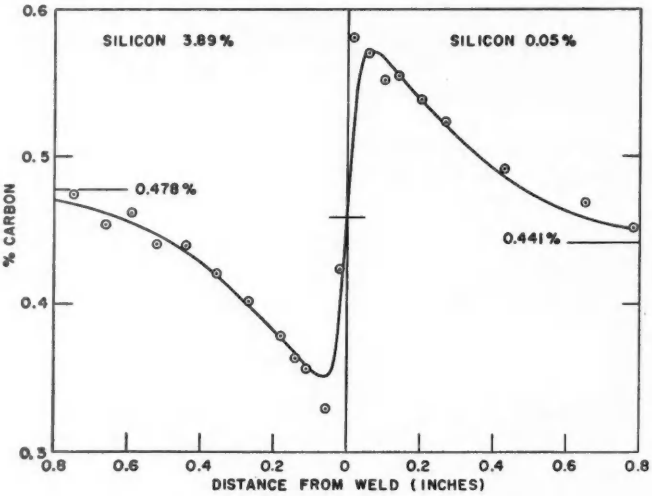

FIG. 1. Interdiffusion in the iron, silicon, carbon system.

To facilitate solution of the condensation of equations (9) applicable to this couple, the following assumptions have been made:

(*a*) D_{11}, D_{22}, and D_{12} are constant,

(*b*) $D_{21}\dfrac{d^2C_1}{d\lambda^2} \ll D_{22}\dfrac{d^2C_2}{d\lambda^2}$.

The final justification of these is that the solution of the differential equation based thereon can be fit quite precisely to the experimental curve. The validity of relation (*b*) is least certain, since for these particular initial conditions the calculated carbon distribution is rather insensitive to assumptions about the relative magnitude of the terms. In the absence of a measurement of the silicon distribution, the relation cannot be confirmed so it remains essentially a mathematical convenience. Should it be invalid, and the terms more nearly equal, the value of D_{22} determined by fitting the curve will be incorrect but D_{11} and D_{12} will be relatively unaffected.

Applying (*a*) and (*b*) to (9), the equations become

$$-\frac{\lambda}{2}\frac{dC_1}{d\lambda} = D_{11}\frac{d^2C_1}{d\lambda^2}+D_{12}\frac{d^2C_2}{d\lambda^2} \tag{12}$$

and

$$-\frac{\lambda}{2}\frac{dC_2}{d\lambda} = 0+D_{22}\frac{d^2C_2}{d\lambda^2}. \tag{13}$$

Equation (13) has the independent solution

$$C_2 = C_2^0 + \frac{C_2^1 - C_2^0}{2}\left[1 - \operatorname{erf}\frac{\lambda}{2\sqrt{D_{22}}}\right], \tag{14}$$

which can be substituted in (12). The solution of equation (12) subject to the approximate conditions stated is

$$C_1 = \frac{C_1^0 + C_1^1}{2} + A\left[\operatorname{erf}\frac{\lambda}{2\sqrt{D_{22}}} - \frac{2A - C_1^0 + C_1^1}{2A}\operatorname{erf}\frac{\lambda}{2\sqrt{D_{11}}}\right], \tag{15}$$

where

$$A = \frac{D_{12}}{D_{11} - D_{22}}\,\frac{C_2^1 - C_2^0}{2}. \tag{16}$$

The coefficient A (and therefore D_{12}) can in general be obtained by fitting equation (15) to the results. In the present case, since $D_{22} \ll D_{11}$, it is sufficient to read A directly from the curves by extrapolation to the origin. For the calculation of the theoretical curve shown in Fig. 1 the following values have been used in equation (15): $C_1^0 = 0.441\%$, $C_1^1 = 0.478\%$, $C_2^1 - C_2^0 = 3.84\%$, $A = 0.135\%$, $D_{11} = 4.8\times10^{-7}$ cm.^{2}/sec. (deduced by trial fits to the experimental curve at points well removed from the origin and in agreement with Darken's values from the same data (Darken 1949)), $D_{22} = 2.3\times10^{-9}$ cm.^{2}/sec. (a very rough value obtained by trial fits near the origin), and $D_{12} = 0.34\times10^{-7}$ cm.^{2}/sec. (calculated from equation (16)).* As we see the final fit is quite good and information has been obtained from this one couple about all three coefficients.

The value of D_{22} used in the calculations shows only order of magnitude agreement with data given by Smithells (1955) for the diffusion of silicon in iron but this is not surprising in view of the meager data for the critical region near the origin and the rather doubtful assumption (*b*).

The value obtained for the off-diagonal coefficient D_{12} indicates a surprisingly large interaction between carbon and a silicon gradient. The significance of such a result can best be made apparent by establishing the relationships between the D_{ik} and the M_{ik} through equation (2).

5. SUMMARY

The very satisfactory description of interdiffusion in the iron, silicon, carbon system as evidenced by Fig. 1 suggests that equations (1) or (9) may be applied with equal directness and facility to other systems and to the solution of various metallurgical problems with simple boundary conditions.

ACKNOWLEDGMENTS

The author is grateful to Dr. P. G. Shewmon of Westinghouse Research Laboratories for his comments on the original manuscript.

*The use of weight per cent as the unit of concentration is approximately valid since the concentrations are low. The accuracy of the data does not justify pursuing the detailed specifications given on p. 436.

REFERENCES

BARDEEN, J. and HERRING, C. 1951. Atom movements (American Society for Metals), p. 87.
BIRCHENALL, C. E., CORREA DA SILVA, L. C., and MEHL, R. F. 1948. Discussion of paper by DARKEN, L. S. Trans. Am. Inst. Mining Met. Engrs. **175**, 197.
BOLTZMANN, L. 1894. Ann. Physik, Leipzig, **53**, 959.
DARKEN, L. S. 1949. Trans. Am. Inst. Mining Met. Engrs. **180**, 430.
——— 1951. Atom movements (American Society for Metals), p. 17.
FICK, A. 1855. Pogg. Ann. **94**, 59.
MATANO, C. 1933. Japan. J. Phys. **8**, 109.
ONSAGER, L. 1945–46. Ann. N.Y. Acad. Sci. **46**, 241.
SMITHELLS, C. J. 1955. Metals reference book, Vol. 2 (Butterworth Scientific Publications, London), p. 555.

SOME SCATTERING PROBLEMS IN CONDUCTION THEORY[1]

P. G. KLEMENS[2]

ABSTRACT

An expression is derived for the scattering of electrons by inhomogeneous strain fields in terms of the scattering of electrons by low frequency lattice vibrations, as deduced from the low temperature intrinsic thermal resistivity and the lattice thermal conductivity. This is applied to the scattering of electrons by dislocations and stacking faults. An expression for the scattering of lattice waves by stacking faults is also derived. The validity of these results is discussed.

INTRODUCTION

In order to interpret changes in the conduction properties of metals at low temperatures due to cold work or irradiation, it is of interest to calculate the scattering by various model imperfections both of electrons and of phonons. The former is related to changes in the residual electrical resistance, the latter to changes in the lattice thermal conductivity.

While the theory of the scattering of electrons by vacancies and interstitials (Jongenburger 1953, 1955; Blatt 1955; Overhauser and Gorman 1956) seems to yield fairly reliable results, the scattering of electrons by extended imperfections seems not as well understood. Hunter and Nabarro (1953) have obtained an expression for the scattering of electrons by static strain fields, and applied this to the scattering by the strain field about a dislocation, deriving the magnitude of the interaction between electrons and the Fourier components of the strain field from first principles. An alternative treatment is developed here, which is formally similar to Hunter and Nabarro's, but in which the interaction is deduced from the magnitude of the electron–phonon coupling as derived from the observed conduction properties.

Care must be taken in interpreting the observed conduction properties, and the most reliable procedure seems to be that of taking the low temperature lattice thermal conductivity, limited by the scattering of phonons by electrons, as a measure of the electron–phonon interaction, since this quantity is not sensitive to details of the electronic band structure. Another reliable measure is the intrinsic electronic thermal conductivity at low temperatures.

The expression for the scattering of electrons by strain fields thus derived is similar to that of Hunter and Nabarro, and is applied to the scattering of electrons by dislocations and stacking faults.

An expression for the scattering of phonons by a static strain field was derived earlier (Klemens 1955), and applied to the cases of dislocations and grain boundaries. An expression for the scattering of phonons by stacking faults is now similarly obtained.

---

[1]Manuscript received December 11, 1956.
Contribution from the Division of Pure Physics, National Research Council, Ottawa, Canada.
Issued as N.R.C. No. 4229.

[2]On leave from Division of Physics, C.S.I.R.O., National Standards Laboratory, Sydney, Australia.

The present treatment is more suited to the case of the scattering of phonons than to the scattering of electrons, because the wave-lengths of the latter are rather short, and most of the scattering arises from regions in the immediate vicinity of the imperfection core, when the elastic continuum theory cannot be expected to apply.

SCATTERING OF ELECTRONS BY STRAIN FIELDS

As pointed out by Hunter and Nabarro (1953), electrons are scattered only in an inhomogeneous strain field, which destroys the periodicity of the lattice, and it is the strain, rather than the displacement, which provides an appropriate description of the deviations from periodicity. Lattice vibrations also produce an inhomogeneous strain field, so that the observed scattering of electrons by lattice waves gives a measure of the scattering of electrons by the various Fourier components of the static strain field, provided the frequencies of the lattice vibrations are sufficiently low to allow the conduction electrons to adjust themselves fully to the ionic displacement, as they must in the case of static strain. One can therefore use the interaction between electrons and low frequency phonons as a measure of the interaction between electrons and the components of a static strain field.

The displacement $\mathbf{u}(\mathbf{x})$ of the lattice point $\mathbf{x}$ due to lattice vibrations is given by

$$\mathbf{u}(\mathbf{x}) = \frac{1}{\sqrt{G}} \sum_{\mathbf{q},j} a(\mathbf{q})\, \boldsymbol{\varepsilon}_j\, e^{i\mathbf{q}\cdot\mathbf{x}} \tag{1}$$

where $\boldsymbol{\varepsilon}_j$ is the polarization vector of the polarization branch j, $\mathbf{q}$ is the wave-vector, ω is the frequency, G is the number of unit cells in the crystal, each of mass M, and $a(\mathbf{q})$ is the harmonic oscillator matrix, whose elements are

$$\begin{aligned} a(\mathbf{q})_{N,N-1} &= \left[\frac{\hbar}{2M\omega} N\right]^{\frac{1}{2}}, \\ a^*(\mathbf{q})_{N,N+1} &= \left[\frac{\hbar}{2M\omega} (N+1)\right]^{\frac{1}{2}}. \end{aligned} \tag{2}$$

The rate of change of the electron distribution function f due to interaction with phonons is given by

$$t\left[\frac{df}{dt}\right] = \frac{2}{9MG\hbar} \sum_{\mathbf{q},j} C_j^{\,2} \frac{q^2}{\omega}\, \mathfrak{A}(\Delta E)[f'(1-f)(N+1) - (1-f')fN], \tag{3}$$

being due to all processes in which an electron $\mathbf{k}$ and a phonon $\mathbf{q}$ combine to form an electron $\mathbf{k}'$ or vice versa, conserving wave-vector

$$\mathbf{k} + \mathbf{q} = \mathbf{k}',$$

and, because of the resonance factor

$$\mathfrak{A}(\Delta E) = 2\,\frac{1-\cos(\Delta E t/\hbar)}{(\Delta E/\hbar)^2}$$

where $\Delta E = E + \hbar\omega - E'$, conserving energy. The constant C_j is the electron–phonon interaction parameter as defined, for example, by Sommerfeld and

Bethe (1933), but generalized to describe the interaction between electrons and phonons of polarization j.

Longitudinal waves cause an inhomogeneous dilatation

$$\operatorname{div} \mathbf{u}(\mathbf{x}) = \frac{i}{\sqrt{G}} \sum_{\mathbf{q}} q\, a(\mathbf{q})\, e^{i\mathbf{q}\cdot\mathbf{x}} \tag{4}$$

whose effect is comparable with that of an inhomogeneous static dilatation $\Delta(\mathbf{x})$, resolved into Fourier components

$$\Delta(\mathbf{x}) = \frac{1}{\sqrt{G}} \sum_{\mathbf{q}} D(\mathbf{q})\, e^{i\mathbf{q}\cdot\mathbf{x}}, \tag{5}$$

so that one can replace $ia(\mathbf{q})q$ in (3) by $D(\mathbf{q})$ to obtain the rate of change of f due to the scattering of electrons by the strain field $\Delta(\mathbf{x})$. Noting the relation (2) between N and a^2, one obtains

$$t\frac{df}{dt}\Big]_{} = \frac{4}{9G\hbar^2} \sum_{\mathbf{q}} C_{\mathrm{I}}{}^2\, D^2(\mathbf{q})\, \Omega(\Delta E)[f'-f] \tag{6}$$

where now $\Delta E = E - E'$, and C_{I} is the electron–phonon coupling constant for longitudinal waves.

Transverse lattice waves similarly cause an inhomogeneous rotation

$$\operatorname{curl} \mathbf{u}(\mathbf{x}) = \frac{i}{\sqrt{G}} \sum_{\mathbf{q}} (\mathbf{q}\times\boldsymbol{\varepsilon})\, a(\mathbf{q})\, e^{i\mathbf{q}\cdot\mathbf{x}} \tag{7}$$

which can be compared with the components of rotation of an inhomogeneous strain field

$$\operatorname{curl} \mathbf{u}(\mathbf{x}) = \mathrm{II}(\mathbf{x}) = \frac{1}{\sqrt{G}} \sum_{\mathbf{q}} \mathbf{P}(\mathbf{q})\, e^{i\mathbf{q}\cdot\mathbf{x}} \tag{8}$$

so that in (3) one can replace $ia(\mathbf{q})q$ for a transverse wave by $\mathbf{P}(\mathbf{q})$ orientated in the direction of $(\mathbf{q}\times\boldsymbol{\varepsilon})$. An expression, similar to (6), can be derived for the scattering by an inhomogeneous rotation field in terms of C_{II}, the coupling constant for transverse vibrations, and $P^2(\mathbf{q})$. If it is assumed that there is no systematic interference between scattering by the dilatation and rotation fields, one obtains for the scattering by an inhomogeneous strain field

$$t\frac{df}{dt}\Big]_{} = \frac{4}{9G\hbar^2} \sum_{\mathbf{q}} \{C_{\mathrm{I}}{}^2\, D^2(\mathbf{q}) + C_{\mathrm{II}}{}^2\, P^2(\mathbf{q})\}\, \Omega(\Delta E)[f'-f]. \tag{9}$$

Since the interaction parameters $C_{\mathrm{I}}{}^2$ and $C_{\mathrm{II}}{}^2$ depend sensitively on the departure of the electron wave-functions from free-electron wave-functions, the estimation of these parameters from first principles is a formidable task,* and we shall rather estimate them from the observed conduction properties. The electronic conduction properties lead to an estimate of $C^2 = C_{\mathrm{I}}{}^2 + 2C_{\mathrm{II}}{}^2$. However, the high temperature resistance does not lend itself easily to an estimate of C^2, because the effects of Umklapp-processes and the dispersion of the lattice waves are not easy to take into account. If these effects were disregarded, one would arrive at an overestimate of C^2. The electrical resistance

*See, for example, Bardeen (1950).

at low temperatures is likewise unsuitable, because it is very sensitive to the shape of the Fermi surface, as discussed elsewhere (Klemens 1954*b*). However, the thermal resistance at low temperatures is not sensitive to the shape of the Fermi surface, and can thus be used to reliably estimate C^2. In Table I values of $(C/\zeta)^2$ are given, estimated from the high temperature resistance (electrical or thermal) and the low temperature thermal resistivity. The latter leads to lower values.

The scattering of phonons by the conduction electrons limits the lattice component of thermal conduction at low temperature, which is thus an additional measure of the electron–phonon interaction. The lattice thermal conductivity varies inversely as either C_{I}^2 or C_{II}^2, whichever is the bigger, because the two polarization branches are closely coupled to each other by phonon–phonon interactions (Klemens 1954*a*, 1956*a*). Comparing the magnitude of the electronic thermal resistivity—which yields C^2—to the lattice thermal conductivity, it has been concluded that

$$C_{\mathrm{I}}^2 \simeq C_{\mathrm{II}}^2 \simeq \tfrac{1}{3}C^2 \tag{10}$$

in the cases of silver (Kemp, Klemens, Sreedhar, and White 1954, 1956) and copper (White and Woods 1954, 1955). In other cases no information is available yet on the lattice thermal conductivity, though it appears likely from the effective ratio of the electrical to thermal resistivities at low temperatures that the electrons interact equally strongly with waves of all polarizations also in the cases of gold and sodium (Klemens 1954*b*).

TABLE I

ESTIMATES OF C^2

Element	$(C/\zeta)_1^2$	$(C/\zeta)_2^2$	$(C_{\mathrm{I}}/\zeta)^2$
Cu	1.23	0.20	0.07
Ag	1.46	0.28	0.09
Au	1.44	0.25	—
Na	1.08	0.20	—

$(C/\zeta)_1^2$ is the estimate from high temperature resistance data,
$(C/\zeta)_2^2$ from the intrinsic thermal resistance at low temperatures, and
$(C_{\mathrm{I}}/\zeta)^2$ from the lattice component of thermal conductivity.

SCATTERING OF ELECTRONS BY DISLOCATIONS

The components of the strain field about a screw dislocation, whose axis lies along the z-axis, are given by

$$\Pi_x = \frac{b}{2\pi r}\cos\theta, \qquad \Pi_y = \frac{b}{2\pi r}\sin\theta \tag{11}$$

where b is the Burgers vector, and (r, θ) are cylindrical coordinates. The strain field of an edge dislocation is

$$\Delta = \frac{b}{2\pi r}\,\frac{1-2\nu}{1-\nu}\sin\theta, \qquad \Pi_z = \frac{b}{2\pi r}\cos\theta \tag{12}$$

where ν is the Poisson ratio (Cottrell 1953).

The expression (9) for the scattering of electrons by a static strain field is formally similar to an expression for the scattering of phonons by a static strain field (Klemens 1955), which had been applied to the scattering by dislocations, so that some of the results derived there can be used for the present purposes. Thus the Fourier transforms of the strain field are

$$P^2(\mathbf{q}) = \frac{G}{G_0^2}\frac{b^2}{a^4 q^2} \tag{13}$$

for screw dislocations, while for edge dislocations they are

$$P^2(\mathbf{q}) = \frac{G}{2G_0^2}\frac{b^2}{a^4 q^2}, \qquad D^2(\mathbf{q}) = \left(\frac{1-2\nu}{1-\nu}\right)^2 \frac{G}{2G_0^2}\frac{b^2}{a^4 q^2} \tag{14}$$

where $\mathbf{q}$ is perpendicular to the z-axis (which implies that scattering by a dislocation cannot alter the z-component of the electron wave-vector), G_0 is the number of unit cells of the crystal in a plane perpendicular to the z-axis, and a is the lattice constant. Noting that, if μ is the direction cosine of $\mathbf{k}$ relative to the field,

$$\sum_q \delta(q_3)\frac{1}{q^2}\left[1-\frac{\mu'}{\mu}\right]\frac{\partial}{\partial t}\Omega(\Delta E) = \frac{a^2 G_0}{(2\pi)^2}\, h\pi\left(k\frac{dE}{dk}\right)_\zeta^{-1} \tag{15}$$

in analogy with a similar summation discussed previously (Klemens 1955), and that this should be multiplied by a factor 0.55 if the dislocations are arranged at random, one obtains for the inverse relaxation time

$$\frac{1}{\tau} = \frac{1}{f^0-f}\frac{df}{dt}\Bigg] = 0.55\,\frac{4\pi}{9}\,\frac{1}{G_0}\,\frac{b^2}{a^2}\,\frac{C_{\mathrm{II}}{}^2}{h(k\,dE/dk)_\zeta} \tag{16}$$

in the case of a screw dislocation. The scattering due to an edge dislocation is of similar magnitude, with a factor

$$\frac{1}{2}\left[C_{\mathrm{II}}{}^2+\left(\frac{1-2\nu}{1-\nu}\right)^2 C_{\mathrm{I}}{}^2\right]$$

in place of $C_{\mathrm{II}}{}^2$. For free electrons $(k\,dE/dk)_\zeta = 2\zeta$, and since $(a^2G_0)^{-1} = N$, the number of dislocation lines per unit area, one obtains

$$\frac{1}{\tau} = 0.55\,\frac{2\pi}{9}\,\frac{C_{\mathrm{II}}{}^2}{h\zeta}\,Nb^2. \tag{17}$$

For copper $\zeta = 7.1$ ev. and $b = 2.5\times10^{-8}$ cm., so that

$$1/\tau = 0.027N \text{ sec.}^{-1} \tag{18}$$

and the increase in electrical resistance at room temperatures due to dislocations is

$$\Delta\rho/\rho \simeq 0.7\times10^{-15}N. \tag{19}$$

The values for the inverse relaxation time and electrical resistance due to dislocations derived here are somewhat smaller* than those derived by Hunter and Nabarro (1953) on the basis of a similar calculation, but using the

*The results of these calculations were presented at the Conference on Electron Transport in Metals and Solids, Ottawa, (Klemens 1956*b*). A numerical error was incurred in going from (17) to (18) and it was erroneously stated that the present considerations lead to a somewhat higher scattering probability than those of Hunter and Nabarro.

deformation potential to estimate the interaction between electrons and the strain field. This is to be expected, since the deformation potential yields values of C of the order of ζ—see Jones (1956).

SCATTERING OF ELECTRONS BY STACKING FAULTS

The present formalism can be used to calculate the scattering of electrons by stacking faults. A face-centered structure can be regarded as composed of closely-packed spheres of radius r, arranged in hexagonal layers, the distance between layers being

$$D = 2r(2/3)^{1/2} \tag{20}$$

and

$$r = 2^{1/6}(a/2) \tag{21}$$

where a^3 is the volume per atom. The layers are stacked one above the other, each being displaced in its plane by a distance

$$S = 2r/\sqrt{3} = a\,2^{1/6}\,3^{-1/2}, \tag{22}$$

successive displacements forming an equilateral triangle.

A stacking fault can be regarded as the displacement of one half of the crystal through a distance S in the layer plane in one of the three possible directions, and thus corresponds to a shear S/D localized within a distance D. Then

$$P(\mathbf{q}) = \frac{\sqrt{G}}{G_3}\frac{S}{D}\,\delta(q_1)\,\delta(q_2) \tag{23}$$

where G_3 is the number of layers in a crystal containing one stacking fault. Thus $P(\mathbf{q})$ vanishes unless $\mathbf{q}$ lies perpendicular to the plane of the stacking fault, which implies that the component of the electron wave-vector $\mathbf{k}$ in the plane of the stacking fault is not changed. Thus an electron can only suffer specular reflection at a stacking fault.

Also

$$\sum_{q_3} \Omega(\Delta E) = G_3 D\left(\frac{dE}{dk}\right)^{-1}\frac{1}{|\cos\theta|}\hbar t \tag{24}$$

where θ is the angle of the incident electron with the normal to the stacking fault plane. Taking an average value for

$$\frac{1}{|\cos\theta|}\left[1-\frac{\mu'}{\mu}\right] = \frac{4}{3} \tag{25}$$

one obtains, on substituting into (9),

$$\frac{1}{\tau} = \frac{16}{27}\frac{C_{II}^{\,2}}{\hbar^2}\frac{1}{v}\frac{S^2}{G_3 D} \tag{26}$$

while in the case of perpendicular incidence, the reflection probability is

$$R = \frac{4}{9}\frac{C_{II}^{\,2}}{\hbar^2}\frac{S^2}{v^2} \tag{27}$$

where v is the velocity of an electron of Fermi energy. In the case of copper, $R \simeq 0.4$.

SCATTERING OF PHONONS BY STACKING FAULTS

It is possible to use the strain-field representation (23) of a stacking fault to calculate the scattering of phonons. It has been pointed out (Klemens 1955) that a static strain field scatters lattice waves because of the anharmonicity of the interatomic forces, and that, in the case of a non-dilatational strain field,

$$\frac{1}{\tau} = \frac{a^3\gamma^2}{54(2\pi)^2}\sum_{j'}\int dS'\, P^2(\mathbf{q})\,\omega^2\,\frac{dk'}{d\omega'}\left[1-\frac{\mu'}{\mu}\right] \tag{28}$$

where γ is the Grueneisen anharmonicity parameter, and the integration is taken over the three surfaces (one for each polarization j') $\omega' = \omega$ in $\mathbf{k}$-space. With the value (23) for $P(\mathbf{q})$, and using (25), the effective relaxation time is given by

$$\frac{1}{\tau} = \frac{a}{18}\gamma^2\omega^2\frac{1}{G_3 c}\frac{4}{3} \tag{29}$$

where c is the velocity of sound. Here again, phonons are specularly reflected, but the reflection probability, in the case of long waves, varies as the square of the frequency, so that the corresponding thermal resistance varies inversely as the absolute temperature. The reflection probability for perpendicular incidence is

$$R = a^2k^2\gamma^2/18 \tag{30}$$

where k is the phonon wave-number.

DISCUSSION

The expression for the scattering of electrons by inhomogeneous strain fields developed here is only valid for slowly varying strain fields, where the important Fourier components are of low wave-number, comparable to the wave-numbers of the phonons important in determining the low temperature thermal resistivities, from which C^2 has been determined. In general the effective value of C^2 changes as the wave-number of phonons is increased (Jones 1956). This is largely due to the inability of the conduction electrons to adjust themselves as well to high frequency vibrations as to low frequency vibrations, an effect which does not arise in the case of static strain fields, so that the use of the present formalism for rapidly varying strain fields does probably not introduce a large error. More serious, however, is the objection that the electrons of Fermi energy have a wave-length of the order of the interatomic distance, so that much of the contribution to the scattering Hamiltonian takes place in regions where the imperfection cannot be adequately described in terms of the strain field alone. This is an objection which does not arise in the case of the scattering of long lattice waves.

Thus in the case of dislocations, for example, the electrons are scattered in the immediate vicinity of the dislocation core, where the displacement of the atom is not adequately described by the continuum theory. This objection applies to the present calculations as well as to those of Hunter and Nabarro (1953). A proper theory of the scattering of electrons by dislocations would

have to take account of the detailed behavior of the conduction electrons at the dislocation core. An attempt along such lines has recently been made by Seeger and Stehle (1956).

When comparing the electrical resistivity increase on plastic deformation with the electrical resistance increase to be expected from (19), or from the corresponding relation obtained by Hunter and Nabarro, the difficulty arises that one is not sure how much of the observed resistance is due to dislocations, and how much due to point imperfections (vacancies, interstitials, or clusters of these). This difficulty has been exhaustively discussed by van Bueren (1955, 1956) and also by Seeger (1956*a*). It appears that in some cases most of the electrical resistance can be ascribed to point imperfections, though this does not necessarily imply that the resistance due to extended imperfections is negligible, as in the case of brasses, where lattice thermal conductivity and electrical resistance were studied simultaneously (Kemp, Klemens, Tainsh, and White 1957). In other cases a substantial fraction of the resistance seems to be due to dislocations. It would then appear that there is a substantial discrepancy between the observed dislocation resistance and that calculated by Hunter and Nabarro, as discussed by van Bueren (1956), and an even greater discrepancy with the present calculations. One way out of this difficulty would be to suppose that a large fraction of the dislocations are split into partial dislocations, joined by stacking faults, and that the stacking faults contribute most of the electrical resistance of this arrangement. This has been suggested, among others, by Seeger and Stehle (1956).

If stacking faults are to contribute an appreciable fraction of the resistance increase due to plastic deformation, the reflection probability for a conduction electron impinging on the stacking fault must be somewhere of the same order as the value calculated here (equation 27), as discussed by Seeger and Stehle (1956) and Seeger (1956*b*).

The electrical resistivity due to stacking faults was estimated by Klemens (1953) by means of a wave-fitting calculation, assuming the electron wave functions to be strongly modulated by the periodic lattice. A reflection probability of 0.5 was obtained in this way. A more general wave-fitting calculation was carried out by Blatt, Ham, and Koehler (1956). As would be expected, the reflection probability depends intimately on the deviation of the electronic band structure from the free electron model: in the case of perfectly free electrons a stacking fault cannot influence the electronic motion, because it has no dilatation. Using a Wigner–Seitz approximation, these authors get a reflection probability which is considerably smaller than the value obtained by Klemens for strong modulation.

It would appear at first sight that the present method of calculating the reflection coefficient in terms of the shear strain field of a stacking fault is not related to the above considerations. However it should be remembered that for free electrons (unmodulated wave functions) $C^2 = 0$, so that C_{II}^2, and hence the reflection probability, depends upon the deviation of the electronic band structure from the free electron model. In the absence of

modulation of the electronic wave function $C_{II}^2 = 0$ and a stacking fault would not scatter electrons.

The fact that the present calculations lead to a reflection probability of the same order of magnitude as that calculated by a wave-fitting method, assuming strongly modulated wave-functions, gives some confirmation that the present method yields scattering probabilities of the correct order of magnitude, and confirms that, at least in the noble metals, the conduction electrons are far from free, as is also apparent from the various intrinsic conduction properties (Klemens 1954*b*, 1956*a*). On the other hand one should not rely on these estimates to more than order of magnitude: firstly one can question the replacement of a stacking fault by a shear over one atomic plane, and more seriously, the applicability of perturbation theory in the present case, when the reflection probability approaches unity, is doubtful. Neither of these effects is likely to change the order of magnitude of the result, but probably falsifies it to some extent.

Another approach still to the problem of the scattering of stacking faults has been made by Seeger (1956*b*), who treated the diffraction of the electron waves due to the displacement of one half of the crystal relative to the other. His result also yields reflection of comparable magnitude.

No reliable experimental results are yet to hand on the effect of stacking faults on the lattice thermal conductivity. The frequency dependence of (29) must be regarded as well established, as it can be derived from quite general arguments. The absolute magnitude of (29) is more questionable, because of the approximations involved, the most serious being the use of the cubic anharmonicities for the case of a very strong shear, where this approximation could break down. Again the present result is probably an estimate of the order of magnitude only. One uncertainty, which is also of importance in the problem of scattering of lattice waves by dislocations, is the correct choice of the Grueneisen constant γ, as discussed by Barron (1956).

The work described here was carried out while the author was on a visiting appointment to the Division of Pure Physics, N.R.C., Ottawa. The author wishes to thank the National Research Council for their hospitality, and Professor F. R. N. Nabarro for helpful discussions.

REFERENCES

BARDEEN, J. 1956. Can. J. Phys. **34**, 1171.
BARRON, T. H. K. 1956. Nature, **178**, 871.
BLATT, F. J. 1955. Phys. Rev. **99**, 1708.
BLATT, F. J., HAM, F. S., and KOEHLER, J. S. 1956. Bull. Am. Phys. Soc. **1**, 114.
VAN BUEREN, H. G. 1955. Z. Metallkunde, **46**, 272.
——— 1956. Thesis, Leiden University.
COTTRELL, A. H. 1953. Dislocations and plastic flow in crystals (University Press, Oxford).
HUNTER, S. C. and NABARRO, F. R. N. 1953. Proc. Roy. Soc. A, **220**, 542.
JONES, H. 1956. Encyclopedia of physics, Vol. 19 (Springer-Verlag, Berlin).
JONGENBURGER, P. 1953. Appl. Sci. Research, B, **3**, 237.
——— 1955. Nature, **176**, 545.
KEMP, W. R. G., KLEMENS, P. G., SREEDHAR, A. K., and WHITE, G. K. 1954. Proc. Phys. Soc. A, **67**, 728.
——— 1956. Proc. Roy. Soc. A, **233**, 41.

KEMP, W. R. G., KLEMENS, P. G., TAINSH, R. J., and WHITE, G. K. 1957. Acta Metallurgica (To be published).
KLEMENS, P. G. 1953. Australian J. Phys. **6**, 122.
——— 1954*a*. Australian J. Phys. **7**, 57.
——— 1954*b*. Australian J. Phys. **7**, 70.
——— 1955. Proc. Phys. Soc. A, **68**, 1113.
——— 1956*a*. Encyclopedia of physics, Vol. 14 (Springer-Verlag, Berlin).
——— 1956*b*. Can. J. Phys. **34**, 1212.
OVERHAUSER, A. W. and GORMAN, R. L. 1956. Phys. Rev. **102**, 676.
SEEGER, A. 1956*a*. Encyclopedia of physics, Vol. 7, Pt. 1 (Springer-Verlag, Berlin).
——— 1956*b*. Can. J. Phys. **34**, 1219.
SEEGER, A. and STEHLE, H. 1956. Z. Physik, **146**, 217, 242.
SOMMERFELD, A. and BETHE, H. 1933. Handbuch der Physik, Vol. 24/2 (Springer-Verlag, Berlin).
WHITE, G. K. and WOODS, S. B. 1954. Phil. Mag. **45**, 1343.
——— 1955. Can. J. Phys. **33**, 58.

A STUDY OF NUCLEON FORCES WITH REPULSIVE CORES

III. LOW ENERGY PROPERTIES OF THE LÉVY POTENTIAL[1]

M. A. PRESTON[2] AND J. SHAPIRO[3]

ABSTRACT

An attempt has been made to select the core radius and coupling constant of the Lévy potential for the interaction of two nucleons in order to fit the binding energy of the deuteron and the singlet state neutron–proton scattering length. It was found that these two quantities cannot be fitted simultaneously. For any given choice of coupling constant, a somewhat larger core radius is required to fit the deuteron binding energy than is required for the scattering length. This spin dependence of the core radius does not preclude the possibility of a fit to the low energy data with the Lévy potential.

An approximate two-nucleon potential has been obtained by Lévy (1952) from symmetrical pseudoscalar meson theory with pseudoscalar coupling by means of the Tamm-Dancoff method. Lévy was able to show that strong repulsions would occur in the relativistic region (i.e. at small separation distances). These were taken into account by using a hard core cutoff. For even parity states (with which we shall be concerned here) the potential is

$$\begin{aligned} V(r) &= \infty \qquad\qquad \text{for } r < r_c, \\ V(r) &= V_c(r) + V_T(r)S_{12} \quad \text{for } r > r_c, \end{aligned} \tag{1}$$

where r_c is the core radius, and

$$V_c(r) = -\mu\hbar c\left[\lambda^2\left(\frac{m_\pi}{2M}\right)^2 \frac{e^{-\mu r}}{\mu r} + 3\lambda^4\left(\frac{m_\pi}{2M}\right) \frac{1}{(\mu r)^2}\left\{\frac{2}{\pi}K_1(2\mu r) + \frac{m_\pi}{2M}\left[\frac{2}{\pi}K_1(\mu r)\right]^2\right\}\right], \tag{2}$$

$$V_T(r) = -\mu\hbar c\lambda^2\left(\frac{m_\pi}{2M}\right)^2\left(1+\frac{3}{\mu r}+\frac{3}{(\mu r)^2}\right)\frac{e^{-\mu r}}{\mu r}. \tag{3}$$

M is the reduced mass of the two-nucleon system, K_1 the Bessel function of imaginary argument, S_{12} the usual tensor operator, and μ is connected with the π-meson mass by $m_\pi = \hbar\mu/c$. Terms up to the fourth order in the pseudoscalar coupling constant G are included ($\lambda^2 = G^2/4\pi\hbar c$). The potential has two parameters (r_c, λ^2) to be determined from experiment. Lévy obtained these by fitting the ^1S NP scattering length a_{sn} and the binding energy of the deuteron, ϵ. Using rather approximate numerical methods he found the result $r_c = 0.38 \pm 0.03$ (in units $\hbar/m_\pi c$, which will be used throughout this paper unless explicitly stated otherwise) and $\lambda^2 = 9.7 \pm 1.3$. With these parameters, the

[1]Manuscript received December 6, 1956.
Contribution from Physics Department, Hamilton College, McMaster University, Hamilton, Ontario, and University of Toronto, Toronto, Ontario. Partially supported by a grant from the National Research Council.

[2]Hamilton College.
[3]National Research Council Student 1951–52, Fellow 1952–53. This paper is based on work submitted for the degree Ph.D. in the University of Toronto. Now at Yale University, New Haven, Connecticut.

potential gave good agreement with the low energy properties of the NP system, except for the deuteron quadrupole moment, which was 20% too low. Lévy also obtained reasonable agreement with the NP differential cross section at 40 Mev. Martin and Verlet (1953) used the Lévy potential to compute the PP differential cross section at 18 and 32 Mev., obtaining good agreement with experiment, provided, however, that the coupling constant was restricted to $\lambda^2 = 10.36 \pm 0.02$.

Klein (1953*a*, *b*) has shown that the term in $[K_1(\mu r)]^2$ should not appear in the fourth order central potential. This term contributes about 10% to the central potential. Calculations have been performed by Blatt and Kalos (1953) and by Jastrow (1953) in the low energy region neglecting this term, and allowing different coupling constants λ, λ' for the second and fourth order terms. They found no potential that simultaneously fitted all the low energy parameters. Nevertheless, the Lévy potential appears to be of some value, even if it is considered only as a phenomenological potential giving reasonable agreement with the experimental data up to 40 Mev. The calculation of G^2 and r_c has been repeated, using the potential of equations (1), (2), and (3). The reason for using the original potential, rather than Klein's modification, was that the computations reported here were nearly completed by the time Klein's work appeared. The calculations were performed on FERUT, the digital computer at the University of Toronto.

The method is the same as that of Lévy. For various choices of the coupling constant, the radial equation for the ^1S state of the NP system was integrated inwards, starting from the asymptotic form

$$u_0 = 1 - r/a_{sn}. \tag{4}$$

The integration proceeded until $u = 0$, which determined the core radius r_c. In this way r_c was determined as a function of λ^2.

This procedure was repeated for the coupled ^3S and ^3D radial equations for the deuteron, starting from the asymptotic radial wave functions

$$\begin{aligned} u &= A \exp(-\gamma r), \\ w &= \rho A \exp(-\gamma r)\left[1 + \frac{3}{\gamma r} + \frac{3}{(\gamma r)^2}\right], \end{aligned} \tag{5}$$

where u and w are the ^3S and ^3D radial wave functions, respectively, and $\gamma^2 = M\epsilon/\hbar^2$. The parameter ρ was varied until both radial wave functions vanished at the same radius r_c. This again determined r_c as a function of λ^2.

The numerical integrations were performed by the predictor–corrector method of Milne (1949). The error in the solution was estimated by performing runs with different interval sizes and different starting points for the integrations. The effect of variation of the meson mass and of the scattering length a_{sn} was investigated in the ^1S case. The effect of the experimental uncertainty in a_{sn} was negligible.

The two curves obtained from fitting the deuteron binding energy and the singlet scattering length are given in Fig. 1, in which λ^2 is plotted against r_c. The singlet case was done for meson masses of $m_\pi = 274\ m_e$, $276\ m_e$, and

278 m_e, the deuteron for $m_\pi = 276\, m_e$. The experimental parameters used were $a_{sn} = -23.69 \times 10^{-13}$ cm., $\epsilon = 2.226$ Mev.

The following points should be noted regarding Fig. 1:

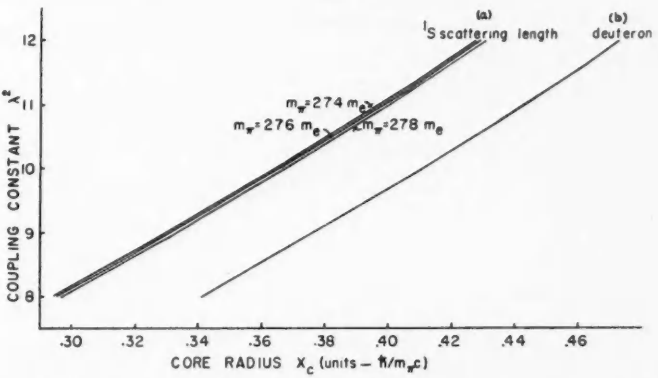

FIG. 1. Coupling constant plotted against core radius for the Lévy potential, as determined from (*a*) the ^1S NP scattering length, (*b*) the binding energy of the deuteron.

(*a*) The two curves are very nearly parallel and do not intersect, at least for the range of core radius used here.

(*b*) For a given λ^2, the core radius obtained from fitting the deuteron binding energy exceeds that obtained from the ^1S scattering length by approximately 0.045.

(*c*) The estimated error of r_c in the calculations is approximately 0.0001 for the ^1S state and 0.004 for the deuteron.

(*d*) The effect on r_c of changing the meson mass by two electron masses in the ^1S case is 0.0014. The effect is expected to be very nearly of the same size and in the same direction for the deuteron, since the potential will be changed in similar ways in both cases.

(*e*) The point of intersection quoted by Lévy lies between the curves obtained here.

The separation of the curves of Fig. 1 is approximately five times the total error of the computations. Thus it must be concluded that one cannot fit simultaneously the singlet scattering length and the deuteron binding energy.

An independent check of our calculations is contained in the work of Jastrow (1953), mentioned above. For $\lambda^2 = \lambda'^2 = 10$, he obtained a singlet core radius of 0.34 and a triplet core radius of 0.38. Both of these are slightly less than those shown in Fig. 1 (as is to be expected, since he used a slightly less attractive potential), but the difference is the same as obtained here.

The possibility of a fit to experiment by the Lévy potential cannot, however, be excluded by the present work. This question has been discussed in Paper II of this series (Shapiro and Preston 1956).

REFERENCES

BLATT, J. M. and KALOS, M. H. 1953. Phys. Rev. **92**, 1563.
JASTROW, R. 1953. Phys. Rev. **91**, 749.
KLEIN, A. 1953*a*. Phys. Rev. **89**, 1158.
——— 1953*b*. Phys. Rev. **90**, 1101.
LÉVY, M. M. 1952. Phys. Rev. **88**, 725.
MARTIN, A. and VERLET, L. 1953. Phys. Rev. **89**, 519L.
MILNE, W. E. 1949. Numerical calculus (Princeton Univ. Press, Princeton, N.J.).
SHAPIRO, J. and PRESTON, M. A. 1956. Can. J. Phys. **34**, 451.

MEASUREMENT BY PHOTOELECTRIC FRINGE SCANNING OF THE PRESSURE SHIFT OF Hg-198 EMISSION LINES[1]

K. M. Baird and D. S. Smith

ABSTRACT

Photoelectric fringe scanning apparatus has been developed at the National Research Laboratories for the measurement of very small wavelength changes (of the order of 5×10^{-5} Å). This paper describes its application to a direct measurement of the shift of some of the visible lines of Hg-198 caused by the presence of the various rare gases used as a carrier. The values found for the shift in wave number are all of the order of 2×10^{-4} cm^{-1} per mm. (Torr) pressure and to the red, except for He, for which it is somewhat less than 1×10^{-4} cm^{-1} per mm. and to the blue.

INTRODUCTION

A spectral line that is to be used as the primary standard of length must be very narrow and symmetrical to enable precise determination of its wavelength. A second requirement is that any variations of the wavelength dependent on conditions of excitation or observation must be small and well known. One source of lines satisfying the first requirement is the electrodeless Hg-198 lamp developed by Meggers and Kessler (1950), who proposed that its bright green line be used as the primary standard.

The wavelengths emitted by this lamp are shifted toward the red by the presence of argon, which is normally used as a carrier gas. The amount of the shift has been inferred by Barrell (1951) from separate determinations of wavelengths of various lamps at the National Physical Laboratory and from wavelength measurements made at other laboratories. He obtained the value of about 4×10^{-4} cm^{-1} per millimeter pressure of argon for the wave number shift. However, the accuracy of this is not great because of errors in separate wavelength determinations as well as in the uncertainty of the argon pressure in the lamp at the time of observation.

Margenau and Watson (1936) give a detailed treatment of the theory of broadening of absorption lines and Barrell (loc. cit.) has summarized information relevant to shift and broadening of the emission lines of Hg-198. Under the conditions of use of Hg-198 lamps with which the present paper is concerned, broadening is mainly due to the carrier gas and is expected to vary linearly with its density.

This paper describes a direct measurement of wavelength shifts for an electrodeless Hg-198 lamp whose carrier gas pressure could be changed and measured at will. The shifts were observed as changes in the fractional order of interference in a Fabry Perot etalon by means of apparatus for scanning the interference fringes photoelectrically. The latter was an adaptation of apparatus previously described by Baird (1954) in application to length measurement. Its sensitivity in a single setting was about $\pm2\times10^{-5}$ Å.

[1]Manuscript received January 7, 1957.
Contribution from the Division of Applied Physics, National Research Council, Ottawa, Canada.
Issued as N.R.C. No. 4268.

Pressure shifts in the range 0 to 10 mm. pressure of Xe, Kr, Ne, and He as well as A were measured for several of the visible lines of the Hg-198 spectrum.

FRINGE SCANNING APPARATUS

The apparatus is shown schematically in Fig. 1. Light from the electrodeless lamp was collimated and passed through the etalon, which was mounted in a

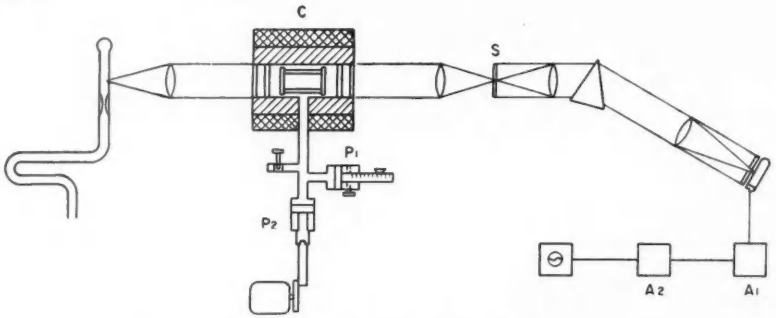

FIG. 1. Schematic diagram of fringe scanning apparatus.

pressure–temperature controlled chamber, C. The circular fringe system was focused and then centered on the slit of the spectrograph at S where a very small aperture allowed only light from the center of the rings (corresponding to 1/50 order) to pass into the spectrograph. At the back of the latter a 1P21 photomultiplier tube received light from the spectral line under study.

The pressure in the chamber C, and therefore the optical separation of the etalon plates, was controlled by two pistons, P_1 and P_2. The piston P_2 was operated by a synchronous motor so as to cause the pressure to oscillate at 15 c.p.s. and at an amplitude such that the corresponding oscillation in the order of interference was approximately equal to the half-width of the bright fringes. The piston P_1 was operated by hand to adjust the average pressure and was equipped with an accurate scale and vernier so that its displacement could be read.

The etalon, of invar, was of an open cage type so that pressure changes and oscillations were transmitted equally to the inside and outside surfaces of the quartz plates. The average temperature in the chamber was controlled to within a few thousandths of a degree and was not subject to rapid drift.

The output of the photomultiplier was fed to a battery powered pre-amplifier A_1, with an L–C filter to remove components much different from 15 c.p.s. The signal was then fed through the Q multiplier A_2, which removed components near 15 c.p.s., and thence to an oscilloscope swept at 30 c.p.s. in phase with the oscillating piston. This arrangement gave a sensitive indication of 15 c.p.s. modulation of the light falling on the photomultiplier, which was in phase with the piston oscillation. The signal was observed as a separation of the positive and negative parts of a sinusoidal signal on the oscilloscope.

The principle of wavelength shift measurement is shown in Fig. 2. The curve represents the variation of total flux entering the phototube with variation of pressure in the etalon chamber. Y_1 and Y_2 represent the limits in the scan amplitude due to the oscillating piston. In general when Y_1 and Y_2

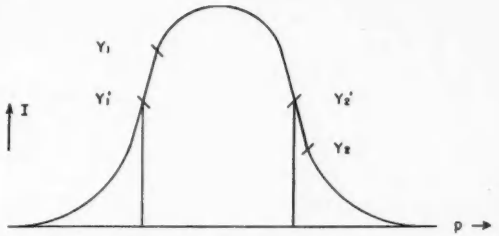

FIG. 2. Variation in flux falling on photomultiplier with pressure in etalon chamber.

were not symmetrical with respect to the peak intensity there was a 15 c.p.s. component to the light modulation due to the difference in intensity at Y_1 and Y_2 and this was indicated on the oscilloscope. On the other hand when the average pressure in the chamber was adjusted by means of P_1 so that the intensities at the limits of the scan were equal, as at Y_1' and Y_2', there was no 15 c.p.s. component; since the higher frequency modulation due to sweep over the peak of the curve was largely filtered out by the electronic circuit, a minimum signal was observed on the oscilloscope.

In order to measure a pressure shift, the piston P_1 was set to give minimum signal (on a bright fringe) under given conditions of the lamp; the pressure in the lamp was changed and the piston displacement required to restore the minimum signal was found. The change in order of interference (and hence the pressure shift) was then determined from a knowledge of the piston displacement required to change from one bright fringe to the next.

This apparatus made possible very convenient and precise determinations of wavelength changes due to lamp operating conditions. In a typical series of settings on the null point at 1-minute intervals over a period of 30 minutes the standard deviation of single settings from the mean was less than 0.001 of an order with a 62.5 mm. etalon. This corresponds to a proportional wavelength change of about $4:10^9$ and included scatter due to temperature variation, backlash and reading errors of P_1, lamp fluctuations, etc.

The above sensitivity was obtained for the Hg green and blue lines; it was somewhat less for the yellow lines and much less at the red end of the spectrum, e.g. at the Cd line 6438 where the photomultiplier sensitivity is very low. Sensitivity could probably be increased by the use of a red-sensitive cell, by refrigeration, and by the use of a detection system of greater sensitivity to phase. However, the first two changes do not have as much benefit as one might expect because the noise, which is largely due to the steady light flux, is not greatly reduced in relation to the signal. In any case the apparatus as described was found adequate for the present investigation.

An important feature of the method of fringe scanning by the use of the central spot of the Haidinger fringes is its great advantage over methods which involve measurements on the outer rings in the elimination of systematic errors due to vignetting, lens distortion, asymmetrical energy distribution in the rings, etc. On asymmetrical spectral lines the wavelength setting will of course depend to a certain extent on the scan amplitude Y_1Y_2 in Fig. 2, but this uncertainty is inherent in the spectral line and must be taken into account for any method of measurement.

Scanning by 15 c.p.s. oscillations is felt to have considerable advantage over d-c. type scanning, as described by Jacquinot and Dufour (1948) and others, in applications such as the present one where drift would introduce important errors. In its present form it does not permit study of line shape but an adaptation for this purpose is under development. It is also pointed out that the principle of scanning with the advantages mentioned in the preceding paragraph is not limited to photoelectric technique, but can be adapted to photography with the added advantage of recording many lines at once.

PROCEDURE

In order to make the pressure shift measurements a Meggers' type Hg-198 lamp containing about 3 mg. of Hg-198 of 98% isotopic purity was directly connected to a vacuum line and to sources of He, Ne, A, Kr, and Xe which could be metered out in small quantities. The pressure of gas in the lamp was read by means of a calibrated oil manometer. The lamp was separated from the rest of the system by a liquid air trap except in the case of Kr and Xe for which a CO_2 trap was used.

Excitation was by means of a special 270 Mc./s. oscillator previously described by Smith (1957). The lamp was water cooled to operate at a temperature of 10° C. No systematic measurement was made of the effect of excitation or temperature on the wavelength. However, deliberate variation of these factors, which was much greater than any likely to occur during the pressure shift measurements, was found to produce no observable effect.

The procedure to obtain a single point on the pressure shift – pressure curve was as follows: first the lamp was operated at well below 0.1 mm. gas pressure and three null settings of P_1 taken at 1-minute intervals; the lamp pressure was then raised to the value for which the shift was being measured and three more settings made at 1-minute intervals; finally, the lamp pressure was reduced to well below 0.1 mm. again and three more readings taken. This procedure was followed for all pressure values for which measurements were made according to a previously determined random schedule.

For argon, measurements were made at all the points indicated in the graph in Fig. 3 on the lines 4047, 4358, 5461, 5770, and 5790 using both a 62.5 mm. etalon and a 25 mm. etalon. Measurements were also made of the difference between a cold cathode Hg-198 lamp supplied by N.P.L. and the Meggers' type lamp at near zero pressure.

For the other gases points were obtained only for 0 mm., 5 mm., and 10 mm.

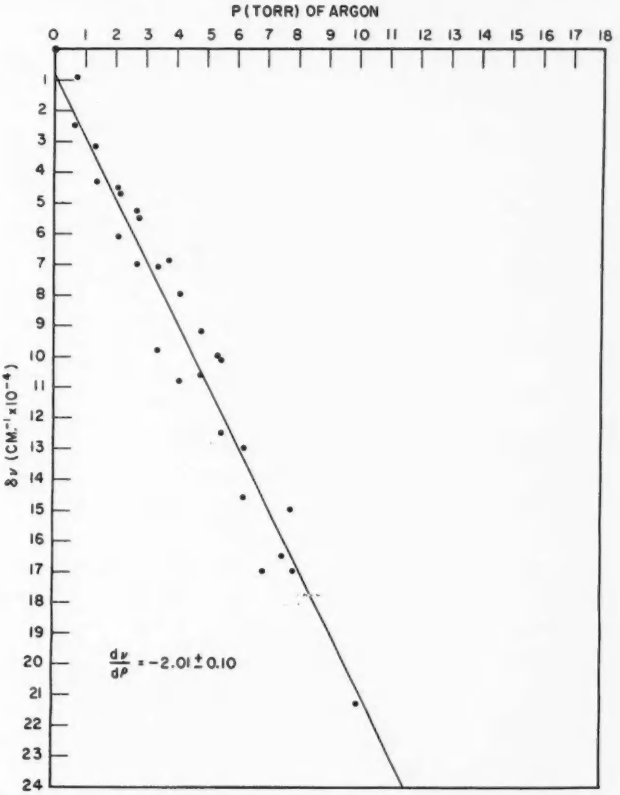

FIG. 3. Wave number shift of Hg-198 line 5461 with argon carrier gas pressure.

lamp gas pressure, and only for one or two lines in each case because poor excitation or interfering lines made observation impractical.

RESULTS

A typical pressure shift curve is shown in Fig. 3, which shows the shift of the 5461 Hg-198 line with argon pressure. The variation is linear as expected and has the value 2.0×10^{-4} cm^{-1}/mm. The probable error of this value calculated from the scatter of single points is $\pm0.1\times10^{-4}$ cm^{-1} per mm., although the difference in the several independent determinations over a period of a few months amounted to about 0.2×10^{-4} cm^{-1}.

The wave number difference between the Geissler type lamp supplied by N.P.L. and the low pressure Meggers' type lamp was found to be 25×10^{-4} cm^{-1} for the 5461 line. As the N.P.L. lamp was said to be filled to 10 mm. pressure of A, the shift per mm. appears somewhat higher than that in-

dicated by the measurements on the electrodeless lamps. This may be due to the different method of excitation.

The values for all the lines measured are given in Table I. It will be seen that except for He the shifts are all to the red and of the same order of magni-

TABLE I

λ (Å)		Shift in $cm^{-1} \times 10^{-4}$ for 10 mm. (Torr) carrier gas pressure				
25.0 mm. etalon	62.5 mm. etalon	He	Ne	A	Kr	Xe
5791				−26±1		
	5791			−17±1		
5770				−30±8		
	5770			−19±1		
5461				−25±1		
	5461	+7.6	−11	−20±1	−21	
4358				−29±2		
	4358	+6.6	−15	−23±1		−20
4047				−21±1		
	4047			−21±1		

tude. The values for A are less than that obtained by Barrell, but together with the value for Ne are in agreement with those found by Kessler (1956) at the National Bureau of Standards.

The interesting blue shift for He carrier gas suggests the possibility of making a lamp containing a mixture of He and A in order to have no net wavelength shift. This has been found to work, but adjustment of the mixture of gases must be done carefully and an envelope impervious to helium would be required if the lamp were to have a long life. Whether the two gases would clean up at the same rate has not been determined.

The slight difference observed in the apparent shift with the two different etalon lengths is thought to be real and to result from the asymmetrical nature of the broadening.

The magnitude of the shift is such that it must be taken into account when the usefulness of the Meggers' lamp as a source for the primary standard is being considered. Lamps filled to 3 to 6 mm. pressure as were the earlier ones would have wavelength errors of the order of nearly one part in 10^7 which would likely change during the life of the lamp. This sort of error would be of importance in precise metrology.

On the other hand lamps filled to only one or two tenths of a millimeter pressure as in Meggers' later lamps could not be in error by more than one or two parts in 10^9 because of pressure shift, an amount which would likely be acceptable at present in a primary standard.

It is of interest to note the corresponding shifts in two other sources proposed as the primary standard. The red line of Cd-114 has been found by Batarchukova and Dubrovskii (1956) to suffer a red shift of 1×10^{-4} cm. per mm.

argon, which is used as the carrier gas. The Kr isotope lamps suffer a shift to the red due to self-broadening that follows the two-thirds law. It amounts to less than 10^{-5} cm^{-1} for the 5650 line at a Kr pressure equal to its vapor tension at the triple point temperature of N_2 (which is the temperature of normal operation). Thus the pressure shift of the Hg-198 green line under present operating conditions is somewhat greater than for these other proposed standards.

REFERENCES

BAIRD, K. M. 1954. J. Opt. Soc. Amer. **44**, 11.
BARRELL, H. 1951. Proc. Roy. Soc. A, **209**, 132.
BATARCHUKOVA, N. R. and DUBROVSKII, G. B. 1956. Optika Spektroskopiia, **1**, No. 3, 330.
JACQUINOT, P. and DUFOUR, C. 1948. J. recherches centre natl. recherche sci., Labs. Bellevue (Paris), **6**, 92.
KESSLER, K. G. 1956. Private communication.
MARGENAU, H. and WATSON, W. W. 1936. Revs. Mod. Phys. **8**, 22.
MEGGERS, W. F. and KESSLER, K. G. 1950. J. Opt. Soc. Amer. **40**, 737.
SMITH, D. S. 1957. Can. J. Technol. **34**, 521.

ELECTRICAL RESISTIVITY OF GRAPHITE IRRADIATED WITH NEUTRONS[1]

R. W. Attree and O. Dahlinger

ABSTRACT

Measurements have been made of the changes in the electrical resistance of an artificial graphite which are induced by neutron irradiation and subsequent annealing. The resistivity increases with irradiation; the increase in resistance is partially removed by annealing at 128° C. These changes have been interpreted using Wallace's theory of the electron structure of graphite. The number of atoms displaced by the irradiation has been calculated using the method of Seitz, and is shown to be consistent with the experimental results.

INTRODUCTION

The physical properties of graphite are markedly changed by irradiation of the material with fast particles. The properties which have been investigated include the thermal and electrical resistivity, Hall coefficient, Young's modulus, thermoelectric power, density, and lattice spacing.[2] Of these, the change in electrical resistivity is the most convenient to measure, although the interpretation of the results is difficult. This difficulty arises from the nature of the conduction process. The electronic conductivity of a solid depends both on the density of electrons which are available for conducting a current, i.e. the density which can be thermally excited above the Fermi level, and upon the effective path length which they traverse before being scattered by grain boundaries, thermal waves, or lattice imperfections. The displaced atoms and vacancies which result from irradiation affect the conductivity in two ways—they act as scattering centers, thus decreasing the mean free path of the electrons, and also trap electrons, thus changing the density of electrons available for conduction.

The changes in resistivity may be partially removed by annealing at temperatures above the irradiation temperature. It may be expected that both the density of scattering centers and the density of trapped electrons will be altered by this treatment.

We have measured the changes of resistance in graphite induced by neutron irradiation, and by subsequent annealing, and, using Wallace's (1947) theory of the electronic structure of graphite, we have shown that a satisfactory interpretation of the results can be given in terms of the density of scattering centers and of conduction electrons.

EXPERIMENTAL METHOD

The specimens were cut from a single block of artificial (petroleum coke) graphite, perpendicular to the direction of extrusion. They were of circular

[1]Manuscript received November 28, 1956.
Contribution from the Research Chemistry Branch, Atomic Energy of Canada Limited, Chalk River, Ontario.
Issued as A.E.C.L. No. 415.

[2]The literature on the subject is large and in general unpublished. Reviews and summaries which have appeared include those by Burton and Neubert (1956), Kinchin (1954, 1956), Woods, Bupp, and Fletcher (1956), and Hennig and Hove (1956). Bowen (1949, 1950) reaches conclusions which are similar to some of those given in this paper.

cross-section with dimensions shown in Fig. 1. Current and potential leads were attached using phosphor-bronze clips with jaws modified to clamp on the circumference of the specimens.

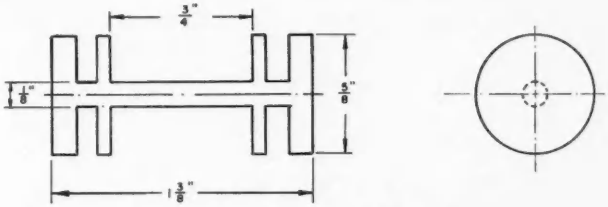

FIG. 1. Dimensions of graphite samples.

The resistance was determined as follows. Three or more measurements of the voltage and current (measured as voltage across a standard manganin resistor immersed in oil) were taken for several rotational positions of the specimen in the clips, and these were averaged. If the result for a position differed from the average by more than 1 part in 500, indicating poor contact between the clips and the specimens, readings were taken for more positions until consistency was obtained. The values for the resistances for each specimen were then averaged, those which indicated poor electrical contact being rejected.

The resistance of two standards was determined in the same manner, whenever specimens were measured, and the specimen resistivities were corrected for any apparent change in the standards. These corrections were of the order of one per cent over a period of several months.

Unirradiated specimens were annealed at 128° C. before use. All specimens were placed in the dry box surrounding the measuring equipment for several hours before measurement. All measurements were made in dry air at 29° C.

Figure 2 illustrates the sequence of measurements in a typical series. The resistances of the three specimens (denoted by A, B, and C in Fig. 2) were measured, and the specimens were then irradiated in the same facility in the NRX reactor. After the irradiation, the resistances were measured. The ratios of the resistances after and before irradiation are denoted by the first point on the upper curve. (These ratios may be taken as the ratio of volume resistivities ρ/ρ_0, since dimensional changes are negligibly small.) Sample A was then annealed at 128° C.; the change in the ratio of resistances is indicated by the vertical broken line. The three samples were irradiated as before, and remeasured. Samples A and B were then annealed. It will be observed that at this stage the values of ρ/ρ_0 are the same for A and B, within the error of the measurements, even though the sequence of annealing and irradiation differs. The samples were then irradiated, measured, annealed, and remeasured, as indicated in Fig. 2. In all, nine specimens, designated A to J, were measured, using three different irradiation facilities in the NRX reactor. The results are given in Table I.

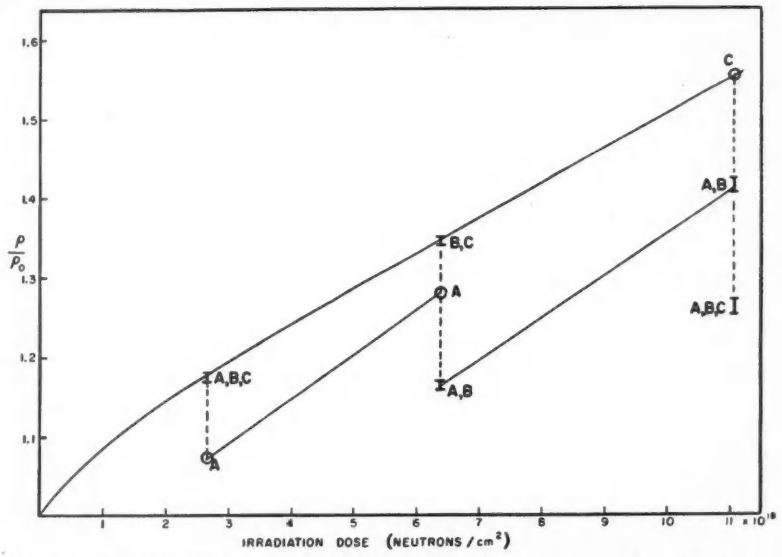

FIG. 2. Resistivity changes in irradiated graphite. The upper curve shows the changes induced by irradiation with no annealing, while the lower curves show changes produced on reirradiating specimens which have been annealed at 128° C. Behavior on annealing is indicated by the vertical broken lines. When more than one sample was measured, the spread of the results is indicated.

TABLE I

VALUES FOR ρ/ρ_0*

Irradiation position	Irradiation dose, ϕ, neutrons/cm.^{2}	ρ/ρ_0		
S-15-5		A	B	C
	2.66×10^{18}	1.175 (1.074) (*a*)	1.175	1.168
	6.40×10^{18}	1.283 (*a*) (1.160) (*b*)	1.341 (1.167) (*a*)	1.349
	11.07×10^{18}	1.424 (*b*) (1.259) (*c*)	1.413 (*a*) (1.254) (*b*)	1.554 (1.275) (*a*)
S-9-5		D	E	F
	3.38×10^{18}	1.216 (1.094) (*a*)	1.205	1.203
	8.40×10^{18}	1.370 (*a*) (1.205) (*b*)	1.418 (1.201) (*a*)	1.408
	13.65×10^{18}	1.467 (*b*) (1.317) (*c*)	1.459 (*a*) (1.312) (*b*)	1.577 (1.326) (*a*)
S-9-4		G	H	J
	2.50×10^{18}	1.091 (1.043) (*a*)	1.086	1.097
	5.07×10^{18}		1.150 (1.065) (*a*)	1.164
	9.00×10^{18}		1.194 (*a*) (1.108) (*b*)	1.257 (1.130) (*a*)

*Values enclosed in brackets are for specimens annealed after irradiation to the total dose indicated. Values for specimens annealed once following an initial irradiation are designated by (*a*); for those annealed twice, by (*b*); and for those annealed three times, by (*c*). The irradiation positions S-9-4, S-9-5, and S-15-5 are located in the graphite reflector outside the calandria of the NRX reactor.

Measurements were made during the course of annealing, which, in some cases, was continued for 10 days. It was found that after long annealing, further changes in the resistance were proportional to the reciprocal of the annealing time. This fact was used to obtain the values for resistance after infinite annealing times, shown in Fig. 3. All samples were annealed for at least 5 days.

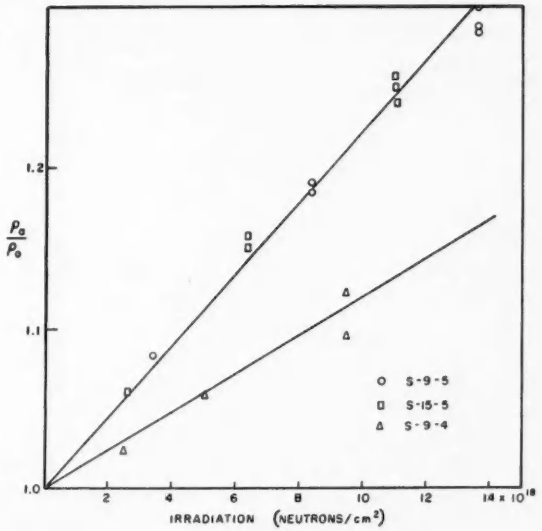

FIG. 3. Ratio of the resistivity after irradiation and annealing at 128° C., ρ_a, to the resistivity before irradiation, ρ_0, as a function of the integrated flux. The lines drawn are the "best" fit as determined by the method of least squares. The lines for irradiation in S-9-5 and S-15-5 facilities coincide.

Thermal neutron fluxes were measured with cobalt monitors. The temperature of the graphite during irradiation was about 70–80° C.

DISCUSSION

One point is immediately evident from the data, that within the accuracy of the measurements a sample which has been irradiated, annealed, re-irradiated, and reannealed has the same resistivity as a sample which has first received the same total amount of irradiation and which has then been annealed. It is possible to imagine that the aggregates of imperfections which remain after irradiation and annealing will either serve as nuclei for the further aggregation of the imperfections produced by a second irradiation, or will be disrupted by the second irradiation. Each of these possibilities will lead to a state different from that arising from a single irradiation and annealing. Because no such difference is found, we conclude that, for the irradiations used, the imperfections introduced by the irradiation do not interact appreciably with the aggregates remaining after the annealing, nor

are these aggregates affected by further slight irradiations, within the accuracy of the measurements. This result is to be expected for the short irradiations used, but would not be expected for longer irradiations.

Using Wallace's (1947) theoretical relations for the energy dependence of the density of the electronic states in graphite, Hennig (1951) has derived an equation for the volume resistivity ρ:

$$\frac{1}{\rho} = \frac{8\pi e^2 \tau}{h^2 c} [2kT \ln\{1+\exp(\Delta/kT)\} - \Delta], \tag{1}$$

where $1/\tau$ is the probability per unit time of scattering an electron, Δ is the difference between the Fermi energy and the energy at a corner of the first Brillouin zone, c is the c-axis lattice spacing, and the other symbols have their usual meaning. Since the value of Δ depends primarily on the number of electrons per atom, and the fraction of these which are trapped, and $1/\tau$ depends on the density of scattering centers, it may be seen that equation (1) is a quantitative statement of the relation between the resistivity, the density of scattering sites, and the fraction of electrons trapped. The relationship between the number of electrons trapped per atom of the solid, m, and Δ has been given by Hennig (1951) as

$$\frac{2.2m}{k^2T^2} = \frac{1}{2}\left(\frac{\Delta}{kT}\right)^2 + \frac{\pi^2}{6} - 2\sum_{n=1}^{\infty} \frac{(-1)^n}{n^2} \exp\frac{-n\Delta}{kT} \tag{2}$$

if kT and Δ are expressed in electron volts.

We shall now determine values of Δ, and hence m and τ, using these equations and the data observed. Let ρ_0 be the initial resistivity of a specimen; $\rho_i(\phi)$ the resistivity after irradiation in an integrated flux ϕ; $1/\tau_0$ the probability per unit time of scattering an electron wave, due to thermal effects and to lattice defects of all kinds which are present in the unirradiated graphite; $1/\tau_i(\phi)$ that due to imperfections introduced on irradiation; and $1/\tau_a(\phi)$ that due to imperfections, other than those in the original lattice, which remain after annealing.

If we assume that the imperfections responsible for the scattering are independent, that is, that the displaced atoms and vacancies formed on irradiation or remaining after annealing are sufficiently far from other scattering centers of all sorts that they do not overlap, and that the concentration of imperfections resulting from irradiation is proportional to the integrated flux ϕ received, we may define constants S_i and S_a such that

$$1/\tau_i(\phi) = S_i\phi, \qquad 1/\tau_a(\phi) = S_a\phi \tag{3a}$$

and, further,

$$\frac{1}{\tau} = \frac{1}{\tau_0} + \frac{1}{\tau_i(\phi)}. \tag{3b}$$

We shall also assume that the number of electrons trapped per atom of carbon, m, is proportional to the integrated flux, and write

$$m = \mu\phi = n\sigma\phi, \tag{4}$$

where n is the number of electrons trapped per displaced atom and σ is the cross section per atom for the displacement of atoms by neutrons. We shall neglect the change in c-axis spacing which appears in equation (1), as this can be shown to introduce a negligible correction to the results.

Substitution of these terms in equation (1) leads to the expression

$$\frac{\rho_i(\phi)}{\rho_0} = (1+S_i\tau_0\phi)\frac{2\ln 2}{2\ln\{1+\exp(\Delta/kT)\}-\Delta/kT} \tag{5}$$

and an analogous expression for $\rho_a(\phi)/\rho_0$.

Experimental values for $\rho_a(\phi)/\rho_0$ are plotted in Fig. 3 as a function of ϕ. It is apparent that the ratio of the resistivity of a specimen annealed at 128° after irradiation, to that of the initial unirradiated resistance, is proportional to the integrated flux received, and hence cannot depend on Δ. Regardless of the form of the dependence of the resistivity on Δ, this can only mean that Δ for such specimens is the same as that for unirradiated specimens. We may therefore conclude independently of Wallace's theory that the imperfections remaining after annealing do not trap appreciable numbers of electrons. Values for $S_a\tau_0$ obtained from the slopes of the lines in Fig. 3 are given in Table II.

TABLE II

VALUES OF THE PARAMETERS GIVING A "BEST" FIT IN EQUATIONS (3), (4), AND (5)

Irradiation facility	S-9-5	S-15-5	S-9-4
$S_i\tau_0$ (cm.²/neutrons)	6.2×10^{-20}	6.1×10^{-20}	3.3×10^{-20}
$S_a\tau_0$ (cm.²/neutrons)	2.2×10^{-20}	2.2×10^{-20}	1.2×10^{-20}
μ (cm.² electrons/atom neutrons)	3.5×10^{-23}	2.8×10^{-23}	1.6×10^{-23}
$S_i\tau_0/\mu$ (atoms/electrons)	1.7×10^{3}	2.2×10^{3}	2.0×10^{3}
S_i/S_a	2.8	2.8	2.7
n (electrons/displaced atom)	1.4	1.1	1.1

A sensitive test of the usefulness of Wallace's theory is provided by comparing the ratios S_i/S_a and $S_i\tau_0/\mu$ obtained in the three irradiation facilities. These ratios are independent of the intensity of the flux, although they will depend on the form of the flux spectrum. Since the form of the spectrum is expected to be very similar in the three positions, constancy of these ratios will be a more stringent test than showing that the data for any one facility can be fitted by an equation of the form (5) by suitable choice of parameters.

Values of $S_i\tau_0$ and μ which give the "best" fit to the data may be obtained for this purpose as follows: a value for μ is assumed; from this and equations (2) and (4) the values of $\Delta(\phi)$ are determined for the appropriate ϕ. These calculated values and the corresponding experimental values of $\rho_i(\phi)/\rho_0$ are then used to determine, by means of a least-squares fit, the value of $S_i\tau_0$. The value of μ which gives the smallest root-mean-square deviation of the experimental points from a straight line, as required by equation (5), is selected as the "best" value. The sensitivity of the root-mean-square deviation to change in μ is shown in Fig. 4 for a typical case. The values of the parameters determined in this way are given in Table II.

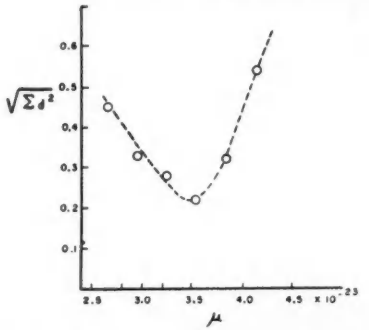

FIG. 4. Root-mean-square deviation of the data from the "best" straight line whose slope is $S_i\tau_0$ for data for S-9-5. μ is expressed in cm.^{2} electrons/atom neutrons, while d is, of course, dimensionless.

It is very desirable to determine a value for the number of electrons trapped per displaced atom, n. This we can do from values obtained for $\mu = n\sigma$, by calculating σ, the cross section per atom for the displacement of atoms, using a method given by Seitz (1949). This method requires a knowledge of the flux spectrum, which we shall assume is given by

$$\eta(E)dE = \frac{\phi_0}{c}\frac{dE}{E},$$

where ϕ_0 is the thermal neutron flux as measured by cobalt monitors, E is the energy of the neutron, and c is the ratio of the density of thermal neutrons as defined above to the density of neutrons in an energy interval ln E. We then find, following Seitz's (1949) procedure, that the fraction of the atoms displaced per unit flux, σ, is $1.0\times10^{-21}/c$ displaced atoms per atom/neutrons per square cm. According to activation experiments by Butler (1956) on gold and cobalt with and without cadmium shielding, values for c are 40 in S-9-5 and S-15-5 positions, and $\sim$66 in S-9-4. Corresponding values for n, the number of electrons trapped by each displaced atom, are given in Table II.

Considering the approximations involved, the agreement between the three values for $S_i\tau_0/\mu$, S_i/S_a, and n is surprisingly good. No reliance should be put on the numerical values for n, as they may all be in error by a common factor of at least two. This error arises both from the approximations used in the calculations, and from the assumption that all the atoms displaced during irradiation remain as displaced atoms at room temperature. Austerman and Hove (1955) have shown that the resistivity changes in graphite irradiated at liquid helium temperatures decrease on annealing to room temperature, but it is not yet established that this is due to annealing or clustering of displaced atoms. We feel, however, that the values of n so obtained are physically reasonable, and conclude from this that the method which Seitz gives for calculating the number of displaced atoms gives at worst a lower limit to the number produced. This is true because, although both the lattice

vacancy and the displaced atom may trap electrons, it is unlikely that more than three or four electrons would be trapped for each atom displaced. Since it is most probable that the atoms displaced by irradiation at temperatures above 0° C. are clustered, we cannot set a lower limit on the number of electrons trapped by each displaced atom. We can, however, conclude that the method of Seitz gives values for the number of displaced atoms which are not too low, for otherwise the values for n would be unreasonably large.

In conclusion, then, we may state that, independent of the theory used, the imperfections left in graphite after short neutron irradiations, followed by an anneal at 128° C., do not trap electrons; that the equation (1) derived by Hennig, based on the Wallace tight binding theory for graphite, can be used to explain the observed facts; and that the method given by Seitz for estimating the average number of atoms displaced by an incident neutron gives in this case values which are not unreasonable, and which are not too small.

ACKNOWLEDGMENTS

We would like to thank Mr. R. L. Cushing for assistance in setting up the apparatus used in the experiment, Dr. R. E. Jervis for assistance with cobalt monitors, and Mr. H. Sheard for some helpful suggestions. We also acknowledge many helpful discussions with Dr. P. J. Dyne and Dr. R. H. Betts.

REFERENCES

AUSTERMAN, S. B. and HOVE, J. E. 1955. Phys. Rev. **100**, 1214.

BOWEN, D. 1949. NAA-SR-33, The electrical conductivity of irradiated graphite, Pt. I; 1950. NAA-SR-39, The electrical conductivity of irradiated graphite, Pt. II. Available on microcards from Reference Services Branch, Technical Information Service, U.S. Atomic Energy Comm., Oak Ridge, Tenn., U.S.A.

BURTON, M. and NEUBERT, T. J. 1956. J. Appl. Phys. **27**, 557. See also the U.S. Atomic Energy Comm. Rept. ANL-5472, Neutron-induced discomposition of graphite.

BUTLER, J. P. 1956. Private communication.

HENNIG, G. R. 1951. J. Chem. Phys. **19**, 922.

HENNIG, G. R. and HOVE, J. E. 1956. Proceedings of the International Conference on the Peaceful Uses of Atomic Energy, Vol. 7 (United Nations, New York), p. 666.

KINCHIN, G. 1954. J. Nuclear Energy, **1**, 124.

——— 1956. Proceedings of the International Conference on the Peaceful Uses of Atomic Energy, Vol. 7 (United Nations, New York), p. 472.

SEITZ, F. 1949. Discussions Faraday Soc. **5**, 271.

WALLACE, P. R. 1947. Phys. Rev. **71**, 622.

WOODS, W. K., BUPP, L. P., and FLETCHER, J. F. 1956. Proceedings of the International Conference on the Peaceful Uses of Atomic Energy, Vol. 7 (United Nations, New York), p. 455.

PHOTONEUTRON EMISSION FROM Th^{232}, U^{233}, U^{238}, AND Pu^{239} [1]

L. KATZ, K. G. MCNEILL,[2] M. LEBLANC,[3] AND F. BROWN[4]

ABSTRACT

Measurements have been made of the numbers of neutrons emitted by the fissile materials Th^{232}, U^{233}, U^{238}, and Pu^{239} under irradiation by betatron X-rays of various energies up to 23 Mev. Yield curves and corresponding cross section curves are given for these nuclides. At low X-ray energies it is found that the yield curves differ from those found with non-fissile heavy elements, corresponding to the fact that even at zero X-ray energy the fissile materials suffer (spontaneous) fission.

INTRODUCTION

The measurement of neutron emission under betatron X-ray irradiation by the fissionable nuclides Th^{232}, U^{233}, U^{238}, and Pu^{239} is of interest both as a continuation of the program of photoneutron investigation carried out in this laboratory and because these data may yield interesting results when analyzed in the light of investigations of photoneutron reactions in non-fissile heavy elements and photofission reactions in these nuclides.

In the study of neutron emission from photoexcited fissile materials there can be no clear-cut distinction between photoneutron and photofission reactions, as some excited nuclei may decay by the emission of one or more neutrons followed by the fissioning of the still-excited daughter nucleus. In fact the total photon capture cross section is

$$\sigma_{\text{total}} = \sigma_{\gamma\gamma'}+\sigma_{\gamma n}+\sigma_{\gamma 2n}+\ldots+\sigma_{\gamma f}+\sigma_{\gamma nf}+\sigma_{\gamma 2nf}+\ldots .$$

Other reactions, involving the emission of charged particles, may be neglected owing to their inhibition by Coulomb forces. Following Gindler, Huizenga, and Schmitt (1956), it is convenient to use the terms:

$$\sigma_{\gamma N} = \sigma_{\gamma n}+2\sigma_{\gamma 2n}+\ldots+\nu\sigma_{\gamma f}+(\nu+1)\sigma_{\gamma nf}+\ldots$$

and

$$\sigma_{\gamma F} = \sigma_{\gamma f}+\sigma_{\gamma nf}+\sigma_{\gamma 2nf}+\ldots$$

to denote the effective cross sections for neutron emission ($\sigma_{\gamma N}$) and photofission ($\sigma_{\gamma F}$). $\sigma_{\gamma n}$ and $\sigma_{\gamma f}$ will be used, as above, to denote single neutron emission or simple fission. In the expression for $\sigma_{\gamma N}$, ν is the average number of neutrons emitted when a nucleus undergoes simple fission (roughly $\nu = 2.5$), and should not be confused with the average number of neutrons that are obtained for every one fission that takes place in a bulk of irradiated material, that is: $\sigma_{\gamma N}/\sigma_{\gamma F}$. ν will probably itself be a function of X-ray energy.

Measurements of the photofission ($\sigma_{\gamma F}$) cross section of U^{238} have been

[1]Manuscript received December 17, 1956.
Contribution from the Department of Physics, University of Saskatchewan, Saskatoon, Sask., and Chemistry Branch, Atomic Energy of Canada Ltd., Chalk River, Ont.
Issued as A.E.C.L. No. 423.
[2]On summer leave of absence from the University of Glasgow, Glasgow, Scotland.
[3]Now at the Department of Physics, University of British Columbia, Vancouver, B.C.
[4]Atomic Energy of Canada Ltd., Chemistry Branch, Chalk River Project, Chalk River, Ont.

made by Katz *et al.* (1955) using chemical separation of the fission products, and similar work has been carried out at the University of Illinois (Gindler, Huizenga, and Schmitt 1956) in U^{238} and Th^{232}. The latter authors also measured radiochemically the cross sections for the reactions $U^{238}(\gamma, n)U^{237}$ and $Th^{232}(\gamma, n)Th^{231}$. Photofission experiments on a number of fissile materials, including U^{233}, U^{238}, Th^{232}, and Pu^{239}, are at present being carried out in this laboratory.

Measurements of neutron emission yields from U have been made by Nathans and Halpern (1954) and from U and Th by Price and Kerst (1950). In Russia, Lazareva, Gavrilov, Valuev, Zarsepina, and Stavinsky (1955) have measured the yield curves and cross sections for neutron emission (γ, N) for Th and U in the energy range 6–28 Mev.

In the present experiments the (γ, N) yield curves and corresponding cross sections have been measured from 23 Mev. down to approximately 5.5 Mev. in the cases of U^{238} and Th^{232}, and down to approximately 6.5 Mev. in the cases of U^{233} and Pu^{239}.

EXPERIMENTAL PROCEDURE

The paraffin-embedded BF_3 long-counter apparatus used in this experiment to detect the emitted neutrons has been previously described (Montalbetti, Katz, and Goldemberg 1953). In order to reduce neutron background, mainly produced by (γ, n) reactions in the lead of the betatron beam collimator, the higher energy work was carried out in a room separated from the betatron by a 7 foot concrete wall, through which a hole was drilled for the X-ray beam. At lower energies the betatron room background is lower, and in order to increase the measured yield in the range of 5–8 Mev., work was carried out in this room. As an additional precaution, the lead collimator was replaced by one of iron.

In the original neutron detection apparatus only one BF_3 counter embedded in paraffin was used. This was so positioned that its response was insensitive to the initial energy of the neutrons. The addition of three other BF_3 counters has been found to increase the detection efficiency of the apparatus fivefold, and not to introduce any appreciable errors due to the fact that these counters were not specifically located in neutron energy insensitive positions (LeBlanc 1954). Therefore the setup with four counters was generally used, but as an additional precaution only the energy insensitive counter was used during the normalization runs in which the neutron emissions from the fissile materials were compared with the neutron emission from copper.

The samples were highly purified samples of Th, U, and Pu shaped in the form of disks. Each disk was embedded in polystyrene, which was placed in a thin cylindrical holder of Al. An aluminum cylinder of the same size as the others, but containing only polystyrene, was used to determine the reaction background from the holders when under irradiation.

Table I lists the compositions and areal densities of the fissile samples used. Although all the compounds used in this work contained oxygen, the contribution of this element to the number of neutrons detected is negligible, amounting at the most to less than 0.1% of the total, owing to the compara-

TABLE I

Nuclide	Compound	Sample thickness, g./cm.^{2}
Th^{232}	ThO_2	1.26
U^{233}	U_3O_8	0.684
U^{238}*	U_3O_8	0.760
Pu^{239}†	PuO_2	0.779

*This sample depleted in U^{235}.
†This sample contained a small amount of Pu^{240}.

tively high threshold energy and low cross section of the $O^{16}(\gamma, n)O^{15}$ reaction.

Calculation of the correction factor for absorption of the bremsstrahlung within the sample has been described by Montalbetti *et al.* (1953). In the present experiment, the necessary correction for X-ray absorption in no case exceeded 3%.

Activity leading to neutron emission may be induced in a sample by bombardments other than by bremsstrahlung. These are:

(*a*) neutrons emitted by the sample itself causing fission in the sample,

(*b*) neutrons in the betatron beam causing fission,

(*c*) neutrons emitted by the sample holders causing fission.

All these possibilities were considered, and it was found that none of these sources could cause 1% of the measured number of neutrons.

Not all emitted neutrons are detected by the BF_3 counters and the absolute efficiency of the apparatus was unknown. Use was therefore made of the fact that the number of neutrons emitted by natural Cu when irradiated with a 22 Mev. maximum energy X-ray beam is known by activation methods to be 2.71×10^8 n./100 r./mole.* A sample of Cu of areal density 0.911 g./cm.^{2} was irradiated at 22 Mev., and the measured yield compared with the measured yields from the fissile samples under identical conditions. The absolute 22 Mev. yield for these samples was thus obtained, and yield versus energy curves for the samples were normalized at this energy. Bremsstrahlung absorption in the Cu necessitated a correction of 1% to the measured copper yield.

The X-ray beam intensity was normally measured by an ionization chamber whose output was integrated. The X-ray energy response of this chamber was checked against a Victoreen chamber placed in an 8 in. lucite block. No absolute beam measurements had to be made, as all results were, as stated above, normalized against the 22 Mev. Cu yield.

RESULTS AND DISCUSSION

The yield curves of the four fissile materials studied, in neutron yield per 100 roentgens per mole, with respect to betatron operating energy are shown at the tops of Figs. 1, 2, 3, and 4. The low energy ends of the yield curves for

*The yield from natural copper used in the paper by Montalbetti, Katz, and Goldemberg (1953) was 3.01×10^8 neutrons per 100 roentgens per mole. Measurements by Johns in our laboratory have shown our Victoreen monitor to read 10% too low at energies above a few Mev. The yield has thus been correspondingly reduced.

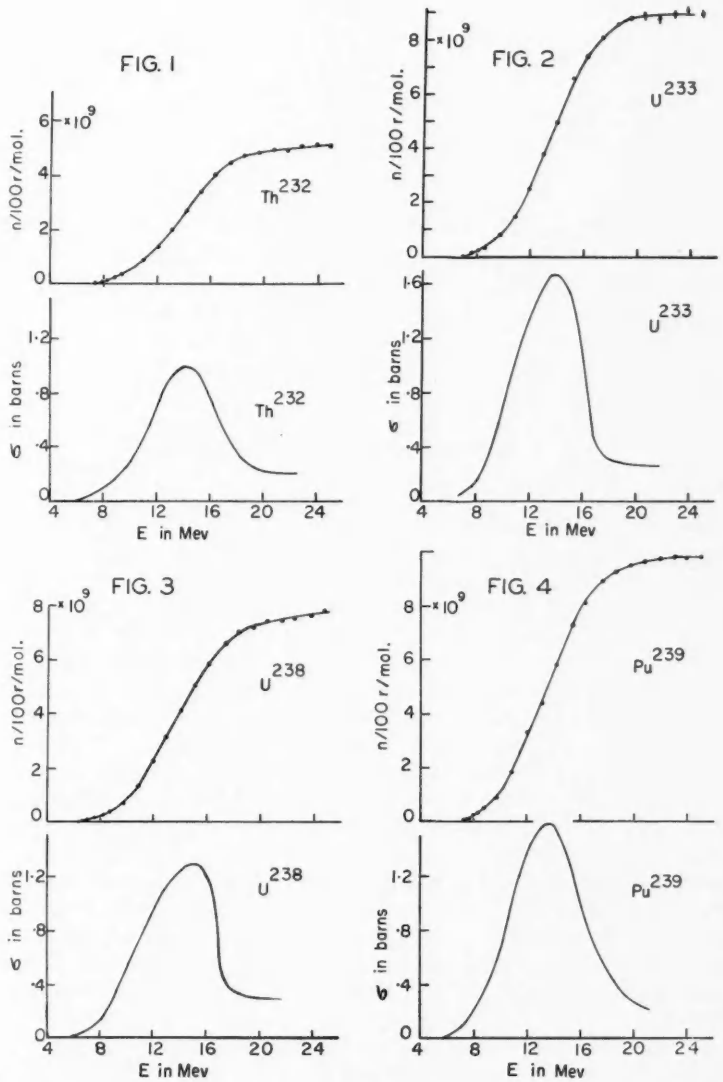

FIG. 1. Yield and cross section curves for the total neutron emission, (γ, N), from Th^{232} under betatron X-ray irradiation.
FIG. 2. (γ, N) yield and cross section curves for U^{233}.
FIG. 3. (γ, N) yield and cross section curves for U^{238}.
FIG. 4. (γ, N) yield and cross section curves for Pu^{239}.

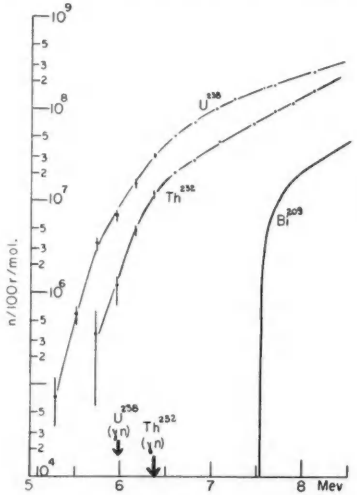

FIG. 5. The low energy section of the U^{238}, Th^{232}, and Bi^{209} neutron yield curves plotted on a logarithmic scale. Compared with the previous figures, the energy scale is expanded.

U^{238} and Th^{232} are shown on an expanded scale in Fig. 5. These curves are believed to be accurate within the statistical accuracy of the individual points. This accuracy varies from about 2% at 22 Mev. to 3% at 12 Mev. and to about 30% at 6 Mev.

To find the cross section curves corresponding to the measured yields the "inverted matrix" method of analysis of Leiss and Penfold (to be published) was used. This is a development of the "photon-difference" method of analysis. The results of these calculations are shown at the bottom of Figs. 1, 2, 3, and 4.

To some extent the smoothing of the yield curves, necessary before the cross sections can be calculated, is arbitrary and subjective. As a result there may be some distortion of the actual shapes of the cross sections. It is regarded that possible errors of 25% should be attributed to any one point of the cross section curve. However, such parameters as the energy of the maximum cross section, and the integrated cross section, $\int\sigma(E)dE$, are not very sensitive to the smoothing process or to the actual shape of the bremsstrahlung spectrum chosen. A greater degree of confidence may thus be placed in these parameters.

In Table II are given the values found in the present experiment of the reaction parameters: maximum cross sections, σ_{max}, the energies corresponding to these maxima, $E(\sigma_{max})$, the half widths of the giant resonances, Γ, the integrated cross sections, $\int_0^{22}\sigma dE$, and the 22 Mev. yields. For comparison, in Table III are listed corresponding values found by other authors, where these are available.

From the tables it will be apparent that there is reasonable agreement between the results of the present work and those of the other authors quoted.

TABLE II

Nuclide	22 Mev. yield, n./100 r./mole	σ_{max}, barns	$E(\sigma_{max})$, Mev.	Γ, Mev.	$\int_0^{22}\sigma_g dE$, Mev-barns
Th^{232}	5.00×10^9	0.99	14.2	6.0	7.15
U^{238}	7.54×10^9	1.29	15.2	6.4	9.74
U^{233}	8.88×10^9	1.67	14.0	6.0	11.2
Pu^{239}	9.51×10^9	1.58	13.6	6.3	11.6
Cu (63 and 65)	2.71×10^8	(normalization figure)			

TABLE III

Nuclide	22 Mev. yield, n./100 r./mole $\times10^9$	σ_{max}, barns	$E(\sigma_{max})$, Mev.	Γ, Mev.	$\int\sigma_g dE$, Mev-barns
Th^{232}	3.9 (*a*)*	0.80±0.10 (*c*)	14.5 (*c*)	5.6 (*c*)	6.6±0.6 (*c*)
U^{238}	5.3 (*a*)	0.98 (*b*)	13.8 (*b*)	6.6 (*b*)	7.15 (*b*)
	5.75 (*b*)	1.18±0.15 (*c*)	14.9 (*c*)	6.8 (*c*)	12.9±1.0 (*c*)

*(*a*) Price and Kerst 1950. (*b*) Nathans and Halpern 1954. (*c*) Lazareva *et al.* 1955.

From Fig. 5 it will be seen that the initial portions of the uranium and thorium yield curves may be divided into three parts. In the high energy and low energy parts, the logarithm of the yield is roughly proportional to the photon energy, whilst the third and middle region is one of transition between the other two. This transition occurs around 6–7 Mev. The upper region from 7 Mev. upwards lies above the (γ, n) threshold (6.0 Mev. for U^{238} (Huizenga *et al.* 1951) and 6.4 Mev. for Th^{232} (Magnusson *et al.* 1951) and also above what is often termed the fission threshold.* This region, indeed the whole curve above 7 Mev., shows a neutron yield – photon energy dependence which is typical of the photon absorption process. We have shown in Fig. 5 the initial portion of the bismuth photoneutron excitation curve (Chidley and Katz 1956). This curve is typical for non-fissile heavy elements; for energies more than 1 Mev. above the (γ, n) threshold it corresponds to the total photon absorption curve since neutron emission is the dominant mode of de-excitation.

The U^{238} and Th^{232} curves above 7 Mev. and the Bi^{209} curve above the Bi(γ, n) threshold are clearly similar. In this region then we may suppose that the probabilities of fission and neutron emission in those U and Th nuclei which have absorbed photons do not vary rapidly with photon energy. This agrees with the fact that the ratio of (γ, f) to (γ, n) in U^{238} is roughly constant over a wide photon energy range (8–22 Mev.) (Duffield and Huizenga 1953). The slope of the curves above 7 Mev. is thus governed chiefly by the increase in the photon absorption cross section with photon energy. It must be emphasized however that one should expect the neutron yield per absorbed photon from U and Th to decrease somewhat above the (γ, n) threshold. This is because below the (γ, n) threshold for each photon absorbed we have 2.5 neutrons (fission), while above this threshold some of the absorbed photons result in only one neutron (γ, n) reaction. A rough estimate of the change in

*This is a somewhat vague term. In the present context it may be taken to mean the energy above which fission accounts for a significant fraction of all de-excitation modes.

slope in the U and Th curves of Fig. 5 as the (γ, n) threshold is crossed shows that it cannot all be accounted for by the presence of (γ, n) competition on the higher energy side. This may indicate a considerable barrier effect against fission.

As the photon energy falls below the (γ, n) threshold the bismuth neutron yield necessarily drops extremely rapidly to zero yield. The uranium and thorium curves pass through a transition region which is longer than the sharp "knee" in the Bi curve and reach a steep but not vertical region extending from 6 or 6.5 Mev. downwards in which the neutron yield is due entirely to fission. In this energy range we must suppose that the probability of fission following photon absorption is strongly energy dependent; probably fission barrier effects have now become important. The steep slope of this curve is therefore due partly to the decrease in photon absorption with decreasing energy and partly to the decrease in the probability of de-excitation by fission as the excitation energy is lowered.

Useful data on Pu^{239} could not be obtained below 6.5 Mev. owing to the high neutron background caused by the spontaneous fission of Pu^{240}.

ACKNOWLEDGMENTS

We wish to acknowledge our thanks to the National Research Council of Canada for providing funds for the University of Saskatchewan Betatron research program.

One of us (K. G. McN.) wishes to express his thanks to the Royal Society of London and to the Nuffield Foundation for making possible his participation in this work, and another of us (M. LeB.) wishes to thank the National Research Council for a bursary held during this research.

REFERENCES

CHIDLEY, B. and KATZ, L. 1956. Unpublished.
DUFFIELD, R. B. and HUIZENGA, J. R. 1953. Phys. Rev. **89**, 1042.
FULLER, E. G. and HAYWOOD, E. 1955. Phys. Rev. **101**, 692.
GINDLER, J. E., HUIZENGA, J. R., and SCHMITT, R. A. 1956. Phys. Rev. **104**, 425.
HUIZENGA, J. R., MAGNUSSON, L. B., FIELDS, P. R., STUDIER, M. H., and DUFFIELD, R. B. 1951. Phys. Rev. **82**, 561.
KATZ, L., KAVANAGH, T. M., CAMERON, A. G. W., BAILEY, E. C., and SPINKS, J. W. T. 1955. Phys. Rev. **99**, 98.
LAZAREVA, L. E., GAVRILOV, B. I., VALUEV, B. N., ZARSEPINA, G. N., and STAVINSKY, V. S. 1955. Division of Physical-Mathematical Sciences, Session of the Academy of Sciences of U.S.S.R. on Peaceful Uses of Atomic Energy, July 1st, 1955, Vol. I, p. 217.
LEBLANC, M. 1954. M.A. Thesis, University of Saskatchewan, Saskatoon, Sask.
MAGNUSSON, L. B., HUIZENGA, J. R., FIELDS, P. R., STUDIER, M. H., and DUFFIELD, R. B. 1951. Phys. Rev. **84**, 166.
MONTALBETTI, R., KATZ, L., and GOLDEMBERG, J. 1953. Phys. Rev. **91**, 659.
NATHANS, R. and HALPERN, J. 1954. Phys. Rev. **93**, 437.
PRICE, G. A. and KERST, D. W. 1950. Phys. Rev. **79**, 725; **77**, 806.

THE GRAVITATIONAL FIELDS OF ELECTRIC AND MAGNETIC DIPOLES[1]

GERALD E. TAUBER

ABSTRACT

Einstein's field equations are solved for cylindrical symmetry in the presence of electric and magnetic singularities (dipoles).

1. INTRODUCTION

Amongst the few known exact solutions of Einstein's field equations are the ones representing the gravitational field of a charged mass or several charged masses distributed with rotational symmetry (Weyl 1917; Curzon 1925; Papapetrou 1947). It would be of some interest to find solutions corresponding to more general situations, say the fields due to rotating magnetic dipoles which occur in some astrophysical problems. Unfortunately the non-linear character of the field equations makes it extremely difficult to find exact solutions of the resulting system of equations.

Recently Bonnor (1954) has shown that some known electrostatic solutions of the field equations can be adapted to the magnetostatic case by the introduction of the conjugate field tensors F^{*ij}. However, if both electric and magnetic sources are present his solutions are not applicable. The property of cylindrical symmetry on the other hand permits us to include both types of sources in the equations. Moreover, the resulting equations for the electromagnetic potentials are of a very simple structure and can be solved by an extension of the work of Curzon (loc. cit.). It is the purpose of this note to discuss this extension of Curzon's work and to obtain the solution of the field equations for electric and magnetic dipoles.

2. THE FIELD EQUATIONS

In canonical co-ordinates the line element for a field with axial symmetry is given by

$$ds^2 = -e^{\lambda}[(dx^1)^2 + (dx^2)^2] - e^{-\rho}(x^2)^2(dx^3)^2 + e^{\rho}(dx^4)^2, \tag{1}$$

where x^1 is the axis of symmetry, x^2 is a radial co-ordinate, x^3 the angular co-ordinate, and x^4 time-like. Both λ and ρ are functions of x^1 and x^3 only. In a region free of matter Maxwell's equations are (cf. Tolman 1934)

$$F_{\mu\nu} = \frac{\partial A_\mu}{\partial x^\nu} - \frac{\partial A_\nu}{\partial x^\mu}, \qquad \frac{\partial(\sqrt{-g}\,F^{\mu\nu})}{\partial x^\nu} = 0, \tag{2}$$

where A_μ are the components of the four-potential and $F_{\mu\nu}$ the electromagnetic field tensor. In accordance with the symmetry requirement of (1) A_μ are functions of x^1 and x^2 only. All non-zero components of the electromagnetic field tensor can be obtained from two components of the potential:

[1]Manuscript received November 30, 1956.
Contribution from the Department of Physics, Western Reserve University, Cleveland, Ohio.

(3) $$\psi = A_4 \text{ and } \phi = A_3.$$

With these conditions the surviving Maxwell's equations (2) then become

(2a) $$\frac{\partial}{\partial x^1}\left(\frac{e^\rho}{x^2}\,\phi_1\right)+\frac{\partial}{\partial x^2}\left(\frac{e^\rho}{x^2}\,\phi_2\right) = 0,$$

(2b) $$\frac{\partial}{\partial x^1}(e^{-\rho}x\,\psi_1)+\frac{\partial}{\partial x^2}(e^{-\rho}x\,\psi_2) = 0.$$

The field equations in the presence of magnetic fields are given by (Tolman, loc. cit.)

(4) $$R^\mu_\nu-\tfrac{1}{2}\,g^\mu_\nu R = -\kappa T^\mu_\nu, \qquad T^\mu_\nu = -F^{\mu\alpha}F_{\nu\alpha}+\tfrac{1}{4}g^\mu_\nu F^{\alpha\beta}F_{\alpha\beta},$$

where κ denotes the gravitational constant and R^μ_ν is the Ricci tensor. For cylindrical symmetry they have already been given by Curzon* (1925):

(4a) $$\lambda_{11}+\lambda_{22}+{\rho_1}^2+\frac{\lambda_2}{x^2} = -\kappa\frac{e^\rho}{(x^2)^2}\,({\phi_1}^2-{\phi_2}^2)+\kappa e^{-\rho}({\psi_1}^2-{\psi_2}^2),$$

(4b) $$\lambda_{11}+\lambda_{22}+{\rho_2}^2-\frac{\lambda_2}{x^2}-\frac{2\rho_2}{x^2} = \kappa\frac{e^\rho}{(x^2)^2}\,({\phi_1}^2-{\phi_2}^2)-\kappa e^{-\rho}({\psi_1}^2-{\psi_2}^2),$$

(4c) $$\rho_1\rho_2-\frac{\rho_1}{x^2}-\frac{\lambda_1}{x^2} = -2\kappa\frac{e^\rho}{(x^2)^2}\,\phi_1\phi_2+2\kappa e^{-\rho}\psi_1\psi_2,$$

(4d) $$\rho_{11}+\rho_{22}+\frac{\rho_2}{x^2} = \kappa\frac{e^\rho}{(x^2)^2}\,({\phi_1}^2+{\phi_2}^2)+\kappa e^{-\rho}({\psi_1}^2+{\psi_2}^2).$$

In equations (2) and (4) and all following ones, the subscript 1 refers to differentiation with respect to x^1 and 2 to differentiation with respect to x^2.

In addition to these equations, the absence of a rotation term g_{34} yields a connection between the components of the four-potential

(4e) $$T^3_4 = T^4_3 = \phi_1\psi_1+\phi_2\psi_2 = 0.$$

It has been shown by Bonnor (1953) that in the case of an electrostatic field it is sufficient to solve equations (2b) and (4d). The presence of another component of the four-potential will not materially change the situation as we shall show in the following sections.

3. THE ELECTRIC DIPOLE

In the absence of any magnetic fields one can set $\phi = 0$ and thus obtain the case previously considered by Curzon *et al.* Assuming that ψ only depends on ρ, (2b) together with (4d) gives an equation for ψ,

(5) $$\psi_{\rho\rho} + \kappa e^{-\rho}\,\psi_\rho{}^3 - \psi_\rho = 0,$$

which has as a solution

(6) $$\psi = A(e^{\frac{1}{2}\rho}-1), \qquad \psi \to 0 \quad \text{as} \quad \rho \to 0,$$

where the constant A is given by

$$A = \sqrt{2/\kappa}.$$

*The difference between the present equations and those given by Curzon is the absence of terms depending on ϕ in his equations.

When this solution is substituted into (4*d*) this equation becomes

$$\rho_{11} + \rho_{22} + \rho_2/x^2 = \tfrac{1}{2}(\rho_1^2 + \rho_2^2), \tag{7}$$

which can be reduced to the axial harmonic

$$\sigma_{11} + \sigma_{22} + \sigma_2/x^2 = 0 \tag{7a}$$

by setting $\rho = -2 \ln \sigma$.

Curzon's solution in terms of two singularities on the axis of symmetry is given by

$$\sigma = K - \frac{\epsilon_1}{r_1} - \frac{\epsilon_2}{r_2}, \qquad K = 1 \quad \text{as} \quad \sigma \to 1, \quad \rho \to 0, \tag{8}$$

where r_1 and r_2 are bipolar co-ordinates of a point P referred to two origins A and B on the x^1-axis (see Fig. 1)

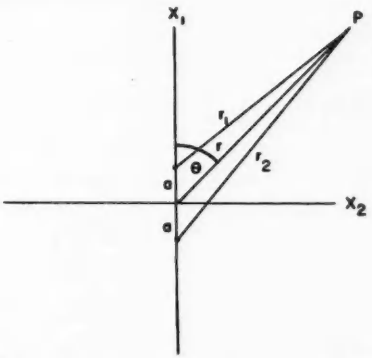

FIG. 1. Bipolar co-ordinates of point singularities in cylindrical co-ordinates. r_1 and r_2 are the bipolar co-ordinates of point P from the singularities, r and θ polar co-ordinates, a the distance from the origin.

$$\begin{aligned} r_1^2 &= (x^1 - a)^2 + (x^2)^2, \\ r_2^2 &= (x^1 + a)^2 + (x^2)^2, \end{aligned} \tag{9}$$

and ϵ_1 and ϵ_2 are constants of integration. Substituting (6) into the remaining equations (4) gives

$$\lambda + \rho = 0, \tag{10}$$

taking $\lambda = 0$ when $\rho = 0$, so that one finally obtains the following solution for two charged point masses along the axis of symmetry:

$$\psi = A\left[\left(1 - \frac{\epsilon_1}{r_1} - \frac{\epsilon_2}{r_2}\right)^{-1} - 1\right], \qquad A = \sqrt{2/\kappa}, \tag{11}$$

$$\lambda = -\rho = 2 \ln\left[1 - \frac{\epsilon_1}{r_1} - \frac{\epsilon_2}{r_2}\right]. \tag{12}$$

It is now simple to see how from (11) and (12) an "electric dipole" solution can be constructed. First of all, we shall assume that the two charges ϵ_1 and

ϵ_2 are of opposite sign but equal magnitude and thus put $\epsilon_1 = -\epsilon_2 = \epsilon$. If one expands r_1 and r_2 in terms of the distance r ($>a$) and aximuthal angle θ (see Fig. 1),

$$r_1^2 = r^2 + a^2 - 2ar\cos\theta,$$

$$r_2^2 = r^2 + a^2 + 2ar\cos\theta,$$

and lets a go to zero and at the same time ϵ go to infinity, so that

$$p = 2a\epsilon$$

remains finite, the potential is now given by

$$\psi = \frac{P\cos\theta}{r^2}, \tag{13}$$

where

$$P = \sqrt{2/\kappa}\, p,$$

while the gravitational potentials can be written as

$$e^{\lambda} = e^{-\rho} = 1 - \frac{p}{r^2}\cos\theta + \frac{p}{2r^4}\cos^2\theta. \tag{14}$$

It is seen that this solution is quite similar to the one corresponding to a charged mass-particle, which for a potential given by $\psi = \epsilon/r$ has as a solution of the field equations (Tolman 1934)

$$e^{\lambda} = e^{-\rho} = 1 - 2\sqrt{\frac{\kappa}{2}}\frac{\epsilon}{r} + \frac{\kappa}{2}\frac{\epsilon^2}{r^2}. \tag{15}$$

In both cases there are two terms, one of the order of the potential and one of its square, the terms having opposite sign.

4. THE MAGNETIC DIPOLE

If we have only magnetic fields, then it is possible to set $\psi = 0$ and to consider only the solution of Maxwell's equation (2*a*). At first sight it would not seem possible to apply the method of Curzon, as the form of this equation differs from the one previously considered (2*b*) and therefore also from the field equation (4*d*). However, if we define a new "potential" such that

$$\Phi_1 = -\frac{e^{\rho}}{x^2}\phi_2 \text{ and } \Phi_2 = \frac{e^{\rho}}{x^2}\phi_1 \tag{16}$$

equation (2*a*) is simply the compatibility condition $\Phi_{21} = \Phi_{12}$.

From the fact that we also demand that $\phi_{12} = \phi_{21}$ an equation for Φ is obtained,

$$\Phi_{11} + \Phi_{22} + \Phi_2/x^2 = \rho_1\Phi_1 + \rho_2\Phi_2. \tag{17}$$

It is seen that this is exactly of the form of (2*b*) and hence will have as a solution

$$\Phi = A'e^{\frac{1}{2}\rho} + B' \tag{18}$$

(assuming, of course, that Φ is only a function of ρ again). The rest of the calculation goes as before and one finally obtains for the two-particle solution

$$\lambda = -\rho = 2\ln\left(1-\frac{m_1}{r_1}-\frac{m_2}{r_2}\right), \tag{19}$$

where again m_1 and m_2 are constants of integration.

In terms of this solution the magnetic field components are given by

$$F_{31} = \phi_1 = -\sqrt{\frac{2}{\kappa}}\left[\frac{m_1(x^2)^2}{r_1^3}+\frac{m_2(x^2)^2}{r_2^3}\right], \tag{20a}$$

$$F_{32} = \phi_2 = \sqrt{\frac{2}{\kappa}}\left[\frac{m_1(x^1-a)\,x^2}{r_1^3}+\frac{m_2(x^1+a)\,x^2}{r_2^3}\right]. \tag{20b}$$

In order to obtain the vector-potential corresponding to a magnetic dipole we shall take $m_1 = m_2 = m$ and let a go to zero and m go to infinity so that

$$\mu = 2am$$

remains finite. Expanding in terms of the quantity a/r we get for the fields

$$\phi_1 = -\sqrt{\frac{2}{\kappa}}\,\frac{3\mu(x^2)^2}{r^4}\cos\theta, \tag{21a}$$

$$\phi_2 = \sqrt{\frac{2}{\kappa}}\left[-\frac{\mu x^2}{r^3}+\frac{3\mu x^1 x^2}{r^4}\cos\theta\right], \tag{21b}$$

and finally for the vector-potential

$$\phi = M\frac{(x^2)^2}{r^3} = \frac{\sin^2\theta}{r^5}, \tag{22}$$

where

$$M = \sqrt{2/\kappa}\,\mu.$$

The appropriate solution of the field equations then again becomes

$$e^{\lambda} = e^{-\rho} = 1-\frac{\mu}{r^2}\cos\theta+\frac{\mu^2}{2r^4}\cos^2\theta. \tag{23}$$

5. THE ELECTRIC AND MAGNETIC DIPOLE

Finally we wish to consider the case when neither ψ nor ϕ vanishes. The simplest possibility, although perhaps not of most physical interest, is to assume the presence of stationary electric and magnetic sources, viz. magnetic and electric dipoles. Outside the singularities, the field equations for empty space and the Maxwell's equation without current and charge distribution hold.

From the result of the last two sections one finds that the scalar and "alternate" vector-potential must be related through

$$\Phi = c\psi + E, \tag{24}$$

where c and E are arbitrary constants. This will also automatically satisfy equation (2e), which connects the two components of the four-potential. As a solution of Maxwell's equations, one again obtains

$$\psi = A''e^{ik\rho} \tag{25}$$

where, now, the constant A'' is given by

$$A'' = \sqrt{\frac{2}{\kappa(1+c^2)}}.$$

The solution of the field equations results in

$$e^{\lambda} = e^{-\rho} = 1 - \frac{d}{r^2}\cos\theta + \frac{d^2}{2r^4}\cos^2\theta, \tag{26}$$

where we have defined

$$d = \lim_{\substack{a\to 0 \\ m\to\infty}} 2am.$$

The corresponding scalar potential is given by

$$\psi = \frac{D\cos\theta}{r^2}, \qquad D = d\sqrt{\frac{2}{\kappa(1+c^2)}}, \tag{27}$$

and the appropriate vector-potential becomes

$$\phi = \frac{\bar{M}\sin^2\theta}{r^5}, \tag{28}$$

where we have defined

$$\bar{M} = cd\sqrt{\frac{2}{\kappa(1+c^2)}}.$$

It is thus seen that c measures the ratio of the electric to magnetic dipoles and that the total gravitational field is due to a superposition of the two. A simple way of seeing this is to express d in terms of D or M and thus write

$$d = \sqrt{\frac{\kappa(1+c^2)}{2}}\,D = \sqrt{\frac{\kappa(1+1/c^2)}{2}}\,\bar{M}. \tag{29}$$

6. CONCLUSION

Thus we have been able to find solutions of Einstein's field equations in empty space in the presence of magnetic and (or) electric fields. Although the solutions are based on rather special assumptions they describe actual physical situations, which may, however, play not too important a part in actual models. In connection with the field of the magnetic dipole it would be of great interest to see what would happen if it were to rotate. Unfortunately the line-element describing rotation is more complicated and so far no solutions have been obtained, although at present work is in progress along these lines.

REFERENCES

BONNOR, W. B. 1953. Proc. Phys. Soc. (London), A, **66**, 145.
——— 1954. Proc. Phys. Soc. (London), A, **67**, 225.
CURZON, H. E. J. 1925. Proc. London Math. Soc. **23**, 477.
PAPAPETROU, A. 1947. Proc. Roy. Irish Acad. **51**, 191.
TOLMAN, R. 1934. Relativity, thermodynamics and cosmology (Oxford at the Clarendon Press).
WEYL, H. 1917. Ann. Physik, **54**, 117.

ADIABATIC OSCILLATIONS IN LIQUID HELIUM II[1]

F. D. MANCHESTER[2] AND J. B. BROWN

ABSTRACT

Oscillations have been observed in an experimental arrangement consisting of an adiabatic container placed in a helium II bath and connected with the bath by means of a "superleak". A "thermal pulse" introduced into the container caused the liquid level to oscillate. Containers of different geometries and employing two different types of superleak were successfully used to observe oscillations. With one of these the temperature dependence of the frequency was measured between 1.39° and 2.065° K. and found to be of the form and magnitude expected from the calculations of Robinson (1951). Other features of the oscillations have been investigated. An analogy between the oscillations in an adiabatic container in liquid helium II and those of a gas in a Helmholtz resonator is suggested and discussed.

INTRODUCTION

In their pioneering paper on the superfluid properties of liquid helium II, Allen and Misener (1939) reported the observation of oscillations of the liquid level in a container which was partly immersed in a bath of the liquid and connected with the bath by means of a superleak, i.e., a flow channel through which only superfluid helium could move easily. These oscillations were later investigated by Atkins (1950), who used the helium II film as the superleak linking the container with the bath. Atkins provided an analysis of the oscillation mechanism taking into account the variations in thickness of the helium II film and from this was able to use measurements on the oscillation period to obtain information on the variation of the thickness of the film with height and with temperature.

Shortly after Atkins' work, Robinson (1951) produced a general analysis of the oscillatory flow of liquid between a container and a bath, which showed that oscillations could be divided into two groups. One group, the isothermal oscillations, were the type already reported by Allen and Misener and by Atkins; the other group, which Robinson called adiabatic oscillations, had not hitherto been observed. The present paper deals with an experimental investigation of these adiabatic oscillations and gives a more detailed account of experiments which were briefly reported on earlier (Manchester 1955 *a*, *b*). The study of these oscillations is of interest because it provides an opportunity for obtaining an experimental check on the equations of motion of liquid helium II in the region of small velocities when the equations are applied to the flow of liquid through a superleak.

OUTLINE OF THE THEORY OF OSCILLATIONS IN LIQUID HELIUM II

Isothermal oscillations have been fully discussed by Atkins (1950) and Robinson (1951). These oscillations occur in a system consisting of a container connected to a helium II bath by means of a superleak and under

[1]Manuscript received in original form June 12, 1956, and, as revised, December 12, 1956. Contribution from The Department of Physics, University of British Columbia, Vancouver, B.C.

[2]Present address: Division of Pure Physics, National Research Council, Ottawa.

conditions where there is very good thermal contact between container and bath. Their mechanism may be viewed as the periodic interchange of energy between the kinetic energy of the superfluid moving in the superleak and the potential energy of the difference in liquid levels. The type of arrangement in which these oscillations have been observed and their typical form are shown in Fig. 1(*a*). Isothermal oscillations have been observed by Allen

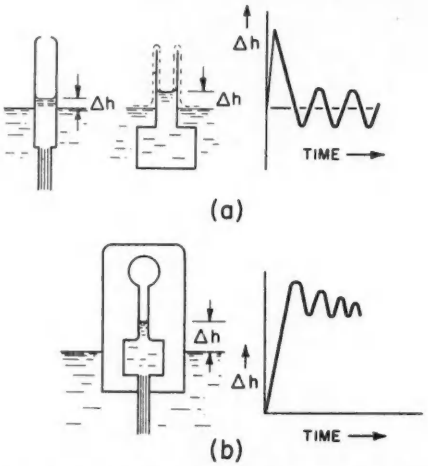

FIG. 1. Representation of (*a*) isothermal and (*b*) adiabatic oscillations. The isothermal case shows both the film and a channel system acting as superleaks.

and Misener (1939), Atkins (1950), and Picus (1954) but only in the case of Atkins' experiments were measures taken to ensure good isothermal conditions.

The case of the adiabatic oscillations may be considered by referring to Fig. 1(*b*). Instead of giving good thermal contact between the container and bath as in the isothermal case, the apparatus is designed to reduce the thermal contact to a minimum. Under these conditions temperature differences can be sustained between container and bath when liquid flows from one to the other. For example, when liquid is flowing from the container to the bath, the temperature of the container liquid rises because of the mechanocaloric effect, setting up a temperature gradient in such a direction that the thermomechanical effect tends to force liquid back into the container. As the superfluid moving in the superleak possesses sufficient inertia, this situation gives rise to oscillations.

A theoretical expression for the frequency of ideal isothermal oscillations was introduced by Allen and Misener and a derivation was later provided by Atkins for the case of the helium II film as superleak. Dash (1954) and Picus (1954) have produced analyses of isothermal oscillations dealing with particular aspects of the helium II film in the role of superleak. From the

analysis due to Robinson (1951) the angular frequency, ω_i, of the isothermal oscillations is given by

$$\omega_i = \left(\frac{\rho_s}{\rho}\frac{g\sigma}{la}\right)^{\frac{1}{2}}, \tag{1}$$

where ρ_s and ρ are the superfluid and bulk liquid densities respectively, g is the acceleration due to gravity, and as is shown in Fig. 2(a), σ is the cross-sectional area of the superleak, l its length, and a the cross-sectional area

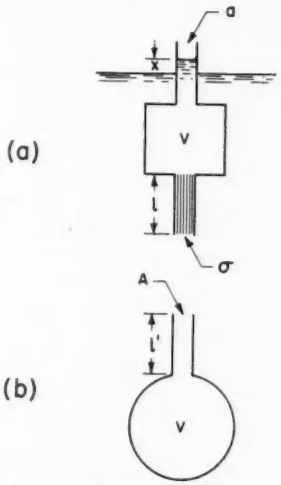

FIG. 2. The adiabatic container, (a), and the Helmholtz resonator, (b), showing geometrical parameters.

of the observational capillary. Atkins found experimentally that the frequency of the oscillations decreased with increasing temperature as expected from (1).

The frequency of ideal adiabatic oscillations ω_a, for the container of Fig. 2(a), is

$$\omega_a = \omega_i(1+\alpha)^{\frac{1}{2}}, \tag{2}$$

where

$$\alpha = \frac{aTS^2}{gVC}\left\{1 - \frac{1}{\rho S}\left(\frac{dp}{dT}\right)_{\text{vap}}\right\}.$$

In the above, S and C are the entropy and specific heat respectively of liquid helium II, $(dp/dT)_{\text{vap}}$ is the gradient of the vapor pressure curve, and T is the absolute temperature. For the derivation of this relation the reader is referred to Robinson's paper. Robinson has shown that the equations of motion describing the flow of superfluid have solutions which can be divided into three regions, according to the degree of thermal linkage between the container and bath. These are: the adiabatic oscillatory region for zero or

very low thermal linkage, an aperiodic region for intermediate values, and the isothermal oscillatory region for good thermal contact. The general solution for x, the position of the meniscus level in the container, may be written for an oscillatory region as

$$x = Ae^{-b\,t/\omega_a}\cos(pt/\omega_a-\phi)+Be^{-L\omega_i^2\,t/\omega_a^2}. \tag{3}$$

For the practical case of a container with some small but finite thermal linkage to the bath, the theoretical picture of the adiabatic oscillations is as follows. If the liquid in the container is suddenly displaced from its equilibrium position to some new position the liquid level will commence to oscillate with angular frequency p/ω_a, the oscillations being damped according to the magnitude of b. During this process and after the oscillations die out, the mean liquid level returns toward its initial position at a rate determined by the second term of the right-hand side of (3). For a particular temperature the p's and b's of (3) are dependent on L, the index of thermal linkage between container and bath ($L = 0$ and $L = \infty$ correspond to ideal adiabatic and ideal isothermal oscillations respectively), and therefore the frequency, damping, and aperiodic decrease observed in a particular experiment should depend on the amount of thermal isolation achieved. The temperature dependence of the ideal isothermal and ideal adiabatic oscillation frequencies, for the particular geometry of one of the containers used in the experiments to be described, is shown by the smooth curves of Fig. 5.

Equation (2) may be expressed in a form which is convenient for the calculation of numerical values:

$$\omega_a = \left(\omega_i^2+\omega_i^2 k\frac{aTS^2}{gVC}\right)^{\frac{1}{2}}$$

$$= (\omega_i^2+k\omega_R^2)^{\frac{1}{2}},$$

where

$$k = \left\{1-\frac{1}{\rho S}\left(\frac{dp}{dT}\right)_{\text{vap}}\right\}$$

and

$$\omega_R^2 = \omega_i^2\frac{aTS^2}{gVC}$$

$$= u_2^2\left(\frac{\rho_n}{\rho}\frac{\sigma}{lV}\right)$$

using equation (1) and the relation

$$u_2^2 = \frac{\rho_s}{\rho_n}\frac{TS^2}{C}$$

for the velocity of second sound (Landau 1941). It is shown in the appendix that ω_R may be identified with the natural frequency of an ideal adiabatic resonator.

The method of calculation used here is very insensitive to the values chosen

for the entropy and specific heat, which is an advantage, because the values of these quantities are somewhat uncertain at the present time (Brewer, Edwards, and Mendelssohn 1955). Geometrical constants of the apparatus are given in Table I and the data used in plotting the smooth curves of Fig. 5 are given in Table II.

TABLE I

GEOMETRICAL CONSTANTS OF THE APPARATUS

	Optical flats apparatus	Wire-filled-tube apparatus
Volume of chamber A	4.0 cm.^{3}	6.6 cm.^{3}
Observational capillary diameter	1.14 mm.	1.10 mm.
Length of superleak	0.68 cm.	11.7 cm.
Cross section of superleak	2×10^{-3} cm.^{2}	7.2×10^{-4} cm.^{2}

TABLE II

THEORETICAL VALUES OF ω_i, ω_R, AND ω_a FOR THE WIRE-FILLED TUBE APPARATUS

T,° K.	k	ω_i, radians/sec.	ω_R, radians/sec.	ω_a, radians/sec.
1.0	0.946	2.50	0.499	2.55
1.1	0.928	2.49	0.684	2.58
1.2	0.923	2.47	0.952	2.63
1.3	0.920	2.45	1.27	2.74
1.4	0.919	2.41	1.66	2.89
1.5	0.920	2.36	2.11	3.11
1.6	0.921	2.27	2.64	3.40
1.7	0.923	2.17	3.11	3.69
1.8	0.925	2.05	3.51	3.95
1.9	0.928	1.86	3.81	4.12
2.0	0.932	1.60	3.91	4.10
2.15	—	0.79	2.32	—
2.19	—	0	0	0

To obtain the calculated values of ω_i, ω_a, and ω_R the following experimental data were used: values of ρ_n/ρ and ρ_s/ρ from Peshkov (1946), second sound velocities from smoothed values quoted by Band and Meyer (1948) and by Maurer and Herlin (1949), the entropy of liquid helium II from Kramers *et al.* (1952), and the vapor pressure relation for liquid helium II from Bleaney and Simon (1939).

EXPERIMENTAL

Two versions of an adiabatic container were used in the experiments, one using the annular gap between two optically flat glass disks to provide a radial flow path which acted as a superleak, and later a container using a wire-filled tube superleak, similar to those used by Allen and Misener (1939), and Brown and Mendelssohn (1947). Some typical results obtained with the apparatus using optical flats have already been published (Manchester 1955*a*). A schematic diagram of the two types of containers and also the essentials of the auxiliary apparatus are shown in Fig. 3.

With both types of container the external experimental arrangements

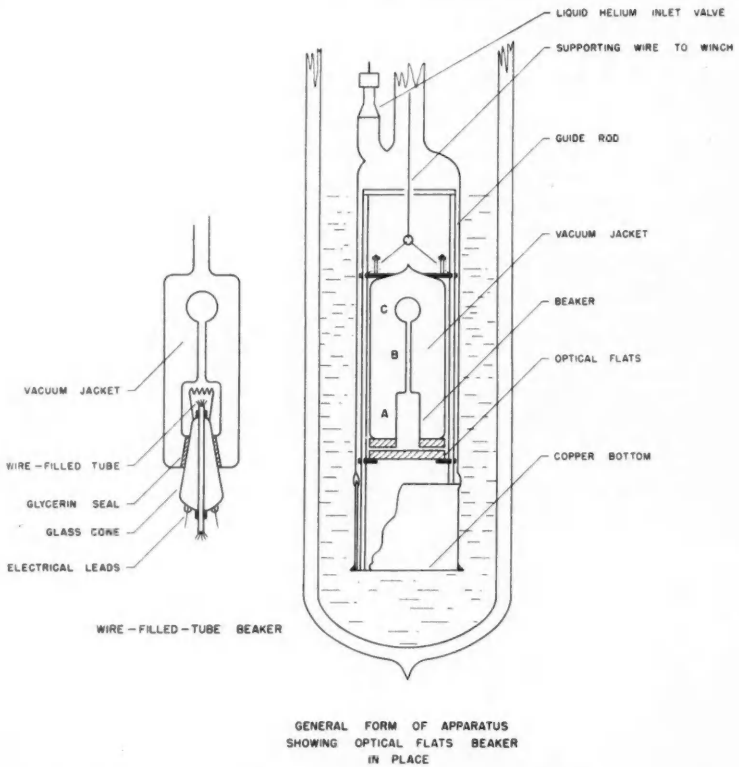

FIG. 3. Schematic diagram showing the general form of the apparatus and the two types of experimental beaker used. A is the main volume containing the heater, B is the observational capillary, and C is designed to minimize any pressure fluctuations above the liquid oscillating in the capillary.

were very similar. The experimental container, henceforth referred to as the "beaker", with its surrounding vacuum jacket, was enclosed in a large glass envelope to which liquid could be admitted from the surrounding liquid helium dewar. The lower end of this glass envelope was provided with a large copper–glass seal and a copper bottom to provide good thermal contact between the liquid in the envelope and the liquid being pumped in the main helium dewar. Arrangement was made for the beaker to be raised or lowered so that its position could be adjusted with respect to the liquid level in the envelope, the "bath level". The temperature of the liquid helium bath was stabilized to 10^{-4} ° K. or better by means of a bridge system of the type described by Boyle and Brown (1954). The main volume A of the experimental beaker was fitted with a heater.

In the case of the optical flats superleak the separation of the flats could

not be measured very reliably; however the general appearance of white light interference fringes indicated that the separation of the flats was approximately 10^{-4} cm., although measurements on oscillations and helium II flow rates obtained in successive experiments indicated that the separation varied from one experiment to the next. Because of these variations in the optical flats superleak and also because a lower frequency of oscillation could be obtained with a longer superleak (see equations (1) and (2)), a wire-filled tube was used.

The wire-filled tube was prepared in the following way. A large number of fine constantan wires (1200) were arranged to thread a cupronickel tube. The tube was then passed through successively smaller holes in a steel die plate to draw it down (Allen and Misener 1939). A photomicrograph taken of a cross section of such a tube showed that the wires were arranged in a regular pattern of closely packed hexagons (Allen and Misener 1939), the separation between parallel sides of neighboring hexagons being the channels available for gas or liquid flow. The mean length of the sides of the hexagons was found by direct measurement with a microscope to be 24.6 μ. For wires of hexagonal cross section, the number of parallel flow channels in the tube is three per wire or 3.1 for the finite number of wires in the particular tube considered here. With the mean channel breadth measured, the depth was determined by careful gas flow measurements and the application of Poiseuille's relation for flow between parallel planes. The value obtained was 7.8×10^{-5} cm. for the average depth and 7.2×10^{-4} cm.^{2} for the total area of cross section of the superleak. This was the value used in computing the theoretical values of ω_a. As in the present case the mean free path of the atoms of the helium gas used in the flow measurements is of the same order of magnitude as the dimensions of the flow channels, Knudsen's relation for gas flow was also used and it gave a value of 5×10^{-5} cm. for the channel depth. As this value is in moderate agreement with that given by Poiseuille's relation, it is possible that the flow was occurring in the transition region between the two types of flow.

The wire-filled tube was fastened by means of Kovar seals along the axis of a glass cone which fitted into a ground-glass socket and formed the bottom of the beaker, as shown in Fig. 3. The cone was also evacuated to provide thermal insulation. Glycerin was used to seal the ground-glass joint.

EXPERIMENTAL RESULTS

The general pattern of oscillation behavior as established in a series of experiments may be summarized as follows.

If the condition of temperature and level equilibrium between beaker and bath is disturbed, the meniscus in the observational capillary will move to some new position and start to oscillate after the position has been reached. The oscillations continue as the mean level of the meniscus returns toward the initial equilibrium position, but as they are fairly strongly damped they die out long before that position is reached. The general form of the oscillations observed at several temperatures is shown in Fig. 4. It was possible to initiate oscillations in several ways (Manchester 1955*a*) but the method used in all

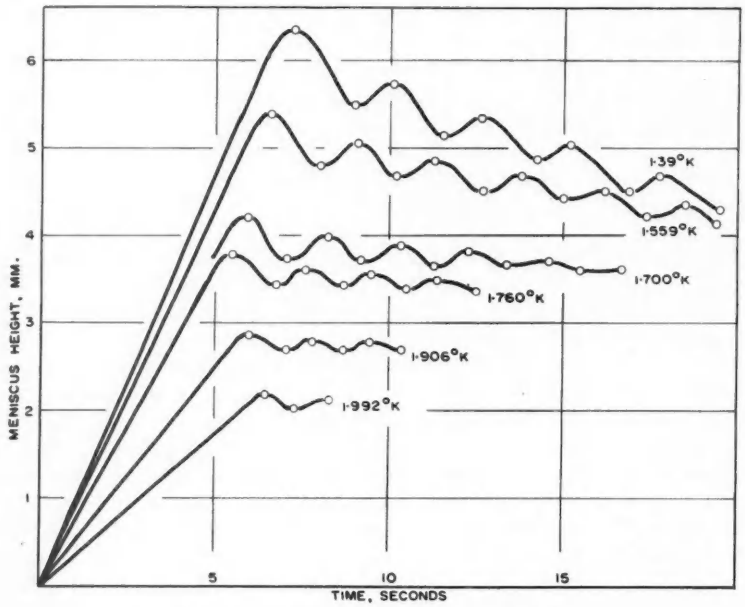

FIG. 4. General form of the adiabatic oscillations.

quantitative work was to discharge a condenser through the heater to release 8.1×10^3 ergs in the beaker.

Some measurements of adiabatic oscillations were obtained with the optical flats apparatus (Manchester 1955*a*) using a stroboscopic flash lamp method of photographing the movement of the meniscus. Such measurements served to establish that the frequency of oscillation was close to that predicted by theory but no useful data were obtained on the temperature dependence of the oscillation frequency, because of the lack of reproducible conditions with the optical flats superleak.

Experiments were then carried out with a similar experimental beaker fitted with a wire-filled tube superleak. The two principal advantages of such a superleak are that its dimensions can be measured with moderate precision and that they remain fairly constant throughout a series of experiments. Because of the different geometry employed (cf. equations (1) and (2)) the frequency of the adiabatic oscillations was much lower with the wire-filled tube. As a result the motion of the meniscus could be followed with the eye, so the stroboscopic flash lamp and camera were replaced with a very simple system using a stop watch, a cathetometer, and a low wattage neon lamp. The observed temperature dependence of the oscillation frequency is displayed in Fig. 5 and Table III. The points plotted in Fig. 5 are the experimental values of the oscillation frequency, the smooth curves being the theoretical values of ω_t and ω_a computed as described previously. Points obtained on a

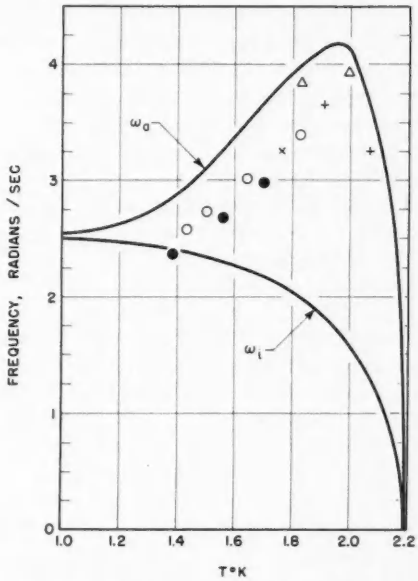

FIG. 5. The temperature dependence of the observed oscillation frequency.

TABLE III

EXPERIMENTAL VALUES OF ω OBTAINED WITH THE WIRE-FILLED TUBE APPARATUS IN THE COURSE OF FIVE DIFFERENT EXPERIMENTS

T, ° K.	ω, radians/sec.	T, ° K.	ω, radians/sec.
1.39	2.37	1.760	3.25
1.432	2.58	1.825	3.39
1.500	2.73	1.826	3.84
1.559	2.68	1.906	3.65
1.640	3.02	1.992	3.93
1.700	2.98	2.065	3.25

particular experimental run are indicated by a common symbol. Temperatures were measured using the 1949 vapor pressure – temperature scale. The measured periodic times are considered reliable to a little better than a tenth of a second. The experimental points agree in form with the temperature dependence of the theoretical curve; the difference between this curve and one fitting the points is presumably due to an uncertainty in the knowledge of the geometry of the apparatus. Because of some blockages which will occur to an unknown extent in the channels of the wire-filled tube it is not practical to estimate the uncertainty in the value for the superleak cross-sectional area and for this reason the curves have been presented in the form of Fig. 5. The most straightforward way to check the geometry factor would be to carry out isothermal oscillation measurements using the same superleak and observational capillary.

It would be desirable to obtain more experimental values in the region above 1.9° K. in order to strengthen the evidence for the curve having a maximum. However such points are difficult to obtain, as the amplitude of oscillation decreases and the damping increases with rising temperature. Also it was more difficult to obtain control over the stability of the meniscus when endeavoring to take readings at a temperature in the region near 2° K. This is because, in the region of lower superfluid velocity, the time between a countering change of the bath temperature and its effect on the meniscus was prolonged, while the sensitivity to temperature imbalance was greater because of the increase of the magnitude of the thermomechanical effect with temperature.

Measurement of the damping of the oscillations could not be carried out very satisfactorily because of the superposition of the damping on the fall of the mean meniscus level and because of the small number of periods available for measurement. Also minute variations in bath temperature tended to produce variations in amplitude which had an appreciable effect when diminution in amplitude was being measured. Such measurements as were made on the damping did not give a value for the thermal linkage between bath and container (the L value, see equation (3)) which agreed at all with that obtained from the data on the aperiodic decrease of the mean meniscus level. However, further examination of this question should be postponed until better experimental data on the damping are available.

The rate of return of the mean meniscus level to the original equilibrium position was measured, that is, the aperiodic decrease represented by the

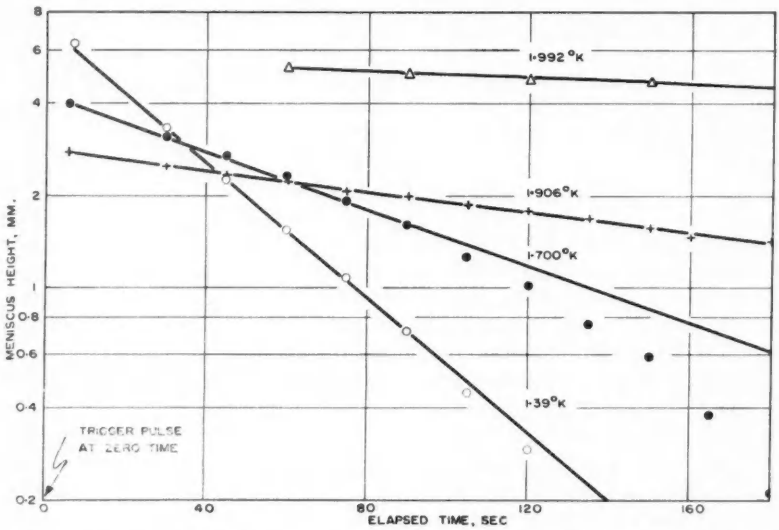

FIG. 6. The aperiodic fall of the meniscus after oscillations ceased. The curve for 1.992° K. is for a triggering pulse of 24,000 ergs.

second term in equation (3). Some results typical of those obtained are shown in Fig. 6. The bending which appears in such curves, and which occurs in all to an extent not necessarily apparent in Fig. 6, is thought to be due to a slight warming of the bath during the period of measurements, presumably because the liquid level in the outer helium dewar was slowly falling. This warming could occur because the temperature-stabilizing bridge controlled the temperature of the outer dewar liquid directly and the helium in the glass envelope by thermal contact through the copper.

The relaxation times for the return were determined by measuring the slopes of the straight line portions of the curves such as those shown in Fig. 6. In Fig. 7 the points are the values of these times plotted against temperature,

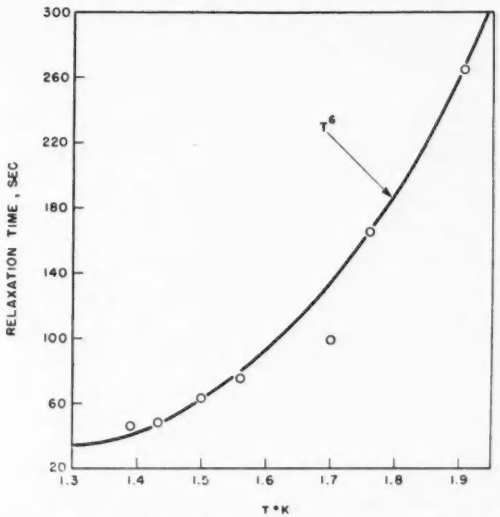

FIG. 7. The temperature dependence of the relaxation time for the fall of the meniscus after oscillatins ceased.

the smooth curve is proportional to T^6. It can be shown that the relaxation time may be written approximately as

$$\tau = \left(\frac{\rho a}{g}\right)\left(\frac{TS^2}{K}\right), \tag{4}$$

where K is an effective coefficient of thermal conduction between the beaker and bath. If it is assumed that the major contribution to the thermal conduction is through the superleak (see below) then K will vary as T^6 for a constant temperature difference as found experimentally by Meyer and Mellink (1947), for a superleak of 0.5 μ width. Using the approximation that the entropy of liquid helium II is proportional to $T^{5.5}$ over the temperature range of interest, the relaxation time is given as proportional to T^6. A more direct comparison between theory and experiment cannot be made because

there is no satisfactory quantitative treatment for heat transport through superleaks of the dimensions used in these experiments.

Calculations were made to determine the magnitude of the heat flux into the container along possible paths such as the electrical leads and the metal of the wire-filled tube. None of these seemed to provide a thermal link of the magnitude required for agreement with the experimental observations. The expected heat flux through the wire-filled tube superleak calculated by means of the relation of London and Zilsel (1948) was too small by a factor of 10^{-2}. This at least is in the same direction and of about the same magnitude as the discrepancies noted by London and Zilsel for superleaks of the dimensions considered here.

The temperature dependence of rates of fluid flow occurring during the oscillations is shown in Fig. 8. These are simply the average velocities between

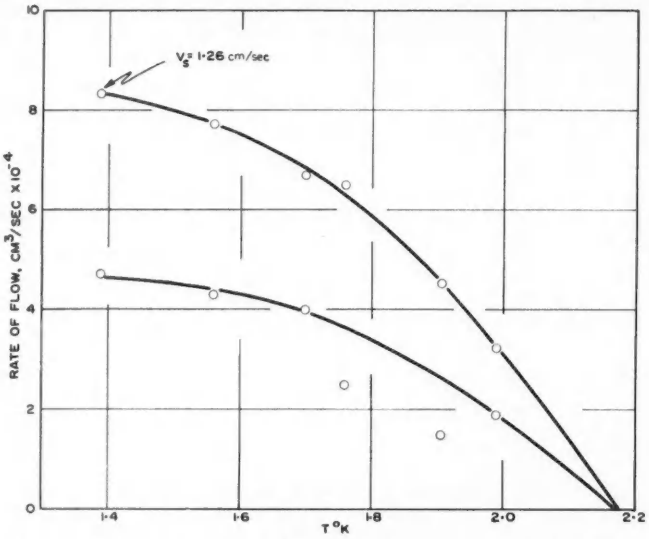

FIG. 8. The temperature dependence of flow rates. Upper curve: the flow rate up to the oscillation point. Lower curve: the flow rate during the first backswing of the oscillation.

turning points. Both of the curves have a form similar to that usually associated with the temperature variation of critical velocities. However, in the present case the velocities are very low; that for the superfluid velocity at 1.39° K. is indicated on the graph and is much lower than published values of critical velocities (see Winkel, Delsing, and Poll 1955). At the time of writing no opportunity has occurred for measuring critical velocities in steady flow experiments with the same wire-filled tube. It was suggested by London (1951) that the study of adiabatic oscillations might yield information on conditions under which there was a critical flow velocity. The present experiments do not provide such information but it is possible that useful data on flow rates may be obtained from a modified experiment to be discussed below.

The equations for the adiabatic oscillations are solvable for the temperature difference as well as the liquid level difference (see Robinson's paper) although from a knowledge of the magnitude of the fountain effect and the amplitude of the liquid level oscillations, the expected temperature oscillations would be of very small amplitude, 10^{-5}° K. or less. In spite of this small amplitude, it was decided to try to detect the temperature oscillations because it was thought possible that their recording might have been more convenient. No temperature oscillations were observed in several attempts, and effort in this direction was then abandoned in favor of concentrating on measurement of the liquid level oscillations. The limitations on the temperature measurements were the extreme sensitivity required of the thermometers together with the necessity for a fast response.

DISCUSSION

The general behavior of the oscillations agrees with the theoretical picture presented by Robinson (1951) while the measured frequency in the range 1.39° K. to 2.065° K. has the same form of temperature dependence and the experimental values are fairly close to those computed theoretically for the apparatus.

The observed agreement with the theoretically predicted values of frequency gives support to the assumption made in the theory that the fluid composition in the superleak is that of the bulk liquid and that it is the superfluid fraction which moves when flow occurs. As the cross section of the superleak is essentially independent of temperature over the range considered, the evidence given here supports the assumption made by Atkins (1950) concerning the substitution of Peshkov's ρ_s/ρ values (Peshkov 1946) in the isothermal oscillation equations.

If the geometry factor could be determined more precisely a better experimental check could be made on the theoretically expected values for the damping, through the quantity p/ω_a (a/ω_a of Robinson's paper). This might be more easily achieved by using a different approach suggested by the resonator analogue discussed in the appendix. This involves the use of a source of second sound placed in the liquid outside the adiabatic container and designed to operate at frequencies in the region of its resonance. Temperature oscillations generated by this source should produce movement of the meniscus in the capillary of the adiabatic container and enable the resonance curve of the container to be traced by visual observation of the amplitude of the meniscus motion. Measurements of the damping carried out in this manner should give much more information than was obtained in the present experiments.

ACKNOWLEDGMENTS

We are grateful to Dr. F. A. Kaempffer and Dr. J. M. Daniels for helpful comments and discussions. We wish to thank Mr. A. J. Fraser and Mr. H. Zerbst for producing the liquid helium, Mr. J. Lees for performing the glass blowing, and the Physics Department workshop staff for help with construction of the apparatus. We are indebted to the National Research Council of

Canada for financially supporting this work through a studentship awarded to one of us (F.D.M.) and a grant toward the cost of the experimental work.

APPENDIX. THE RESONATOR ANALOGUE

Equation (2) may be simplified by making the approximations that

$$\alpha = aTS^2/gVC$$

and that α is much larger than unity. Then

$$\omega_a = \left\{\frac{\rho_s}{\rho}\frac{\sigma}{lV}\frac{TS^2}{C}\right\}^{\frac{1}{2}}$$

and making use of the relation for u_2, the second sound velocity (Landau 1941),

$$u_2^{\,2} = \frac{\rho_s}{\rho_n}\frac{TS^2}{C}$$

the expression for ω_a becomes

$$\omega_a = u_2\left(\frac{\rho_n}{\rho}\frac{\sigma}{lV}\right)^{\frac{1}{2}}. \tag{I}$$

Equation (I) gives the frequency for ideal adiabatic oscillations assuming that $\omega_a \gg \omega_t$ and neglecting the effect of the vapor pressure over the liquid in the container. For reasons which will be given below the expression for ω_a in the form of equation (I) will be denoted by ω_R. It is possible to derive the relation for ω_R from an exact treatment of a simplified case which takes only thermal effects into account and neglects gravitation. For higher temperatures in the liquid helium II region, where the thermomechanical effect is relatively very large, the temperature dependence of ω_R is close to that of ω_a as given by equation (2), but with decreasing temperature the value of ω_R falls to zero at 0° K. whereas ω_a tends to ω_i, the isothermal value.

It is interesting to compare equation (I) with the expression given by standard acoustical theory for the resonant frequency of a Helmholtz resonator in a gaseous medium. For such a resonator, in the region of long wavelengths, the frequency of resonance is given by (see for instance Stewart and Lindsay 1930)

$$\omega_H = c(A/l'V)^{\frac{1}{2}},$$

where c is the velocity of sound in the gas, A the cross-sectional area of the resonator neck or opening, l' the effective length of the neck, and V the volume of the resonator, Fig. 2(*b*). There is good reason, therefore, for regarding the ideal adiabatic container in the second sound field as analogous to the Helmholtz resonator in the first sound field, both being considered for the long wavelength case only.

Considered from this point of view of association with second sound, the adiabatic container may be thought of as either a resonator or an oscillator. As an oscillator emitting radiation it could be regarded as a source similar to that used by Peshkov (1948), who placed a superleak in front of a mechanical

transducer emitting first sound so that relative motion of super and normal fluid was produced and the device acted as a source of second sound.

It should be noted that the approximation $\omega_a \gg \omega_t$ used above is affected by the geometry of the adiabatic container. In the experiments described in this paper the geometry of the container was chosen to give a low value of ω_a so that experimental observation would be easier. Thus in this particular case the approximation $\omega_a \gg \omega_t$ is not a good one but experimental conditions could easily be chosen to make it much better.

REFERENCES

ALLEN, J. F. and MISENER, A. D. 1939. Proc. Roy. Soc. (London), A, **172**, 467.
ATKINS, K. R. 1950. Proc. Roy. Soc. (London), A, **203**, 119, 240.
BAND, W. and MEYER, L. 1948. Phys. Rev. **74**, 389.
BLEANEY, B. and SIMON, F. 1939. Trans. Faraday Soc. **35**, 1205.
BOYLE, W. S. and BROWN, J. B. 1954. Rev. Sci. Instr. **25**, 359.
BREWER, D. P., EDWARDS, D. O., and MENDELSSOHN, K. 1955. Comm. Intern. Conf. Low Temp., Paris, p. 40.
BROWN, J. B. and MENDELSSOHN, K. 1947. Nature, **160**, 670.
DASH, J. G. 1954. Phys. Rev. **94**, 1091.
KRAMERS, H. C., WASCHER, J. D., and GORTER, C. J. 1952. Physica, **18**, 329.
LANDAU, L. 1941. J. Phys. U.S.S.R. **5**, 71.
LONDON, F. 1951. Proc. Intern. Conf. Low Temp., Oxford, p. 5.
LONDON, F. and ZILSEL, P. R. 1948. Phys. Rev. **74**, 1148.
MANCHESTER, F. D. 1955*a*. Can. J. Phys. **33**, 146.
——— 1955*b*. Comm. Intern. Conf. Low Temp., Paris, p. 105.
MAURER, R. D. and HERLIN, M. A. 1949. Phys. Rev. **76**, 950.
MEYER, L. and MELLINK, J. H. 1947. Physica, **13**, 197.
PESHKOV, V. P. 1946. Rept. Intern. Conf. Low Temp., Cambridge, p. 19.
——— 1948. J. Exptl. Theoret. Phys. (U.S.S.R.), **18**, 867.
PICUS, G. S. 1954. Phys. Rev. **94**, 1459.
ROBINSON, J. E. 1951. Phys. Rev. **82**, 440.
STEWART, G. W. and LINDSAY, R. B. 1930. Acoustics (D. Van Nostrand Company, Inc., New York, N.Y.), p. 47.
WINKEL, P., DELSING, A. M. G., and POLL, J. D. 1955. Physica, **21**, 331.

ON THE THEORY OF MULTIPLE MESON PRODUCTION[1]

YASUSHI TAKAHASHI[2]

In a previous paper (Takahashi 1956*a*), a general expression for the *S*-matrix for multiple meson production was derived, and the relation between Fermi's thermodynamic approach and the field theoretical treatment discussed, by determining the most probable value of the meson production probability, neglecting meson correlation.

On the other hand, it has been pointed out that the Fermi model is too simple to explain experimental data available so far (Bethe and de Hoffman 1955; Landau 1951). This point has been discussed in detail by Landau and a Japanese group (Koba 1956), who stress the importance of the meson–meson interaction.

In this note, the meson–meson correlation is discussed starting from the general expression of the *S*-matrix (Takahashi 1956*b*). According to the previous paper (Takahashi 1956*b*), the probability for the n-meson production is generally given as

$$(1) \qquad w_n = \frac{1}{n!}\int_{(\text{con.})}\cdots\int\prod_{i=1}^{n}\frac{d\mathbf{k}_i}{(2\pi)^3\,2K_i^3}\,|\phi_p(\mathfrak{k}_1,\ldots,\mathfrak{k}_n)|^2,$$

where

$$\phi_p(\mathfrak{k}_1,\ldots,\mathfrak{k}_n) = \sum_{(\text{permutation})}\phi(\mathfrak{k}_1,\ldots,\mathfrak{k}_n),$$

$$(2)^* \qquad \phi(\mathfrak{k}_1,\ldots,\mathfrak{k}_n) = \int_{-\infty}^{\infty}\cdots\int\prod_{i=1}^{n}\{(dx_i)\exp(-i\mathfrak{k}_i x_i)\} \times\langle\Phi_0', T^*(\dot{\mathbf{O}}(x_1),\ldots,\dot{\mathbf{O}}(x_n))\Phi_0\rangle.$$

Since the function $|\phi_p(\mathfrak{k}_1,\ldots,\mathfrak{k}_n)|^2$ in (2) is a positive symmetric function with respect to the $\mathfrak{k}$'s, it can be expanded in the following way:

$$(3) \qquad |\phi_p(\mathfrak{k}_1,\ldots,\mathfrak{k}_n)|^2 = \prod_i\phi_1(\mathfrak{k}_i)\prod_{(i,j)}\phi_2(\mathfrak{k}_i,\mathfrak{k}_j)\prod_{(i,j,k)}\phi_3(\mathfrak{k}_i,\mathfrak{k}_j,\mathfrak{k}_k)\ldots,$$

where (i, j) signifies the product over all possible combinations of i and j and (i, j, k) the product over all possible combinations of i, j, k, and so on. The expansion of a symmetric function in the form (3) is always possible but is not always unique. This will be discussed in a detailed paper later. We suppose, at any rate, that the $\phi_2(\mathfrak{k}_i, \mathfrak{k}_j)$, $\phi_3(\mathfrak{k}_i, \mathfrak{k}_j, \mathfrak{k}_k)$, ... are determined as close to unity as possible, and we will neglect, for the sake of simplicity, the

[1]Issued as N.R.C. No. 4286.

[2]Department of Physics, State University of Iowa, Iowa City, Iowa, U.S.A.; on leave during the summer of 1956 at the National Research Council, Division of Pure Physics, Ottawa, Canada.

*The notation used in this note is the same as that in the article in the *Nuovo Cimento*.

terms which include more than two arguments. If we express (3) in terms of the meson occupation number, we get

$$(4)\qquad |\phi_p(\mathfrak{k}_1, \ldots, \mathfrak{k}_n)|^2 = n! \prod_r \frac{1}{n_r!} \{\phi_1(\mathfrak{k}_{(r)})\}^{n_r} \prod_r \{\phi_2(\mathfrak{k}_{(r)}, \mathfrak{k}_{(r)})\}^{\frac{1}{2}n_r(n_r-1)} \times \prod_s \prod_{r\neq s} \{\phi_2(\mathfrak{k}_{(r)}, \mathfrak{k}_{(s)})\}^{\frac{1}{2}n_s \cdot n_r},$$

where n_1 is the number of mesons with the momentum $\mathfrak{k}_{(1)}$, n_2 the number of mesons with the momentum $\mathfrak{k}_{(2)}$, and so on.

The total probability is

$$(5)\qquad W_n = \sum_{n=n_1+n_2+\cdots} dW_n(n_1, n_2, \ldots),$$

where

$$(6)\quad dW_n(n_1, n_2, \ldots) = \prod_r \frac{1}{n_r!} \left\{\frac{1}{V}\Omega(\mathfrak{k}_{(r)})\right\}^{n_r} \prod_r \{\phi_2(\mathfrak{k}_{(r)}, \mathfrak{k}_{(r)})\}^{\frac{1}{2}n_r(n_r-1)} \times \prod_s \prod_{r\neq s} \{\phi_2(\mathfrak{k}_{(r)}, \mathfrak{k}_{(s)})\}^{\frac{1}{2}n_r \cdot n_s}$$

and

$$(7)\qquad \Omega(\mathfrak{k}_{(s)}) \equiv \frac{1}{2K_{(s)}^3}\, \phi_1(\mathfrak{k}_{(s)}).$$

We can easily determine the most probable $dW_n(n_1, n_2, \ldots)$, subject to the energy conservation law, by taking a variation with respect to n_r of the quantity

$$(8)\qquad I = \log dW_n(n_1, n_2, \ldots) + \beta(\Delta E - \sum K_{(s)}\, n_{(s)}).$$

Thus,

$$(9)\qquad 0 = \sum_r \frac{\partial I}{\partial n_r}\, \delta n_r = -\sum_r \delta n_r \log n_r + \sum_r \delta n_r \log \frac{\Omega(\mathfrak{k}_{(r)})}{V} - \beta \sum_r K_{(r)} \delta n_{(r)} + \sum_r \sum_s \delta n_r \,.\, n_s \log\{\phi_2(\mathfrak{k}_{(r)}, \mathfrak{k}_{(s)})\}.$$

We have, therefore,

$$(10)\qquad \begin{aligned} n_r &= \frac{1}{V}\Omega(\mathfrak{k}_{(r)}) \exp(-\beta K_{(r)}) \prod_{s=1}^{\infty} \{\phi_2(\mathfrak{k}_{(r)}, \mathfrak{k}_{(s)})\}^{n_s} \\ &= \frac{1}{V}\Omega(\mathfrak{k}_{(r)}) \exp(-\beta K_{(r)}) \prod_{s=1}^{\infty} \exp(\lambda_{rs}\, n_s) \\ &= \frac{1}{V}\Omega(\mathfrak{k}_{(r)}) \exp(-\beta K_{(r)}) \exp(\bar{\lambda}_r\, n), \end{aligned}$$

where we put

$$(11)\qquad \begin{aligned} &\phi_2(\mathfrak{k}_{(r)}, \mathfrak{k}_{(s)}) \equiv \exp \lambda_{rs}, \\ &\bar{\lambda}_r \equiv \sum_s \lambda_{rs}\, n_s \Big/ \sum_s n_s. \end{aligned}$$

The last factor of (10) takes care of the effect coming from the meson–meson interaction and effectively modifies the "spectrum volume" $\Omega(\mathfrak{f})$. This is encouraging in view of the fact that raising the volume Ω is suggested to bring the ratio of two-meson to one-meson events into agreement with experiment.

The relation between equation (10) and Landau's theory will be discussed in the next paper.

The author would like to thank Dr. G. Herzberg and Dr. T. Y. Wu for their kind hospitality. He is also indebted to Dr. G. R. Allcock for his stimulating discussion.

BETHE, H. A. and DE HOFFMAN, F. 1955. Mesons and fields, Vol. II (Row, Peterson & Co., Evanston, Ill.).
KOBA, Z. 1956. Private communication. See also the Proceedings of the Rochester Conference, 1956.
LANDAU, L. D. 1951. Izvest. Akad. Nauk. S.S.S.R. **17**, 51.
TAKAHASHI, Y. 1956*a*. Can. J. Phys. **34**, 378.
——— 1956*b*. Nuovo cimento (10), **4**, 531.

RECEIVED AUGUST 23, 1956.
DIVISION OF PURE PHYSICS,
NATIONAL RESEARCH COUNCIL,
OTTAWA, CANADA.

A SIMPLE FORMULA FOR EVALUATING THE MADELUNG CONSTANT OF AN NaCl-TYPE CRYSTAL

J. K. MACKENZIE

In a recent paper, Benson (1956) gave a new formula for the Madelung constant of a crystal of the NaCl type. The purpose of this note is to give a direct proof of this formula.

The Madelung constant α_M is given by the triple summation

$$-\alpha_M = \sum_{l_1, l_2, l_3}{}'^{\infty}_{-\infty} (-1)^{l_1+l_2+l_3}(l_1^2+l_2^2+l_3^2)^{-\frac{1}{2}}, \tag{1}$$

where the prime on the summation means that the term with $l_1 = l_2 = l_3 = 0$ is omitted. By means of a physical model with repulsive forces, Benson showed that

$$\alpha_M = 48\pi \sum_{p}^{\infty}{}_1 \nu_p \exp(-\pi p^{\frac{1}{2}})/[1+\exp(-\pi p^{\frac{1}{2}})]^2, \tag{2}$$

where ν_p is the number of ways $p = l_1^2+l_2^2$ can be represented as the sum of squares of positive odd integers. He also showed that equation (2) gives the correct value of α_M to at least nine significant figures.*

*The last two digits of the first entry in the second column of his Table I should read 63 instead of 54. With this change 10 significant figures are obtained correctly.

It is clear that

$$(3)\quad -\alpha_M = 3\sum_{l_1,\,l_2,\,l_3=-\infty}^{\infty\prime}(-1)^{l_1+l_2+l_3}\,l_1^{\,2}(l_1^{\,2}+l_2^{\,2}+l_3^{\,2})^{-3/2},$$

$$(4)\quad = 6\pi^{-\frac{1}{2}}\sum_{l_1,\,l_2,\,l_3=-\infty}^{\infty\prime}(-1)^{l_1+l_2+l_3}\,l_1^{\,2}\int_0^\infty u^{\frac{1}{2}}\exp[-(l_1^{\,2}+l_2^{\,2}+l_3^{\,2})u]du,$$

on using the integral which defines the gamma function. Interchange of the order of the summation and the integration can be justified and further, since all terms in equation (4) with $l_1 = 0$ are zero, the summation can be extended over all values of l_1, l_2, l_3. Thus

$$(5)\quad -\alpha_M = 12\pi^{-\frac{1}{2}}\sum_{l_1=1}^{\infty}(-1)^{l_1}\,l_1^{\,2}\int_0^\infty \exp(-l_1^{\,2}u)f(u)\,u^{\frac{1}{2}}du,$$

where

$$(6)\quad f(u) = \sum_{l_2,\,l_3=-\infty}^{\infty}(-1)^{l_2+l_3}\exp[-(l_2^{\,2}+l_3^{\,2})u],$$

$$(7)\quad = (\pi/u)\sum_{l_2,\,l_3\text{odd}=-\infty}^{\infty}\exp[-(l_2^{\,2}+l_3^{\,2})\pi^2/4u],$$

on using a known result (Whittaker and Watson 1935). When the series for $f(u)$ given by equation (7) is substituted into equation (5), interchange of the order of summation and integration can again be justified and the integrals can be evaluated by using the result (see Watson 1944)

$$(8)\quad \int_0^\infty u^{n-1}\exp[-(a^2u+b^2/u)]du = 2(b/a)^n\,K_n(2ab).$$

Finally, when $K_{\frac{1}{2}}(x)$ is put equal to $(\pi/2x)^{1/2}e^{-x}$ and the summation over l_1 performed, the result given in equation (2) follows.

Similar methods can be used to evaluate other lattice sums but the resulting series do not always converge more rapidly than the series which are already known. This is so, for example, in the case of the series obtained by the present method for the Madelung constant for a CsCl-type lattice.

Benson, G. C. 1956. Can. J. Phys. **34**, 888.
Watson, G. N. 1944. Theory of Bessel functions, 2nd ed. (Cambridge University Press, London), p. 181.
Whittaker, E. T. and Watson, G. N. 1935. Modern analysis, 4th ed. (Cambridge University Press, London), p. 124.

Received January 4, 1957.
Division of Tribophysics,
Commonwealth Scientific and Industrial Research Organization,
University of Melbourne,
Melbourne, Australia.

THERMAL CONTACT IN A PARAMAGNETIC SALT[1]

J. S. DUGDALE, D. K. C. MACDONALD, AND A. A. M. CROXON

In recent measurements of the electrical resistance of metals below 1° K. (Dugdale and MacDonald 1957) we wished to measure the thermal contact resistance between a gold wire and a paramagnetic salt which had been crystallized onto it. To do this, an experiment was made with two "pills" of the salt (iron ammonium alum) each of which was crystallized onto a specimen of the gold wire. The two gold wires were joined by a copper wire whose thermal resistance was estimated to be considerably less than the thermal contact resistance to be measured. In one of the pills a rhodium–platinum resistance element was embedded to act as an electrical heater. Both salts were then demagnetized from the same field at about 1° K. in the normal way; after demagnetization, the temperatures of the two pills were measured (by their magnetic susceptibilities) at regular intervals. From time to time known quantities of heat were supplied to one salt by means of the heater, and from the temperature–time graphs of the two salts a value of the thermal contact resistance was deduced.

However, a peculiar phenomenon was also observed. As soon as the heater was switched on in the "hot" pill, the temperature of the "cold" pill was found to *fall* and it was not until later that the flux of heat from the "hot" pill caused the temperature of the cold pill to start to rise in the expected manner. It was suggested that an adsorbed helium film showing superfluidity might be responsible for this behavior,* and we were then concerned whether the presence of such a film might also play a significant role in the observed normal thermal conduction. If this were so, our estimate of the thermal contact resistance between wire and paramagnetic salt might be seriously in error. We have, therefore, carried out further experiments with a double pill arrangement to examine this question.

We assumed that any heat flow through the helium film would depend essentially on the perimeter of the link joining the two pills. We therefore made two experiments with the same pills and gold wires but with different links. These had the same length and over-all perimeter but quite different thermal resistances. In the first experiment connection between the pills was made by a heavy copper wire of 0.1 in. diameter (some of the results are shown in Fig. 1(*a*)). In the second experiment the link was made of manganin. It consisted of 20 manganin wires of the same length as the copper and of 0.005 in. diameter giving thus the same total perimeter; its thermal resistance however was estimated to be at least a hundred times bigger than that of the copper. The results with the manganin link are shown in Fig. 1(*b*). It is clear that in this case the two pills remain effectively isolated even when the temperature of the "hot" pill has risen as high as 0.5° K.

From these experiments we deduce that with the copper connecting rod the total thermal conductance is about 50 ergs/sec.deg., and with the manganin

[1]Issued as N.R.C. No. 4237.

*We are grateful to Dr. F. D. Manchester for making this suggestion.

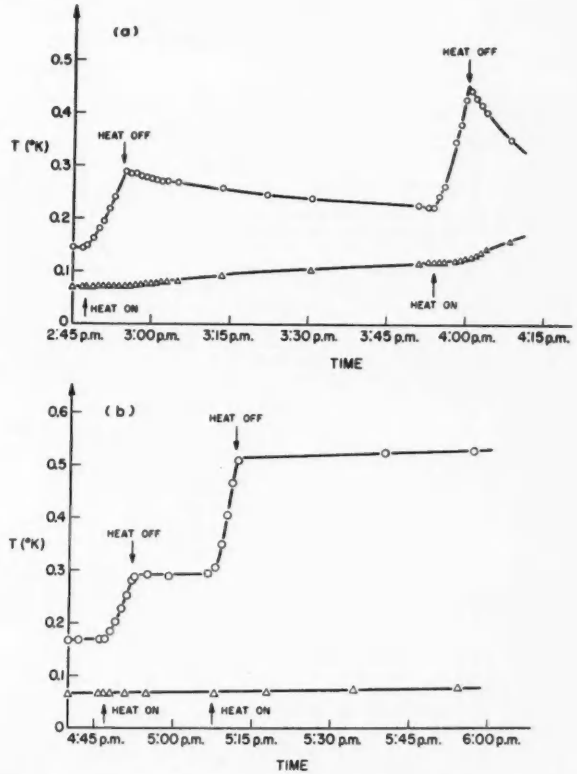

FIG. 1. (*a*) Temperature–time curves for pills connected by heavy copper wire.
(*b*) Temperature–time curves for pills connected with manganin wires.

connection only about 3 ergs/sec. deg. in the comparable temperature range. Therefore, even if we attribute all of the latter heat flow to the helium film it is still small compared with that when the copper link is used. Consequently it appears that the thermal conductance of the contact between each salt pill and the gold wire is of the order of 100 ergs/sec. deg. at these temperatures, which is even better than we thought originally.

It may be remarked that in the present experiments the anomalous cooling of the "cold" pill is much less noticeable than in the earlier work. We believe that this may be due to the achievement of a better vacuum in the present experiments, so reducing the formation and/or superfluid flow of the helium film.

DUGDALE, J. S. and MACDONALD, D. K. C. 1957. Can. J. Phys. **35**, 271.

RECEIVED JANUARY 3, 1957.
DIVISION OF PURE PHYSICS,
NATIONAL RESEARCH COUNCIL,
OTTAWA, CANADA.

LETTERS TO THE EDITOR

Under this heading brief reports of important discoveries in physics may be published. These reports should not exceed 600 words and, for any issue, should be submitted not later than six weeks previous to the first day of the month of issue. No proof will be sent to the authors.

Structure de la molécule CH_2=CH—C≡N par diffraction des électrons*

Nous avons obtenu, au moyen du diffracteur électronique de l'Université de Montréal (Grégoire et Rouault 1951) des photographies de diffraction d'électrons de 50 kv. par les vapeurs du cyanure de vinyle CH_2=CH—C≡N. Un faisceau sensiblement parallèle d'électrons rencontre un faisceau moléculaire de gaz. Les électrons diffractés impressionnent une émulsion photographique placée dans le plan focal d'une lentille magnétique. La répartition de l'intensité I des électrons diffractés en fonction de $s = 4\pi(\sin\theta/2)/\lambda$ (θ = angle de diffraction, λ = longueur d'onde associée aux électrons) a été tracée au moyen d'un microphotomètre Leeds and Northrup, en faisant tourner la photographie autour du centre des anneaux de diffraction pendant l'enregistrement (Bélair et Rouault 1951). La structure de la molécule a été étudiée par la méthode de comparaison des courbes expérimentale et théorique représentant la fonction s^3I (Rouault 1940).

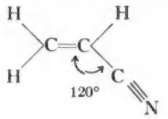

FIG. 1.

La structure des composés à double liaisons conjuguées et des composés de C≡N et l'étude du spectre hertzien (Wilcox, Goldstein, et Simons 1954) du cyanure de vinyle rendaient très probable la structure plane de la fig. 1 avec les caractéristiques suivantes:

C=C = 1.38 Å	C—C = 1.46 Å	C≡N = 1.16 Å
C—H = 1.09 Å	∠C=C—C = 120°	∠H—C—C = 120°

La fig. 2 reproduit la courbe théorique correspondant à ce modèle et la courbe expérimentale déduite de l'étude de la photographie. L'intensité I des électrons diffractés par un gaz constitue de ces molécules et donnée par la formule:

$$s^3I = \Sigma_i\Sigma_j\phi_i\phi_j \frac{\sin sl_{ij}}{sl_{ij}},$$

où

$$\phi_i(s) = \frac{Z_i - F_i(s)}{s^2},$$

$F_i(s)$ = facteur de diffusion pour rayons X de l'atome i,
l_{ij} = distance des 2 atomes numéros i et j.

La courbe II de la fig. 2 représente cette fonction s^3I. La courbe expérimentale (courbe III) a une forme générale un peu différente due très probablement à une erreur dans la détermination de la courbe de sensibilité de l'émulsion utilisée; mais l'influence sur les abscisses des maxima et minima de s^3I est faible. Si la forme choisie pour la molécule (rapport des différentes distances interatomiques) est bonne, on peut calculer une distance particulière l, C=C par exemple, en écrivant pour chaque point caractéristique, maximum ou minimum, $s_{exp}\, l_{exp} = s_{th} l_{th}$; les résultats de ce calcul sont présentés dans le tableau I; les différentes valeurs de ce tableau sont en bon accord et ne montrent pas de dérive systématique en fonction de s dans une même photographie. On peut en conclure (Rouault 1940) que le modèle choisi est en accord avec nos mesures. La moyenne des nombres du tableau I est 1.38 Å, confirmant non seulement la forme de la molécule, mais aussi sa grandeur.

Le résultat ci-dessus est confirmé par le calcul de la fonction s^3I pour un modèle pour lequel les distances des liaisons sont inchangées sauf la distance C=C qui a été prise égale à 1.35 Å;

*Subventionné par le Conseil National de Recherches du Canada.

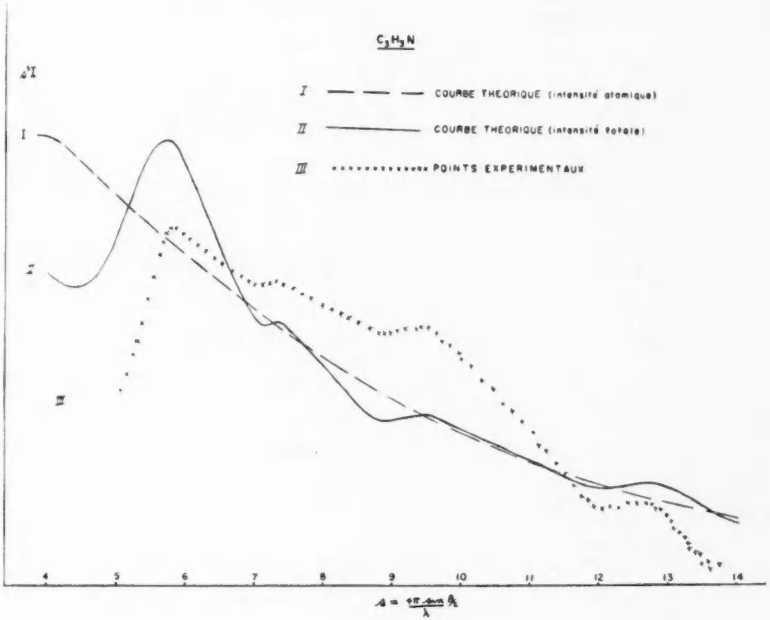
C_2H_3N
I COURBE THEORIQUE (intensité atomique)
II COURBE THEORIQUE (intensité totale)
III POINTS EXPERIMENTAUX
4 5 6 7 8 9 10 11 12 13 14

FIG. 2.

TABLEAU I
DISTANCE C=C

	10 juin, série no 4				10 juin, série no 2				10 juin, série no 3	
	Plaque no 1	Plaque no 2	Plaque no 3	Plaque no 4	Plaque no 1	Plaque no 2	Plaque no 3	Plaque no 4	Plaque no 1	Plaque no 2
M_3	1.371	1.378	1.375	1.378	1.384	1.375	1.370	1.380	1.384	1.370
m_4	1.376	1.380	1.380	1.372	1.383	1.380	1.388	1.380	1.376	1.384
M_4	1.376	1.378	1.380	1.376	1.376	1.387	1.387	1.378	1.382	1.376
m_5					1.381	1.388	1.372	1.375	1.375	
M_5	1.374	1.377	1.374	1.373	1.375	1.371	1.378	(1.391)	1.374	1.380
m_6					1.382	1.373	1.380	1.375		
M_6					1.373	1.388	1.386	1.382		
Moy.	1.374	1.378	1.377	1.375	1.379	1.380	1.380	1.378	1.378	1.377

Moyenne générale: C=C → 1.38 Å.

le tableau des distances C=C calculées comme ci-dessus non seulement montre des résultats deux fois plus dispersés, mais une augmentation systématique des valeurs de C=C déduite des maxima successifs d'une même photographie lorsqu'on se déplace vers les s croissants (fig. 3).

L'écart quadratique moyen déduit du même tableau I est $\sqrt{\overline{\Delta l^2}} \simeq 5\times10^{-3}$, soit en valeur relative 4×10^{-3}. Mais à cause de l'incertitude sur la forme de la molécule, incertitude difficile à chiffrer, on ne peut pas dire que la distance C=C soit connue à mieux que 0.01 Å près.

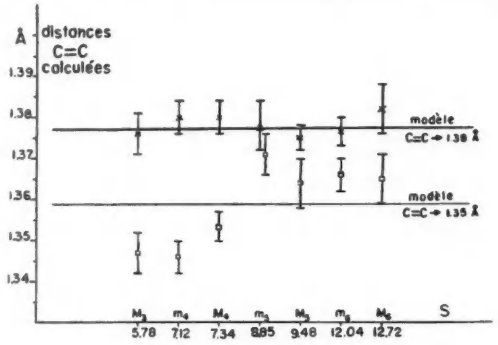

FIG. 3.

BÉLAIR, R. et ROUAULT, M. 1951. Ann. ACFAS, **17**, 80.
GRÉGOIRE, L. et ROUAULT, M. 1951. Ann. ACFAS, **17**, 75.
ROUAULT, M. 1940. Ann. phys. **14**, 78.
WILCOX, W. S., GOLDSTEIN, J. H., et SIMONS, J. W. 1954. J. Chem. Phys. **22**, 517.

REÇU LE 12 DÉCEMBRE 1956.
DÉPARTEMENT DE PHYSIQUE,
UNIVERSITÉ DE MONTRÉAL,
MONTRÉAL, QUÉBEC.

Marcel Rouault
Claude St-Arnaud

THE PHYSICAL SOCIETY

MEMBERSHIP of the Society is open to all who are interested in Physics.

FELLOWS pay an Entrance fee of £1 1*s*. ($3.00) and an Annual Subscription of £2 2*s*. ($6.00).

STUDENTS: A candidate for Studentship must be between the ages of 18 and 26, and pays an Annual Subscription of 5*s*. ($0.75).

MEETINGS: Fellows and Students may attend all Meetings of the Society including the annual Exhibition of Scientific Instruments and Apparatus.

PUBLICATIONS include the *Proceedings of the Physical Society*, published monthly in two sections, and *Reports on Progress in Physics*, published annually. Volume XIX, 1956, is now available (price 50*s*. ($7.15)). Members are entitled to receive any of the Publications at a reduced rate.

Further information can be obtained from:

THE PHYSICAL SOCIETY

1, LOWTHER GARDENS, PRINCE CONSORT ROAD

LONDON, S.W.7, ENGLAND

CANADIAN JOURNAL OF PHYSICS

Notes to Contributors

Manuscripts

(i) ***General.*** Manuscripts, in English or French, should be typewritten, double spaced, on paper 8½×11 in. **The original and one copy are to be submitted.** Tables and captions for the figures should be placed at the end of the manuscript. Every sheet of the manuscript should be numbered.

Style, arrangement, spelling, and abbreviations should conform to the usage of this journal. Names of all simple compounds, rather than their formulas, should be used in the text. Greek letters or unusual signs should be written plainly or explained by marginal notes. Superscripts and subscripts must be legible and carefully placed.

Manuscripts and illustrations should be carefully checked before they are submitted. Authors will be charged for unnecessary deviations from the usual format and for changes made in the proof that are considered excessive or unnecessary.

(ii) ***Abstract.*** An abstract of not more than about 200 words, indicating the scope of the work and the principal findings, is required, except in Notes.

(iii) ***References.*** References should be listed **alphabetically by authors' names,** unnumbered, and typed after the text. The form of the citations should be that used in current issues of this journal; in references to papers in periodicals, titles should not be given and only initial page numbers are required. The names of periodicals should be abbreviated in the form given in the most recent *List of Periodicals Abstracted by Chemical Abstracts.* All citations should be checked with the original articles and each one referred to in the text by the authors' names and the year.

(iv) ***Tables.*** Tables should be numbered in roman numerals and each table referred to in the text. Titles should always be given but should be brief; column headings should be brief and descriptive matter in the tables confined to a minimum. Vertical rules should be used only when they are essential. Numerous small tables should be avoided.

Illustrations

(i) ***General.*** All figures (including each figure of the plates) should be numbered consecutively from 1 up, in arabic numerals, and each figure referred to in the text. The author's name, title of the paper, and figure number should be written in the lower left corner of the sheets on which the illustrations appear. Captions should not be written on the illustrations (see Manuscripts (i)).

(ii) ***Line Drawings.*** Drawings should be carefully made with India ink on white drawing paper, blue tracing linen, or co-ordinate paper ruled in blue only; any co-ordinate lines that are to appear in the reproduction should be ruled in black ink. Paper ruled in green, yellow, or red should not be used unless it is desired to have all the co-ordinate lines show. All lines should be of sufficient thickness to reproduce well. Decimal points, periods, and stippled dots should be solid black circles large enough to be reduced if necessary. Letters and numerals should be neatly made, preferably with a stencil (**do NOT use typewriting**) and be of such size that the smallest lettering will be not less than 1 mm. high when reproduced in a cut 3 in. wide.

Many drawings are made too large; originals should not be more than 2 or 3 times the size of the desired reproduction. In large drawings or groups of drawings the ratio of height to width should conform to that of a journal page but the height should be adjusted to make allowance for the caption.

The original drawings and one set of clear copies (e.g. small photographs) are to be submitted.

(iii) ***Photographs.*** Prints should be made on glossy paper, with strong contrasts. They should be trimmed so that essential features only are shown and mounted carefully, with rubber cement, on white cardboard with no space or only a **very** small space (less than 1 mm.) between them. In mounting, full use of the space available should be made (to reduce the number of cuts required) and the ratio of height to width should correspond to that of a journal page (4¾×7½ in.); however, allowance must be made for the captions. Photographs or groups of photographs should not be more than 2 or 3 times the size of the desired reproduction.

Photographs are to be submitted in duplicate; if they are to be reproduced in groups one set should be mounted, the duplicate set unmounted.

Reprints

A total of 50 reprints of each paper, without covers, are supplied free. Additional reprints, with or without covers, may be purchased.

Charges for reprints are based on the number of printed pages, which may be calculated approximately by multiplying by 0.6 the number of manuscript pages (double-spaced typewritten sheets, 8½×11 in.) and including the space occupied by illustrations. An additional charge is made for illustrations that appear as coated inserts. The cost per page is given on the reprint requisition which accompanies the galley.

Any reprints required in addition to those requested on the author's reprint requisition form must be ordered officially as soon as the paper has been accepted for publication.

Contents

Page

The Lattice Spacings of Nickel Solid Solutions—*W. B. Pearson and L. T. Thompson* - - - - - - - - - - - - 349

Lattice Distortion in Terminal Solid Solutions of the First Long Period Transition Metals and Copper—*W. B. Pearson* - - - 358

The Velocity Dependence of Čerenkov Radiation from μ-Mesons —*C. H. Millar and E. P. Hincks* - - - - - - - - - 363

High Resolution Raman Spectroscopy of Gases. VIII. Rotational Spectra of Acetylene, Diacetylene, Diacetylene-d_2, and Dimethylacetylene—*J. H. Callomon and B. P. Stoicheff* - - 373

Rheology of the Earth: The Basic Problem of Geodynamics—*A. E. Scheidegger* - - - - - - - - - - - - 383

Variations in the Amounts of Positronium Formed in Liquids and Amorphous Solids—*R. E. Green and R. E. Bell* - - - - 398

Steady State Heat Transfer to Fully Developed Turbulent Flow in a Curved Channel—*A. W. Marris* - - - - - - - - 410

Diffusion in Multicomponent Metallic Systems—*J. S. Kirkaldy* - 435

Some Scattering Problems in Conduction Theory—*P. G. Klemens* 441

A Study of Nucleon Forces with Repulsive Cores. III. Low Energy Properties of the Lévy Potential—*M. A. Preston and J. Shapiro* 451

Measurement by Photoelectric Fringe Scanning of the Pressure Shift of Hg-198 Emission Lines—*K. M. Baird and D. S. Smith* - 455

Electrical Resistivity of Graphite Irradiated with Neutrons—*R. W. Attree and O. Dahlinger* - - - - - - - - - 462

Photoneutron Emission from Th^{232}, U^{233}, U^{235}, and Pu^{239}—*L. Katz, K. G. McNeill, M. LeBlanc, and F. Brown* - - - - - - 470

The Gravitational Fields of Electric and Magnetic Dipoles—*Gerald E. Tauber* - - - - - - - - - - - - - - - 477

Adiabatic Oscillations in Liquid Helium II—*F. D. Manchester and J. B. Brown* - - - - - - - - - - - - - 483

Notes:

On the Theory of Multiple Meson Production—*Yasushi Takahashi* - - - - - - - - - - - - - - - 498

A Simple Formula for Evaluating the Madelung Constant of an NaCl-type Crystal—*J. K. Mackenzie*- - - - - 500

Thermal Contact in a Paramagnetic Salt—*J. S. Dugdale, D. K. C. MacDonald, and A. A. M. Croxon* - - - - - 502

Letters to the Editor:

Structure de la molécule $CH_2{=}CH{-}C{\equiv}N$ par diffraction des électrons—*Marcel Rouault and Claude St-Arnaud* - - 504

Printed in Canada *by* University of Toronto Press